



Indu Ambat

APPLICATION OF DIVERSE FEEDSTOCKS FOR BIODIESEL PRODUCTION USING CATALYTIC TECHNOLOGY



Indu Ambat

APPLICATION OF DIVERSE FEEDSTOCKS FOR BIODIESEL PRODUCTION USING CATALYTIC TECHNOLOGY

Dissertation for the degree of Doctor of Science (Technology) to be presented with due permission for public examination and criticism in the Viipuri-hall at Lappeenranta-Lahti University of Technology LUT, Lappeenranta, Finland on the 24th of March, 2020, at noon.

Acta Universitatis
Lappeenrantaensis 900

Supervisors Professor Tuomo Sainio
LUT School of Engineering Science
Lappeenranta-Lahti University of Technology LUT
Finland

Dr. Varsha Srivastava
LUT School of Engineering Science
Lappeenranta-Lahti University of Technology LUT
Finland

Reviewers Professor Adam Lee
Department of Applied chemistry and Environmental science
Royal Melbourne Institute of Technology (RMIT)
Australia

Associate professor Yohannes Kiros
Department of Chemical Engineering
KTH Royal Institute of Technology
Sweden

Opponent Professor Dmitry Murzin
Laboratory of Industrial Chemistry and Reaction Engineering
Johan Gadolin Process Chemistry Centre
Åbo Akademi University
Finland

ISBN 978-952-335-494-4
ISBN 978-952-335-495-1 (PDF)
ISSN-L 1456-4491
ISSN 1456-4491

Lappeenranta-Lahti University of Technology LUT
LUT University Press 2020

Abstract

Indu Ambat

Application of diverse feedstocks for biodiesel production using catalytic technology

Lappeenranta 2020

88 pages

Acta Universitatis Lappeenrantaensis 900

Diss. Lappeenranta-Lahti University of Technology LUT

ISBN 978-952-335-494-4, ISBN 978-952-335-495-1 (PDF), ISSN-L 1456-4491, ISSN 1456-4491

Recently the rise in population and demand in energy for growth and development of countries leads to more consumption of fossil fuels which is a non-renewable source. The excessive usage of non-renewable resources results in depletion of limited energy reserves, environmental pollution, and global warming. Therefore, there is a genuine need to discover an alternative energy source to meet the global energy demand for the present and future. Based on various explored choices for alternative fuels, biodiesel is one of the attractive alternatives because of its various benefits like renewability, biodegradability, non-toxicity, high flash point, and eco-friendly nature when compared to conventional diesel. Biodiesel can be synthesized by transesterification of oil or fats with methanol in the presence of a suitable catalyst. This research work focuses on the development of sustainable ways to reduce issues related to conventional energy usage. The present work focused on the exploration of different kinds of feedstocks, such as rapeseed oil, linseed oil, lard oil, waste cooking oil, and algal oil for biodiesel production. Various kinds of nanocatalysts such as the potassium doped TiO_2 ($TiO_2-0.5C_4H_5KO_6$), lithium impregnated CaO ($CaO-0.5LiOH$), nano-magnetic potassium doped ceria ($Fe_3O_4-CeO_2-25K$), Sr-Al double oxides (Sr: 0.33Al) were used for transesterification of different oils. The detailed characterization of synthesized catalysts was investigated using different techniques, and results were summarized in this research work. The regeneration and reusability of the catalysts makes the biodiesel process cost-effective and more eco-friendly.

Moreover, the study also revealed the positive influence of co-solvent on biodiesel production by resolving problems related to the transesterification reaction. During the progress of this thesis work, sustainable bioenergy production using algal cultivation in aquaculture wastewater also provided promising results. The synthesized biodiesel was analyzed by various analytical techniques, and results were discussed in this thesis. The properties of obtained biodiesel were within ASTM /ENISO limits. The brief overview of this Ph.D. thesis involves the exploration of different potential feedstocks and nanocatalysts, identification of potential impacts of the co-solvent in transesterification reaction, and synergic approach of biodiesel production combined with wastewater treatment.

Keywords: Biodiesel production, transesterification, nanocatalysts, potassium doped TiO_2 , lithium doped CaO , potassium impregnated $\text{Fe}_3\text{O}_4\text{-CeO}_2$, Sr-Al double oxides, aquaculture wastewater, co-solvent extraction, microalgae, nutrient removal.

Acknowledgements

The framework of this research thesis is a compilation of five articles within the scope of sustainable biodiesel production from diverse feedstocks and exploring different ways to initiate developments towards cost-effective and eco-friendly ways of energy production. The nine-tenths of this thesis work was executed in the Department of Separation Science at Lappeenranta-Lahti University of Technology LUT, Finland. The thesis work could not have been accomplished without the support and fabulous research collaboration with the following individuals from the university and institute.

First, I would like to express my gratitude to my previous supervisor, Prof. Mika Sillanpää who gave me this opportunity to carry out my research work under his supervision and to be part of an outstanding research group. Your constant encouragement, support, fruitful and inspiring discussions, and guidance helped me to focus more on research and pursue my passion.

Second, I would like to express my heartfelt thanks to my current supervisor Professor Tuomo Sainio for the help and support during the sudden change in the organization.

I would also like to thank Dr. Varsha Srivastava. As my secondary supervisor, you made me very comfortable to work, always supported, and encouraged my research ideas and become my friend. I will be grateful for your guidance throughout my research work and in the final drafting of the manuscript.

Thanks to my thesis committee members for their comment in my thesis work. I would like to acknowledge Professor Adam Lee and Associate professor Yohannes Kiros for reviewing my thesis, and providing their valuable comments helps to improve the quality of the thesis. I am grateful to Professor Dmitry Murzin for acting as an opponent.

Great thanks to Dr. Anne Ojala and Dr. Elina Peltomaa from the University of Helsinki for providing me algal strains for research work, introducing me to the algological lab, shared their expertise in algal cultivation, providing me support and encouragement

during my algal studies. Thanks to both of them for revising my manuscript related to algal studies.

I would like to extend my appreciation to Laboratory engineer Mr. Esa Haapaniemi, the University of Jyväskylä, for helping with NMR analysis. Many thanks to Dr. Jouni Vielma and Mr. Jani Pulkkinen, from Natural Resources Institute Finland (Luke) for providing guidance with recirculation aquaculture systems (RAS) and for helping with aquaculture wastewater sample collection.

Thanks to all researchers in the Department of Separation Science, who have been wonderful colleagues. My warmest thanks to my friends Deepika, Sidra, Mahsa, Zhao, Mirka, Bhairavi, Evgenia, Fangping, Khum, Tam, Feiping, Olga, Nikolai, Sabina, Changbai, and Huabin for making the working environment very relaxed and inspiring. My special thanks to Ms. Sanna Tomperi for her support in administrative tasks.

Last but not least, many thanks to my parents who have been there for me, unconditionally with their love, care, and support that helps me to follow my dreams. I also want to extend my thanks to my husband's parents, brother, and his wife and my niece for their support and encouragement. My heartfelt thanks to my husband, Manu Bose Ambat, who has shown immense love, support, encouragement, trust, and motivation to go forward at harder times. My special thanks to my son Bose Imanuel Ambat precious gift of my life made me evolve personally and showed patience during my long writing nights and days.

Indu Ambat

29 October 2019

Mikkeli, Finland

Contents

Abstract

Acknowledgements

Contents

List of publications	9
Author's contribution in the publications	10
Other publications by same author in related field	11
Nomenclature	13
1 Introduction	15
1.1 Importance and demand for energy.....	15
1.2 Challenges in energy supply.....	16
1.3 Carbon dioxide emission and global warming	17
1.4 Transition towards sustainable and renewable energy sources	18
1.5 Towards biodiesel.....	20
1.6 Source of biodiesel	21
1.7 Different technologies for biodiesel production.....	25
1.7.1. Non- catalytic technology for biodiesel production	25
1.7.2. Catalytic technology for biodiesel production	25
1.8. Mechanism of acid and base catalysed transesterification reaction.....	27
1.8.1. Alkali-catalysed reaction	27
1.8.2. Acid-catalysed reaction	28
1.9 Application of nanocatalyst in biodiesel production.....	29
2 Objectives and goals	33
3 Materials and Methods	35
3.1 Feedstocks	35
3.2 Materials	35
3.3 Synthesis of nanocatalysts	36
3.4 Characterization of nanocatalysts.....	37
3.5 Sustainable microalgae cultivation, extraction of algal lipids and nutrient removal	38
3.6 Biodiesel production from different feedstocks and optimization of the reaction conditions	39
3.7 Characterization of synthesized biodiesel	40

3.8 Recovery and Reuse of catalysts	41
4 Results and discussion	43
4.1 Characterization of nanocatalysts.....	43
4.2 Algal biomass productivity, lipid content and nutrient removal	53
4.3 Characterization of biodiesel.....	55
4.4 NMR analysis of biodiesel	58
4.5 Effect of reaction parameters on FAME production (yield) or biodiesel production (yield).	62
4.6 Properties of the synthesized biodiesel	66
4.7 Regeneration and reusability of nanocatalysts	67
4.8 Comparison of main outcomes of biodiesel production with existing literature	
69	
5 Conclusion	71
6 Future research	75
References	77
Publications	

List of publications

- I. **I. Ambat**, V. Srivastava, E. Haapaniemi, M. Sillanpää, Application of Potassium Ion Impregnated Titanium Dioxide as Nanocatalyst for Transesterification of Linseed Oil, *Energy Fuels* 32 (2018) 11645–11655.
- II. **I. Ambat**, V. Srivastava, E. Haapaniemi, M. Sillanpää, Effect of lithium ions on the catalytic efficiency of calcium oxide as a nanocatalyst for the transesterification of lard oil. *Sustainable Energy Fuels* 3 (2019), 2464–2474.
- III. **I. Ambat**, V. Srivastava, E. Haapaniemi, M. Sillanpää, Nano-magnetic potassium impregnated ceria as catalyst for the biodiesel production. *Renewable Energy* 139 (2019), 1428–1436.
- IV. **I. Ambat**, V. Srivastava, S. Iftekhar, E. Haapaniemi, M. Sillanpää, Effect of different co-solvents on biodiesel production from various low-cost feedstocks using Sr-Al double oxides. *Renewable Energy* 146 (2020), 2158–2169.
- V. **I. Ambat**, S. Bec, E. Peltomaa, A. Ojala, V. Srivastava, M. Sillanpää, Phototropic technology for aquaculture wastewater treatment coupled with biodiesel production using the co-solvent method of lipid extraction. Submitted manuscript.

Author's contribution in the publications

- I. Indu Ambat is the principal author and investigator who planned, performed all experiments, analyzed all data, interpreted results and wrote the first draft of the manuscript. Esa Haapaniemi helped with NMR data collection.
- II. Indu Ambat is the primary researcher and principal author, who planned, performed all experiments, analyzed all data, interpreted results, and wrote the first draft of the manuscript. Esa Haapaniemi helped with NMR data collection.
- III. Indu Ambat is the principal author and investigator, who planned, performed all experiments, analyzed all data, interpreted results, and wrote the first draft of the manuscript. Esa Haapaniemi helped with NMR data collection.
- IV. Indu Ambat is the principal author and investigator, who planned, performed all experiments, analyzed all data, interpreted results, and wrote the first draft of the manuscript. Sidra Iftekhar and Esa Haapaniemi helped with catalyst preparation and NMR data collection, respectively.
- V. Indu Ambat is the primary researcher and principal author, who planned, performed experiments, collected all data except nutrient removal, analyzed all data, interpreted results, and wrote the first draft of the article. Sabina Bec collected data related to nutrient removal.

Other publications by same author in related field

- I. **I. Ambat**, V. Srivastava, M. Sillanpää, Recent advancement in biodiesel production methodologies using various feedstock : A review, *Renewable Sustainable Energy Reviews* 90 (2018) 356–369.
- II. **I. Ambat**, W. Tang, M. Sillanpää, Statistical analysis of sustainable production of algal biomass from wastewater treatment process, *Biomass and Bioenergy* 120 (2019) 471–478.
- III. **I. Ambat**, V. Srivastava, S. Iftekhar, E. Haapaniemi, M. Sillanpää, Dual application of divalent ion anchored catalyst: biodiesel synthesis and photocatalytic degradation of carbamazepine, *Catalysis in Green Chemistry and Engineering* 2 (2019) 25–42.
- IV. **I. Ambat**, V. Srivastava, E. Haapaniemi, M. Sillanpää, Novel Functionality of Lithium-Impregnated Titania as Nanocatalyst, *Catalysts*, 9 (2019) 943
- V. **I. Ambat**, S. Bec, E. Peltomaa, V. Srivastava, A. Ojala, M. Sillanpää, A synergic approach for nutrient recovery and biodiesel production by the cultivation of microalga species in the fertilizer plant wastewater. *Scientific Reports*, 9, (2019), 19073.

Nomenclature

List of symbols

<i>wt.</i>	weight percentage	%
<i>C</i>	percentage conversion of oil to FAME	%
P/P _o	Relative pressure	-
BE	Binding energy	eV
θ	(theta)	

Abbreviations

ITASA	Intercollegiate taiwanese american students association
WEC	World energy council
IEA	International energy agency
CAS	Chemical abstract service
EMIM DEP	1-Ethyl-3-methylimidazolium diethyl phosphate
THF	Tetrahydrofuran
WCO	Waste cooking oil
FFA	Free fatty acid
AqWW	Aquaculture wastewater
RAS	Recirculating aquaculture system
MWC	Modified WC medium
FAME	Fatty acid methyl esters
FTIR	Fourier transform infrared spectroscopy
XRD	X-ray power diffraction
SEM	Scanning electron microscopy
EDS	Energy dispersive X-ray spectroscopy
TEM	Transmission electron microscopy
BET	Brunauer-Emmett-Teller
AFM	Atomic force microscope
XPS	X-ray photoelectron spectroscopy

ASTM	American Society for Testing and Materials
GC-MS	Gas chromatography with mass spectrometry
NMR	Nuclear magnetic resonance
ICP-OES	Inductively coupled plasma optical emission spectroscopy
EN ISO	European International standard organization
IUPAC	International Union of Pure and Applied Chemistry
BE	Binding energy
CN	Cetane number
SV	Saponification value
IV	Iodine Value
DW	Dry weight
COD	Chemical oxygen demand
TN	Total nitrogen
TP	Total phosphorus

1 Introduction

1.1 Importance and demand for energy

Energy plays a crucial role in social-economic development of a country [1], [2]. The industrial growth and economic growth are interrelated to energy availability [3]. Moreover, the need for energy and energy services is inevitable to satisfy human economic and social development[4]. The rise in population increases the demand for energy and scarcity in energy leads to constraints in the development of the economy [3],[4]. The energy consumption and population growth projections of different continents are shown in Fig.1[5], [6].

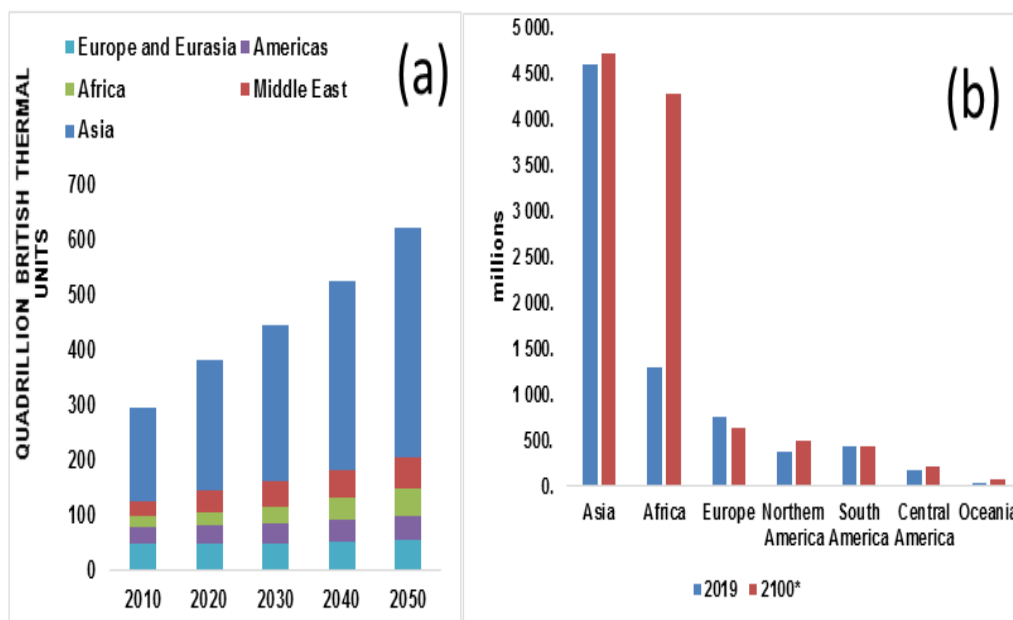


Fig.1. (a) The global energy consumption by different regions and (b) prediction of world population in 2019 and 2100 [5],[6].

Based on Fig1a, more than half of the energy consumption of the world is in Asia due to the increased population and robust economic growth in this region [5]. As per projection in Fig 1b, population proliferates in 2100 compared to 2019 resulting in increased demand for energy, and it would be challenging to fulfill the energy needs of the world. Besides, based on previously reported studies, the global population growth rises at the rate of 1.14% per year, whereas the demand for total energy in the world increases at the rate of 1.56 % per year [7]. The international outlook 2017 projects that global energy consumption increases by 28% by 2040 whereas, EIA estimate approximately 50% rise in world energy usage by 2050, mainly due to the high demand for energy in Asia [5], [8].

1.2 Challenges in energy supply

Nowadays, the world perceives the growing energy supply as depicted in Fig. 2. Energy is inevitable for industrialization, urbanization, and modernization and, thereby, overall development of the world [2], [9], [10]. Furthermore, Fig.2 also shows the dependency of the world on non-renewable energy sources. The need for energy is mainly for the growth and development of a country. The consumption of energy depends on the population, economic, and social development of a country. The exploitation of coal, crude oil, and natural gas is increasing to meet the rising energy supply; however, 50 % of coal resources were lowered from 1980 to 2005 [9]. The usage of non-renewable resources continue this way leading to depletion of natural gas and crude oil and cannot be replenished in our lifetimes or even many lifetimes [10]. Therefore, fossil fuels and other non-renewable resources are limited, and thus it is the primary global challenge [2], [11], [12].

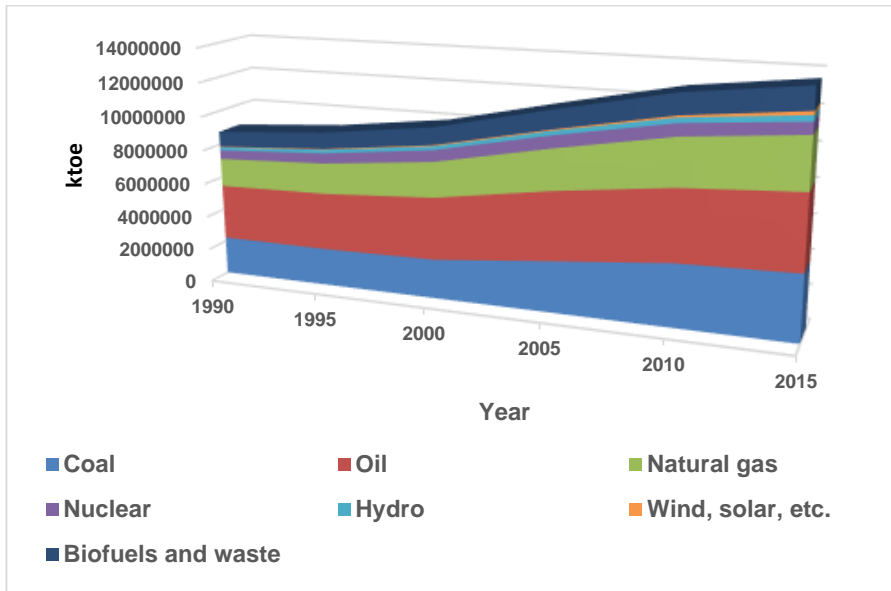


Fig.2. The total major energy supply over a period of 1990 -2015 by various sources [13].

1.3 Carbon dioxide emission and global warming

The increased consumption of conventional fuels such as fossil fuels should be petroleum or oil, coal, and natural gas results in environmental pollution and global warming [2], [12], [14]. After the industrial revolution, the demand of energy for social, economic, and industrial development was huge. Moreover, the large intake of non-renewable energy sources results in increased emission of CO₂ and other gases [15], [16]. Fig. 3 represents that CO₂ emission increases parallel to the energy demand of the respective countries. The exponential increase in the CO₂ emission, which could be one of the causes connected to global warming.

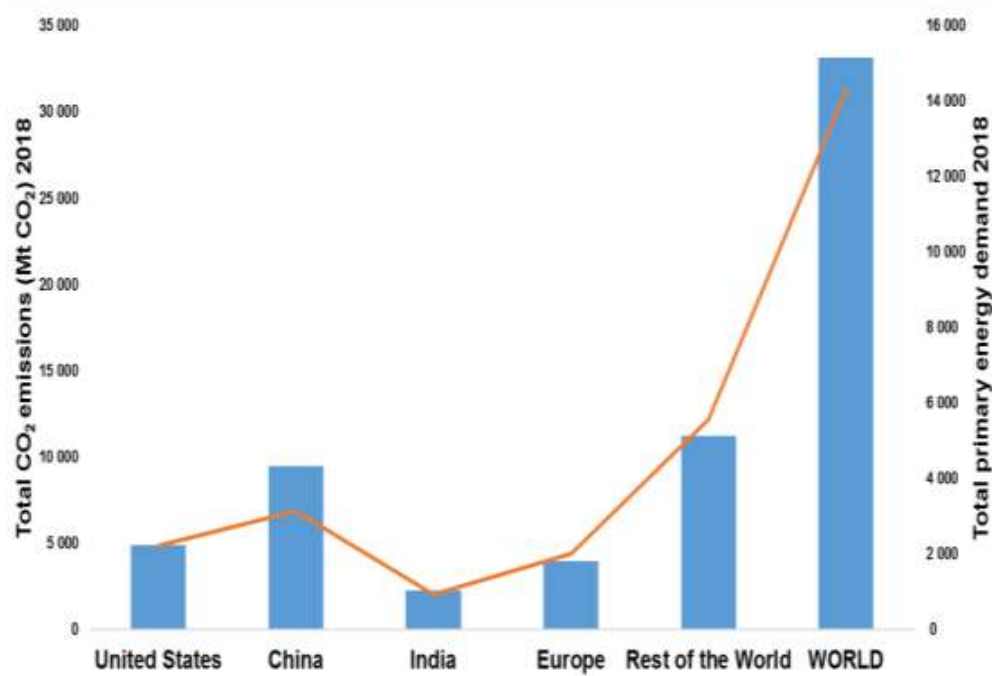


Fig.3. The total CO₂ emission and total primary energy demand of different countries [14].

1.4 Transition towards sustainable and renewable energy sources

The use of renewable energy resources could attain sustainable economic development. The excess utilization of fossil fuels leads to issues such as the depletion of energy reserves, global warming, and environmental pollution [5], [6], [12]. Moreover, the availability of fossil fuels mostly depends on the consumption rate [9], [11]. All these problems form an unsustainable condition. Sustainability can be accomplished by reducing analyzing risk factors and environmental impacts and reduce it to a certain extent [15], [16]. An alternative substitute is required to solve issues related to fossil fuels. Renewable energy supply can act as an alternative to fossil fuel because of its unlimited availability. Furthermore, an alternative for fossil fuel should possess certain factors such

as lower environmental pollution or global warming [4], [12]. With a broad range of potential renewable energy resources such as wind, hydrothermal, organic (includes bioethanol, biodiesel, and biogas), solar, or hydrogen energy, the idea and suggested benefits progressing from the use of biofuels are exciting [12], [17].

Bioenergy has the capacity to fulfill the needs of both developing and developed countries. Additionally, in the current scenario, 10-15 % of global energy use is supported by bioenergy [10], [15]. Recent studies also show the shift from non-renewable to renewable sources to meet energy demands for sustainable socio-economic development [5]. Fig. 4 illustrates the change in energy demand to meet up the world energy requirements. It also shows that consumption of non-renewable energy sources such as coal and oil reduced more than 50%, whereas natural gas remains the same, and usage of renewable sources doubled from 2015-2040. Fig.4 also represents the transition of the world towards the utilization renewable energy sources from conventional non-renewable resources.

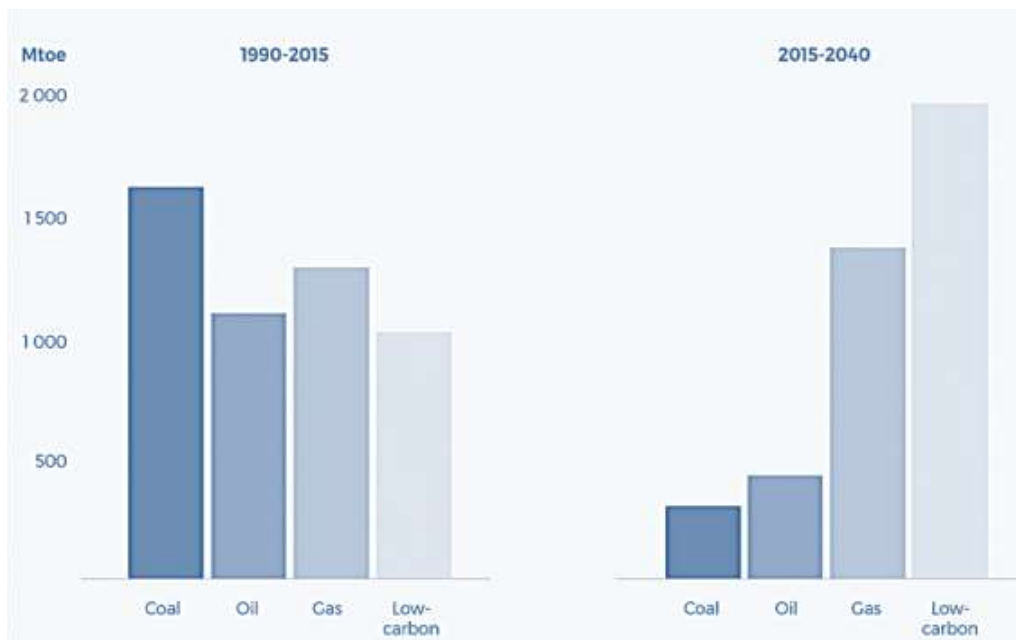


Fig.4. The change in primary energy demand to meet the global requirements [16].

1.5 Towards biodiesel

During the investigation of various biofuels, it was observed that in World's exhibition in Paris in 1898, German inventor Rudolf Diesel used peanut oil as fuel for the demonstration of his first diesel engine [12], [17]. Even though vegetable oil has great potential to act as an alternative fuel, the viscosity of oil was 10 to 17 times greater than petroleum diesel fuel[18]. Apart from that, another challenge includes low volatility and lower efficiency under cold conditions [12], [19]. To overcome these issues, more research have been focused on derivatives of oils/fats. The chemical transformation of the oil to its corresponding fatty acid ester known as biodiesel is known by a process called transesterification. Biodiesel, a derivative of oil, have shown physical properties close to that of diesel. Thus, biodiesel has received greatest attention [12], [18], [20], [21]. Fig. 5 shows the demand for petroleum-based products increasing from 2010 to 2017. The substitute for petrodiesel is technically possible by the production of biodiesel. Moreover, biodiesel offers better properties such as renewability, biodegradability, non-toxicity, high flash point, lower greenhouse gas (GHG) emissions, and eco-friendly nature by replacing petro diesel [12],[20-22]. The biodiesels made nowadays can be used without any alterations in the diesel engine [17]. Long-term use of biodiesel can reduce the emission of pollutants and carcinogens[12].

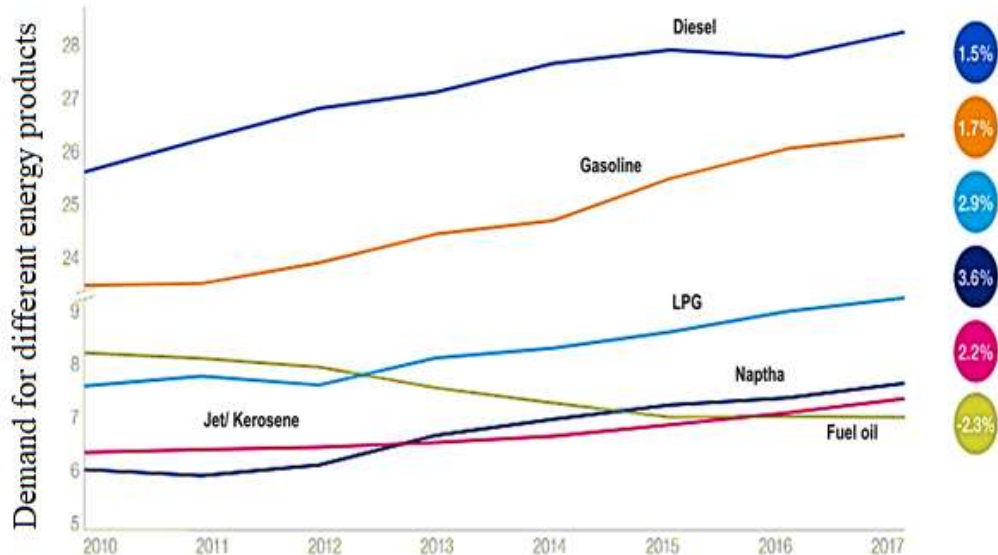


Fig.5. Demand for different energy products across the world [23].

1.6 Source of biodiesel

Presently more than 350 oil-bearing crops are identified, and out of those, some non-edible and edible crops are explored for biodiesel production [18]. The edible oils, non-edible oils, algal oils, animal fats, and waste cooking oil (WCO) serve as feedstock for biodiesel production [12],[24]. The feedstock for biodiesel production generally depends on the crops amenable to the local environment [12], [19]. The screening of raw materials for biodiesel production can be performed based on the kind of sources and availability [12], [25]. Soybean oil serves as a leading raw material for biodiesel production in the United States, whereas palm oil is commonly used as feedstock for biodiesel in Malaysia and Indonesia. In Europe, rapeseed is the primary fuel source, while in India and Southeast Asia, Jatropha serves as the primary source of biodiesel [12], [18], [19], [26].

Biodiesel is categorized into three main classes based on feedstock from which they are derived. The edible oil, such as rapeseed, soybean, peanut, sunflower, olive, coconut, mustard, and palm, serves as feedstock for first-generation biodiesel. The main drawback is that it has adverse effect on food market and price of biodiesel [12], [24-37]. The second-generation biodiesel can be produced from various non-edible oil as raw materials like stillingia, jatropha, karanja, neem, linseed, castor, and rubber seed [12], [38-46]. The main benefits of second-generation biodiesel do not compete with the food market, reduced biodiesel production cost, and smaller land area for cultivation [12], [47]. Algal oil derived biodiesel is known as third-generation biodiesel. Algae can be grown in any place where there is sunshine. The main merits of algal biodiesel are the increased growth rate and productivity, a significant amount of oil content, no adverse effects on the balance of food chain, reduced greenhouse effect. However, the main demerits are the requirement of sunlight, and large consumption of solvents for oil extraction [12],[48-52].

Besides, from these three categories of biodiesel, also other feedstocks are explored for biodiesel production. The WCO also serves as feedstock for biodiesel production and does not openly conflict with food imbalance [12], [53-55]. Animal fat also serves as raw material for biodiesel production and has environmental, economic, and food security benefits over edible oils [12],[56-58]. The sustainability of raw materials and the oil content of feedstock play a vital role in biodiesel production [12], [59]. Table 1 shows the different kinds of sources and oil content of various raw materials used for biodiesel production. The animal fat and waste cooking oil sources are entirely oils unless they are not contaminated with water. Besides, the oil content of algae and microbes depends on the type of organism.

Table 1. Summarizes the oil content of various feedstock for biodiesel production[12], [60-63].

Edible oils	Oil content (%)	Non edible oils	Oil content (%)	Animal Fat & other sources	Oil content (%)
Sunflower	25–35	Jatropha	30-40	Mutton Fat	
Soybean	15-20	Chinese tallow seed (stillingia)	44.15	Broiler chicken waste	
Rapeseed	38-46	Karanja(Pongamia pinnata)	27-39	Algae oil	
Peanut	45-55	Neem	20-30	Waste cooking oil	
Olive	45-70			Microbial oils	
Canola	30.6-48.3	Castor	45-50	Waste fish oil	
Palm	30-60	Sylbum marianum		Micro algae	30-70
Coconut	63-65	Rubber seed	53.7-68.4	Pine seed	31-68
Mustard	22.4 – 38.9			Kapok seed	27.5
Linseed	40-44				

The fatty acid distribution of different sources used for biodiesel production is depicted in Table 2. It provides information about the percentage distribution of saturated and unsaturated fatty acids [12]. The information of different feedstocks helps not to rely on a single source for biodiesel production and helps in the exploration of the feasibility of different feedstock to biodiesel in a more economical and environmentally friendly way.

Table 2. The fatty acid composition in various biodiesel feedstocks [12]

Composition of fatty acid (wt %) in various biodiesel sources										
	Tauric C _{12:0}	Myristic C _{14:0}	Palmitic C _{16:0}	Stearic C _{18:0}	Oleic C _{18:1}	Linoleic C _{18:2}	Linolenic C _{18:3}	Arahydroic C _{20:0}	Eicosenoic C _{20:1}	Eruic C _{22:1}
Edible										
Sunflower	5-8	2-6	15-40	30-70	3-5					
Rapeseed, high erucic	1-3	0-1	10-15	12-15	8-12	7-10				45-60
Soybean	6-10	2-5	20-30	50-60	5-11					
Peanut	8-9	2-3	50-65	20-30						
Olive	9-10	2-3	72-85	10-12	0-1					
Palm	0.5-2	39-48	3-6	36-44	9-12					
Mustard		1-2	8-23	10-24	8-18					
Coconut	45-53	16-21	7-10	2-4	5-10	1-2.5				
Almond Kernel	6.5		1.4	70.7	20	0.9				
Walnut kernel	7.2		1.9	18.5	56	16.2				
Sesame	13	4	53	30						
Non-edible										
Linseed [10]	4-7	2-4	25-40	35-40	25-60					
Neem [100]	13.6-16.2		49.1-61.9							
Jatropha [100]	14.1-15.3	0.13	34.3-45.8	14.1-15.3	0-0.3					
Cotton seed [100]		22.96-28.33	0.8-0.9	13.27-18.3	0.2					
Rubber [120]	2.2	10.2	8.7	24.6	39.6	16.3				
Karanja		3.7-7.9	2.4-8.6	44.5-71.3	10.8-18.3					
Pongamia	11.65			51.5	11.65					
Stillingia	0.4	0.1	7.5	2.3	16.7	31.5	41.5			
Animal fat & Other sources										
Chicken fat	3.1	19.82	3.06	37.62						
Waste cooking oil		8.5	3.1	21.2	55.2	5.9				
Tallow	23.3	19.3	42.4	2.9	0.9	2.9				
Brown grease	1.66	22.83	12.54	42.36	12.09	0.82				
Microalgal	12-15	10-20								
Yellow grease	2.43	23.24	12.96	44.32	6.97	0.67				

1.7 Different technologies for biodiesel production

1.7.1. Non-catalytic technology for biodiesel production

Generally, the most common method used for a non-catalytic process for biodiesel production is the supercritical methanol method. The faster reaction is attained in the supercritical method due to the high miscibility of methanol and oil at supercritical conditions. The main disadvantages are the requirement of high energy to achieve supercritical conditions and is susceptible to corrosion and salt deposition [12], [52-54].

Pyrolysis and micro-emulsion are other non-catalytic methods used for biodiesel production. The conversion of organic matter to fuel by application of heat in the absence of oxygen is referred to as pyrolysis. The colloidal balance dispersions of isotropic fluid are made from a single or various ionic amphiphiles and two non-miscible liquids in the micro-emulsion method for biodiesel production [12],[19] [21],[42],[55].

1.7.2. Catalytic technology for biodiesel production

Transesterification procedure is a catalytic technology used for the conversion of oils/fats to biodiesel with the help of alcohol (ethanol or methanol) in the presence of a catalyst [12],[59],[64]. The different types of catalysts involved in transesterification reactions are homogeneous catalyst, heterogeneous catalyst, and enzyme catalyst [12],[19], [21],[47]. Fig. 6 demonstrates the conversion of oil or fat to biodiesel via transesterification reaction. The chemical reaction involves that one mole of triglyceride reacts with three moles of alcohol in the presence of a catalyst that can be acid/ base/biocatalyst. The R', R'', R''' letters in triglyceride denote alkyl groups [12], [19], [47], [65].

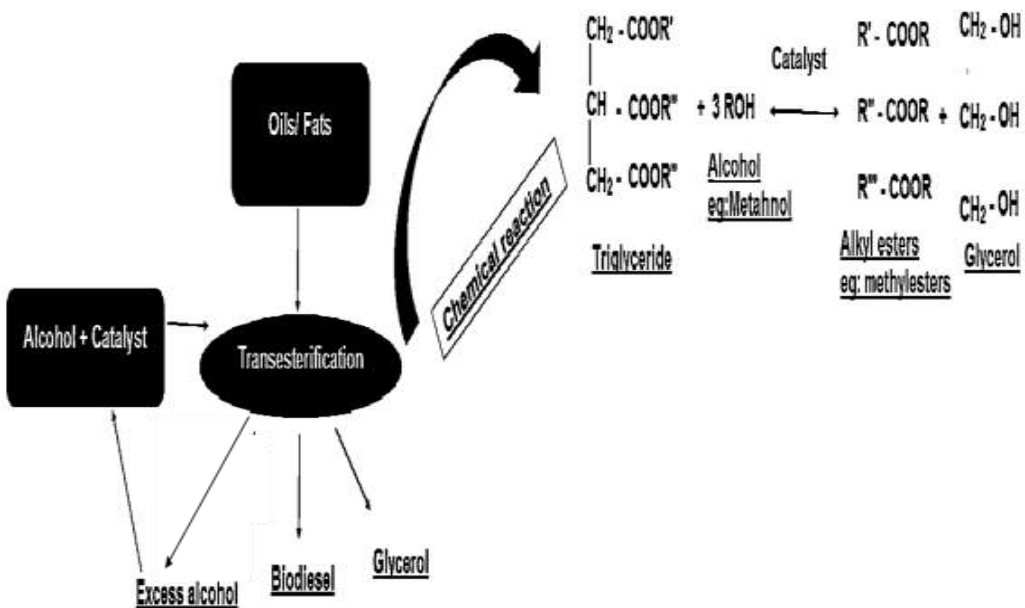


Fig.6. The biodiesel production via transesterification reaction[12].

Fig. 7 represents the different catalysts used in the conversion of oil or fat to biodiesel. Homogenous and heterogeneous catalyst are either acidic or basic in nature. Biodiesel production can be achieved in a shorter time and at lower temperature homogeneous catalysts (base or acid). The main disadvantage of homogenous catalysts is the practical difficulty in the separation of the catalyst after the reaction. Therefore, a large amount of water is consumed for cleaning, and thus separation of products results in a huge amount of wastewater. Heterogeneous catalysts are easy to recover after the transesterification reaction. Hence, it can solve the issues related to homogeneous catalysis and simultaneously reduce the material and processing cost. However, heterogeneous catalyst has some drawbacks like diffusion limitations and mass transfer issues [12], [19], [47], [62], [63]. The enzyme catalyst transesterification reaction was carried out by using lipase. The lipase is a common enzyme produced by microorganisms, plants, and animals. The main cons of enzyme-based transesterification techniques are restricted process temperature due to denaturing of enzymes at a higher temperature and high cost of enzymes [12], [21], [66], [67].

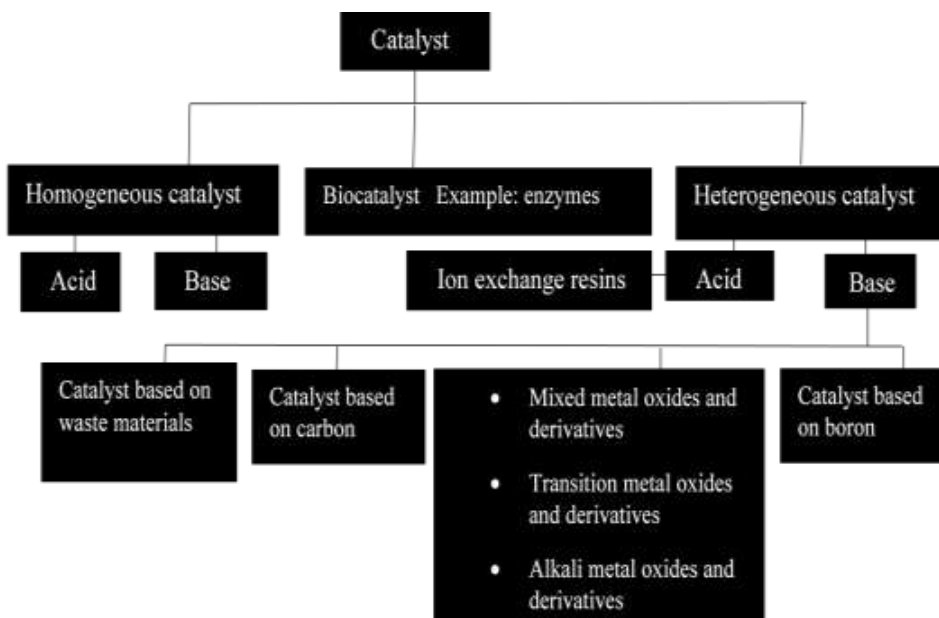


Fig. 7. Various catalyst used in biodiesel production process [12].

1.8. Mechanism of acid and base catalysed transesterification reaction

1.8.1. Alkali-catalysed reaction

The detailed transesterification reaction stages involving basic catalysts are given in Fig. 8. The mechanism of alkali-catalyzed reaction includes the formation of alkoxide and protonated catalysts because of the interaction of alkali and methanol. The tetrahedral intermediate is formed by the reaction of the carbonyl atom of the triglyceride molecule and nucleophilic alkoxide, with the reaction of the alcohol with the tetrahedral structure to revive the anion. Later, the tetrahedral structure endures structural reformation to form a diglyceride and fatty acid ester.

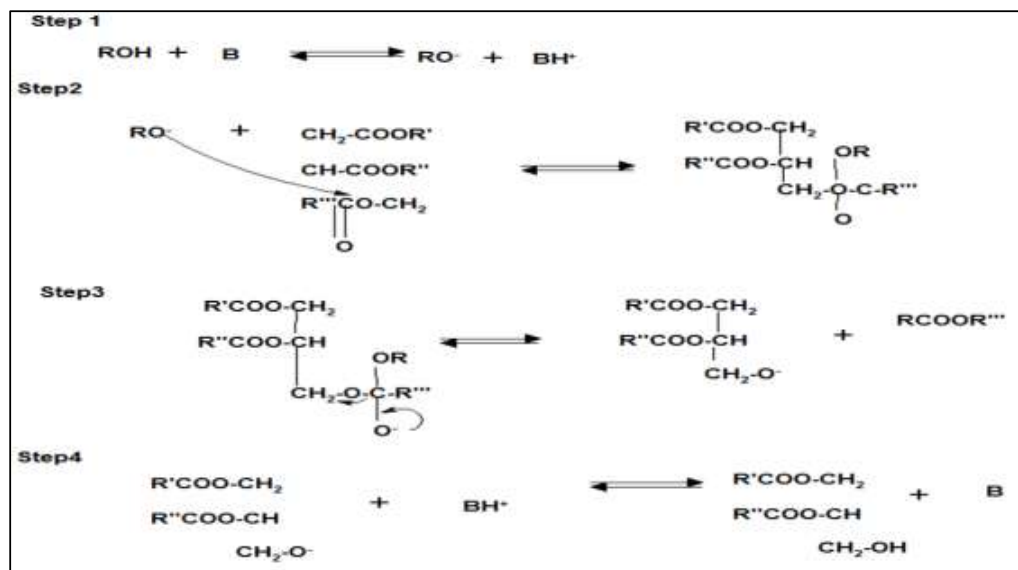


Fig. 8. Mechanism of transesterification reaction via alkali based catalyst [12].

1.8.2. Acid-catalysed reaction

Fig. 9 shows the transesterification reaction steps by the acid catalyst. The carbocation in acid-catalysed reaction is achieved by protonation of a carbonyl group. The protonated carbonyl group is exposed to a nucleophilic action of alcohol to produce tetrahedral intermediate. The removal of glycerol, catalyst recovery, and ester production are obtained due to intermediate formation [12], [19], [68].

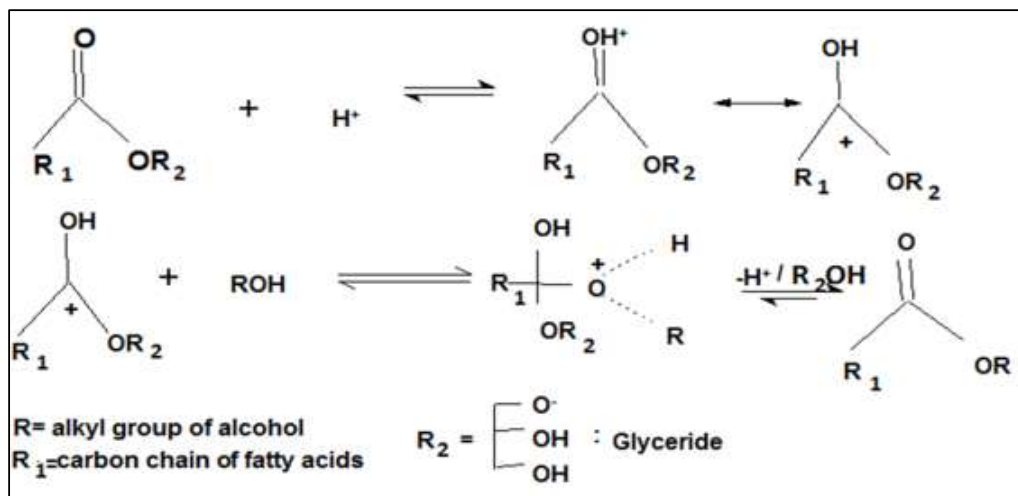


Fig. 9. Mechanism of transesterification reaction via acid based catalyst[12].

1.9 Application of nanocatalyst in biodiesel production

Presently, nanocatalysts show a vital part in the conversion of different sources such as edible/non-edible oil, fat /waste cooking oil, and algal oil to biodiesel. Nanocatalyst is highly recommended for the transesterification process because of its increased catalytic activity, economical, and environmentally friendly nature. Moreover, the nanomaterials perform a significant role in biodiesel production due to their improved surface area, reusability, and lower problems in mass transfer [12], [33], [44]. Table 3 describes different nanocatalyst used in biodiesel production process.

Table 3. Details of different nanocatalyst involved in biodiesel production from various sources [12], [69-73].

No	Feedstock	Catalyst	Size (nm)	Temp. (°C)	Alcohol to oil ratio	Reaction time (min)	Catalyst (wt %)	Biodiesel yield (%)
1.	Soybean oil [12]	ZrO ₂ /C ₄ H ₉ O ₆ HK	10-40	60	16:1	120	6	98.03
2.	Stillingia oil [12]	KF/Ca ₃ Fe ₅ O ₄	50	65	12:1	180	4	95
3	Palm oil [12]	ZnO	28.4	60	6:1	300		83.2
4	Palm oil [12]	TiO ₂ -ZnO	34.2	60	6:1	300		92.2
5	Chinese tallow seed oil [12]	KF/CaO	30-100	65	12:1	150	4	96
6	Soybean oil [12]	Nano MgO supported on KF/CaO-MgO	100-300	150-225	18:1	60	0.1-7	95
7	Rapeseed oil [12]	MgO	50-200	600		180		95
8	Rapeseed oil [12]	MgO	50-200	70-310	4:1	40-120		98
9	Sunflower oil [12]	Sr-Ti nanocomposite	50-100	70-310	4:1	40-120		98
10	Soybean oil [12]	C ₅ A ₁ Fe ₃ O ₄	30-35	58	14:1	120	4	94.8
11	Sunflower oil [12]	Li/MgO	17	65	12:1	40	5	
12	Button fat [12]	CaO-Al ₂ O ₃	29.9	100	5:1	180		82.3
13	Jatropha curcas oil [12]	ZnO ₂ /Al ₂ O ₃	20.59-29.86	81	12:1	120	1	90.47
14	Oleic acid [12]	Li-CaO	65	12:1	60	5	>99	
15	Karanja oil [12]	Li-CaO	65	12:1	120	5	>99	
16	Jatropha oil [12]	CaO	55	9:1			1.25	96.3
17	Algal oil [12]	CaO	66±3	5.15:1	13.3:1	0.2:1		98.54
18	Jatropha oil [12]	CaO-MgO	7:1	360				98.95
19	Recycled waste cooking oil	Sr ₃ Al ₂ O ₆		25:1	61	1.3		95.7±0.5
20	Soybean oil [12]	CaO-Au nanoparticle	65	9:1	150	3		
21	Sunflower oil [12]	(Ca(OCH ₃) ₂)	80	30:1	150	3		99
22	Algal lipids [12]	Cu-ZnO	55	10:1	60	10		97.18
23	Neem oil [12]	Cs-Ca/SiO ₂ -TiO ₂	45	60	12:1	120		98
24	Vegetable oil [12]	CZO	55	8:1	50	12		97.71
25	Waste cooking oil [12]	CsH ₂ PW ₁₂ O ₄₀ /FeSiO ₂	38-42	60	12:1	240	4	81
26	Sunflower oil [12]	Fe/ZnO	55	10:1	55	12		93
27	Pongamia oil [12]	lipase on	50	37	1:1	720		93
28	Soybean oil [12]	Cs-MgO	17.5±5.3	90	30:1	1,440	2.8	93
29	Olive oil [12]	Heteropoly acid coated	5-29	55±5		300	3	98
30	Madhuca indica oil [12]	CaO nanoparticles/NaX	60	6:1	360	10		93.5
31	Sunflower oil [12]	TiO ₂ /PrSO ₄ H	8.2-42	60	15:1	340	4.5	98.3
32	Used cooking oil [12]	MgO/MgAl ₂ O ₄	21.3	110	12:1	180	3	95.7
33	Sunflower oil [12]	Ti(SO ₄) ₂ O	25	75	9:1	180	1.5	97.1
34	Used cooking oil [12]	MgO-La ₂ O ₃	21.1	65	18:1	300		97.7
35	Sunflower oil [12]	SBC	100-150	60	7.5:1	120	1.2	96.13
36	Linseed oil [65]	BBC	100-120	60	5.5:1	120	0.8	94.41
37	Linseed oil [65]	Ni/ZnO	55	8:1	60	11		95.2
38	Castor oil [66]	Al ₂ O ₃ /Fe ₃ O ₄	193	99.8	32.1:1	177	5	99.1
39	WCO	S-ZrO ₂ /MCM-41	1-30	60	9:1	30	5	96.9
40	Sunflower oil [68]	KOH/Ca ₁₂ Al ₁₄ O ₃₃		15:1	30	4		98.8
41	Canola oil							

Usually, nanocatalyst is prepared by vacuum deposition, impregnation, precipitation, and sol-gel techniques. In vacuum deposition evaporation of the different materials such as molecules, alloys or compounds is attained by applying a thermal source. The heating of the substrate molecule is performed under vacuum and pressure. The optimum deposition rate was observed at pressure 1.3 Pa. [12], [74]. The production of nanocatalyst by chemical precipitation was achieved through the reaction of soluble components. During this method, the dopant introduction to the primary solution is done before precipitation, and the separation of particles formed is performed using surfactants [12],[34], [74]. The nanocatalyst production using a liquid phase technique is known as a sol-gel method. In this process, colloidal particle production mainly takes place through the hydrolysis reactions; the addition of suitable amount of substrate results in the precipitation of nanoparticles. The main qualities of the sol-gel method are that shaping and inserting can be accomplished easily, the higher temperature is not required for the reaction, and the process is flexible [12], [75], [76]. As in the impregnation method the aqueous solution comes into contact with the solid support, dried and calcined at an appropriate temperature. Different rates of adsorption of the active phases are observed during the impregnation processes [12], [77], [78]. Moreover, it is a simple, low cost and well-known process in which particle size controlling is difficult. The nanocatalysts properties can be altered by modifying the synthesis parameters such as concentration, calcination temperature, and reducing agent [12], [33].

2 Objectives and goals

The world is facing severe environmental and energy issues. Global warming and dependency of the world on limited energy resources are two significant global issues. In this research work, an effort towards sustainable development with minimization of problems related to both energy and environment was dealt with. The research work is focuses on the accomplishment of sustainability by exploring biodiesel as a renewable energy source. Throughout this work, investigation of various categories of feedstocks with different fatty acid compositions was used for biodiesel production. The exploration of suitable catalyst that can provide high yield and good quality biodiesel and is able to meet challenges faced by commonly used catalysts and by increasing the economic sustainability of the biodiesel production process.

To summarize, the aims and objectives of this research work are:

- ✓ To explore various kinds of sustainable feedstocks belonging to different source categories for biodiesel production.
- ✓ To synthesize various kinds of nanocatalysts, characterization of synthesized catalysts, and investigate the activity of catalysts for biodiesel production.
- ✓ To determine the economic viability and eco-friendly nature of catalyst by measuring reusability cycles and loss of activity of each catalyst after each cycle.
- ✓ To optimize the reaction conditions for better conversion of feedstock to biodiesel.
- ✓ To characterize the synthesized biodiesel and estimate the percentage conversion of feedstocks to biodiesel.
- ✓ To evaluate the properties of produced biodiesel based on ASTM standard methods/ EN 14214 methods.

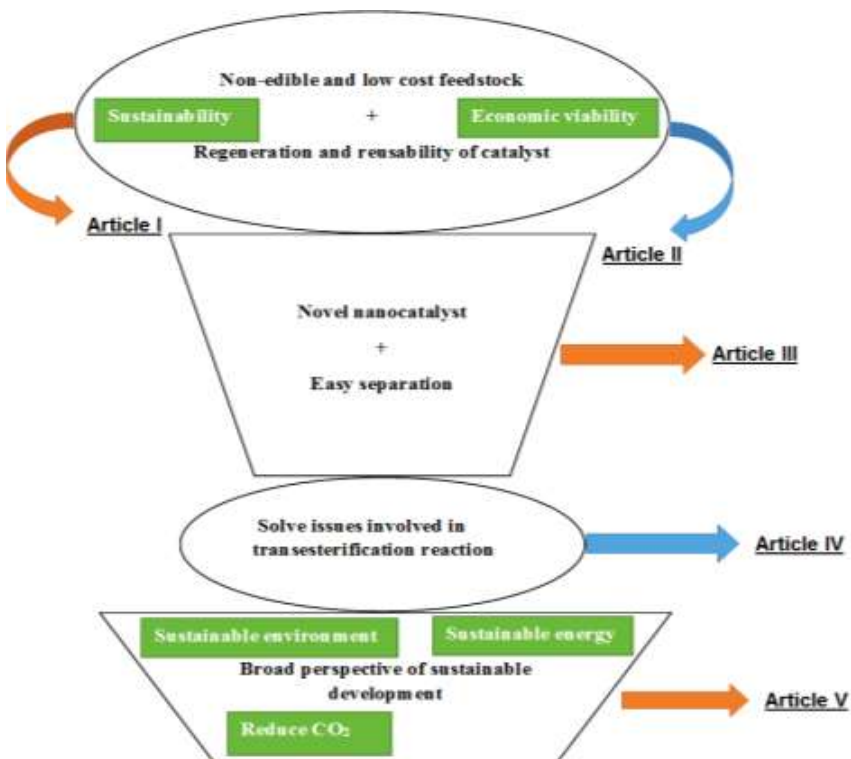


Fig. 10. Logic connection between objectives and papers.

Biodiesel serves as a potential source of renewable energy for sustainable development. Based on Fig. 10 the initial focus or Article I explores feedstock that do not compete with the food market which are available as low-cost feedstock and conversion to biodiesel using a catalyst that can offer higher activity and regeneration capacity. Article II focused on the preparation of novel nanocatalysts that offers easy separation after each biodiesel production process. To resolve issues related to transesterification reactions such as low reaction rate, weak phase separation, and soap formation are explored in Article IV. Article V discusses the integrated approach of algal biodiesel production and wastewater treatment. It offers a feasible solution for sustainable development via sustainable energy and environment.

3 Materials and Methods

3.1 Feedstocks

The present work includes the utilization of different kinds of feedstocks for biodiesel production. Linseed oil is non-edible oil, with oil content comparable to that of edible oils such as rapeseed oil and higher than that of soybean and sunflower oils. Linseed oil (acid value = 0.606 mg KOH/g), was explored as feedstock for biodiesel production (Article I). Lard oil (FFA % = 0.423) is a low-cost raw material that belongs to an animal fat category, and it was used as a source for biodiesel production (Article II). Rapeseed oil (FFA % = 0.442) is a significant source for biodiesel production in the whole of Europe. Hence, it was also employed as raw material for biodiesel production. (Article III). Waste cooking oil (FFA % = 0.634) is another economically sustainable feedstock and was utilized as feedstock for biodiesel production (Article IV). Algae lipids derived from algal species grown in aquaculture wastewater was explored as a source for biodiesel production (submitted manuscript, V).

3.2 Materials

The materials and chemicals used in this work are listed in Table 4. The chemicals were used as received form from the supplier without further purification. The aquaculture wastewater (AqWW) used in this research work was collected from a recirculating aquaculture system (RAS) operated at the Laukaa fish farm of the Natural Resources Institute Finland. The algal strain such viz. *Chlamydomonas* sp., *Scenedesmus ecornis*, and *Scenedesmus communis* used in the present work was provided by, University of Helsinki, Finland. The Modified WC Medium (MWC) was used to pre-culture and maintain all the algal species. Methanol, heptane, acetone, tetrahydrofuran (THF),

hexane, and chloroform were used for experimental analysis. All the solvents were purchased from Sigma-Aldrich and they were of analytical grade.

Table 4. Details of materials and chemicals used in the present work.

Materials/ Chemicals	Product description
Titanium dioxide (TiO_2) nano powder	CAS Number 13463-67-7, Sigma-Aldrich, particle size- 21 nm.
Potassium bitartrate ($\text{C}_4\text{H}_5\text{KO}_6$)	CAS Number 868-14-4, Sigma-Aldrich.
Calcium oxide (CaO) nanopowder	CAS Number 1305-78-8, Sigma-Aldrich, particle size lower than 160nm.
Magnesium oxide (MgO) nanopowder	CAS Number 1309-48-4, Sigma-Aldrich, particle size - \leq 50 nm
Zinc oxide (ZnO) nanopowder	CAS Number 1314-13-2, Sigma-Aldrich, particle size - <50 nm.
Lithium hydroxide (LiOH)	CAS Number 1310-65-2, Sigma-Aldrich.
Cerium (III) nitrate hexahydrate ($\text{Ce}(\text{NO}_3)_3 \cdot 6 \text{H}_2\text{O}$)	CAS Number 10294-41-4, Sigma-Aldrich.
Iron (II) chloride tetrahydrate ($\text{FeCl}_2 \cdot 4\text{H}_2\text{O}$)	CAS Number 13478-10-9, Sigma-Aldrich.
Iron (III) chloride hexahydrate ($\text{FeCl}_3 \cdot 6\text{H}_2\text{O}$)	CAS Number 10025-77-1, Sigma-Aldrich.
Potassium Hydroxide (KOH)	CAS Number 1310-58-3, Sigma-Aldrich.
Aluminium nitrate nonahydrate ($\text{Al}(\text{NO}_3)_3 \cdot 9 \text{H}_2\text{O}$)	CAS Number 7784-27-2, Sigma-Aldrich.
Citric acid monohydrate ($\text{HOOC}(\text{COOH})(\text{CH}_2\text{COOH})_2 \cdot \text{H}_2\text{O}$)	CAS Number 5949-29-1, Sigma-Aldrich.
Strontium nitrate ($\text{Sr}(\text{NO}_3)_2$)	CAS Number: 10042-76-9, VWR.
1-Ethyl-3-methylimidazolium diethyl phosphate ($\text{C}_{10}\text{H}_{21}\text{N}_2\text{O}_4\text{P}$, EMIM DEP)	CAS Number 848641-69-0, Sigma-Aldrich.
Ammonia solution	Sigma-Aldrich

3.3 Synthesis of nanocatalysts

The various types of nanocatalysts, TiO_2 modified by $\text{C}_4\text{H}_5\text{KO}_6$ ($\text{TiO}_2-0.5\text{C}_4\text{H}_5\text{KO}_6$), Lithium doped CaO ($\text{CaO}-0.5\text{LiOH}$), nanomagnetic potassium impregnated ceria ($\text{Fe}_3\text{O}_4-\text{CeO}_2-25\text{K}$) and Sr-Al double oxides (Sr-0.33Al) were prepared for biodiesel production.

Concisely, the TiO₂ doped by C₄H₅KO₆ was synthesized by an impregnation method (Article I). Lithium modified CaO was prepared by the incipient wetness impregnation method (Article II). The magnetic nanoparticles loaded with 25 wt. % ceria was prepared by the co-precipitation method. Later potassium doping was performed using the incipient wetness impregnation method (Article III). The Sr-Al metal oxides were synthesized by the sol-gel citrate method (Article IV). The detailed description of the preparation of different nanocatalysts was presented in Articles I-IV.

3.4 Characterization of nanocatalysts

The prepared nanocatalysts were examined by X-ray powder diffraction (XRD) with a Co-K α of 0.178 nm as an X-ray source at 40 mA and 40 kV over a 2 θ range of 10-120°. X-ray diffractometer (PANalytical – Empyrean, Netherlands) was used to record the XRD patterns of synthesized catalysts (Article I-IV). The functional groups of synthesized catalysts were analyzed using Fourier transform infrared spectroscopy equipped with platinum attenuated total reflection (FTIR-ATR). The IR spectra of catalysts were captured in the range of 400-4000 cm⁻¹ using Vertex 70 Bruker, Germany, shown in Articles I-IV. The surface structure and morphology of the catalysts were observed using scanning electron microscopy (SEM) with energy dispersive X-ray spectroscopy (EDS). SEM images of catalysts were obtained by dispersion a sample on colloidal graphite with 5 kV accelerating voltage (Hitachi SU3500, Japan) as depicted in Article I-IV. The elemental distribution in the prepared catalysts was studied with the help of EDS (Article III, IV). A further illustration of the surface structure of the synthesized catalysts was collected using an Atomic force microscope (AFM). AFM images of the nanocatalysts were obtained using a Park Systems NX10, South Korea (Article I). The size of the catalyst particles was confirmed using transmission electron microscopy (TEM). Hitachi HT7700, Japan, was used to obtain TEM images of the catalyst samples in Article I-IV. The surface area, pore volume, and pore size were determined by Brunauer-Emmett-Teller (BET) analysis. The N₂ adsorption-desorption

isotherm plots and parameters of the synthesized catalysts were analyzed using were analyzed using Micromeritics Tristar II plus, USA, in Article I-IV. The binding energies (BEs) and surface properties (BEs) of elements in catalysts were studied using X-ray photoelectron spectroscopy (XPS). Thermo Fisher Scientific ESCALAB 250Xi (UK) with monochromatic Al K α (1486.6 eV) was used for XPS analysis of catalysts (Article I, IV). The basic strength of the catalyst was determined with the help of the Hammett indicator analysis (Article I-III). The properties of the nanomagnetic catalyst were measured using the SQUID magnetometer (Cryogenic S700X-R, UK) in Article III.

3.5 Sustainable microalgae cultivation, extraction of algal lipids and nutrient removal

The freshwater microalgae viz. *Chlamydomonas* sp., *Scenedesmus ecornis*, and *Scenedesmus communis* were used for sustainable biodiesel production by cultivating them in two sets of wastewater (AqWW1 and AqWW2) collected from recirculating aquaculture system (RAS) operated at the Laukaa fish farm of the Natural Resources Institute Finland. The physical parameters such as temperature, light intensity, and carbon dioxide amount for all the algal species were optimized to obtain maximum biomass. The growth of each algal species was examined on alternate days by measuring optical density (OD) at 680 nm using a spectrophotometric method and was confirmed by dry weight measurements. The biomass productivity at the late lag phase was calculated using the gravimetric method represented in Equation 1. The co-solvent system consists of 1-ethyl-3-methyl imidazolium diethyl phosphate, [Emim] DEP, and methanol in 1.2:1 (v/v) ratio at 65 °C for a time period of 18 hours was used for extraction of lipids from different algal sources. The total content of lipid in each algal species was determined gravimetrically, and the lipid content of each alga was expressed as a percentage of dry weight. The lipid productivity of each algal species was calculated using Equation 2. The comprehensive explanation about algal cultivation and extraction of lipids from algal species for biodiesel production is elucidated in the submitted manuscript, V.

$$\text{Biomass productivity } (\text{mgL}^{-1}\text{d}^{-1}) = \frac{\text{Biomass yield } (\text{mgL}^{-1})}{\text{No. of days}} \quad (\text{Eq. 1})$$

$$\begin{aligned} \text{Lipid productivity } (\text{mgL}^{-1}\text{d}^{-1}) \\ = \text{Biomass productivity} \times \frac{\text{Lipid content}}{100} \quad (\text{Eq. 3}) \end{aligned}$$

The nutrient removal competence of different algal strains was determined by collecting samples on alternative days, and it was then centrifuged and filtered. The filtered samples were analyzed for COD, total nitrogen (TN), and total phosphorus (TP). The detailed report about the determination of nutrient removal efficiency by various algae in Aquaculture wastewater in Submitted article V.

3.6 Biodiesel production from different feedstocks and optimization of the reaction conditions

The production of fatty acid methyl ester (FAME) from various feedstocks was achieved by conducting a transesterification reaction in a three-neck round bottom flask with a mechanical stirrer and reflux condenser at a specific temperature for a specific time interval. During the transesterification reaction, the known amount of catalyst and the known ratio of methanol to oil were mixed with feedstock. After the transesterification process, the separation of FAME, excess methanol, and catalyst were obtained by centrifugation of the reaction mixture. The excess of methanol recovered by a rotary vacuum evaporator (IKA RV 10, Germany). The obtained biodiesel was subjected to the characterization procedure. The optimization of the reaction conditions such as oil to methanol ratio, temperature, reaction time, and catalyst amount was performed to obtain the maximum yield of biodiesel. The thorough explanation about biodiesel production from various feedstocks in Articles I-V and optimum conditions specific to each feedstock and catalyst were described in Articles I-IV.

3.7 Characterization of synthesized biodiesel

The characterization of biodiesel/ FAME was performed using gas chromatography with mass spectrometry (GC-MS, Agilent-GC6890N, MS 5975, US), ^1H , and ^{13}C nuclear magnetic resonance (NMR, Bruker Avance III, Germany). The GC-MS analysis was conducted with Agilent DB-wax FAME column (dimensions 30 m, 0.25 mm, 0.25 μm) at operation conditions such as inlet temperature was 250 °C and oven temperature was programmed at 50 °C for 1 minute and it raised at the rate of 25 °C/minute to 200 °C, and then at 3 °C /minute to 230 °C to be held for 23 minutes. For the NMR analysis, FAME was examined by ^1H NMR and ^{13}C NMR at 400 MHz with chloroform (CDCl_3) as the solvent. The percentage of conversion of feedstock to fatty acid methyl esters (C %) and the percentage of biodiesel yield are determined by equation (3) and equation (4), respectively. The biodiesel profile was validated using GC-MS chromatogram and National Institute of Standards and Technology (NIST, Agilent) 2014 MS library.

$$C(\%) = \frac{2 \times \text{Intergration value of protons of methyl ester}}{3 \times \text{Intergraton value of methyl protons}} \times 100 \quad (\text{Eq. 3})$$

$$\text{Biodiesel yield (\%)} = \frac{\text{mass of biodiesel}}{\text{mass of oil}} \times 100 \quad (\text{Eq. 4})$$

The properties and quality of produced biodiesel were determined using the American Society for Testing and Materials (ASTM D6751) method or European International standard organization (EN ISO 14214) method. The complete description of the characterization, chemical composition, and properties of the obtained biodiesel was shown in Articles 1-IV. The algal biodiesel properties such as cetane number (CN), saponification value (SV), and iodine value (IV) were estimated using the empirical formula given below.

$$\text{Cetane number (CN)} = 46.3 + \frac{5458}{SV} - 0.225 \times IV \quad (\text{Eq 5})$$

Where IV is iodine value ((g I 100g⁻¹) and SV is saponification value (mg KOH g⁻¹)

The saponification value and iodine value of algal FAME can be determined using the empirical formula given below.

$$IV = \Sigma \frac{254 \times F \times D}{MW} \quad (Eq \ 6)$$

$$SV = \Sigma \frac{560 \times F \times D}{MW} \quad (Eq \ 7)$$

Where, MW is the molecular weight, F is the percentage weight of each fatty acid, and D is the number of double bonds of the respective fatty acid (Submitted article V).

3.8 Recovery and Reuse of catalysts

The recovery and reusability of catalyst play a significant role in an economically viable and eco-friendly biodiesel production method. The details about the regeneration capacity of different nanocatalysts were defined in Articles I-IV. Briefly, the regeneration of catalyst was performed using organic solvents and calcination process. The reusability of the regenerated catalyst was investigated by performing various cycles of transesterification reaction. The stability of recycled catalyst was also analyzed.

4 Results and discussion

4.1 Characterization of nanocatalysts

FTIR analysis provides information about functional groups on the surface of nanocatalysts and helps to confirm the integration of doped ions to the catalyst surface. Fig. 11 represents different nanocatalysts used for the conversion of various raw materials to biodiesel. The FTIR spectra of $\text{TiO}_2\text{-}0.5\text{C}_4\text{H}_5\text{KO}_6$ (Article I) show peaks at 464 cm^{-1} , and 765 cm^{-1} that are from anatase titania and Ti-O-Ti stretching respectively[79]. The bands at 895.82 cm^{-1} , 1368.324 cm^{-1} , and 1458.00 cm^{-1} are due to the integration of potassium ions into the TiO_2 structure. The broadband in the range of 2900 cm^{-1} to 3300 cm^{-1} is from stretching vibrations of the Ti-O-K bond (Article I). The IR bands of $\text{CaO}\text{-}0.5\text{LiOH}$ observed in Fig.11b in the region of 1350 cm^{-1} , 3600 cm^{-1} and 1350 cm^{-1} are corresponding to bending and stretching of OH bonds, respectively. The peaks at 489.85 cm^{-1} , 713.57 cm^{-1} , and 1087.71 cm^{-1} are probably from Li-O stretching (Article II). Fig. 11c shows, FTIR spectrum of $\text{Fe}_3\text{O}_4\text{-CeO}_2\text{-}25\text{K}$ in which peaks at around 1009 cm^{-1} and 1370 cm^{-1} are from the vibration of CeO_2 . The IR bands identified in the range of 500 cm^{-1} to 700 cm^{-1} represent the Fe–O metal-oxygen bond that specifying the presence of Fe_3O_4 . The bands at around 833 cm^{-1} and 1390 cm^{-1} show the impregnation of potassium to the catalyst (Article III). The FTIR spectrum of Sr-0.33Al shown in Fig.11d indicates IR peaks in the region of 445 cm^{-1} to 602 cm^{-1} from the frequency vibrations of AlO_6 groups. The bands observed around 723 cm^{-1} to 872 cm^{-1} are due to the stretching and vibration of AlO_4 . The IR band at 1440.64 cm^{-1} shows the existence of Sr-O vibrations. The FTIR peaks at about $3,400\text{ cm}^{-1}$, $3,600\text{ cm}^{-1}$, and $1,640\text{ cm}^{-1}$ are from bending vibrations of OH groups and water molecule crystallization respectively (Article IV).

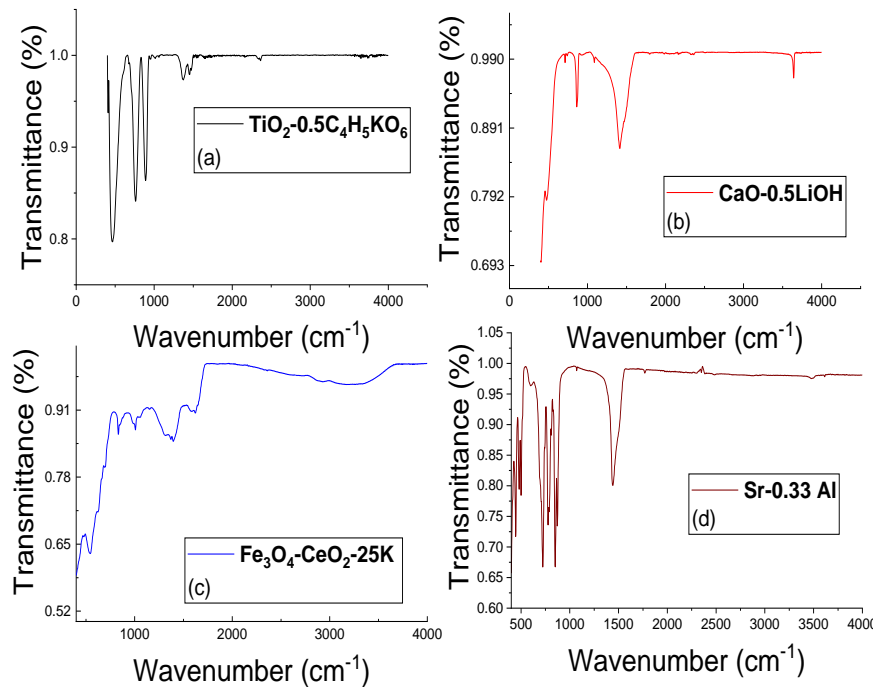


Fig. 11. FTIR spectra (a) TiO_2 - $0.5\text{C}_4\text{H}_5\text{KO}_6$ (Article I), (b) $\text{CaO}-0.5\text{LiOH}$ (Article II), (c) Fe_3O_4 - CeO_2 -25K (Article III), and (d) $\text{Sr}:0.33\text{Al}$ (Article IV) nanocatalysts used in the biodiesel production.

Fig. 12 illustrates the XRD spectra of different catalysts used for the biodiesel production process. The diffractogram of Potassium Titanium Oxide (tetragonal structure) achieved by modification of TiO_2 with 0.5 molar $\text{C}_4\text{H}_5\text{KO}_6$ offers an excellent match to the reference standard code ICSD: 73465, ICDD: 98-007-3465 (Article I). The XRD spectra of lithium-ion impregnated CaO ($\text{CaO}-0.5\text{LiOH}$) provides a consistent harmony to the reference standard code ICDD: 98-041-3207 (Article II). The XRD pattern of Fe_3O_4 - CeO_2 -25K peaks at 35.36° , 41.51° , 50.8° , 63.6° , 67.7° , 74.7° indicates the presence of Fe_3O_4 - CeO_2 and peak at 38.72° that is from the impregnation of potassium ions to Fe_3O_4 - CeO_2 nanocatalyst shown in Fig. 12c (Article III). Fig. 12d represents the XRD spectra

of sr-0.33Al in which diffraction patterns at 37.1° , 45.8° , 56° , 57.1° , 58.6° , 67.1° are consigned to the typical peaks of $\text{Sr}_3\text{Al}_2\text{O}_6$ and show as a match to JCPDS file No. 24-1187. The low intense peaks around 18° , 24.3° , 29.9° , 34.9° , 40.5° , 49.9° , 53.6° , 60.5° , 70.24° show the slight presence of SrCO_3 (Article IV). Out of all these four catalysts, more sharp peaks were observed for Sr: 0.33 Al and CaO-0.5LiOH due to the better crystalline nature of the catalyst.

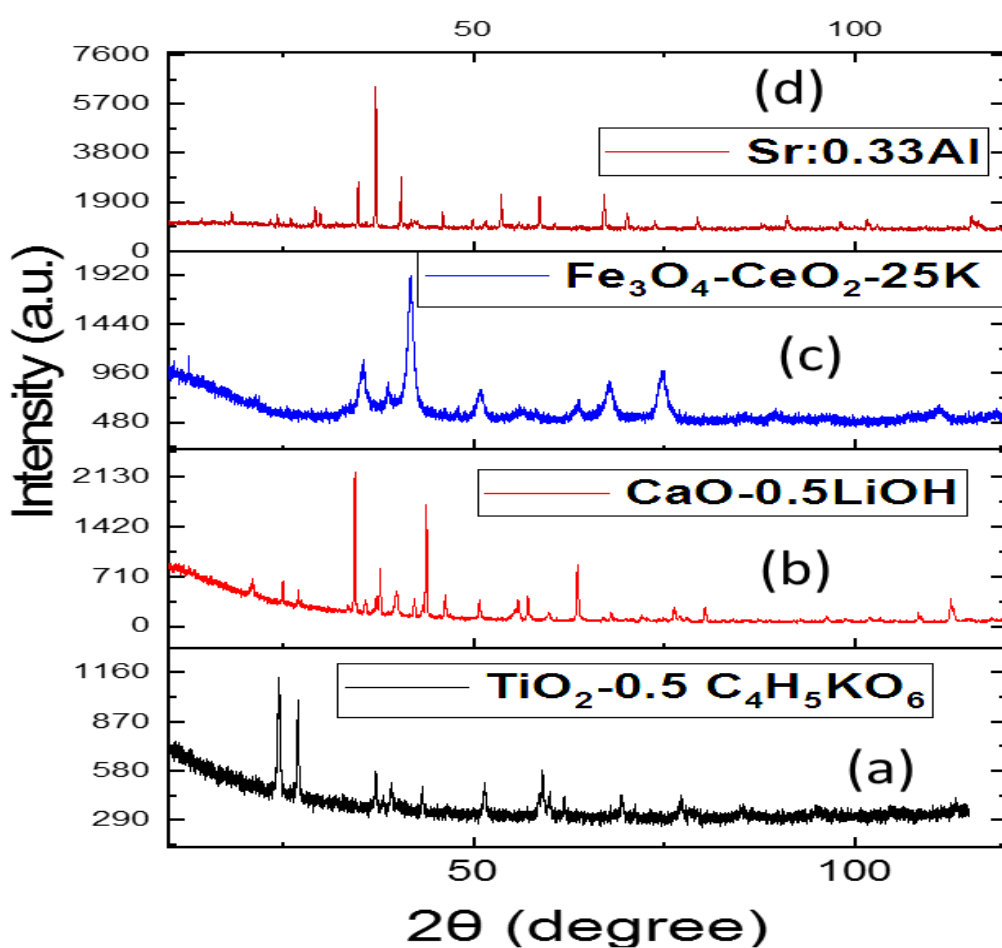


Fig.12. XRD patterns of (a) TiO_2 - $0.5\text{C}_4\text{H}_5\text{KO}_6$ (Article I), (b) CaO - 0.5LiOH (Article II), (c) Fe_3O_4 - CeO_2 - 25K (Article III), and (d) Sr:0.33Al (Article IV) nanocatalysts used in the biodiesel production.

SEM image of TiO_2 - 0.5C₄H₅KO₆ depicted in Fig.13a specifies a flat surface of various shapes was dispersed on the catalytic material that altering the morphology of TiO_2 , which also confirmed the modification and integration of potassium in the structure of TiO_2 (Article I). Fig.13 b represents the lithium doped CaO (CaO-O.5LiOH) in which irregular flat surface indicates the impregnation of lithium ions to CaO nanomaterial. The addition of lithium results in agglomeration of the particles and a decline in the porosity of catalyst (Article II).The SEM image of Fe_3O_4 -CeO₂-25K depicts a coating of potassium on the catalyst as illustrated in Fig.13 c (Article III). SEM image of Sr-0.33Al represents a similar morphology of particles all over the image with minor agglomeration (Article IV).

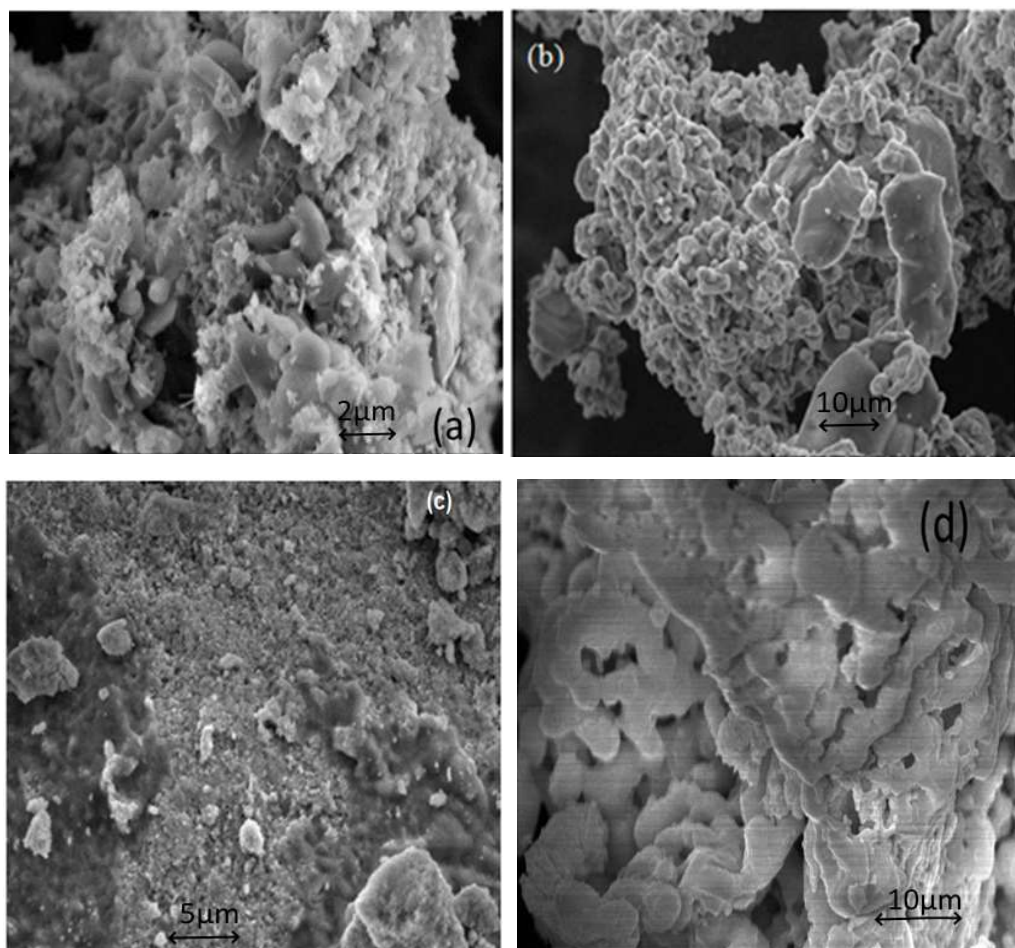


Fig.13. SEM images of (a) TiO₂- 0.5C₄H₅KO₆ (Article I), (b) CaO-0.5LiOH (Article II), (c) Fe₃O₄-CeO₂-25K (Article III), and (d) Sr: 0.33Al (Article IV) nanocatalysts used in biodiesel production.

The TEM studies of TiO₂-C₄H₅KO₆ represented in Fig. 14a confirms the particle size of the catalyst as 26-179 nm. The TEM image of TiO₂-0.5C₄H₅KO₆ demonstrates a long flat surface structure besides the evenly distributed particles with aggregates (Article I). TEM results of the CaO-0.5LiOH catalyst confirm that the particle size of catalyst is in the range of 54.5- 127 nm and is shown in Fig.14b. The agglomeration of the particles due to lithium impregnation was observed in the TEM image (Article II). The TEM Fe₃O₄-CeO₂-25K depicted in Fig. 14c indicates a flat cover of potassium as a coating on the nanomaterial (Article III). Fig.14d illustrates the TEM image of Sr: 0.33Al catalyst which indicates the distribution of similarly shaped particles throughout the image. TEM analysis confirms the particle size of Sr: 0.33Al catalyst as 57-100 nm (Article IV).

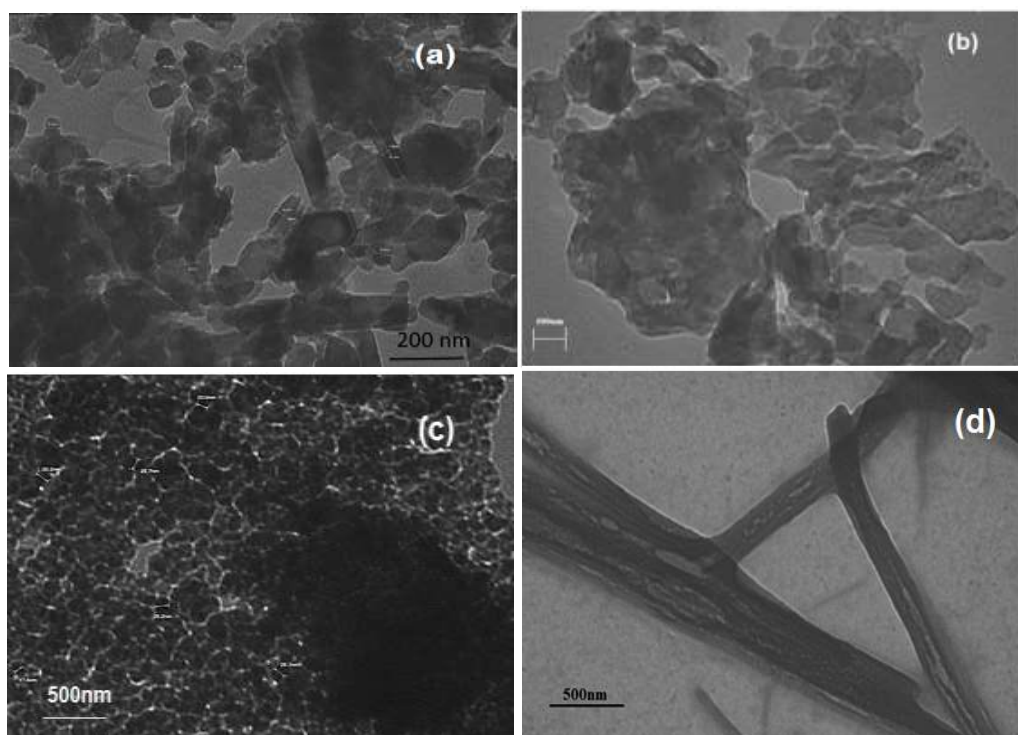


Fig.14. TEM images of (a) TiO₂- 0.5C₄H₅KO₆ (Article I), (b) CaO-0.5LiOH (Article II), (c) Fe₃O₄-CeO₂-25K (Article III), and (d) Sr: 0.33Al (Article IV) nanocatalysts used in the biodiesel production.

Table 5 shows the surface area, pore size, and pore volume of the different catalysts used for biodiesel production (Article I-IV). The addition of alkali metals to nanocatalytic material leads to the increase of catalyst sintering and causes a reduction in surface area and a rise in the basicity of catalysts. The alkaline earth metals also boost the basicity of catalyst[80]. The surface areas are highest for Fe₃O₄-CeO₂-25K (Article III) and the lowest for Sr: 0.33Al (Article IV). Fig. 15 shows N₂ adsorption and desorption isotherms of the various catalysts used for biodiesel production. Based on the International Union of Pure and Applied Chemistry (IUPAC) classification, the isotherms of TiO₂-0.5C₄H₅KO₆, CaO-0.5LiOH, and Sr: 0.33Al exhibit type III, H₃ hysteresis loop (Article I, II and IV). The nature Fe₃O₄-CeO₂-25K (Article III) isotherm display type IV, H₂ hysteresis [81], [82].

Table 5. The results of BET analysis of various catalyst used for biodiesel production.

Parameters	TiO ₂ - 0.5C ₄ H ₅ KO ₆	CaO- 0.5LiOH	Fe ₃ O ₄ -CeO ₂ - 25K	Sr- 0.33Al
BET surface area (m ² /g)	16.25	2.41	72.84	0.95
Single point adsorption total pore volume of pores (cm ³ /g)	0.03	0.006	0.18	0.002
Adsorption average pore	7.24	10.32	9.99	8.5

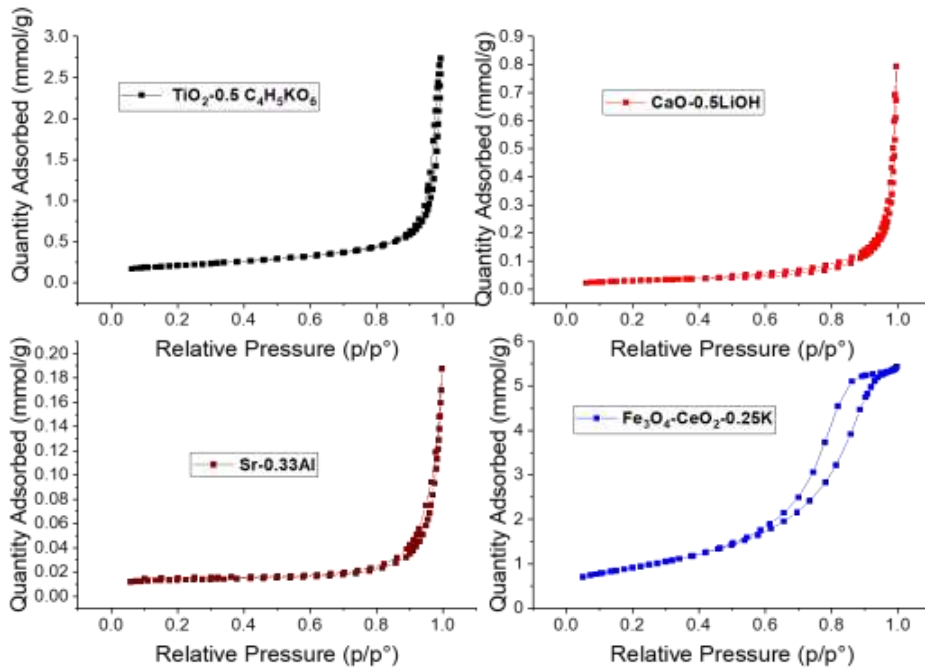


Fig.15. N₂ adsorption-desorption of different nanocatalyst used in biodiesel production.

Fig. 16 a represents XPS fitted spectra of TiO₂-C₄H₅KO₆, and Gaussian curve-fitting was used for the simulation of the chemical environment of Ti, O, K. The Ti 2p signals of TiO₂-C₄H₅KO₆ is with two peaks assigned to Ti 2p_{1/2} and 2p_{3/2} at binding energies of 463.66 and 457.96 eV, respectively. Based on the BE gap between these two-core level orbitals, the chemical valance state of Ti is +4 in the synthesized nanocatalyst. The O 1s spectra of TiO₂-0.5C₄H₅KO₆ displays BE at 530.1 eV that assigns to O²⁺, forming an oxide with the metals. The K 2p with binding energies at 292.37 eV and 294.97 eV corresponds to 2p_{3/2} and 2p_{1/2} in the K-O group of TiO₂-0.5C₄H₅KO₆ (Article I). The chemical environment of Sr, Al, O, and C were simulated by Gaussian curve-fitting of the Sr 3d, Al 2p, O 1s, and C 1s spectra fitted the Sr: 0.33Al as shown in Fig. 16b. The binding energies of 133.1 and 134.9 eV observed in Sr: 0.33Al consigned to Sr 3d_{5/2} and

$3d_{3/2}$, correspondingly. The binding energy at 73 eV in Al 2p spectra of Sr: 0.33Al corresponds to pure Al. The spectra of Sr: 0.33Al represents the existence of weakly adsorbed oxygen while stronger binding of adsorbed oxygen with aluminium atoms were defined by a signal at 531 eV. The C 1s core-level spectrum of Sr: 0.33Al shows binding energies at 284.6 eV and 289 eV assigned to C–C, C=O, respectively (Article IV).

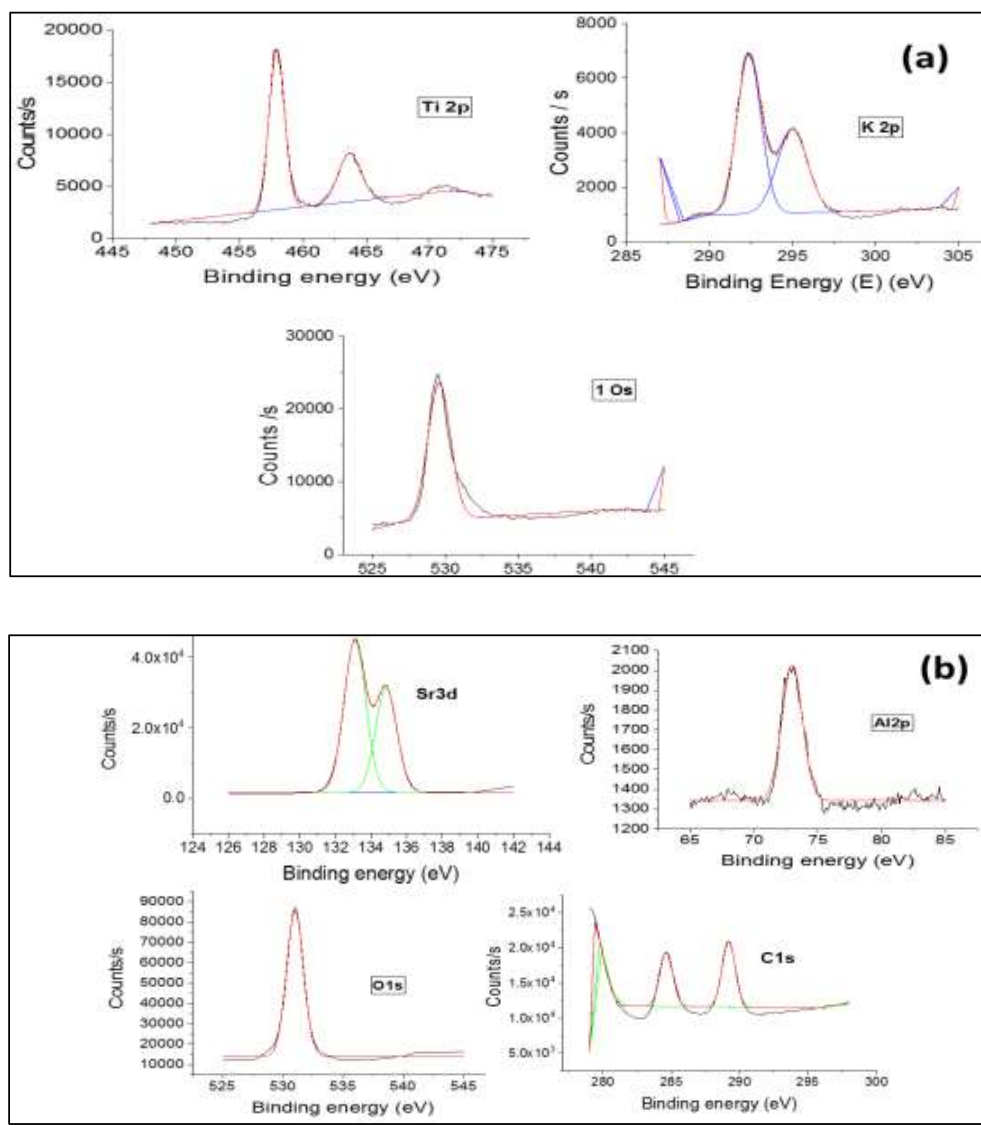


Fig.16. XPS spectra of (a) TiO₂-C₄H₅KO₆ (Article I) and (b) Sr: 0.33Al (Article IV) nanocatalyst used for transesterification reaction.

The basic strength of different catalysts used for biodiesel production is represented in Table 6. CaO-0.5 LiOH showed the maximum total basicity. The doping of alkali metals to the nanocatalytic material increases the basic strength of the catalyst, and the basicity of catalyst depends on the optimum loading amount of the alkali metal (Article I-III). The alkaline earth metals containing catalyst also shows high basic strength [80].

Table 6. The basicity test results of various catalyst used for biodiesel production.

Catalyst	Catalyst basic strength	Total basicity (mmol g ⁻¹)
TiO ₂ -0.5C ₄ H ₅ KO ₆	9.8<H<15	1.80
CaO-0.5 LiOH	15<H<18.4	1.85
Fe ₃ O ₄ -CeO ₂ -25K	9.8<H<15	1.18
Sr:0.33Al	9.8<H<15	1.63

The EDS of Fe₃O₄-CeO₂-25K and Sr: 0.33Al is illustrated in Fig. 17. The elemental distribution of Fe₃O₄-CeO₂-25K confirms the composition of catalyst as Fe (34.9 wt %), K (16.4 wt %), Ce (13.5 wt %), and O (28.8 wt %) shown in Fig. 17a (Article III). The EDS spectra of Sr: 0.33Al in Fig. 17b (Article IV) shows the elemental composition of the catalyst as Sr (59.80 wt %), Al (3.04 wt %), and O (15.69 wt %).

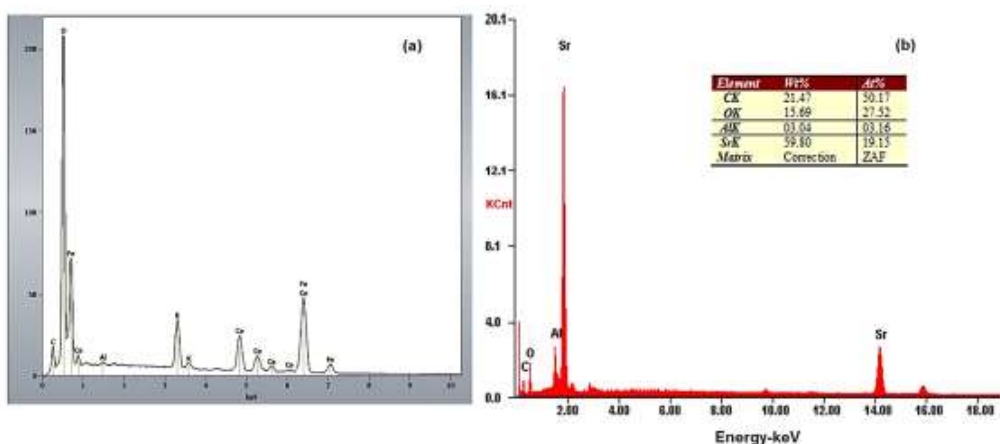


Fig.17. EDS of (a) Fe₃O₄-CeO₂-25K (Article III) and (b) EDS of Sr: 0.33Al (Article IV).

Further characterization of TiO₂ and TiO₂-0.5C₄H₅KO₆ with AFM (Fig. 18) is in good agreement with those of TEM and SEM results. AFM results confirm the integration of potassium ions into titanium dioxide nanocatalyst, and the particle size matches with TEM studies (Article I).

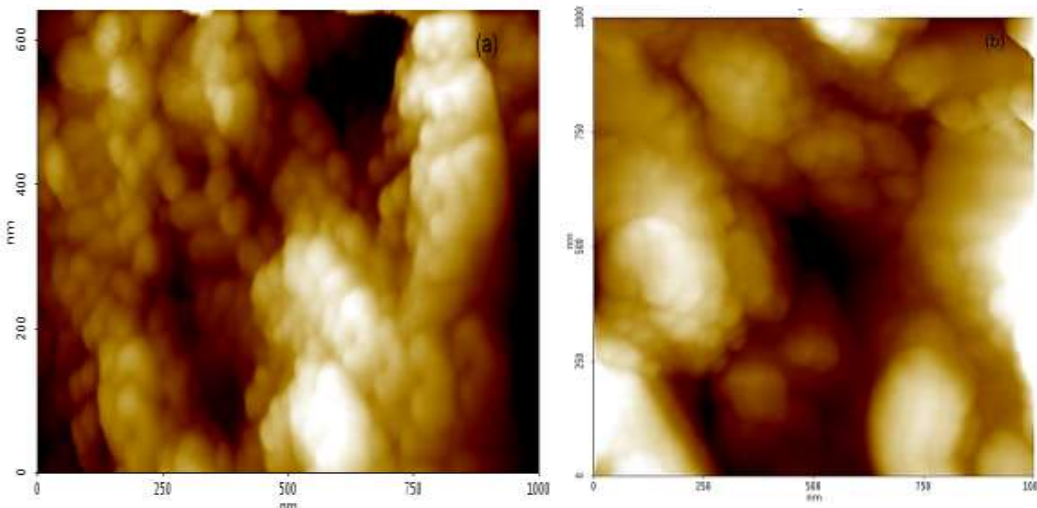
**Fig.18.** AFM image of (a) TiO₂ and (b) TiO₂-0.5C₄H₅KO₆ (Article I).

Fig. 19 demonstrates the magnetization versus magnetic field dependencies of Fe₃O₄-CeO₂-25K at 300 K, and shows remanent magnetization for the nanomagnetic catalyst sample is 0.75 emu/g. The separation of the catalyst from the reaction mixture are also shown in Fig.19 (Article III).

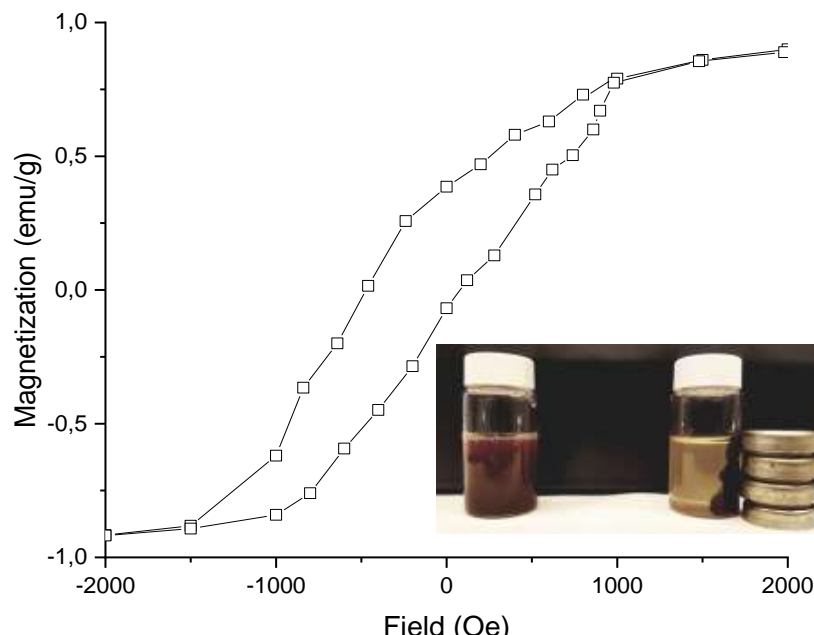


Fig. 19. The magnetization versus magnetic field of $\text{Fe}_3\text{O}_4\text{-CeO}_2\text{-25K}$ (Article III).

4.2 Algal biomass productivity, lipid content and nutrient removal

The biomass productivity, lipid content, and lipid productivity of *Chlamydomonas* sp., *S. ecornis*, and *S. communis* in aquaculture wastewater samples (AqWW1 and AqWW2) are represented in Fig. 20a. The cultivation of algal strains was carried out at optimum biomass production conditions at 20 °C with a continuous light intensity of 230 $\mu\text{mol m}^{-2}\text{s}^{-1}$ without CO₂ supply for *Chlamydomonas* sp. and 20% (v/v) amount of CO₂ for *S. ecornis*, and *S. communis*, respectively. The biomass productivity of *Chlamydomonas* sp. was higher in AqWW1 and *S. ecornis*, and *S. communis* in AqWW2. The biomass productivity of *Chlamydomonas* sp. was 251 mg L⁻¹d⁻¹ and 246 mg L⁻¹d⁻¹ in AqWW1 and AqWW2, respectively. The *S. ecornis* and *S. communis* shows biomass productivity of 129 mg L⁻¹d⁻¹ and 143 mg L⁻¹d⁻¹ in AqWW1, whereas 159 mg L⁻¹d⁻¹ and 181 mg L⁻¹d⁻¹ in

AqWW2, correspondingly. The maximum lipid content was observed in *Chlamydomonas* sp. (38.5%), followed by *S. communis* (31.1 %) and *S. ecornis* (29 %) in AqWW1 (Article V).

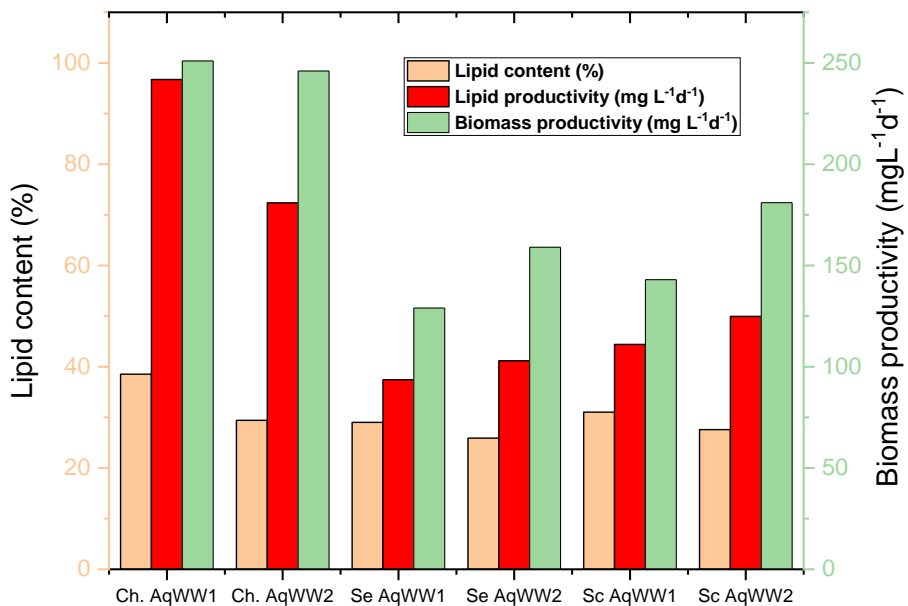


Fig. 20a. The biomass productivity, lipid content and lipid productivity of *Chlamydomonas* sp. (represented as Ch), *S. ecornis* (represented as Se), and *S. communis* (represented as Sc) in aquaculture wastewater samples (AqWW1 and AqWW2).

The nutrient removal ability by *Chlamydomonas* sp., *S. ecornis*, and *S. communis* in the aquaculture wastewater samples (AqWW1 and AqWW2) are summarized in Fig. 20b. The *Chlamydomonas* sp., *S. communis*, and *S. ecornis* exhibited 95.5 %, 89.1 %, and 85.4 % of COD removal in AqWW1 respectively whereas 92.9 %, 91.9 %, and 87.0 % in AqWW2 respectively. The *Chlamydomonas* sp. showed maximum percentage removal of TN and TP in AqWW1 while *S. communis*, and *S. ecornis* exhibited significant removal of TN and TP in AqWW2, correspondingly (submitted Article V).

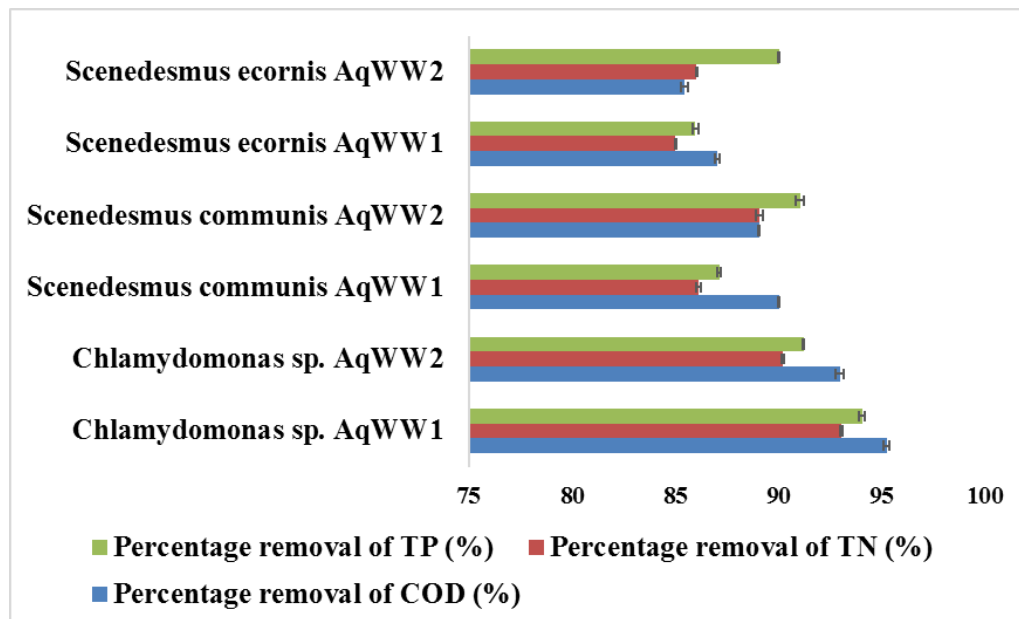


Fig. 20b. The nutrient removal efficiency of different algal strains in aquaculture wastewater (AqWW1 and AqWW2).

4.3 Characterization of biodiesel

The FAME (biodiesel) obtained was validated using results from GC-MS chromatogram and National Institute of Standards and Technology (NIST) 2014 MS library. The FAME results after the transesterification of various feedstocks using different catalysts are summarized in Table 7 (Article I-IV) and Table 8 (Submitted, Article V).

Table 7. The composition of biodiesel obtained after transesterification of various feedstocks with different nanocatalysts.

Linseed oil - TiO₂- 0.5 C₄H₅KO₆

Peak	FAME		Compound name
	Retention time (min)	Library match (%)	
1	8.38	91.2	Hexadecanoic acid, methyl ester
2	9.89	93.6	Methyl stearate
3	10.09	94	9-Octadecenoic acid, methyl ester
6	10.48	94.3	9, 12- Octadecenoic acid (Z,Z)-, methyl
7	11.19	92.9	9,12,15 Octadecatrienoic acid, methyl

Lard oil- CaO-0.5LiOH

Peaks	FAME		Compound name
	Retention time (min)	Library match (%)	
1	7.26	91.7	Tridecanoic acid, 12 methyl-methyl
2	8.35	91.5	Hexadecenoic acid , methyl ester
3	8.52	94.35	9-Hexadecenoic acid , methyl ester
4	9.87	93.51	Methyl stearate
5	10.08	96.01	13-Octadecenoic acid, methyl ester
6	10.52	96.53	11, 14 - Octadecadienoic acid, methyl
7	11.21	89.09	9,12,15- Octadecatrienoic acid, methyl

Rapeseed oil- Fe₃O₄-CeO₂-25K

Peaks	FAME		Compound name
	Retention time (min)	Library match (%)	
1	8.35	91.77	Hexadecanoic acid, methyl ester
2	9.87	92.74	Methyl stearate
3	10.09	93.73	9-Octadecenoic acid, methyl ester
4	10.51	96.67	11,14-Octadecadienoic acid, methyl
5	11.19	92.22	9,12,15 Octadecatrienoic acid, methyl
6	12.02	88.15	Eicosanoic acid, methyl ester
7	12.25	92.08	11- Eicosanoic acid, methyl ester

Waste cooking oil- Sr: 0.33Al

Peaks	FAME		Compound name
	Retention time (min)	Library match (%)	
1	5.4	89.9	Methyl decanoate
2	6.4	84.6	Methyl dodecanoate
3	7.3	92.9	Methyl 12-methyltridecanoate
4	8.4	90.3	Methyl hexadecanoate
5	8.8	85	Methyl 14-methylpentadecanoate
6	10.1	96.8	Methyl (E)-octadec-13-enoate
7	10.5	96.4	Methyl (11E,14E)-octadeca-11,14-
8	11.2	93.2	Methyl (9Z,12Z,15Z)-octadeca-9,12,15-

The FAME of *Chlamydomonas* sp., *S. ecornis*, and *S. communis* was mainly comprised of palmitic acid methyl ester (C16:0), stearic acid methyl ester (C18:0), palmitoleic acid methyl ester (C16:1), oleic acid methyl ester (C18:1n9c), linoleic acid methyl ester

(C18:2n6c), and α -linolenic acid methyl ester (C18:3n3) (Table 8). The algal FAME percentage profiling was performed using GC-MS with the help of FAME mix C₄-C₂₄ and pentadecanoic acid methyl ester as a quantitative standard and as an internal standard, respectively. The *Chlamydomonas* sp., *S. communis*, and *S. ecornis* attained FAME yields of 23.1%, 11.0%, and 10.5% of DW in AqWW1, respectively. The increased content of FAME (% DW) in the current work compared to previously reported studies is possibly due to co-solvent lipid extraction (Article V).

Table 8. Summary of FAME composition of different algal species in aquaculture wastewater within ten days.

FAME Composition	<i>Chlamydomonas</i> sp.		<i>S. communis</i>		<i>S. ecornis</i>	
Retention time (min)	AqWW1	AqWW2	AqWW1	AqWW2	AqWW1	AqWW2
Saturated fatty acids (% of total FAME)						
C16:0	8.4	28.24	26.12	37.45	35.56	23.12
C18:0	9.9	2.80	3.1	2.1	2.9	1.50
Unsaturated fatty acids (% of total FAME)						
C 16:1	8.5	2.79	2.18	2.55	1.89	3.4
C18:1n9c	10.2	27.20	23.42	44.5	40.03	32.18
C18:2n6c	10.5	26.4	22.10	3.6	2.84	9.16
C18:3n3	11.2	5.0	6.94	10.4	12.67	12.3
Total FAME (%DW)		23.12	14.65	11.04	9.38	10.45
						7.92

4.4 NMR analysis of biodiesel

The methoxy group (A_{ME}) of FAME and the methylene group (A_{CH_2}) were well-defined by signals at 3.6 ppm and 2.27 ppm in 1H NMR spectra as depicted in Fig.21. Moreover, these signals also correspond to the confirmation of methyl ester in the biodiesel sample. Besides, the signals used for the calculation of FAME conversion percentage, there were other signals like 0.83 to 0.97 ppm for the latter methyl group. The existence of the methylene group and olefinic groups were confirmed by the signal in the range of 1.22 to 2.34 and at 5.3 ppm, respectively. The signal at 3.4 ppm range assigns to the solvent residual signal (Article I-IV).

The existence of ester carbonyl $-COO-$ and C-O were verified by signals at the range of 174 ppm and 51 ppm in ^{13}C NMR, correspondingly as shown in Fig.22. The unsaturation in FAME samples was indicated by signals over the range of 126-132 ppm. The signals in the region of 21-35 ppm support the presence of $-CH_2$ group. Apart from these signals, the presence of terminal $-CH_3$ groups was substantiated by signals at 14.03 ppm and 14.2 ppm (Articles I-IV).

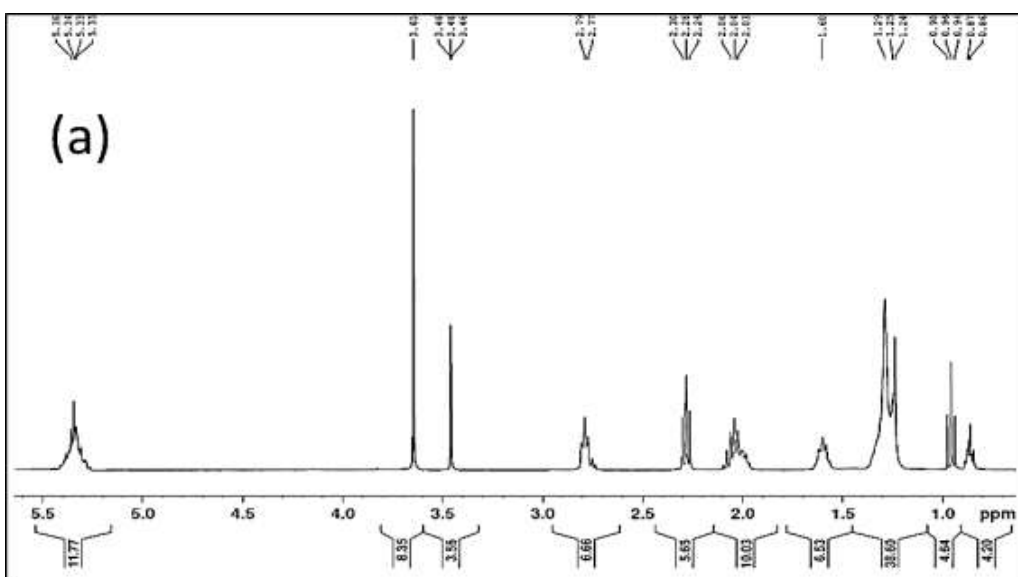


Fig.21a. The ^1H NMR for the FAME sample obtained with TiO_2 - $0.5\text{C}_4\text{H}_5\text{KO}_6$ (Article I).

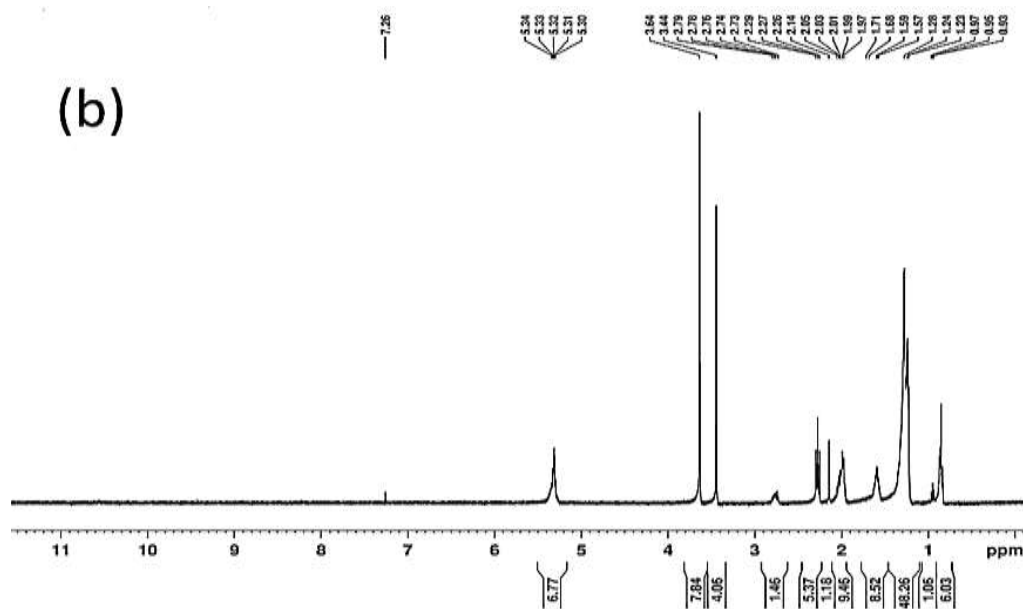


Fig.21b. The ^1H NMR for the FAME sample obtained with CaO-0.5LiOH (Article II).

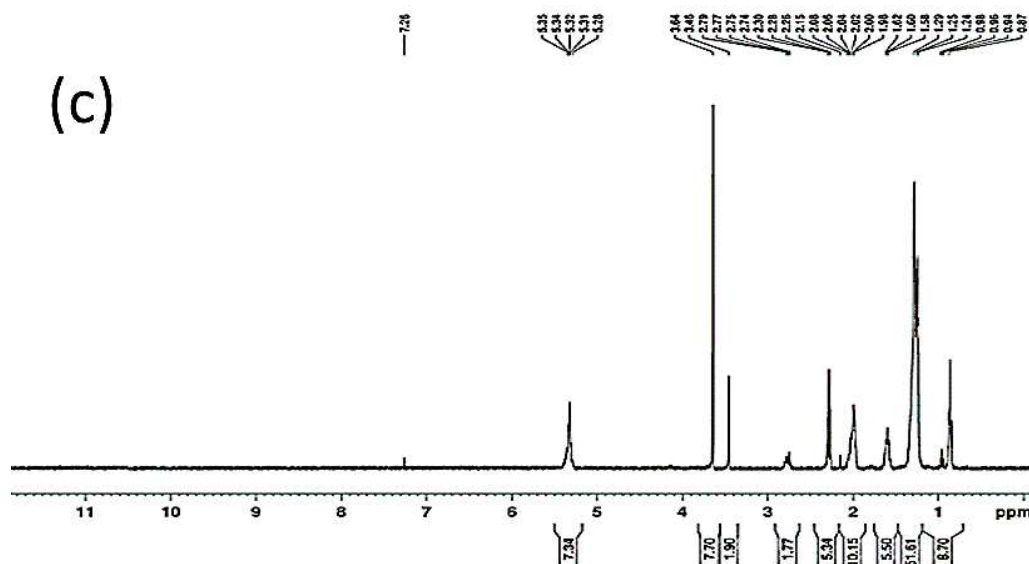


Fig.21c. The ^1H NMR for the FAME sample obtained with $\text{Fe}_3\text{O}_4\text{-CeO}_2\text{-25K}$ (Article III).

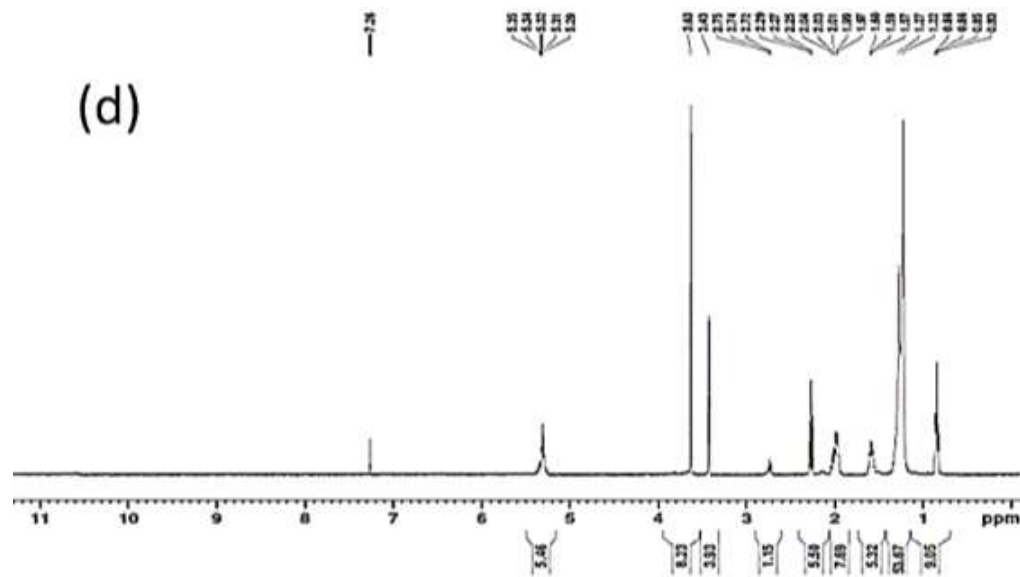


Fig.21d. The ^1H NMR for the FAME sample obtained with Sr: 0.33Al (Article IV).

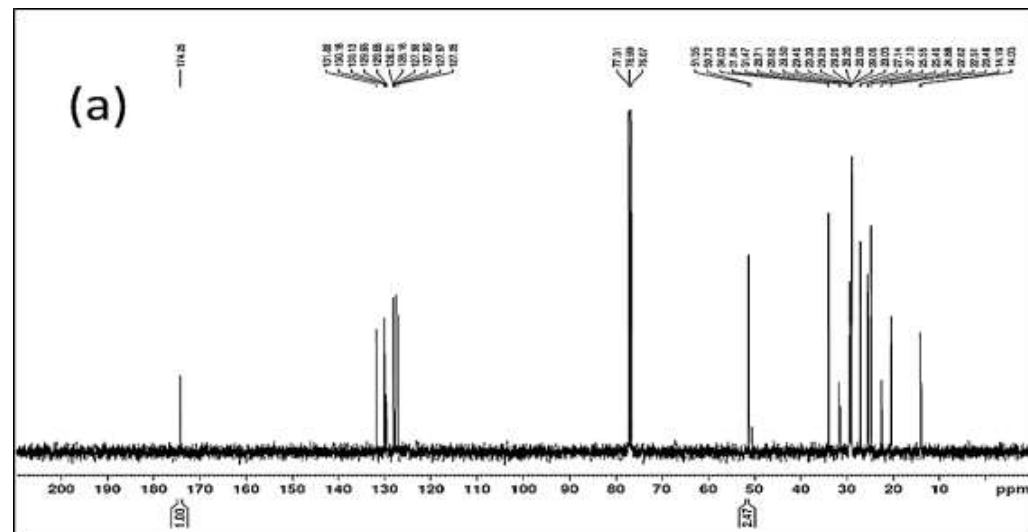


Fig.22a. The ^{13}C NMR for the FAME sample obtained with TiO_2 - 0.5C₄H₅KO₆ (Article I).

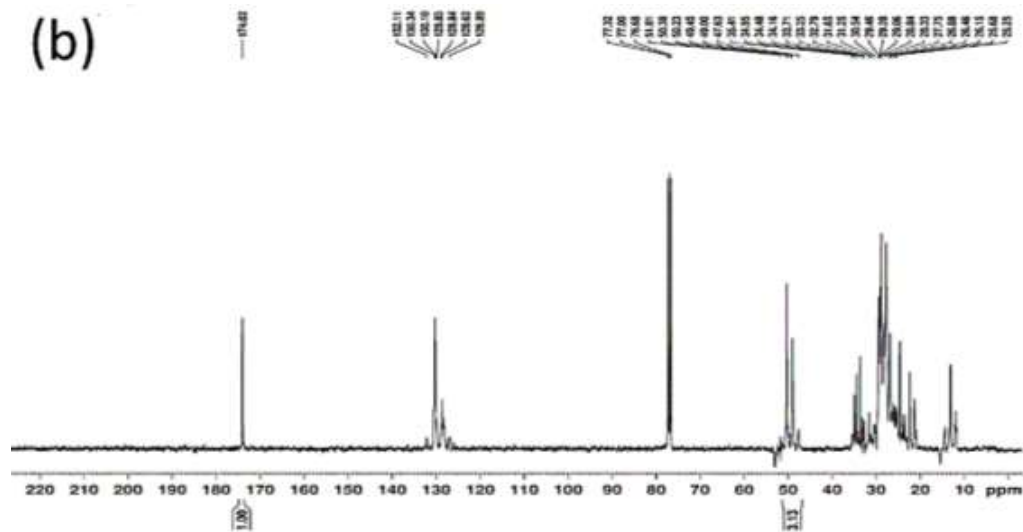


Fig.22b. The ^{13}C NMR for the FAME sample obtained with CaO-0.5LiOH (Article II).

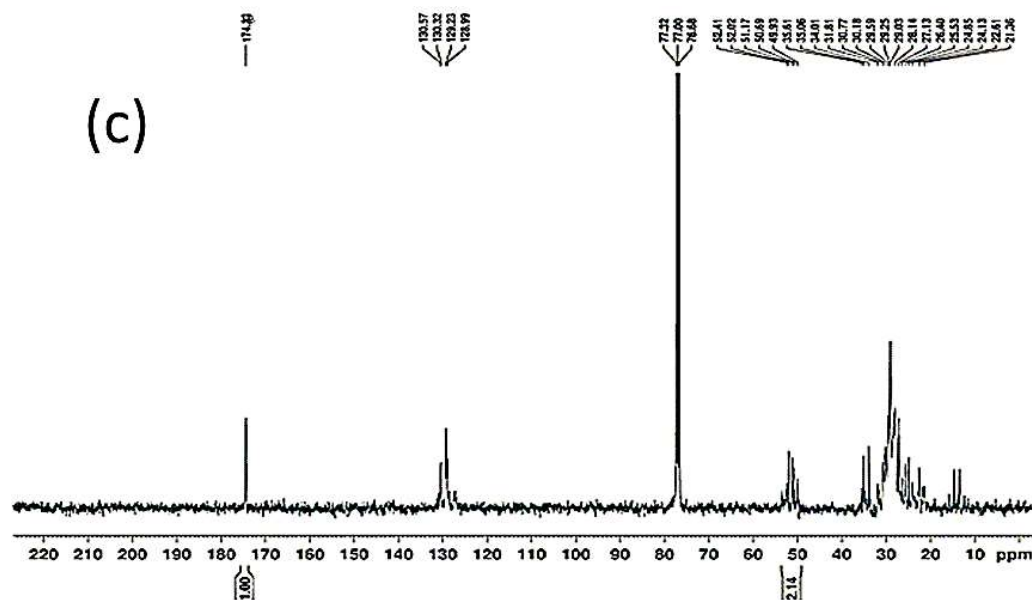


Fig.22c. The ^{13}C NMR for the FAME sample obtained with $\text{Fe}_3\text{O}_4\text{-CeO}_2\text{-25K}$ (Article III).

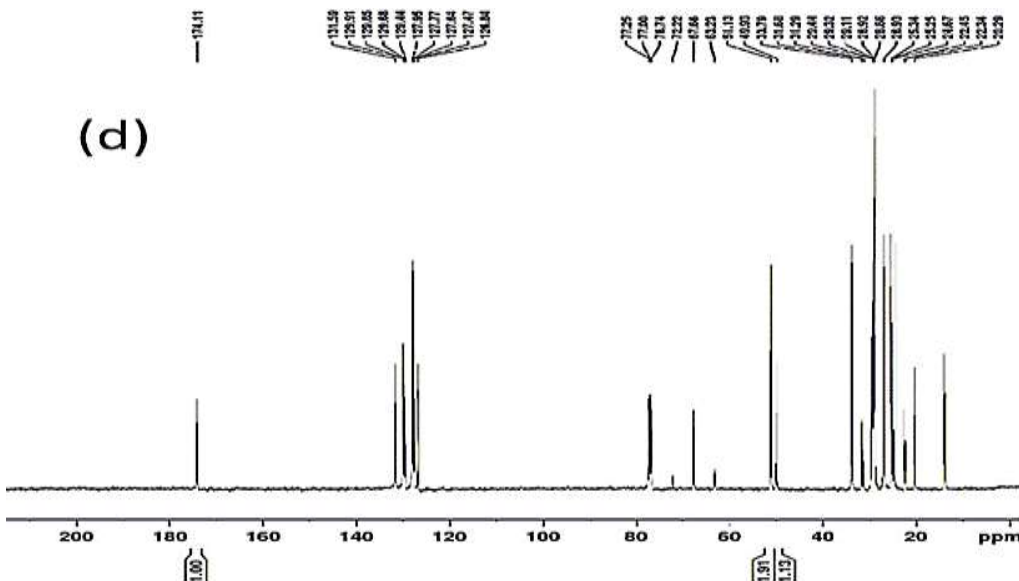


Fig.22d. The ^{13}C NMR for the FAME sample obtained with Sr: 0.33Al (Article IV).

4.5 Effect of reaction parameters on FAME production (yield) or biodiesel production (yield).

Based on Table 9 and Fig. 23, the TiO_2 - 0.5 $\text{C}_4\text{H}_5\text{KO}_6$, CaO -0.5 LiOH , Fe_3O_4 - CeO_2 -25K, Sr:0.33Al showed a maximum biodiesel yield of 98.5 %, 97.33 %, 96.13 %, and 99.4 % from raw materials such as linseed oil, lard oil, rapeseed oil, and waste cooking oil, respectively. The Sr: 0.33Al nanocatalyst also exhibited 99.7% FAME yield from lard oil at optimum reaction conditions. The yield of biodiesel was influenced by the reaction conditions such as oil to methanol ratio, reaction temperature, reaction time, and catalyst amount. The biodiesel production is lower when catalyst amount is less than the optimum amount, and there is a decrease in FAME conversion due to a decrease in the availability of active sites and a hindrance to phase separation with increased amount of catalyst above the optimal value (Article I-IV).

Generally, the FAME yield was negatively affected by an increase in methanol concentration beyond the optimum value due to mainly the excess and the solubility of

glycerol to the ester phase, making the separation of biodiesel difficult. The surplus methanol possibly favors the reverse reaction than the production of biodiesel. Furthermore, biodiesel production drops with a rise in temperature due to the possible evaporation of methanol at elevated temperature. Fig. 23 shows the optimum methanol concentration and reaction temperature for each transesterification reaction performed using various nanocatalysts (Articles I-IV). The biodiesel yield remains constant or decreases with an increase in reaction time after optimum value. The decline in FAME production is due to the hydrolysis of esters (Articles I-IV). Fig. 23d, the maximum biodiesel yield was achieved in a shorter reaction time with a lower amount of catalyst and an oil to methanol ratio. This is due to the reduction of possible saponification by lowering the phase boundary in reactants and offering a faster separation of biodiesel and glycerol (Article I-IV).

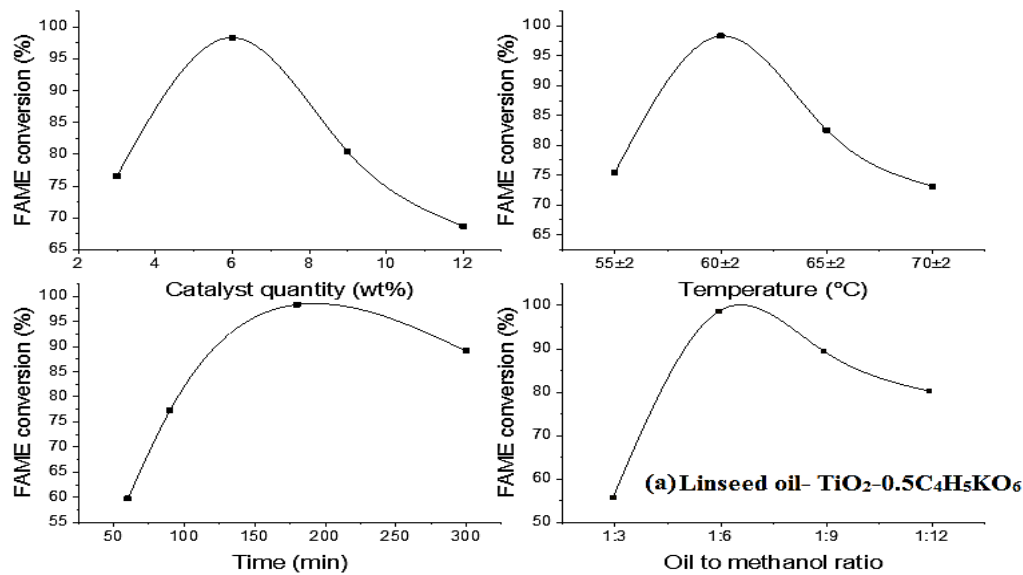


Fig. 23a. Influence of transesterification conditions on biodiesel yield using $\text{TiO}_2\text{-}0.5\text{C}_4\text{H}_5\text{KO}_6$ (Article I).

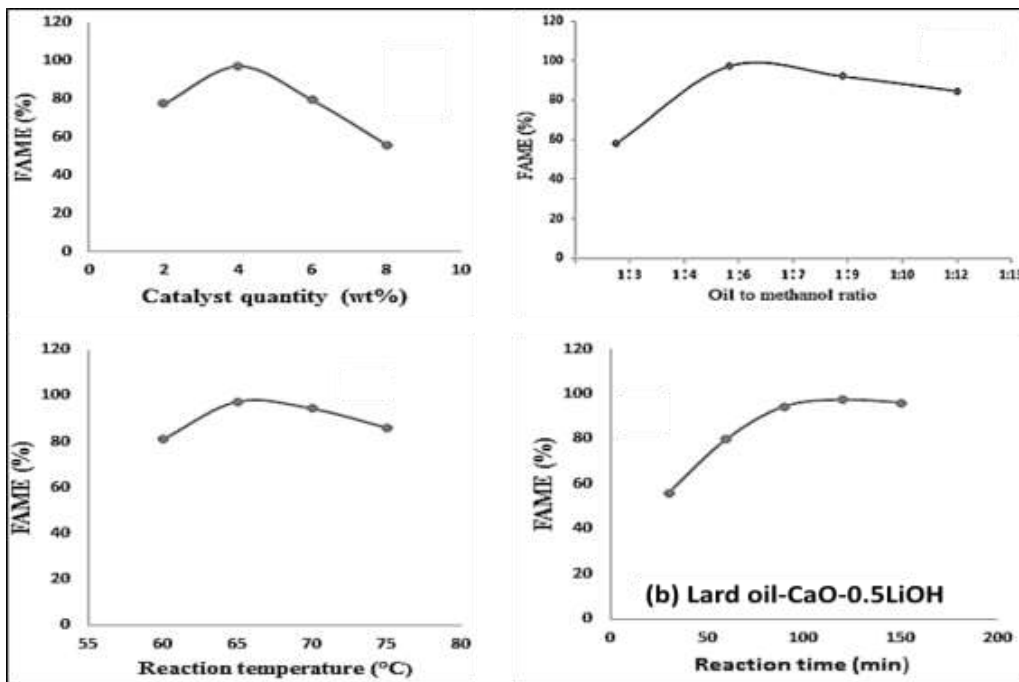


Fig. 23b. Influence of transesterification conditions on biodiesel yield using CaO-0.5LiOH (Article II).

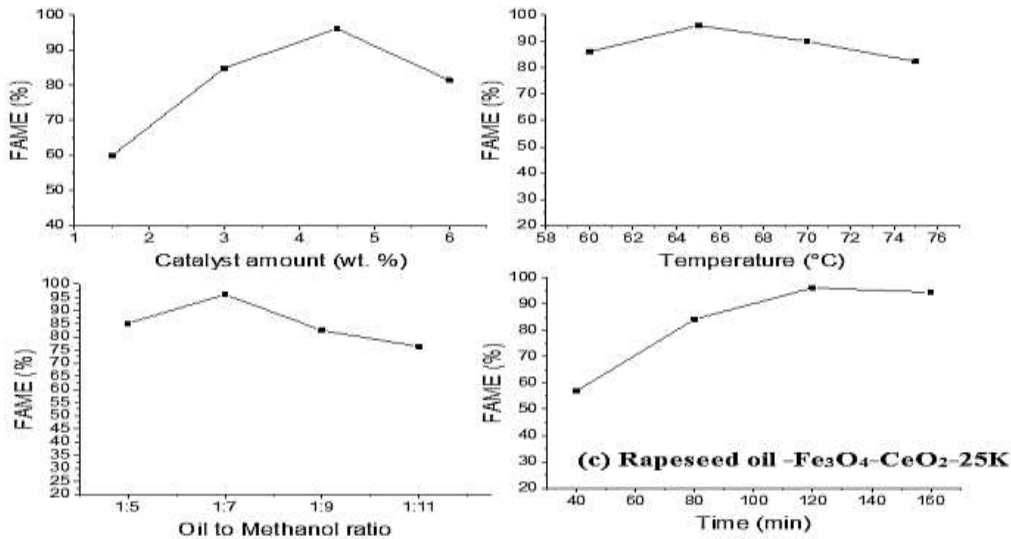


Fig. 23c. Influence of transesterification conditions on biodiesel yield using Fe₃O₄-CeO₂-25K (Article III).

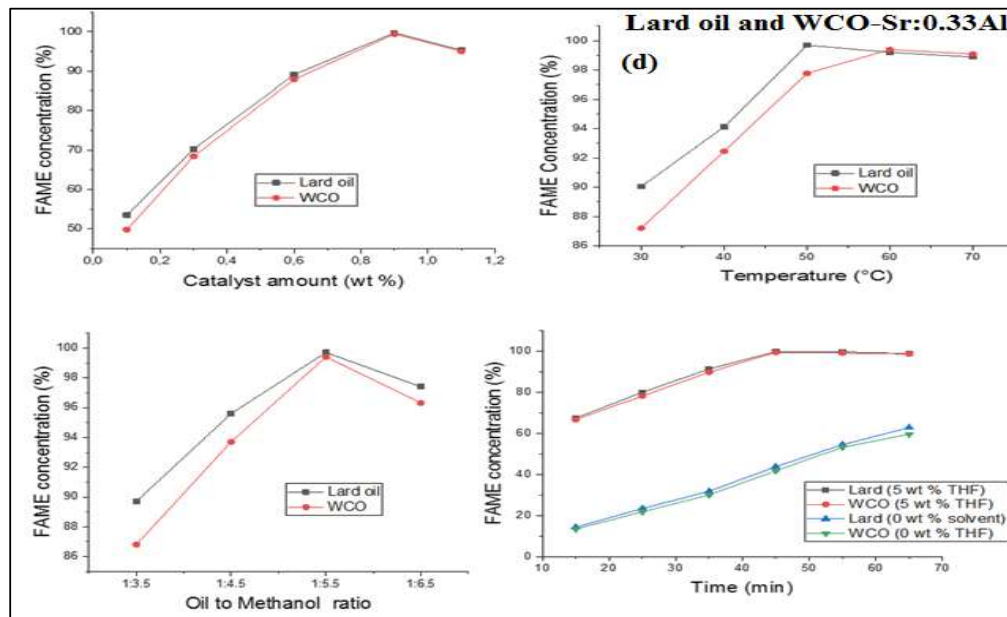


Fig. 23d. Influence of transesterification conditions on biodiesel yield using Sr: 0.33Al (Article IV).

Table 9. Maximum biodiesel production from various sources using different nanocatalysts (Article I-IV).

Feedstock	Catalyst	Particle size (nm)	Temp. (°C)	Oil to methanol ratio	Reaction time (min)	Catalyst wt. %	Biodiesel yield %
Linseed oil	TiO ₂ -0.5C ₄ H ₉ KO ₆	26-179	60	1:6	180	6	98.5
Lard oil	CaO-0.5LiOH	54.5-127	65	1:6	120	4	97.33
Rapeseed oil	Fe ₃ O ₄ -CeO ₂ -25K	20-33.9	65	1:7	120	4.5	96.13
Waste cooking oil	Sr:0.33Al	57-100	60	1:5.5	45	0.9	99.4
Lard oil	Sr-0.33Al	57-100	50	1:5.5	45	0.9	99.7

4.6 Properties of the synthesized biodiesel

The parameters of obtained biodiesel were measured using the EN 14214/ ASTM D6751 method, as shown in Table 10 a. The algal FAME properties such as cetane number (CN) and iodine value (IV) were determined using the empirical formula (Eq.5 and Eq.6) depicted in Table 10b. All the properties depicted in Table 10 have a significant role in biodiesel quality. The high acid value beyond ASTM and EN ISO limits cause problems such as engine filter clogging and corrosion of engine rubber parts. The density and kinematic viscosity values above standard value result in issues in fuel injection operation and lead to the formation of engine deposits. Flashpoint is a crucial property of fuel, and it is critical to establish flash point value for fuel management and storage. The rest of the chosen features, such as cloud point, calorific value, iodine value, pour point, and cetane number are also within the limits of EN ISO/ASTM standards (Article I-IV and submitted Article V).

Table 10 a. Properties of FAME from different feedstocks using nanocatalysts.

Property	FAME from linseed oil (using TiO₂-0.5C₄H₅KO₆)	FAME from lard oil (using CaO-0.5 LiOH)	FAME from rapeseed oil (using Fe₃O₄-CeO₂-25K)	FAME from lard oil (using Sr: 0.33Al)	FAME from WCO (using Sr: 0.33Al)
Acid value (mg KOH/g)	0.3	0.282	0.308	0.29	0.31
Density at 15°C (kg/m ³)	891.52	881.76	880.30	882.1	885.6

Kinematic viscosity at 40°C mm ² /s	3.5709	4.08	4.37	3.98	4.01
Flash point (°C)	173	130	171	131	138
Cetane Number	57	62.6	-	63	67
Cloud point (°C)	4	7	-	8	9
Pour point (°C)	2	5	-	5	7
Calorific value (MJ/kg)	40.89	41.23	-	39.92	40.45

Table 10b. FAME properties of different algal species grown in aquaculture wastewater with in ten days.

Properties	<i>Chlamydomonas</i> sp		<i>S. communis</i>		<i>S. ecornis</i>	
	AqWW1	AqWW2	AqWW1	AqWW2	AqWW1	AqWW2
Iodine value	88.74	82.25	77.54	77.69	82.57	76.24
(g l 100g ⁻¹)						
Cetane number	55.05	59.44	55.11	56.38	60.25	65.53

4.7 Regeneration and reusability of nanocatalysts

Catalyst reusability shows a significant part in an eco-friendly biodiesel production process, and the regeneration of nanocatalysts after transesterification was initially done by washing with heptane or methanol or their combination. The washed catalysts were

dried and calcined to reactivate the used catalyst. The catalyst deactivation was mainly due to deposition of impurities, minor changes in the catalyst structure and composition, reduction in BET surface area, oil content or thermal deactivation, and metal leaching. The stability of nanocatalysts after different cycles was evaluated by determining the leached metal ion concentration after each cycle with the help of ICP-OES (Article I-IV). Table 11 shows the reduction in biodiesel production efficiency and stability of various nanocatalysts after five cycles of transesterification.

Table 11a. Reduction in activity of different nanocatalysts after five cycles.

Nano catalysts	Biodiesel yield cycle I (%)	Biodiesel yield cycle V (%)
TiO ₂ -0.5C ₄ H ₅ KO ₆	98.5	93.1
CaO-0.5LiOH	97.33	94.4
Fe ₃ O ₄ -CeO ₂ -25K	96.13	80.94
Sr: 0.33Al (Lard oil)	99.7	95.1
Sr:0.33Al (WCO)	99.4	93.7

Table 11b. Stability of different nanocatalysts after five cycles of transesterification.

Nano catalysts	Total metal leaching after five cycles (mg/L)						
	Ti	K	Ca	Li	Ce	Sr	Al
TiO ₂ -0.5C ₄ H ₅ KO ₆	0.043	0.0004	-	-	-	-	-
CaO-0.5LiOH	-	-	-	0.32	-	-	-
Fe ₃ O ₄ -CeO ₂ -25K	-	0.56	-	-	0.038	-	-
Sr: 0.33Al	-	-	-	-	-	0.024	0.0072

4.8 Comparison of main outcomes of biodiesel production with existing literature

Table 12 presents comparison of biodiesel production using the synthesized catalysts during in this research with other previously reported catalysts. Biodiesel production from linseed and lard oils using a heterogeneous catalyst that has not been explored earlier, has been successfully implemented in this research work. The conversion of these oils to biodiesel was better with our synthesized catalysts than other reported catalysts. The synthesized Fe₃O₄-CeO₂-25K showed better efficiency in the conversion of rapeseed oil to biodiesel compared to KF/CaO-MgO nanocatalyst but lower than MgO. Moreover, in comparison to other reported nanomagnetic catalysts presented in Table 3, Fe₃O₄-CeO₂-25K showed better production of FAME but lower than Al₂O₃/Fe₃O₄. The MgO and Al₂O₃/Fe₃O₄ nanocatalyst require high temperature for optimum production of biodiesel compared to Fe₃O₄-CeO₂-25K. The synthesized Sr: 0.33Al nanocatalyst showed a better

conversion of lard and WCO compared to other reported catalysts. Furthermore, in the current research work, *Scenedesmus* sp. showed a FAME yield of 11.0% and 10.5% of DW. The obtained FAME (% DW) in this study is slightly higher than in other previously reported studies [90], [91].

Table 12. Comparison of obtained biodiesel yield using various catalysts

Feed stock	Catalyst	Co-solvent	Biodiesel yield (%)	Reference
Linseed oil	NaOH	-	88-96	[87]
Linseed oil	CaO	Diethyl ether	98.08	[88]
Linseed oil	TiO ₂ -0.5C ₄ H ₅ KO ₆	-	98.5	Article I
Lard oil	KOH	-	96	[89]
Lard oil	CaO-0.5LiOH	-	97.33	Article II
Lard oil	Sr-0.33Al	THF	99.7	Article IV
Rapeseed oil	KF/CaO-MgO	-	95	[12]
Rapeseed oil	MgO	-	98	[12],[34]
Rapeseed oil	Fe ₃ O ₄ -CeO ₂ -25K	-	96.13	Article III
Recycled waste cooking oil	CaO-MgO		98.95	[12]
WCO	Al ₂ O ₃ /Fe ₃ O ₄	-	99.1	[67]
Used cooking oil	Ti(SO ₄)O	-	97.1	[12]
Used cooking oil	TiO ₂ /PrSO ₃ H	-	98.3	[12]
WCO	Sr-0.33Al	THF	99.4	Article IV

5 Conclusion

The conversion of various feedstock such as edible, non-edible, animal fat, waste oil, and algal oil derived from various algal biomass to biodiesel was successfully investigated in this thesis work. The potassium doped TiO_2 ($\text{TiO}_2\text{-}0.5\text{C}_4\text{H}_5\text{KO}_6$), lithium impregnated CaO ($\text{CaO}\text{-}0.5\text{LiOH}$), nano-magnetic potassium doped ceria ($\text{Fe}_3\text{O}_4\text{-CeO}_2\text{-}25\text{K}$), Sr-Al double oxides (Sr:0.33Al) were used for nanocatalytic transesterification of different oils such as linseed oil, lard oil, rapeseed oil, and waste cooking oil. The characterization of the synthesized nanocatalysts and impregnation of alkali metal on to nanomaterials were confirmed by FTIR, XRD, TEM, SEM, XPS, BET, and basicity test using Hammett indicators benzene carboxylic acid titration method. The regeneration and reusability test of the catalyst was effectively completed. The optimum reaction conditions for each feedstock using respective nanocatalysts were determined. The characterization and quality of obtained biodiesel were successfully evaluated. The current work also illustrates the efficient cultivation of different algal strains such as *Chlamydomonas* sp., *S. ecornis*, and *S. communis* in aquaculture wastewater (AqWW1 and AqWW2) as a nutrient medium for biodiesel production, which provides potential benefits in environmental and energy perspective.

The potassium impregnated TiO_2 showed better conversion of linseed oils to biodiesel compared to other reported catalysts. Lithium doped CaO nanocatalysts was prepared using lithium hydroxide as a new precursor, which resulted in a FAME yield of 97.33 %. The novel nano-magnetic potassium doped ceria ($\text{Fe}_3\text{O}_4\text{-CeO}_2\text{-}25\text{K}$) as a catalyst for

transesterification of rapeseed oil showed the FAME yield of 96.13 %. However, the biodiesel yield was slightly lower than of other nanocatalysts is due to lower basicity of catalyst. The synthesized Sr: 0.33Al nanocatalyst showed a better conversion of lard and WCO compared to other previously reported catalysts. All the synthesized catalysts in this research work showed a promising solution for efficient biodiesel production. The impregnation of alkali metals and the presence of alkaline earth metals enhances basicity, thereby improves the transesterification efficiency of nanocatalysts.

The reusability test of catalyst showed that CaO-0.5LiOH showed better stability than TiO₂-0.5C₄H₅KO₆ and Fe₃O₄-CeO₂-25K. The existence of co-solvent in transesterification reaction raises the reaction rate, decreases the amount of catalyst used, and reduction in methanol consumption for maximum yield of biodiesel compared to the usual transesterification reaction. The regeneration of catalysts and co-solvent studies help to determine the economic viability and eco-friendly nature of catalyst and to resolve issues related to transesterification reactions respectively.

The synergic approach of algal biodiesel production and wastewater treatment was also studied in this research work. The *S. ecornis*, and *S. communis* species showed better carbon dioxide tolerance than *Chlamydomonas* sp. The lower nutrient concentration in wastewater enhances the content of triglycerides. The co-solvent lipid extraction from different algal strains resulted in improved FAME content. Therefore, it is a promising solution to the world energy crisis, climate change and also for the removal of pollutants such as COD, TN, and TP from wastewater.

The biodiesel production from different potential renewable feedstocks was successfully achieved with the reusable catalyst in a sustainable approach. The properties of all obtained biodiesel were within EN ISO / ASTM limits. Thereby resulted biodiesel can as a fuel with preferred features.

6 Future research

The results of this work can serve as a foundation for further research in the future. The increased stability, easy, and efficient reusability of catalyst for transesterification of feedstock with high water content or FFA content can be attained by the 3D printed nanostructured catalyst. All the catalyst prepared in this research work was metallic in nature so they can be easily 3D printed using metallic printers for continuous flow reactors to carry out biodiesel production process [12], [83]. Moreover, glycerol, the by-product obtained after the transesterification reaction can be converted to hydrogen because fossil fuels are the primary source for hydrogen production [84]. Moreover, algal biomass after lipid extraction are rich in carbohydrates (starch and cellulose) and can be used for the production of ethanol by fermentation, and the remaining residues of algal biomass after biodiesel and ethanol production can be used for biogas production [85],[86].

References

- [1] E. Bergasse, The relationship between energy and economic and social development in the southern Mediterranean with the support of Wojciech Paczynski and contributions by Marek Dabrowski and Luc Dewulf, 2013.
- [2] N. Zhang, N. Lior, H. Jin, The energy situation and its sustainable development strategy in China, Energy. 36 (2011) 3639–36–49. doi:10.1016/j.energy.2011.01.035.
- [3] D.I. Stern, The Role of Energy in Economic Growth, in: R. Costanza, K. Limburg, I. Kubiszewski (Eds.), Ecol. Econ. Rev., Ann. N.Y. Acad. Sci, 2011: pp. 26–51. doi:doi/abs/10.1111/j.1749-6632.2010.05921.x.
- [4] P.A. Owusu, S. Asumadu-sarkodie, A review of renewable energy sources , sustainability issues and climate change mitigation, Cogent Eng. 3 (2016) 1–14.
- [5] U.S. Energy Information Administration International Energy Outlook 2019, 2019. <https://www.eia.gov/outlooks/ieo/>
- [6] United Nations, UN DESA, World Population Prospects: The 2019 Revision, 2019. <https://population.un.org/wpp/Download/Standard/Population/>.
- [7] M.G. Azad, Kalam Rasul, M.M.K. et. al Khan, Introduction to sustainable and alternative ecofuels, Adv. Eco-Fuels a Sustain. Environ. (2019) 1–14. doi:doi.org/10.1016/B978-0-08-102728-8.00001-2.
- [8] U.S. Energy Information Administration International Energy Outlook 2017, 2017. <https://www.eia.gov/todayinenergy/detail.php?id=32912>.
- [9] S. Shafiee, E. Topal, When will fossil fuel reserves be diminished?, Energy Poli. 37 (2009) 181–189.

- [10] H.C. Ong, T.I. Mahlia, H.H. Masjuki, A review on energy scenario and sustainable energy in Malaysia, *Renew. Sustain. Energy Rev.* 15 (2011) 639–647. doi:10.1016/j.rser.2010.09.043.
- [11] S. Saito, Role of nuclear energy to a future society of shortage of energy resources and global warming, *J. Nucl. Mater.* 398 (2010) 1–9. doi:10.1016/j.jnucmat.2009.10.002.
- [12] I. Ambat, V. Srivastava, M. Sillanpää, Recent advancement in biodiesel production methodologies using various feedstock : A review, *Renew. Sustain. Energy Rev.* 90 (2018) 356–369.
- [13] World Energy Balances, International energy Agency (IEA), IEA (International Energy Agency), 2019. <https://www.iea.org/statistics/>.
- [14] Global energy and CO₂ status, International Energy Agency (IEA), International energy agency, 2018. <https://www.iea.org/geco/emissions/>.
- [15] M.F. Demirbas, M. Balat, H. Balat, Potential Contribution of Biomass to the Sustainable Energy Development, *Energy Convers. Manag.* 50 (2009) 1746–1760.
- [16] World energy outlook, International Energy Agency (IEA), 2016. <https://www.iea.org/newsroom/news/2016/november/world-energy-outlook-2016.html>.
- [17] R. Luque, R. Luque, L. Herrero-davila, J.M. Campelo, J.H. Clark, J.M. Hidalgo, D. Luna, M. Marinas, A.A. Romero, Biofuels : a technological perspective, 1 (2008). doi:10.1039/b807094f.
- [18] A. Demirbas, Importance of biodiesel as transportation fuel, *Energy Policy*. (2007). doi:10.1016/j.enpol.2007.04.003.
- [19] S.P. Singh, D. Singh, Biodiesel production through the use of different sources and

- characterization of oils and their esters as the substitute of diesel: A review, Renew. Sustain. Energy Rev. 14 (2010) 200–216. doi:10.1016/j.rser.2009.07.017.
- [20] T. Nguyen, L. Do, D.A. Sabatini, Biodiesel production via peanut oil extraction using diesel-based reverse-micellar microemulsions, Fuel. 89 (2010) 2285–2291. doi:10.1016/j.fuel.2010.03.021.
- [21] G. Baskar, R. Aiswarya, Trends in catalytic production of biodiesel from various feedstocks, Renew. Sustain. Energy Rev. 57 (2016) 496–504. doi:10.1016/j.rser.2015.12.101.
- [22] W. Shi, J. Li, B. He, F. Yan, Z. Cui, K. Wu, L. Lin, X. Qian, Y. Cheng, Biodiesel production from waste chicken fat with low free fatty acids by an integrated catalytic process of composite membrane and sodium methoxide, Bioresour. Technol. 139 (2013) 316–322. doi:10.1016/j.biortech.2013.04.040.
- [23] World energy statistics , International energy Agency (IEA), Energy Insights- Global energy perspective, 2017.
- [24] E. Bet-Moushoul, K. Farhadi, Y. Mansourpanah, A.M. Nikbakht, R. Molaei, M. Forough, Application of CaO-based/Au nanoparticles as heterogeneous nanocatalysts in biodiesel production, Fuel. 164 (2016) 119–127. doi:10.1016/j.fuel.2015.09.067.
- [25] A. Karmakar, S. Karmakar, S. Mukherjee, Properties of various plants and animals feedstocks for biodiesel production, Bioresour. Technol. 101 (2010) 7201–7210. doi:10.1016/j.biortech.2010.04.079.
- [26] E. Rashtizadeh, F. Farzaneh, Transesterification of soybean oil catalyzed by Sr-Ti mixed oxides nanocomposite, J. Taiwan Inst. Chem. Eng. 44 (2013) 917–923. doi:10.1016/j.jtice.2013.02.008.

- [27] F. Sanchez, P.T. Vasudevan, Enzyme catalyzed production of biodiesel from olive oil., *Appl. Biochem. Biotechnol.* 135 (2006) 1–14. doi:10.1385/ABAB:135:1:1.
- [28] M.P. Dorado, E. Ballesteros, M. Mittelbach, F.J. López, Kinetic parameters affecting the alkali-catalyzed transesterification process of used olive oil, *Energy and Fuels.* 18 (2004) 1457–1462. doi:10.1021/ef034088o.
- [29] R. Madhuvilakku, S. Piraman, Biodiesel synthesis by TiO₂-ZnO mixed oxide nanocatalyst catalyzed palm oil transesterification process, *Bioresour. Technol.* 150 (2013) 55–59. doi:10.1016/j.biortech.2013.09.087.
- [30] D. Kumar, G. Kumar, Poonam, C.P. Singh, Fast, easy ethanolysis of coconut oil for biodiesel production assisted by ultrasonication, *Ultrason. Sonochem.* 17 (2010) 555–559. doi:10.1016/j.ultsonch.2009.10.018.
- [31] J. Hossain, Bio-Diesel from Mustard Oil: A Renewable Alternative Fuel for Small Diesel Engines, *Mod. Mech. Eng.* 1 (2011) 77–83. doi:10.4236/mme.2011.12010.
- [32] A. Gashaw, A. Lakachew, Production of Biodiesel from Non Edible Oil and its Properties, *Int. J. Sci. Environ. Technol.* 3 (2014) 1544–1562.
- [33] M. Akia, F. Yazdani, E. Motaei, D. Han, H. Arandian, A review on conversion of biomass to biofuel by nanocatalysts, *Nanocatalysts. Biofuel Res. J. Biofuel Res. J.* 1 (2014) 16–25.
- [34] M. Verziu, B. Cojocaru, J. Hu, R. Richards, C. Ciuculescu, P. Filip, V.I. Parvulescu, Sunflower and rapeseed oil transesterification to biodiesel over different nanocrystalline MgO catalysts, *Green Chem.* 10 (2008) 373. doi:10.1039/b712102d.
- [35] L. Mguni, R. Meijboom, K. Jalama, Biodiesel Production over nano-MgO Supported on Titania, *Int. Sch. Sci. Res. Innov.* 6 (2012) 380–384. <http://www.waset.org/publications/13050>.

-
- [36] L.H.A. and H.E.T. M.F.C. Andrade, A.L.A. Parussulo, C.G.C.M. Netto, Lipase immobilized on polydopamine-coated magnetite nanoparticles for biodiesel production from soybean oil, *Biofuel Res. J.* 10 (2016) 403–409. doi:10.18331/BRJ2016.3.2.5.
 - [37] J. Gardy, A. Hassanpour, X. Lai, M.H. Ahmed, Synthesis of Ti(SO₄)O solid acid nano-catalyst and its application for biodiesel production from used cooking oil, *Appl. Catal. A Gen.* 527 (2016) 81–95. doi:10.1016/j.apcata.2016.08.031.
 - [38] L. Wen, Y. Wang, D. Lu, S. Hu, H. Han, Preparation of KF / CaO nanocatalyst and its application in biodiesel production from Chinese tallow seed oil, *Fuel.* 89 (2010) 2267–2271. doi:10.1016/j.fuel.2010.01.028.
 - [39] R. Anr, A.A. Saleh, M.S. Islam, S. Hamdan, M.A. Maleque, Biodiesel Production from Crude Jatropha Oil using a Highly Active Heterogeneous Nanocatalyst by Optimizing Transesterification Reaction Parameters, *Energy and Fuels.* 30 (2016) 334–343. doi:10.1021/acs.energyfuels.5b01899.
 - [40] M. Naik, L.C. Meher, S.N. Naik, L.M. Das, Production of biodiesel from high free fatty acid Karanja (*Pongamia pinnata*) oil, *Biomass and Bioenergy.* 32 (2008) 354–357. doi:10.1016/j.biombioe.2007.10.006.
 - [41] B. Gurunathan, A. Ravi, Process optimization and kinetics of biodiesel production from neem oil using copper doped zinc oxide heterogeneous nanocatalyst, *Bioresour. Technol.* 190 (2015) 424–428. doi:10.1016/j.biortech.2015.04.101.
 - [42] J.M. Dias, J.M. Araújo, J.F. Costa, M.C.M. Alvim-Ferraz, M.F. Almeida, Biodiesel production from raw castor oil, *Energy.* 53 (2013) 58–66. doi:10.1016/j.energy.2013.02.018.
 - [43] M. Morshed, K. Ferdous, M.R. Khan, M.S.I. Mazumder, M.A. Islam, M.T. Uddin, Rubber seed oil as a potential source for biodiesel production in Bangladesh, *Fuel.*

- 90 (2011) 2981–2986. doi:10.1016/j.fuel.2011.05.020.
- [44] S. Hashmi, S. Gohar, T. Mahmood, U. Nawaz, H. Farooqi, Biodiesel Production by using CaO-Al₂O₃ Nano Catalyst, *Int. J. Eng. Res. Sci.* 2 (2016) 2395–6992.
- [45] S. Hu, Y. Guan, Y. Wang, H. Han, Nano-magnetic catalyst KF/CaO-Fe₃O₄ for biodiesel production, *Appl. Energy.* 88 (2011) 2685–2690. doi:10.1016/j.apenergy.2011.02.012.
- [46] F. Halek, A. Delavari, Production of biodiesel as a renewable energy source from castor oil, (2013) 1063–1068. doi:10.1007/s10098-012-0570-6.
- [47] E.F. Aransiola, T. V. Ojumu, O.O. Oyekola, T.F. Madzimbamuto, D.I.O. Ikhu-Omoregbe, A review of current technology for biodiesel production: State of the art, *Biomass and Bioenergy.* 61 (2014) 276–297. doi:10.1016/j.biombioe.2013.11.014.
- [48] I. Ambat, W. Tang, M. Sillanpää, Statistical analysis of sustainable production of algal biomass from wastewater treatment process, *Biomass and Bioenergy.* 120 (2019) 471–478. doi:<http://dx.doi.org/10.1016/j.biombioe.2018.10.016>.
- [49] M. Tariq, S. Ali, N. Khalid, Activity of homogeneous and heterogeneous catalysts, spectroscopic and chromatographic characterization of biodiesel: A review, *Renew. Sustain. Energy Rev.* 16 (2012) 6303–6316. doi:10.1016/j.rser.2012.07.005.
- [50] R.R. Kumar, P.H. Rao, M. Arumugam, Lipid extraction methods from microalgae : a comprehensive review, *Front. Energy Res.* 2 (2015) 1–9. doi:10.3389/fenrg.2014.00061.
- [51] L. Chen, T. Liu, W. Zhang, X. Chen, J. Wang, Biodiesel production from algae oil high in free fatty acids by two-step catalytic conversion, *Bioresour. Technol.* 111 (2012) 208–214. doi:10.1016/j.biortech.2012.02.033.

-
- [52] S. Siva, C. Marimuthu, Production of biodiesel by transesterification of algae oil with an assistance of nano-CaO catalyst derived from egg shell, *Int. J. ChemTech Res.* 7 (2015) 2112–2116.
 - [53] V. Singh, F. Bux, Y.C. Sharma, A low cost one pot synthesis of biodiesel from waste frying oil (WFO) using a novel material, β -potassium dizirconate (β -K₂Zr₂O₅), *Appl. Energy.* (2016). doi:10.1016/j.apenergy.2016.02.135.
 - [54] M. Feyzi, L. Nourozi, M. Zakarianezhad, Preparation and characterization of magnetic CsH₂PW₁₂O₄₀/Fe–SiO₂ nanocatalysts for biodiesel production, *Mater. Res. Bull.* 60 (2014) 412–420. doi:10.1016/j.materresbull.2014.09.005.
 - [55] G. Baskar, R. Aiswarya, Biodiesel production from waste cooking oil using copper doped zinc oxide nanocomposite as heterogeneous catalyst, *Bioresour. Technol.* 188 (2015) 124–127. doi:<http://dx.doi.org/10.1016/j.biortech.2015.01.012>.
 - [56] M. Paul Abishek, J. Patel, A. Prem Rajan, Algae Oil: A Sustainable Renewable Fuel of Future., *Biotechnol. Res. Int.* 2014 (2014) 272814. doi:10.1155/2014/272814.
 - [57] P. Adewale, M.J. Dumont, M. Ngadi, Recent trends of biodiesel production from animal fat wastes and associated production techniques, *Renew. Sustain. Energy Rev.* 45 (2015) 574–588. doi:10.1016/j.rser.2015.02.039.
 - [58] J. Abraham, R.S. Kumar, F. Xavier, D. Mathew, A.R. Materials, H.F. Proper, J.E. Testi, K.S. An, A.D.B. R, Biodiesel Production from Broiler Chicken Waste, 9 (2015) 1154–1157.
 - [59] A. Demirbas, Biofuels securing the planet's future energy needs, *Energy Convers. Manag.* 50 (2009) 2239–2249. doi:10.1016/j.enconman.2009.05.010.
 - [60] M. B, Ö. MM, A.J. F, Some rape/canola seed oils: fatty acid composition and

- tocopherols., *Z Naturforsch C J Biosci.* 71 (2016) 73–77. doi:10.1515/znc-2016-0003.
- [61] G.A. Antova, M.I.A. Romova, Z.Y. Petkova, O.T. Teneva, M.P. Marcheva, Lipid composition of mustard seed oils (*Sinapis alba L.*), *Bulg. Chem. Commun.* 49 (2017) 55–60.
- [62] R.L. Wolff, C.C. Bayard, Fatty acid composition of some pine seed oils, *J Am Oil Chem Soc.* 72 (1995) 1043–1046.
- [63] F. Anwar, U. Rashid, S.A. Shahid, M. Nadeem, Physicochemical and Antioxidant Characteristics of Kapok (*Ceiba pentandra Gaertn.*) Seed Oil, *J Am Oil Chem Soc.* 91 (2014) 1047–1054. doi:10.1007/s11746-014-2445-y.
- [64] J.J. Woodford, C.M.A. Parlett, J.P. Dacquin, G. Cibin, A. Dent, J. Montero, K. Wilson, A.F. Lee, Identifying the active phase in Cs-promoted MgO nanocatalysts for triglyceride transesterification, *J. Chem. Technol. Biotechnol.* 89 (2014) 73–80. doi:10.1002/jctb.4098.
- [65] S. Koohikamali, C.P. Tan, T.C. Ling, Optimization of Sunflower Oil Transesterification Process Using Sodium Methoxide, *Sci. World J.* 475027 (2012). doi:10.1100/2012/475027.
- [66] S. Karthikumar, V. Ragavanandham, S. Kanagaraj, R. Manikumar, A. Asha, A. Achary, Preparation, characterization and engine performance characteristics of used cooking sunflower oil based bio-fuels for diesel engine, *Adv. Mater. Res.* Vols. (2014) 913–923. doi:10.4028/www.scientific.net/AMR.984-985.913.
- [67] M. Aarthy, P. Saravanan, M.K. Gowthaman, C. Rose, N.R. Kamini, Enzymatic transesterification for production of biodiesel using yeast lipases: An overview, *Chem. Eng. Res. Des.* 92 (2014) 1591–1601. doi:10.1016/j.cherd.2014.04.008.
- [68] U. Schuchardt, R. Sercheli, R. Matheus, Transesterification of Vegetable Oils : a

- Review General Aspects of Transesterification Transesterification of Vegetable Oils Acid-Catalyzed Processes Base-Catalyzed Processes, 9 (1998) 199–210.
- [69] I. Ambat, V. Srivastava, S. Iftekhar, E. et al Haapaniemi, Dual application of divalent ion anchored catalyst: biodiesel synthesis and photocatalytic degradation of carbamazepine, *Catal. Green Chem. Eng.* 2 (2019) 25–42. doi:<http://dx.doi.org/10.1615/CatalGreenChemEng.2019030878>.
- [70] G. Baskar, I.A.E. Selvakumari, R. Aiswarya, Bioresource Technology Biodiesel production from castor oil using heterogeneous Ni doped ZnO nanocatalyst, *Bioresour. Technol.* 250 (2018) 793–798. doi:[10.1016/j.biortech.2017.12.010](https://doi.org/10.1016/j.biortech.2017.12.010).
- [71] A. Bayat, M. Baghdadi, G.N. Bidhendi, Tailored magnetic nano-alumina as an efficient catalyst for transesterification of waste cooking oil_ Optimization of biodiesel production using response surface methodology.pdf, *Energy Convers. Manag.* 177 (2018) 395–405.
- [72] S. Dehghani, M. Haghghi, Sono-sulfated zirconia nanocatalyst supported on MCM-41 for biodiesel production from sunflower oil_ Influence of ultrasound irradiation power on catalytic properties and performance.pdf, *Ultrason. Sonochem.* 35 (2017) 142–151.
- [73] H. Nayebzadeh, M. Haghghi, N. et al Saghatoslami, Influence of carbon source content on the structure and performance of KOH/Ca₁₂Al₁₄O₃₃C nanocatalyst used in the transesterification reaction via microwave irradiation.pdf, *J. Alloys Compd.* 743 (2018) 672–681.
- [74] N. Rajput, Methods of preparation of nanoparticles- A review, *Int. J. Adv. Eng. Technol.* 7 (2015) 1806–1811.
- [75] C. a. Charitidis, P. Georgiou, M. a. Koklioti, A.-F. Trompeta, V. Markakis, Manufacturing nanomaterials: from research to industry, *Manuf. Rev.* 1 (2014) 11.

- doi:10.1051/mfreview/2014009.
- [76] K. Tahvildari, Y.N. Anaraki, R. Fazaeli, S. Mirpanji, E. Delrish, The study of CaO and MgO heterogenic nano-catalyst coupling on transesterification reaction efficacy in the production of biodiesel from recycled cooking oil., *Iran. J. Environ. Heal. Sci. Eng.* 13 (2015) 1–9. doi:10.1186/s40201-015-0226-7.
- [77] J. Haber, J.H. Block, B. Delmon, Manual of methods and procedures for catalyst characterization (Technical Report), *Pure Appl. Chem.* 67 (1995) 1257–1306. doi:10.1351/pac199567081257.
- [78] H. Nayebzadeh, N. Saghatoleslami, M. Tabasizadeh, Optimization of the activity of KOH/calcium aluminate nanocatalyst for biodiesel production using response surface methodology, *J. Taiwan Inst. Chem. Eng.* 68 (2016) 379–386. doi:10.1016/j.jtice.2016.09.041.
- [79] P. Praveen, G. Viruthagiri, S. Mugundan, N. Shanmugam, Structural , optical and morphological analyses of pristine titanium di-oxide nanoparticles-Synthesized via sol-gel route, *Spectrochim. Acta Part A Mol. Biomol. Spectrosc.* 117 (2013) 622–629.
- [80] Q. Meng, C. Qiu, G. et. al. Ding, Role of alkali earth metals over Pd/Al₂O₃ for decarbonylation of 5-hydroxymethylfurfural, *Catal. Sci. Technol.* 6 (2016) 4377–4388.
- [81] Z.A. Alothman, A Review: Fundamental Aspects of Silicate Mesoporous Materials, 5 (2016) 2874–2902. doi:10.3390/ma5122874.
- [82] Y. Zhang, D. Shao, J. Yan, X. Jia, Y. Li, P. Yu, T. Zhang, The pore size distribution and its relationship with shale gas capacity in organic-rich mudstone of Wufeng-Longmaxi Formations , Sichuan Basin , China, *J. Nat. Gas Geosci.* (2016) 1–8.

-
- [83] M.E. Borges, L. Hernández, J.L.G. Fierro, P. Esparza, Use of 3D printing for biofuel production: efficient catalyst for sustainable biodiesel production from wastes, *Clean Technol. Environ. Policy.* 19 (2017) 2113–2127. doi:10.1007/s10098-017-1399-9.
 - [84] C.A. Schwengber, H.J. Alves, R.A. et al. Schaffner, Overview of glycerol reforming for hydrogen production, *Renew. Sustain. Energy Rev.* 58 (2016) 259–266.
 - [85] J. Benemann, Microalgae for Biofuels and Animal Feeds, *Energies.* 6 (2013) 5869–5886. doi:10.3390/en6115869.
 - [86] A. Guldhe, F.A. Ansari, P. et al Singh, Heterotrophic cultivation of microalgae using aquaculture wastewater: A biorefinery concept for biomass production and nutrient remediation, *Ecol. Eng.* 99 (2017) 47–53. doi:<https://doi.org/10.1016/j.ecoleng.2016.11.013>.
 - [87] R. Kumar, P. Tiwari, S. Garg, Alkali transesterification of linseed oil for biodiesel production, *Fuel.* 104 (2013) 553–560. doi:10.1016/j.fuel.2012.05.002.
 - [88] M.H. Gargari, S.M. Sadrameli, Investigating continuous biodiesel production from linseed oil in the presence of a Co-solvent and a heterogeneous based catalyst in a packed bed reactor, *Energy.* 148 (2018) 888–895. doi:10.1016/j.energy.2018.01.105.
 - [89] C.B. Ezekannagha, C.N. Ude, O.D. Onukwuli, Optimization of the methanolysis of lard oil in the production of biodiesel with response surface methodology, *Egypt. J. Pet.* (2017). doi:10.1016/j.ejpe.2016.12.004.
 - [90] V.T. Duong, F. Ahmed, S.R. Thomas-hall, S. Quigley, High protein- and high lipid-producing microalgae from northern Australia as potential feedstock for animal feed and biodiesel, *Front. Bioeng. Biotechnol.* 3 (2015) 1–7.

doi:10.3389/fbioe.2015.00053.

- [91] T. Marika, K. Chopra, K. Silja, V. Kalle, S.A. K, S. Suvigya, O. Anne, R. Martin, Conversion of biowaste leachate to valuable biomass and lipids in mixed cultures of *Euglena gracilis* and chlorophytes, *Algal Res.* 35 (2018) 76–84.

Publication I

I. Ambat, V. Srivastava, E. Haapaniemi, M. Sillanpää

**Application of Potassium Ion Impregnated Titanium Dioxide as Nanocatalyst for
Transesterification of Linseed Oil**

Reprinted with permission from

Energy Fuels

Vol. 32, pp. 11645-11655

© 2018, ACS

Application of Potassium Ion Impregnated Titanium Dioxide as Nanocatalyst for Transesterification of Linseed Oil

Indu Ambat,*[†] Varsha Srivastava,[†] Esa Haapaniemi,[‡] and Mika Sillanpää[†]

[†]Department of Green Chemistry, School of Engineering Science, Lappeenranta University of Technology, Sammonkatu 12, FI-50130 Mikkeli, Finland

[‡]Department of Organic Chemistry, University of Jyväskylä, FI-40014 Jyväskylän, Finland

See https://pubs.acs.org/sharingguidelines for options on how to legitimately share published articles.

ABSTRACT: The current work comprises the investigation of biodiesel production from linseed oil using TiO_2 and a potassium L-tartrate monobasic ($\text{C}_4\text{H}_5\text{KO}_6$)-modified TiO_2 nanocatalyst. Different amounts of $\text{C}_4\text{H}_5\text{KO}_6$ were considered for TiO_2 modification. The nanocatalyst $\text{TiO}_2-0.5\text{C}_4\text{H}_5\text{KO}_6$ (1:0.5 molar ratio) showed the best conversion rate for biodiesel production. The nanocatalyst was characterized by FTIR, XRD, TEM, BET, and XPS, and the Hammett indicator–benzenecarboxylic acid titration method was used for basicity measurement. The biodiesel was characterized by GC-MS and ^1H and ^{13}C NMR. Furthermore, the optimum reaction parameters for transesterification reaction were analyzed, and the yield was determined by GC-MS and ^1H NMR. The maximum yield of 98.5% was obtained with 6 wt% catalyst amount and 1:6 oil-to-methanol ratio at 60 °C for 3 h. The properties of biodiesel obtained from linseed oil were determined using the EN 14214/ASTM D6751 method. The reusability of the catalyst was tested up to five cycles and showed promising results.

1. INTRODUCTION

The energy crisis is a major issue confronting the whole world due to the dependency on conventional energy reserves.^{1,2} Ongoing increases in population result in the growing utilization of fossil fuels, which leads to two major issues: direct environmental pollution and global warming.^{2–4} Biodiesel is a fatty acid methyl ester (FAME) compound that has been suggested as a suitable alternative fuel, produced by the transesterification of fats/oils using alcohol—mainly methanol or ethanol—with a suitable catalyst.^{5–8} FAMEs can act as renewable sources of energy due to their features such as biodegradability and eco-friendly nature.⁹

Generally, vegetable oils, algal oils, and animal fat/oils are used as feedstock for biodiesel production.^{10–12} It is preferred that the feedstock used for biodiesel production be less expensive and not in competition for food production.^{13,14} Hence, linseed oil was tested as feedstock for biodiesel production. The oil content of linseed oil is similar to that of edible oils such as rapeseed oil and higher than that of soybean and sunflower oils. Moreover, the linolenic acid content ($\text{C}_{18:3}$) in linseed oil is higher compared to other acids in other oils.¹³ Kumar et al.¹⁵ reported 88–96% conversion efficiency of linseed oil with alkali transesterification. Gargari and Sadrameli¹⁶ observed that FAMEs yield up to 98.08% biodiesel in the presence of diethyl ether as a co-solvent and calcium oxide as a heterogeneous-based catalyst in a fixed-bed reactor.

The transesterification reaction is commonly conducted using a homogeneous catalyst, heterogeneous catalyst, or biocatalyst.^{8,9,13,17} Heterogeneous nanocatalysts have received great attraction in the field of biodiesel production due to features such as increased stability, activity, and selectivity.^{5,17,18} Previous research reports suggest that potassium-doped metal oxides provide promising results in biodiesel production; for example, potassium doped on titanium dioxide (TiO_2 , also called titania) using potassium bitartrate as

precursor resulted in good biodiesel yields with both edible and non-edible oils.^{3,19–22} Additionally, TiO_2 alone serves as a catalyst for transesterification and also acts as a good support in heterogeneous catalysis due to its high chemical stability, thermal constancy, and commercial availability.^{7,23} Therefore, potassium impregnated on titania using potassium bitartrate as precursor was used for biodiesel production from linseed oil.

In the present study we target the production of biodiesel from linseed oil using a heterogeneous nanocatalyst. The purpose of our work is to investigate the effect of heterogeneous nanocatalysis on linseed oil, which has not been explored yet. Hence potassium impregnated TiO_2 as a nanocatalyst was synthesized. The effect of $\text{C}_4\text{H}_5\text{KO}_6$ loading on catalytic activity was also investigated. The $\text{TiO}_2-0.5\text{C}_4\text{H}_5\text{KO}_6$ nanocatalyst showed significant conversion of linseed oil to biodiesel. Characterization of the synthesized nanocatalyst was done using Fourier transform infrared spectroscopy (FTIR), scanning electron microscopy (SEM), X-ray diffraction (XRD), X-ray photoelectron spectroscopy (XPS), transmission electron microscopy (TEM), atomic-force microscopy (AFM), and Brunauer–Emmett–Teller (BET) analysis. Further, the nanocatalyst was used for transesterification reactions, where production conditions such as temperature, molar ratio of oil to methanol, catalyst amount, and time were optimized. The biodiesel was analyzed by gas chromatography–mass spectrometry (GC-MS) and ^1H and ^{13}C nuclear magnetic resonance (NMR) spectroscopy.

2. MATERIALS AND METHODS

2.1. Material. Linseed oil (acid value = 0.606 mg KOH/g, average molecular weight = 887.9354), titanium dioxide nanopowder (TiO_2),

Received: September 21, 2018

Revised: October 23, 2018

Published: October 27, 2018

potassium bitartrate ($C_4H_5KO_6$), and methanol were purchased from Sigma-Aldrich. All the chemicals used were of analytical grade.

2.2. Synthesis and Screening of Catalyst. The TiO_2 modified by $C_4H_5KO_6$ was synthesized by an impregnation method. In this method, catalysts were prepared by mixing $TiO_2/C_4H_5KO_6$ in molar ratios of 1:0.25, 1:0.5, 1:0.75, and 1:1. The solutions were stirred continuously for 5 h and subsequently dried at 90 °C. Finally, dried samples were calcined at 500 °C in a muffle furnace (Naberthermb180). The unmodified TiO_2 and the series of catalysts synthesized by mixing of $TiO_2/C_4H_5KO_6$ in various molar ratios were screened for fatty acid methyl ester (FAME) production. Furthermore, a series of the catalysts was synthesized by doping various concentrations of potassium ion to titania to allow us to investigate the capability of different catalysts in the transesterification of linseed oil as well as to reveal the effect of $C_4H_5KO_6$ loading on the catalytic activity of TiO_2 .

2.3. Characterization of Catalyst. FTIR spectra of the catalysts were recorded using a Bruker Vertex 70 spectrometer in the range of 400–4000 cm⁻¹. TEM images of the samples were obtained using a Hitachi HT7700 transmission electron microscope. The nanocatalyst was dispersed in ethanol with the help of sonication in order to obtain dispersed particles in suspension. A drop of the suspension was added to a carbon-coated copper grid. SEM images of catalysts were recorded using a Hitachi SU3500 scanning electron microscope to examine sample spread on colloidal graphite with 5 kV accelerating voltage. XRD patterns were obtained with a PANalytical Empyrean X-ray diffractometer over a 2θ range of 10–120° with a Co $K\alpha$ X-ray source of 0.178 nm at 40 mA and 40 kV. The surface area of the catalysts was determined using Micromeritics Tristar II plus instrument for BET analysis. The catalyst samples were degassed at 80 °C overnight to remove moisture from the samples.

AFM images of the nanocatalysts were collected using a Park Systems NX10 atomic force microscope for better illustration. The surface composition and the binding energies of elements in the nanocatalysts were examined using an ESCALAB 250 X-ray photoelectron spectrometer with an Al K X-ray source of 1486.6 eV. The basicity of the catalysts was tested with help of a titration method. Hammett indicator–benzenecarboxylic acid (0.02 mol L⁻¹ anhydrous methanol solution) titration was performed to determine the basic strength of the synthesized catalysts using Hammett indicators such as neutral red (H_{6.8}), bromothymol blue (H_{7.2}), phenolphthalein (H_{9.8}), and 2,4-dinitroaniline (H₁₅).^{24,25}

2.4. Biodiesel Production. Linseed oil was used as feedstock for biodiesel production. The reaction for screening the different catalysts was performed by mixing oil and methanol in a 1:6 molar ratio and with 6 wt% of each catalyst. All the reactions were carried out in a 250 mL three-neck round-bottom flask with mechanical stirrer and reflux condenser at 60 °C for 3 h. After the reaction, the samples were centrifuged, resulting in three separate phases: catalyst at the bottom, methyl ester at the top, and glycerol in the middle. The catalyst was isolated, excess methanol was removed by an evaporator, and the obtained biodiesel was analyzed by GC-MS (Agilent-GC6890N, MS 5975) with an Agilent DB-wax FAME analysis GC column of dimensions 30 m, 0.25 mm, 0.25 μm. The inlet temperature was 250 °C, and the oven temperature was programmed at 50 °C for 1 min, increasing at a rate of 25 °C/min to 200 °C, and then at 3 °C/min to 230 °C, where it was held for 23 min. The concentration and presence of ester carbonyl groups of FAMEs were determined by ¹H and ¹³C NMR at 400 MHz with CDCl₃ as solvent. The percentage of linseed oil conversion to FAME (C %) was determined by the equation given below:¹³

$$C(\%) = \frac{2 \times \text{integration value of protons of methyl ester}}{3 \times \text{integration value of methyl protons}} \times 100 \quad (1)$$

3. RESULT AND DISCUSSION

3.1. Screening and Selection of Nanocatalyst for Transesterification of Linseed Oil. The nanocatalyst for biodiesel production from linseed oil was selected by screening the catalytic activity of different catalysts such as TiO_2 and $TiO_2/C_4H_5KO_6$ with 1:0.25, 1:0.5, 1:0.75, and 1:1 molar ratios at 60 °C with 6 wt% of each catalyst and 1:6 oil-to-methanol molar ratio for 3 h. The catalyst composition, surface area, total basicity of synthesized catalyst, and catalytic performance of each catalyst are summarized in Table 1. The basic nature and

Table 1. Efficiency of Various Catalysts for Transesterification of Linseed Oil

catalyst	molar ratio	total basicity (mmol g ⁻¹)	BET surface area (m ² g ⁻¹)	FAME conversion (%)
TiO_2	—	0.1	37.58	no reaction
$TiO_2/C_4H_5KO_6$	1:0.25	0.3	25.43	<5
$TiO_2/C_4H_5KO_6$	1:0.5	1.80	16.25	98.54
$TiO_2/C_4H_5KO_6$	1:0.75	1.56	10.65	80.10
$TiO_2/C_4H_5KO_6$	1:1	0.89	7.37	50.88

total basicity of the synthesized catalyst were determined by Hammett indicator–benzenecarboxylic acid titration.^{8,24–26} The TiO_2 showed no reaction, probably due to its lower basic strength. The basicity of the catalyst increases with increasing loading amount of $C_4H_5KO_6$, which increases the activity of the catalyst. Further increase in the amount of $C_4H_5KO_6$ after the optimum value reduces the catalytic activity, possibly due to a decrease in both surface area and basicity. The $TiO_2/C_4H_5KO_6$ with a 1:0.5 ratio showed significant conversion of biodiesel from linseed oil due to the optimum loading of $C_4H_5KO_6$. Therefore, $TiO_2-0.5C_4H_5KO_6$ was selected for the optimization of reaction parameters for higher yielding production of biodiesel.

3.2. Characterization of Catalyst. The FTIR spectra of unmodified TiO_2 and $TiO_2-0.5C_4H_5KO_6$ are shown in Figure 1. The FTIR spectrum of $TiO_2-0.5 C_4H_5KO_6$ shows new peaks at 895.82, 1368.324, and 1458.00 cm⁻¹. New peaks could be due to the integration of potassium ions into the TiO_2 structure. However, the spectrum also shows a broad band in range of 2900–3300 cm⁻¹ due to stretching vibrations of the Ti–O–K bond.^{3,19}

Figure 2 shows the XRD pattern of both unmodified TiO_2 and $TiO_2-0.5C_4H_5KO_6$. XRD analysis of unmodified TiO_2 depicts a good match to standard reference codes ICSD: 154607 and ICDD: 98-015-4607. The XRD pattern of potassium–titanium–oxide obtained as result of modification of TiO_2 with 0.5 molar $C_4H_5KO_6$ provides a consistent harmony to reference standard code ICSD: 73465, ICDD: 98-007-3465. The crystallographic parameters of synthesized catalysts are shown in Table 2.

Surface morphology of catalyst was analyzed by SEM. Figure 3 shows the SEM images of unmodified TiO_2 and $TiO_2-C_4H_5KO_6$ (1:0.5 molar ratio) with 5 kV magnification. By comparing two images, it was observed that there was a significant difference in the structure of $TiO_2-C_4H_5KO_6$ (1:0.5 molar ratio) due to the doping of potassium. The unmodified TiO_2 catalyst looks fluffier and comparatively uniform particles with some aggregates. It is very clear from SEM image of $TiO_2-0.5C_4H_5KO_6$ that flat surface of different shapes was dispersed in the catalytic material indicates a different

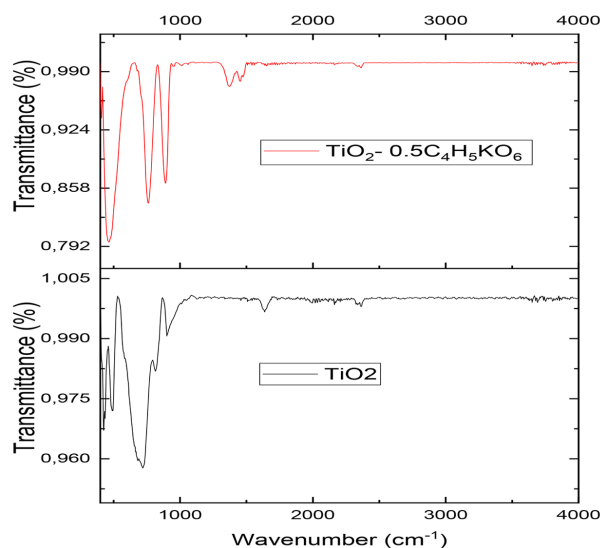


Figure 1. FTIR spectra of TiO_2 (unmodified) and $\text{TiO}_2-\text{C}_4\text{H}_5\text{KO}_6$ (1:0.5 molar ratio).

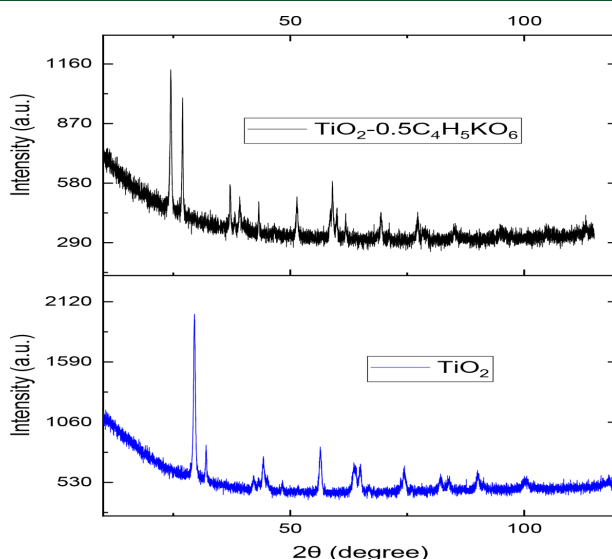


Figure 2. XRD pattern of TiO_2 (unmodified) and $\text{TiO}_2-\text{C}_4\text{H}_5\text{KO}_6$ (1:0.5 molar ratio).

Table 2. Crystallographic Parameters of Unmodified TiO_2 and $\text{TiO}_2-0.5\text{C}_4\text{H}_5\text{KO}_6$

catalyst	crystal structure	a (nm)	b (nm)	c (nm)	α (deg)	β (deg)	γ (deg)
TiO_2	tetragonal	0.379	0.379	0.941	90	90	90
$\text{TiO}_2-0.5\text{C}_4\text{H}_5\text{KO}_6$	tetragonal	1.02	1.02	0.296	90	90	90

morphology of particles due to impregnation of potassium particles on the surface of TiO_2 (Figure 3b).

The TEM images of unmodified TiO_2 and $\text{TiO}_2-\text{C}_4\text{H}_5\text{KO}_6$ (1:0.5 molar ratio) are depicted in Figure 4. The unmodified

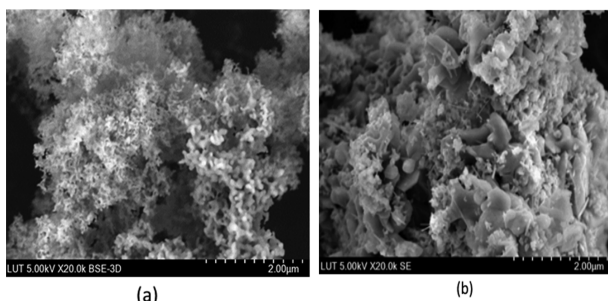


Figure 3. SEM images of (a) TiO₂ (unmodified) and (b) TiO₂-C₄H₅KO₆ (1:0.5 molar ratio).

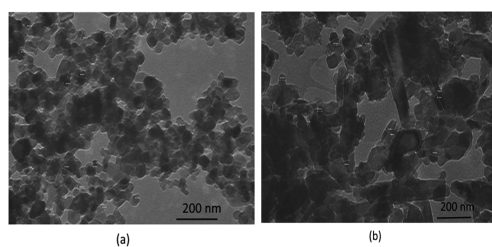


Figure 4. TEM images of (a) TiO₂ (unmodified) and (b) TiO₂-C₄H₅KO₆ (1:0.5 molar ratio).

TiO₂ catalyst has a particle size of 23–46.7 nm, whereas TiO₂-C₄H₅KO₆ (1:0.5 molar ratio) modified catalyst has a particle size of 26–179 nm. The size of the particles in the catalyst was confirmed from the TEM images. Moreover, the TEM image of unmodified TiO₂ also shows a large quantity of well distributed uniform particle with agglomerates, while TEM studies of TiO₂-0.5C₄H₅KO₆ show a long, flat structure in addition to uniform particles with aggregates. SEM results also match with TEM images.

The AFM images of TiO₂ and TiO₂-C₄H₅KO₆ are portrayed in Figure 5 with scan rate and amplitude of 0.26 Hz and 15.04 × 10³ nm, respectively. The AFM images also agree with the benefit of integration of potassium ions into

TiO₂ nanocatalyst. All the dimensions are shown in nanoscale. Particle dimensions measured from the AFM images agree well with TEM analysis and support potassium loading. All the catalyst characterization confirms the impregnation of potassium ion to titania.

The surface area, pore volume, and pore size were determined by BET analysis. Surface area analysis of unmodified TiO₂ and TiO₂-0.5 C₄H₅KO₆ using the BET method is shown in Table 3. The decrease in porosity of TiO₂ modified with C₄H₅KO₆ catalyst was due to the insertion of potassium ions.²⁵ Even though there is a decrease in porosity and surface area, there is an increase in catalytic activity for transesterification, which is seen in Table 1. This may be due to the strength of basic sites in the catalyst.²⁵ The N₂ adsorption-desorption isotherm for TiO₂ and TiO₂ modified with C₄H₅KO₆ from BET analysis is given in Figure 6. The hysteretic loop isotherm indicates the presence of mesoporous materials.

XPS was applied to examine the surface properties and binding energies (BEs) of elements in unmodified TiO₂ and TiO₂-C₄H₅KO₆ (1:0.5 molar ratio). The chemical environment of Ti, O, and K was simulated by Gaussian curve-fitting of the Ti 2p, K 2p, and O 1s spectra of unmodified TiO₂ and TiO₂-0.5C₄H₅KO₆. Figure 7 depicts XPS fitted spectra of unmodified TiO₂ and TiO₂-0.5C₄H₅KO₆ nanocatalyst. Both unmodified TiO₂ and TiO₂-0.5C₄H₅KO₆ give Ti 2p signals with two peaks at BEs of 463.66 and 457.96 eV, assigned to Ti

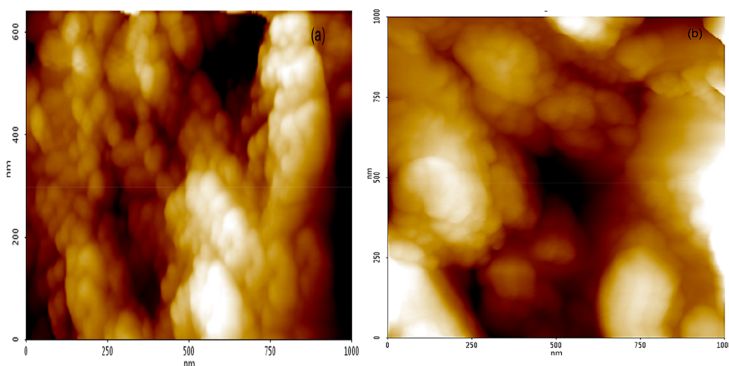


Figure 5. AFM images of (a) TiO₂ (unmodified) and (b) TiO₂-C₄H₅KO₆ (1:0.5 molar ratio).

Table 3. Results of Brunauer–Emmett–Teller Surface Area Analysis

parameters	unmodified TiO_2	$\text{TiO}_2\text{--C}_4\text{H}_5\text{KO}_6$ (1:0.5 molar ratio)
Surface area		
BET surface area (m^2/g)	37.58	16.25
BJH adsorption cumulative surface area of pores (m^2/g)	34.32	12.49
BJH desorption cumulative surface area of pores (m^2/g)	34.41	12.75
Pore volume		
single-point adsorption total pore volume of pores (cm^3/g)	0.06	0.03
BJH adsorption cumulative volume of pores (cm^3/g)	0.10	0.09
BJH desorption cumulative volume of pores (cm^3/g)	0.11	0.09
Pore size		
adsorption average pore width (\AA)	64.31	72.43
BJH adsorption average pore diameter (\AA)	122.41	296.76
BJH desorption average pore diameter (\AA)	129.24	291.11

$2p_{1/2}$ and $2p_{3/2}$, respectively. The BE gap between these two core-level orbitals suggests that the chemical valence state of Ti in the synthesized nanocatalyst is +4. The O 1s spectra of unmodified TiO_2 and $\text{TiO}_2\text{--}0.5\text{C}_4\text{H}_5\text{KO}_6$ show BE = 530.1 eV, which corresponds to O^{2+} forming an oxide with the metal.²⁷ Figure 7b represents K 2p with BE = 292.37 and 294.97 eV, which are assigned to $2p_{3/2}$ and $2p_{1/2}$ in the K–O group of $\text{TiO}_2\text{--}0.5\text{C}_4\text{H}_5\text{KO}_6$.²⁸

3.3. Characterization of Biodiesel. The FAME made from the linseed oil was characterized by GC-MS, ^1H NMR, and ^{13}C NMR. The quality of the produced biodiesel was tested using the EN 14214/ASTM D6751 method.

The chemical composition of biodiesel was demonstrated by comparison of the GC-MS chromatogram with the National Institute of Standards and Technology (NIST) 2014 MS library. The components of biodiesels obtained after transesterification of linseed oil with $\text{TiO}_2\text{--}0.5\text{C}_4\text{H}_5\text{KO}_6$ were identified with the help of a library match, as represented in Table 4.

The analysis of FAME from linseed oil was conducted by ^1H and ^{13}C NMR spectroscopy. The biodiesel yield was calculated

using eq 1, which was already discussed above. With the help of ^1H NMR, the FAME conversion percentage of the sample obtained after transesterification with $\text{TiO}_2\text{--}0.5\text{C}_4\text{H}_5\text{KO}_6$ was found to be 98.5%. Figure 8 illustrates the ^1H and ^{13}C NMR spectra of the FAME sample obtained with help of $\text{TiO}_2\text{--}0.5\text{C}_4\text{H}_5\text{KO}_6$ catalyst. These spectra help to characterize the FAME and can be used to confirm the existence of methyl esters in the biodiesel. Moreover, the proposed catalyst resulted in better conversion of linseed oil to biodiesel in comparison with previously reported studies using alkali as well as CaO solid catalysts.^{15,16}

In ^1H NMR spectra, a signal at 3.65 ppm indicates a methoxy group (A_{ME}) of FAMEs, and a signal at 2.28 ppm corresponds to a methylene group (A_{CH_2}). The presence of these signals in the biodiesel sample verifies the presence of methyl ester. Apart from the signal used for the quantification, there are other identifiable peaks, such as a signal at 0.86–0.87 ppm for $\text{CH}_2\text{--CH}_3$ or for the latter methyl group. The peaks in the range of 1.24–2.34 ppm represent CH_2 (methylenic group). The signal at 5.3 ppm indicates the presence of $\text{CH}=\text{CH}$ (double bond) groups or olefinic groups.^{29–31} In ^{13}C NMR spectra, signals at 174.25 and 51.35 ppm indicate ester carbonyl $-\text{COO}-$ and C=O , respectively. The unsaturation in the biodiesel sample was confirmed by the presence of signals at 131.88 and 127.05 ppm. In addition to these signals, there are other signals at 14.03 and 14.19 ppm, indicating the presence of terminal $-\text{CH}_3$ groups. The presence of a $-\text{CH}_2$ group was revealed by signals in the region of 22–34 ppm.²⁹

3.4. Influence of Various Parameters on Biodiesel Production.

The yield of biodiesel depends on reaction conditions such as catalyst amount, oil-to-methanol ratio, temperature, and time (Figure 9). Based on the preliminary screening of catalysts, $\text{TiO}_2\text{--C}_4\text{H}_5\text{KO}_6$ (1:0.5 molar ratio) was found to be an efficient catalyst for the conversion of linseed oil to FAME. The optimum reaction conditions for higher conversion of linseed oil to biodiesel using $\text{TiO}_2\text{--}0.5\text{C}_4\text{H}_5\text{KO}_6$ were determined by a series of transesterification reactions.

3.4.1. Catalyst Amount (wt%). The influence of catalyst concentration on transesterification was studied by performing reactions at various catalyst concentration from 3 wt% to 12 wt % of the oil. A 98.5% biodiesel conversion was obtained within 3 h of reaction time at 60 °C by using 6 wt% catalyst and 1:6 oil-to-methanol molar ratio (Figure 9a). The conversion of oil to biodiesel depends on the catalyst amount: if the catalyst

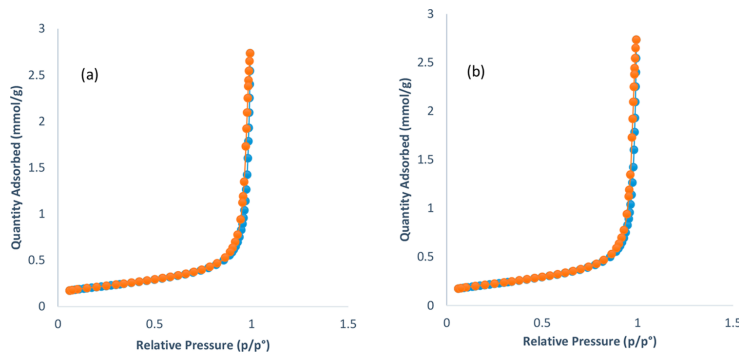


Figure 6. N_2 adsorption–desorption isotherms of (a) TiO_2 (unmodified) and (b) $\text{TiO}_2\text{--C}_4\text{H}_5\text{KO}_6$ (1:0.5 molar ratio).

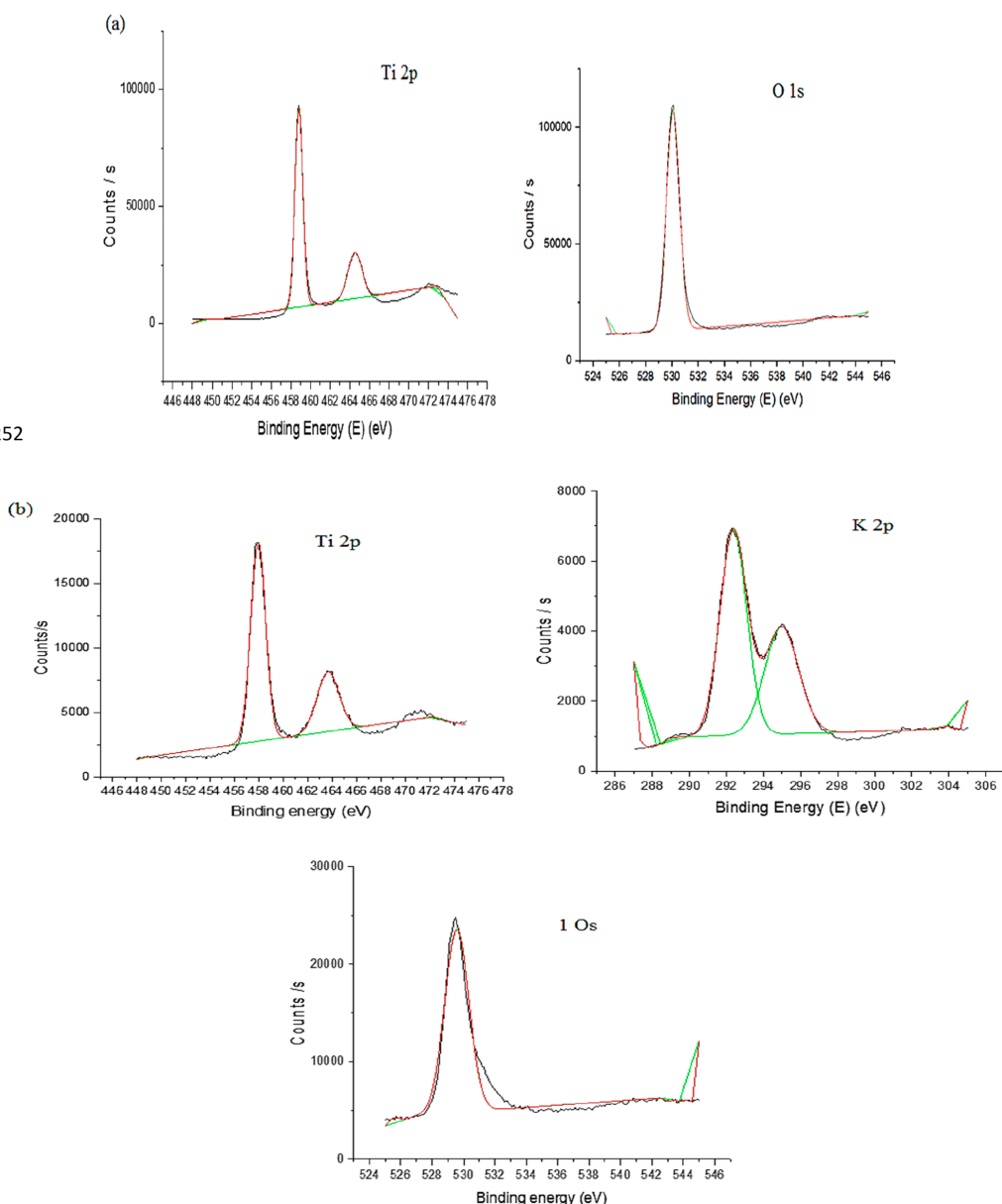


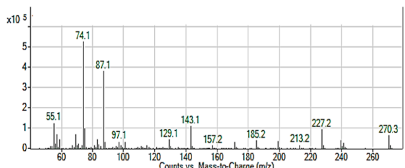
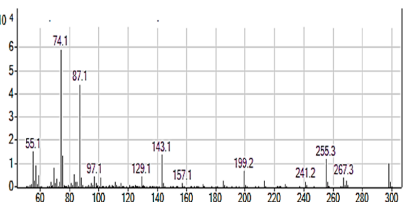
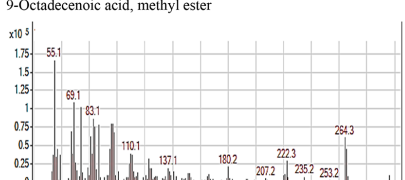
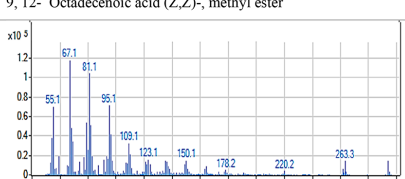
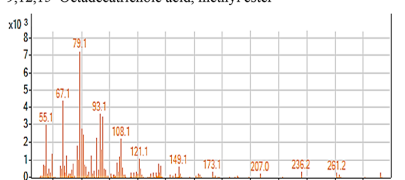
Figure 7. XPS spectra of (a) TiO_2 (unmodified) and (b) $\text{TiO}_2-\text{C}_4\text{H}_5\text{KO}_6$ (1:0.5 molar ratio).

amount is lower than the optimum concentration, there is a reduction in FAME conversion due to a decrease in the availability of active sites and hindrance to phase separation.^{19,25,32}

3.4.2. Oil-to-Methanol Molar Ratio. Figure 9b depicts the progressive increase in biodiesel conversion when the oil-to-

methanol molar ratio was increased from 1:3 to 1:6. The reaction was carried out at 6 wt% catalyst at 60 °C for 3 h of reaction time. The biodiesel conversion was negatively affected by increasing the methanol concentration above the optimum value, which was due to the increased solubility of glycerol in the ester phase, resulting in difficulty in separation of biodiesel.

Table 4. Composition of Biodiesel Attained after Transesterification with TiO_2 –0.5 $\text{C}_4\text{H}_5\text{KO}_6$

Peak	FAME		Compound name & mass spectrum
	Retention time (min)	Library match (%)	
1	8.38	91.2	Hexadecanoic acid, methyl ester 
2	9.89	93.6	Methyl stearate 
3	10.09	94	9-Octadecenoic acid, methyl ester 
6	10.48	94.3	9, 12- Octadecenoic acid (<i>Z,Z</i>)-, methyl ester 
7	11.19	92.9	9,12,15 Octadecatrienoic acid, methyl ester 

It may also favor the reverse reaction over the production of biodiesel.^{33,34}

3.4.3. Temperature. The effect of temperature on biodiesel yield was investigated by conducting the reaction at various

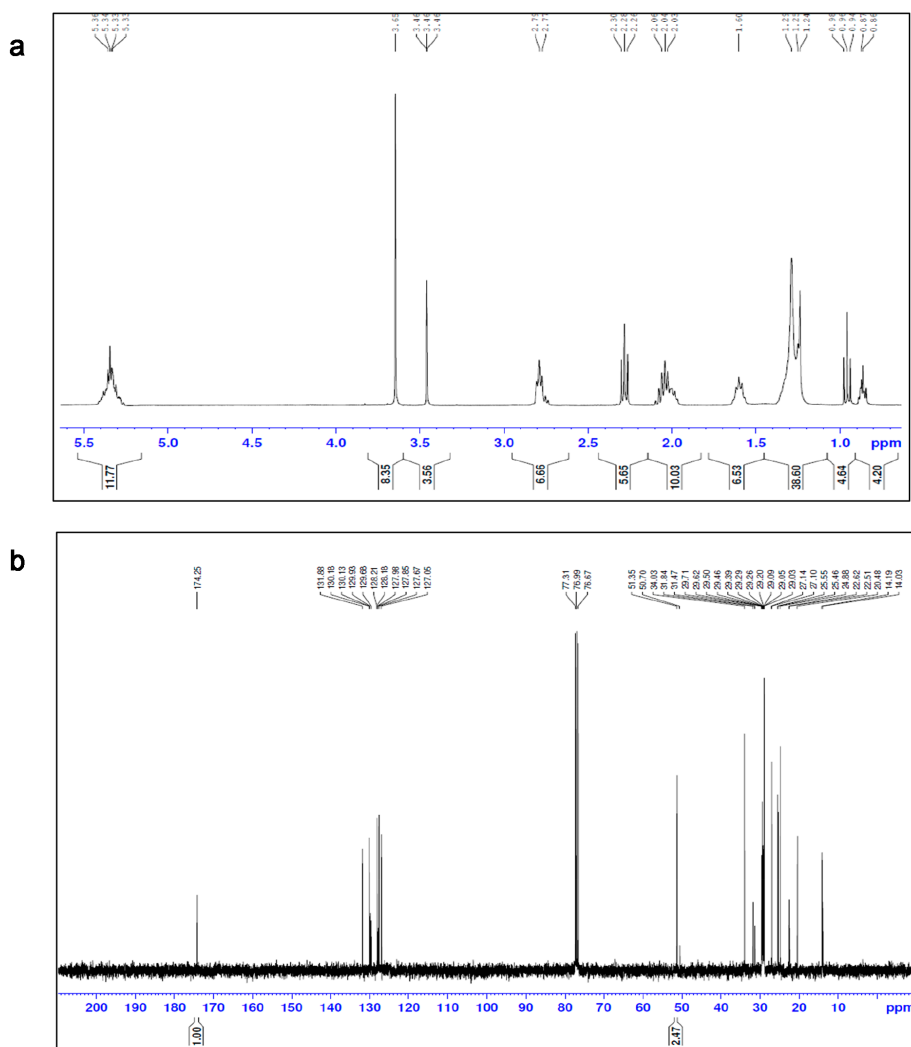


Figure 8. (a) ¹H and (b) ¹³C NMR spectra for the biodiesel sample obtained with TiO₂-0.5C₄H₉KO₆.

temperatures using 6 wt% catalyst and 1:6 oil-to-methanol molar ratio for 3 h reaction time (Figure 9c). The FAME conversion increased significantly up to 60 °C, which resulted in the optimum yield of FAME. After 60 °C, biodiesel conversion decreased with increasing temperature, which is due to the fact that elevated temperature favors vaporization of methanol.^{25,35,36}

3.4.4. Time. The influence of reaction time on the transesterification reaction was examined by performing reactions for different time intervals using 6 wt% catalyst and 1:6 oil-to-methanol molar ratio at 60 °C as depicted in Figure 9d. The percentage of FAME conversion rose with the increase in reaction time up to 180 min, where it reached its maximum.

After 180 min, instead of an increase in the yield of biodiesel, reduction in ester content with an increase in reaction time was observed. This is due to the reversible nature of the transesterification reaction. After a prolonged reaction time, backward reaction/reverse of the transesterification reaction is favored, which leads to the hydrolysis of esters.^{35,37}

3.5. Properties of Synthesized Biodiesel from Linseed Oil. The properties of linseed oil methyl esters were determined using the EN 14214/ASTM D6751 method as shown in Table 5. All these parameters play important roles in biodiesel quality. The acid value of linseed oil methyl ester was found to be 0.3 mg KOH/g, within the limits of the EN ISO method. Increases in the acid value can create issues like

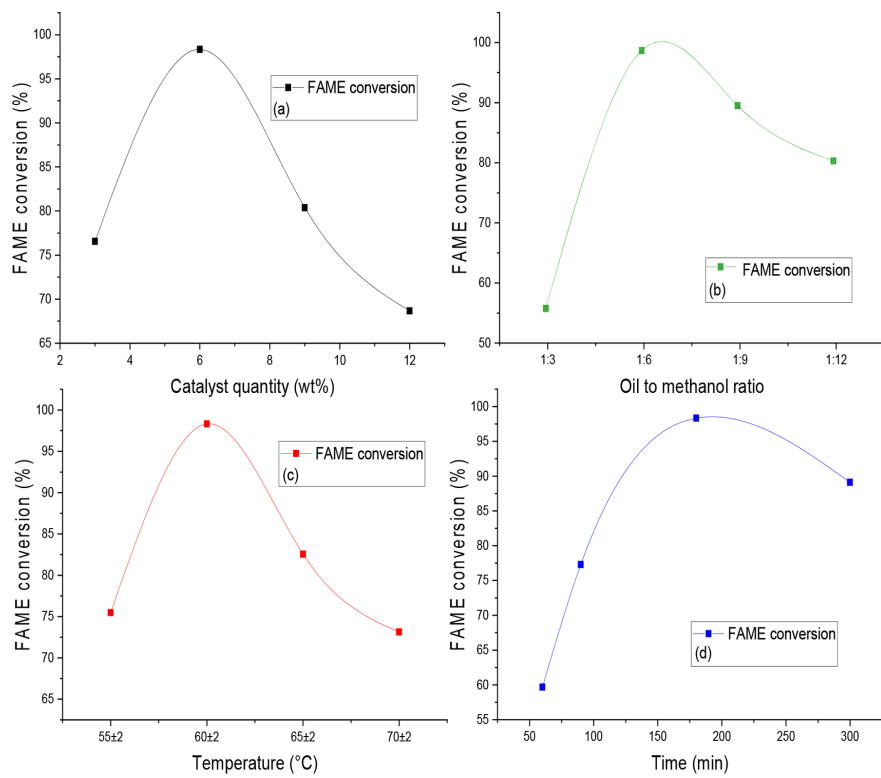


Figure 9. Influence of reaction conditions on biodiesel yield: (a) catalyst amount, (b) oil-to-methanol molar ratio, (c) reaction temperature, and (d) reaction time.

Table 5. Properties of Linseed Oil Methyl Esters^a

property	EN 14214 test method	limits	value for methyl ester from linseed oil
acid value (mg KOH/g)	Pr EN 14104	0.5 max	0.3
density at 15 °C (kg/m ³)	EN ISO 12185	860–900	891.52
kinematic viscosity at 40 °C (mm ² /s)	EN ISO 3104	3–5	3.5709
flash point (°C)	EN ISO 2719	–	173 °C
cetane number	EN ISO 5165	≥51	57
cloud point (°C)	ASTM D2500	–	4
pour point (°C)	ISO 3016	–	2
calorific value (MJ/kg)	ASTM D6751	–	40.89

^aReaction conditions: TiO₂–0.5 C₄H₅KO₆ catalyst at 6 wt% concentration, 1:6 oil-to-methanol ratio, reaction temperature 60 °C, and reaction time 3 h.

corrosion of rubber parts of engines and filter clogging.³⁸ The other two important fuel parameters which influence the fuel injection operation are density and kinematic viscosity. Higher values of these parameters can adversely affect the fuel injection process and result in the formation of engine deposits.^{39,40} The density and kinematic viscosity of linseed

oil methyl esters were 891.52 kg/m³ and 3.5709 mm²/s, respectively. Another important parameter is the flash point, which indicates the minimum temperature at which fuel starts to ignite—it is important to know the flash point value for fuel handling and storage.⁴¹ The rest of the measured features, including calorific value, cloud point, cetane number, and pour point, are also within EN ISO/ASTM limits.

3.6. Reusability and Stability of Catalyst. The reusability of the catalyst makes the transesterification process cost-effective and more eco-friendly. Catalyst deactivation is mainly due to deposition of impurities, oil content, or thermal deactivation. Regeneration of the catalyst was usually attained with the help of suitable solvent washing and calcination.⁴² To analyze the reusability of TiO₂–0.5 C₄H₅KO₆ nanocatalyst, first it was separated from linseed oil methyl esters and glycerol. After transesterification, the separated catalyst was washed several times with heptane to remove impurities. The washed catalyst was dried at 90 °C and calcined at 500 °C for 3 h to reactivate it. The catalytic reusability of TiO₂–0.5 C₄H₅KO₆ over linseed oil using 6 wt% catalyst and 1:6 oil-to-methanol molar ratio within 180 min of reaction time at 60 °C is represented in Figure 10. Conversion of linseed oil to FAME decreased from 98.5% to 93.1% over five cycles.

The stability of the nanocatalyst after each cycle was evaluated by determining the leached metal ion concentration,

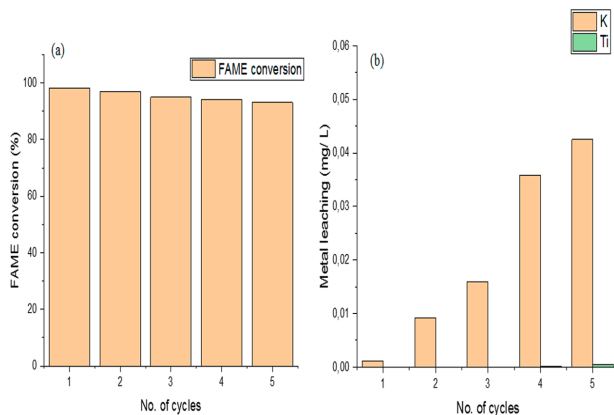


Figure 10. Reusability analysis of $\text{TiO}_2\text{-}0.5 \text{C}_4\text{H}_5\text{KO}_6$ catalyst up to five transesterification reactions.

as depicted in Figure 10. Metal concentration was measured with an Agilent 5110 inductively coupled plasma-optical emission spectrometry (ICP-OES) system. It was detected that from cycle 1 to cycle 5, the Li concentrations in solution were less than 0.043 mg/L. Moreover, Ti concentration in solution was null up to three cycles; after that, there was a slight leaching of Ti ions to solution which was less than 0.0004 mg/L.

4. CONCLUSION

Biodiesel was successfully synthesized from linseed oil with the help of $\text{TiO}_2\text{-}0.5 \text{C}_4\text{H}_5\text{KO}_6$ nanocatalyst. Modification of TiO_2 with $\text{C}_4\text{H}_5\text{KO}_6$ enhanced the properties of the nanocatalyst due to impregnation of potassium and showed better conversion in comparison to unmodified TiO_2 . FTIR, XRD, SEM, TEM, and AFM confirmed the integration of potassium ions into the TiO_2 nanostructure. The best activity was obtained at an optimum loading of $\text{C}_4\text{H}_5\text{KO}_6$ to TiO_2 in 0.5:1 molar ratio. The nanocatalyst yielded 98.5% fatty acid methyl ester using 6 wt% catalyst amount and 1:6 oil-to-methanol ratio at 60 °C within a reaction time of 3 h. The properties of this biodiesel, such as acid value, density, kinematic viscosity, and flash point, were within the EN 14214 limits. Thus, the FAME obtained was of good quality. All these results support the efficient performance of $\text{TiO}_2\text{-}0.5 \text{C}_4\text{H}_5\text{KO}_6$ as a catalyst for biodiesel production from linseed oil as a feedstock. The reusability of the catalyst also showed a promising result, which makes it economically feasible.

■ AUTHOR INFORMATION

Corresponding Author

*E-mail: indu.ambat@outlook.com.

ORCID

Indu Ambat: [0000-0002-8236-2050](https://orcid.org/0000-0002-8236-2050)

Notes

The authors declare no competing financial interest.

■ REFERENCES

- (1) Demirbas, A. Importance of biodiesel as transportation fuel. *Energy Policy* **2007**, *35*, 4661–4670.
- (2) Singh, S. P.; Singh, D. Biodiesel production through the use of different sources and characterization of oils and their esters as the substitute of diesel: A review. *Renewable Sustainable Energy Rev.* **2010**, *14*, 200–216.
- (3) Li, Y.; Qiu, F.; Yang, D.; Li, X.; Sun, P. Preparation, characterization and application of heterogeneous solid base catalyst for biodiesel production from soybean oil. *Biomass Bioenergy* **2011**, *35*, 2787–2795.
- (4) Rashtizadeh, E.; Farzaneh, F. Transesterification of soybean oil catalyzed by Sr-Ti mixed oxides nanocomposite. *J. Taiwan Inst. Chem. Eng.* **2013**, *44*, 917–923.
- (5) Hu, S.; Guan, Y.; Wang, Y.; Han, H. Nano-magnetic catalyst KF/CaO- Fe_3O_4 for biodiesel production. *Appl. Energy* **2011**, *88*, 2685–2690.
- (6) Liu, H.; Su, L.; Shao, Y.; Zou, L. Biodiesel production catalyzed by cinder supported CaO/KF particle catalyst. *Fuel* **2012**, *97*, 651–657.
- (7) Madhuviilaku, R.; Piraman, S. Biodiesel synthesis by $\text{TiO}_2\text{-ZnO}$ mixed oxide nanocatalyst catalyzed palm oil transesterification process. *Bioresour. Technol.* **2013**, *150*, 55–59.
- (8) Qiu, F.; Li, Y.; Yang, D.; Li, X.; Sun, P. Heterogeneous solid base nanocatalyst: Preparation, characterization and application in biodiesel production. *Bioresour. Technol.* **2011**, *102*, 4150–4156.
- (9) Kaur, M.; Ali, A. Lithium ion impregnated calcium oxide as nano catalyst for the biodiesel production from karanja and jatropha oils. *Renewable Energy* **2011**, *36*, 2866–2871.
- (10) Baskar, G.; Selvakumari, I. A. E.; Aiswarya, R. Biodiesel production from castor oil using heterogeneous Ni doped ZnO nanocatalyst. *Bioresour. Technol.* **2018**, *250*, 793–798.
- (11) Ding, H.; Ye, W.; Wang, Y.; Wang, X.; Li, L.; Liu, D.; et al. Process intensification of transesterification for biodiesel production from palm oil: Microwave irradiation on transesterification reaction catalyzed by acidic imidazolium ionic liquids. *Energy* **2018**, *144*, 957–967.
- (12) Teo, S. H.; Islam, A.; Taufiq-Yap, Y. H. Algae derived biodiesel using nanocatalytic transesterification process. *Chemical engineering research and design* **2016**, *111*, 362–370.
- (13) Ambat, I.; Srivastava, V.; Sillanpää, M. Recent advancement in biodiesel production methodologies using various feedstock: A review. *Renewable Sustainable Energy Rev.* **2018**, *90*, 356–369.
- (14) Aransiola, E. F.; Ojumu, T. V.; Oyekola, O. O.; Madzimbamuto, T. F.; Ikuo Omorogbe, D. I. O. A review of current technology for biodiesel production: State of the art. *Biomass Bioenergy* **2014**, *61*, 276–297.
- (15) Kumar, R.; Tiwari, P.; Garg, S. Alkali transesterification of linseed oil for biodiesel production. *Fuel* **2013**, *104*, 553–560.

- (16) Gargari, M. H.; Sadrameli, S. M. Investigating continuous biodiesel production from linseed oil in the presence of a Co-solvent and a heterogeneous based catalyst in a packed bed reactor. *Energy* **2018**, *148*, 888–895.
- (17) Akia, M.; Yazdani, F.; Motaei, E.; Han, D.; Arandiyani, H. A review on conversion of biomass to biofuel by nanocatalysts. *Biofuel Res. J.* **2014**, *1*, 16–25.
- (18) Hashmi, S.; Gohar, S.; Mahmood, T.; Nawaz, U.; Farooqi, H. Biodiesel Production by using CaO-Al₂O₃ Nano Catalyst. *Int. J. Eng. Res. Sci.* **2016**, *2*, 2395–6992.
- (19) Takase, M.; Chen, Y.; Liu, H.; Zhao, T.; Yang, L.; Wu, X. Biodiesel production from non-edible Silybum marianum oil using heterogeneous solid base catalyst under ultrasonication. *Ultrason. Sonochem.* **2014**, *21*, 1752–62.
- (20) Fadhil, A. B.; Al-tikriti, E. T. B.; Khalaf, A. M. Transesterification of non-edible oils over potassium acetate impregnated CaO solid base catalyst. *Fuel* **2018**, *234*, 81–93.
- (21) Fadhil, A. B.; Aziz, A. M.; Altamer, M. H. Optimization of methyl esters production from non-edible oils using activated carbon supported potassium hydroxide as a solid base catalyst. *Arab J. Basic Appl. Sci.* **2018**, *25*, 56–65.
- (22) Buasri, A.; Worawanitchaphong, P.; Trongyong, S.; Loryuenyong, V. Utilization of Scallop Waste Shell for Biodiesel Production from Palm Oil - Optimization Using Taguchi Method. *APCBE Proc.* **2014**, *8*, 216–221.
- (23) Bagheri, S.; Julkapli, N. M.; Hamid, S. B. A. Titanium Dioxide as a Catalyst Support in Heterogeneous Catalysis. *Sci. World J.* **2014**, *2014*, 727496.
- (24) Thitsartarn, W.; Kawi, S. An active and stable CaO – CeO₂ catalyst for transesterification of oil to biodiesel. *Green Chem.* **2011**, *13*, 3423–3430.
- (25) Singh, V.; Bux, F.; Sharma, Y. C. A low cost one pot synthesis of biodiesel from waste frying oil (WFO) using a novel material, β -potassium dizirconate (β -K₂Zr₂O₅). *Appl. Energy* **2016**, *172*, 23–33.
- (26) Yan, S.; Kim, M.; Salley, S. O.; Ng, K. Y. S. Oil transesterification over calcium oxides modified with lanthanum. *Appl. Catal., A* **2009**, *360*, 163–170.
- (27) Wang, X.; Xiang, Q.; Liu, B.; Wang, L.; Luo, T.; Chen, D.; Shen, G. TiO₂ modified FeS Nanostructures with Enhanced Electrochemical Performance for Lithium-Ion Batteries. *Sci. Rep.* **2013**, *3*, 2007.
- (28) Hu, S.; Li, F.; Fan, Z.; Wang, F.; Zhao, Y.; Lv, Z. Band gap tunable potassium doped graphitic carbon nitride with enhanced mineralization ability. *Dalton Trans.* **2015**, *44*, 1084–1092.
- (29) Tariq, M.; Ali, S.; Ahmad, F.; Ahmad, M.; Zafar, M.; Khalid, N.; et al. Identification, FT-IR, NMR (1H and 13C) and GC/MS studies of fatty acid methyl esters in biodiesel from rocket seed oil. *Fuel Process. Technol.* **2011**, *92*, 336–341.
- (30) Thangaraj, B.; Piraman, S. Heteropoly acid coated ZnO nanocatalyst for Madhuca indica biodiesel synthesis. *Biofuels* **2016**, *7*(1), 13–20.
- (31) Mello, V. M.; Oliveira, F. C. C.; Fraga, W. G.; do Nascimento, C. J.; Suarez, P. A. Z. Determination of the content of fatty acid methyl esters (FAME) in biodiesel samples obtained by esterification using 1 H-NMR spectroscopy. *Magn. Reson. Chem.* **2008**, *46*, 1051–1054.
- (32) Encinar, J. M.; Pardal, A.; Sánchez, N. An improvement to the transesterification process by the use of co-solvents to produce biodiesel. *Fuel* **2016**, *166*, 51–58.
- (33) Banhani, F. F. Transesterification and Production of Biodiesel from Waste Cooking Oil: Effect of Operation Variables on Fuel Properties. *Am. J. Chem. Eng.* **2016**, *4*, 154–160.
- (34) Ayetor, G. K.; Sunnu, A.; Parbey, J. Effect of biodiesel production parameters on viscosity and yield of methyl esters: *Jatropha curcas*, *Elaeis guineensis* and *Cocos nucifera*. *Alexandria Eng. J.* **2015**, *54*, 1285–1290.
- (35) Eevera, T.; Rajendran, K.; Saradha, S. Biodiesel production process optimization and characterization to assess the suitability of the product for varied environmental conditions. *Renewable Energy* **2009**, *34*, 762–765.
- (36) Abbah, E. C.; Nwandikom, G. I.; Egwuonwu, C. C.; Nwakuba, N. R. Effect of Reaction Temperature on the Yield of Biodiesel From Neem Seed Oil. *Am. J. Energy Sci.* **2016**, *3*, 16–20.
- (37) Ofoefule, A. U.; Ibeto, C. N.; Ugwu, L. C.; Eze, D. C. Determination of Optimum Reaction Temperature and Reaction Time for Biodiesel Yield from Coconut (*Cocos nucifera*) Oil. *Int. Res. J. Pure Appl. Chem.* **2014**, *4* (1), 108–117.
- (38) Chhetri, A. B.; Watts, K. C.; Islam, M. R. Waste Cooking Oil as an Alternate Feedstock for Biodiesel Production. *Energies* **2008**, *1*, 3–18.
- (39) Demirbas, A. *Biodiesel: A realistic fuel alternative for diesel engines*; Springer-Verlag: London, 2008; DOI: 10.1007/978-1-84628-995-8.
- (40) Knothe, G.; Steidle, K. R. Kinematic viscosity of biodiesel fuel components and related compounds. Influence of compound structure and comparison to petrodiesel fuel components. *Fuel* **2005**, *84*, 1059–1065.
- (41) Aleme, H. G.; Barbeira, P. J. S. Determination of flash point and cetane index in diesel using distillation curves and multivariate calibration. *Fuel* **2012**, *102*, 129–134.
- (42) Prescott, W. V.; Schwartz, A. I. *Nanorods and Nanomaterials Research Progress*; Nova Science Publishers, 2008.

Publication II

I. Ambat, V. Srivastava, E. Haapaniemi, M. Sillanpää

Effect of lithium ions on the catalytic efficiency of calcium oxide as a nanocatalyst for the transesterification of lard oil.

Reprinted with permission from

Sustainable Energy Fuels

Vol.3, pp. 2464-2474

© 2019, RSC



Cite this: *Sustainable Energy Fuels*,
2019, 3, 2464

Effect of lithium ions on the catalytic efficiency of calcium oxide as a nanocatalyst for the transesterification of lard oil†

Indu Ambat,  *^a Varsha Srivastava,^a Esa Haapaniemi^b and Mika Sillanpää^a

The present work encompasses the effect of Li⁺ ions on CaO nanoparticles for the transesterification of lard oil. The modification of CaO nanoparticles was achieved by the impregnation of different molar ratios of lithium hydroxide. Later, each catalyst was screened for the catalytic conversion of lard oil to a fatty acid methyl ester (FAME). The nanocatalyst CaO–0.5LiOH (1 : 0.5 molar ratio) showed the best conversion rate for FAME. The synthesized nanocatalyst was characterized using Fourier transform infrared spectroscopy (FTIR), scanning electron microscopy (SEM), X-ray diffraction (XRD), transmission electron microscopy (TEM), Brunauer–Emmett–Teller (BET) analysis, and Hammett indicators for the basicity test. The obtained FAME was analyzed by gas chromatography with mass spectrometry (GC-MS) and ¹H and ¹³C nuclear magnetic resonance (NMR). The effect of optimum reaction parameters such as catalyst weight percentage, oil-to-methanol ratio, reaction time, reaction temperature, and reusability of the catalyst for the transesterification reaction was analyzed by ¹H NMR. The maximum FAME yield of 97.33% was obtained with 4 wt% catalyst amount and 1 : 6 oil-to-methanol ratio at 65 °C in 120 minutes. The physical properties of the synthesized FAME were also determined.

Received 2nd April 2019

Accepted 7th July 2019

DOI: 10.1039/c9se00210c

rsc.li/sustainable-energy

1. Introduction

FAME is the ester of fatty acids obtained by the transesterification of fats/oils with methanol in the presence of various kinds of catalysts. It can act as a substitute for conventional fuels because it is readily accessible, technically feasible, and renewable and has a sustainable nature.^{1–3,30,33} Moreover, FAME is a renewable fuel that can be produced from various sources such as vegetable oils, algal oils, and animal fat/oils.^{1–6}

Usually, vegetable oils such as rapeseed, sunflower, and soybean oils are used as the feedstock for FAME production. The feedstock used in the present work was lard oil because it is less expensive and does not compete with food production.^{2,7,8,39,40} Moreover, FAME synthesized from animal fat has a higher calorific value and cetane number in comparison with FAME obtained from vegetable oils.⁹

Currently, nanocatalysts play a significant role in FAME production from different feedstocks due to their higher catalytic activity, increased surface area, reusability, easy operational procedures, and reduced mass transfer resistance.^{1,3,10}

CaO-based nanocatalysts are recommended for FAME production because they are cost-effective and eco-friendly and have higher basicity.^{11,12,37,38}

The present work was reported to enable the production of FAME from lard oil using lithium ion-doped CaO as the nanocatalyst. One way to reduce the FAME production costs is to use less expensive feedstocks. Thus, lard oil was selected as the feedstock for FAME production. The selection of CaO as the nanocatalyst for the transesterification of lard oil was due to the positive response of CaO when compared to those of other commercially available nanocatalysts such as MgO, TiO₂, and ZnO. Later, lithium ions having various concentrations were impregnated into CaO nanoparticles using lithium hydroxide as a precursor to determine the doping effect of lithium ions on the catalytic activity. Moreover, to the best of our knowledge, to date, the transesterification of lard oil using lithium-doped CaO has not been investigated. In previous research studies, the transesterifications of sunflower oil, cottonseed oil, and soybean oil were performed using LiNO₃-doped CaO, nanocrystalline lithium doped CaO, and Li₂CO₃-doped CaO, respectively, whereas the current study focused on the transesterification of lard oil using LiOH-doped CaO.^{17,19,20} FTIR, SEM, XRD, TEM, BET, and the use of Hammett indicators for basicity tests were carried out for the characterization of the synthesized catalyst. Moreover, the synthesized catalyst was used for the transesterification of lard oil, where the reaction parameters such as the molar ratio of oil and methanol, temperature, catalyst amount, and time of transesterification were optimized. FAME

^aDepartment of Green Chemistry, School of Engineering Science, Lappeenranta University of Technology, Sammonkatu 12, FI-50130 Mikkeli, Finland. E-mail: indu.ambat@outlook.com

^bDepartment of Organic Chemistry, University of Jyväskylä, Finland

† Electronic supplementary information (ESI) available. See DOI: 10.1039/c9se00210c

was analyzed by GC-MS and ^1H and ^{13}C NMR techniques to investigate its various important characteristics.

2. Experimental

2.1 Chemicals

Lard oil (FFA% = 0.423, average molecular weight = 866.82), calcium oxide nanopowder (CaO), magnesium oxide nanopowder (MgO), titanium oxide nanopowder (TiO_2), zinc oxide (ZnO) nanopowder, methanol ($\geq 99.8\%$), and lithium hydroxide were purchased from Sigma-Aldrich. All the chemicals were of analytical grade.

2.2 Catalyst synthesis and selection

The conversion of lard oil using different catalysts (MgO , TiO_2 , ZnO , and CaO) was conducted by mixing oil to methanol in 1 : 6 molar ratio with 4 wt% of each commercial catalyst at 65°C for 2 h. After the investigation of the primary result of transesterification, CaO was selected for Li^+ ion impregnation and was further used for lard oil transesterification. Later, CaO nanoparticle modification by Li^+ ion impregnation was carried out by the incipient wetness impregnation method.

The catalysts were prepared by blending CaO/LiOH in different molar ratios of 1 : 0.15, 1 : 0.25, 1 : 0.5, and 1 : 0.75. The reason behind the selection of LiOH instead of lithium carbonate or lithium nitrate was to avoid nitrate and carbonate ion residues over the nanocatalyst as the leftover residual concentration of anions can affect the surface properties of the catalyst and hence the FAME synthesis from lard oil. The $\text{CaO}-\text{LiOH}$ solutions were stirred continuously for 7 h at room temperature and later dried at 50°C .^{2,3,13} The dried samples were calcined at 400°C in a muffle furnace (Nabertherm 180) for 4 h. The as-prepared Li^+ ion-impregnated CaO nanocatalysts ($\text{Li}-\text{CaO}$) with different molar ratios of 1 : 0.15, 1 : 0.25, 1 : 0.5, and 1 : 0.75 were screened for fatty acid methyl ester (FAME) production. Moreover, the effect of lithium ions on the enhancement of CaO catalytic activity in the transesterification of lard oil was examined with a set of lithium-impregnated CaO catalysts.

2.3 Catalyst characterization

The XRD patterns of bare and modified nanocatalysts were collected by a PANalytical – Empyrean X-ray diffractometer with

an X-ray source with $\text{Co-K}\alpha$ of 0.178 nm at 40 mA and 40 kV over an FTIR instrument. The SEM images of the catalysts were scanned by SEM Hitachi SU3500 with 5 kV accelerating voltage. The TEM images of the samples were recorded using HT7700 (Hitachi) TEM by dissolving the sample in ethanol. The catalyst samples were degassed at 40°C overnight to remove the moisture, followed by BET analysis (BET, Micromeritics Tristar II plus) to determine the surface area of the nanocatalyst.

The Hammett indicator–benzenecarboxylic acid (0.02 mol L $^{-1}$ anhydrous methanol solution) titration was conducted to determine the total basicity of the catalyst. Hammett indicators such as bromothymol blue ($\text{H}_{-7.2}$), phenolphthalein ($\text{H}_{-9.8}$), 2,4-dinitroaniline (H_{-15}), and 4-nitroaniline ($\text{H}_{-18.4}$) were used to determine the basic strength of the synthesized nanocatalyst with different molar ratios of $\text{CaO} : \text{LiOH}$ and also for TiO_2 , MgO , ZnO , and CaO with the help of the titration method.^{3,13,14}

2.4 FAME production

FAME production from lard oil *via* the transesterification process using different catalysts was done by blending oil to methanol in a 1 : 6 molar ratio with 4 wt% of each nanocatalyst. The reactions were carried out in triplicates in a 250 mL three-neck round bottom flask with a mechanical stirrer and reflux condenser at 65°C for 120 min in order to select the best catalyst among all the synthesized nanocatalysts for FAME production. Moreover, various methanol-to-oil ratios, temperatures, catalyst amounts, and reaction times were reported for the transesterification studies and theoretically, the 3 : 1 molar ratio was enough for the transesterification reaction. Besides, different reported research works indicate that there is more chance of methanol vaporization after 65°C and the CaO -based catalyst amounts of 3–5 wt% show better results in the transesterification studies. Due to these facts, the above-mentioned reaction conditions were selected for the initial research studies.^{1,2,12,14,20} The centrifugation of the samples was followed by the reaction to obtain the fatty acid methyl ester. Excess methanol in the ester phase was recovered by a rotary evaporator. FAME was analyzed by GC-MS (Agilent-GC6890N, MS 5975) with an Agilent DB-wax FAME analysis GC column having the following dimensions: 30 m, 0.25 mm, and 0.25 μm . The inlet temperature was 250°C and the oven temperature was programmed

Table 1 The efficiency of various catalysts for the transesterification of lard oil

No.	Catalyst	Molar ratio	Catalyst basic strength	FAME yield (%)	Total basicity (mmol g $^{-1}$)	BET surface area (m 2 g $^{-1}$)
1	MgO	—	$\text{H}_{-} < 7.2$	No reaction	0.25	23.5
2	ZnO	—	$\text{H}_{-} < 7.2$	No reaction	0.1	24.2
3	TiO_2	—	$\text{H}_{-} < 7.2$	No reaction	0.1	37.58
2	CaO	—	$7.2 < \text{H}_{-} < 9.8$	66.55	0.68	22.09
3	$\text{CaO} : \text{LiOH}$	1 : 0.15	$9.8 < \text{H}_{-} < 15$	71.25	0.96	11.95
4	$\text{CaO} : \text{LiOH}$	1 : 0.25	$9.8 < \text{H}_{-} < 15$	83.30	1.23	6.37
5	$\text{CaO} : \text{LiOH}$	1 : 0.5	$15 < \text{H}_{-} < 18.4$	97.33	1.85	2.41
6	$\text{CaO} : \text{LiOH}$	1 : 0.75	$15 < \text{H}_{-} < 18.4$	85.09	1.45	1.51

at 50 °C for 1 min. It was raised at the rate of 25 °C min⁻¹ to 200 °C and that of 3 °C min⁻¹ to 230 °C; then, it was held for 23 min. Moreover, the esters of lard oil after the transesterification reaction were analyzed by ¹H and ¹³C NMR (Bruker). The fatty acid methyl esters were analyzed by ¹H NMR and ¹³C NMR at 400 MHz with CDCl₃ as the solvent. The conversion percentage of lard oil to fatty acid methyl esters (C%) and the percentage of the FAME yield were estimated by eqn (1) and (2), respectively.^{2,3,34}

$$C(\%) = \frac{2 \times \text{integration value of protons of methyl ester}}{3 \times \text{integration value of methyl protons}} \times 100 \quad (1)$$

$$\text{Biodiesel yield (\%)} = \frac{\text{mass of biodiesel}}{\text{mass of oil}} \times 100 \quad (2)$$

Furthermore, in the current study, optimization was done using the best catalyst obtained after the screening process. This was conducted by varying the oil-to-methanol molar ratio, catalyst amount, reaction time, and reaction temperature.

3. Results and discussion

3.1. Screening and selection of the nanocatalyst for FAME production from lard oil

The transesterification of lard oil using a series of catalysts such as MgO, ZnO, TiO₂, CaO, and CaO/LiOH (1 : 0.15, 1 : 0.25, 1 : 0.5, and 1 : 0.75 molar ratios) was performed using oil to methanol in the molar ratio of 1 : 6 with 4 wt% of each nanocatalyst at 65 °C for 120 min in order to select the best catalyst. The catalytic performance of each catalyst is shown in Table 1. Moreover, the reaction parameters for the chosen catalyst were optimized to obtain a high yield of the fatty acid methyl esters (FAME).

Based on Table 1, we can see that CaO shows a positive reaction in the conversion of lard oil to FAME compared to other catalysts such as MgO, TiO₂, and ZnO. This is probably due to two factors: one is that the activity of the catalyst depends on the chemical composition of the feedstock and the other one is the basicity of the catalyst. Therefore, the transesterification ability of the CaO catalyst improved after impregnation of different molar ratios of LiOH. The CaO : LiOH ratio for which a relatively high conversion of feedstock into FAME was obtained was 1 : 0.5, showing the best conversion of lard oil to FAME. This is due to the optimum loading of the lithium ions into CaO, which offers sufficient active sites for the fatty acids to bind with the catalyst as well as the basic nature of the catalyst.^{3,13,29,31} Moreover, the increase in the amount of LiOH after the optimum value reduced the catalytic activity possibly due to the decrease in both the surface area and basicity.^{2,3} On the basis of the preliminary examination of the conversion of lard oil to FAME, CaO : LiOH with 1 : 0.5 ratio (named as CaO-0.5LiOH) was selected for the optimization of other reaction parameters for FAME production.

3.2. Characterization of the nanocatalyst

The FTIR spectra of CaO, CaO-0.5LiOH, and regenerated CaO-0.5LiOH are shown in Fig. 1. The peaks observed at 3600 and 1350 cm⁻¹ are due to the OH stretching and bending, respectively. The FTIR bands at 489.85 cm⁻¹, 713.57 cm⁻¹, 1087.71 cm⁻¹ are possibly due to Li-O stretching.¹⁵ The FTIR bands due to Li-O stretching, especially the band at 489.85 cm⁻¹, were more intense and sharper for the CaO-0.5LiOH catalyst. Furthermore, the non-regenerated and regenerated CaO-0.5LiOH samples showed similar FTIR spectra.

Fig. 2 shows the XRD patterns of bare CaO, lithium ion-impregnated CaO-0.5LiOH, and regenerated CaO-0.5LiOH nanocatalysts. The X-ray diffraction pattern of unmodified CaO matched well to the standard reference code ICDD: 98-002-8905. Concisely, the diffractogram of lithium ion-impregnated CaO is

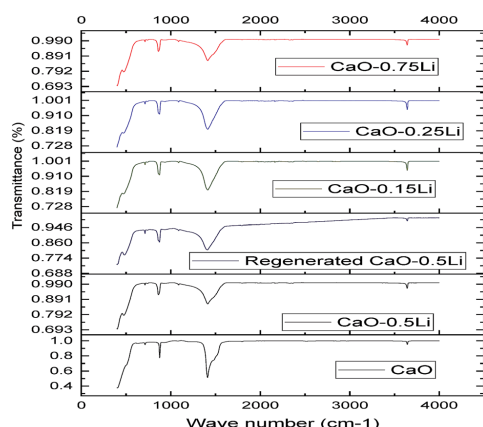


Fig. 1 FTIR spectra of CaO, CaO/LiOH in different molar ratios and the regenerated CaO-0.5LiOH.

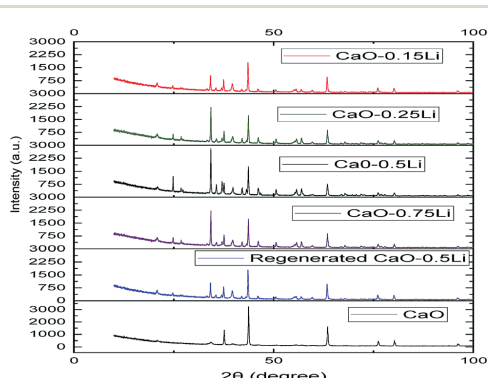


Fig. 2 XRD patterns of CaO, CaO/LiOH in different molar ratios and regenerated CaO-0.5LiOH.

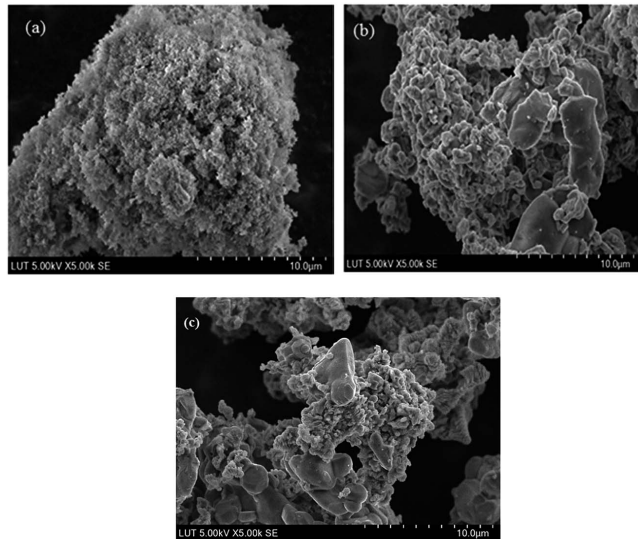


Fig. 3 SEM images of (a) CaO, (b) CaO–0.5LiOH and (c) regenerated CaO–0.5LiOH.

consistent with the reference standard code ICDD: 98-041-3207. The intensity of the XRD peaks due to lithium impregnation is higher for CaO–0.5LiOH. Moreover, the lithium ion-impregnated peaks are also visible for regenerated CaO–

0.5LiOH. Thus, both the XRD and FTIR results supported the impregnation of lithium ions into the CaO nanostructure.^{15–17}

The surface structure and composition of nanocatalysts were studied by SEM. Fig. 3a and b depict the SEM images of

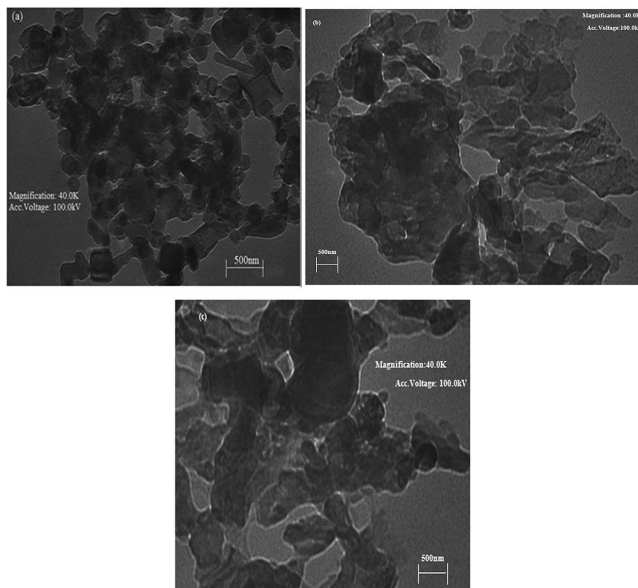


Fig. 4 TEM images of (a) CaO, (b) CaO–0.5LiOH and (c) regenerated CaO–0.5LiOH.

Table 2 The results of Brunauer–Emmett–Teller surface area analysis

	Parameters	Unmodified CaO nanocatalyst	CaO–0.5LiOH nanocatalyst
Surface area	BET surface area ($\text{m}^2 \text{ g}^{-1}$)	22.09	2.41
	BJH adsorption cumulative surface area of pores ($\text{m}^2 \text{ g}^{-1}$)	19.14	2.03
	BJH desorption cumulative surface area of pores ($\text{m}^2 \text{ g}^{-1}$)	19.00	2.83
Pore volume	Singl point adsorption total pore volume of pores ($\text{cm}^3 \text{ g}^{-1}$)	0.04	0.006
	BJH adsorption cumulative volume of pores ($\text{cm}^3 \text{ g}^{-1}$)	0.08	0.023
	BJH desorption cumulative volume of pores ($\text{cm}^3 \text{ g}^{-1}$)	0.09	0.028
Pore size	Adsorption average pore width (\AA)	70.60	103.26
	BJH adsorption average pore diameter (\AA)	177.30	455.41
	BJH desorption average pore diameter (\AA)	189.23	389.56

unmodified CaO and CaO–0.5LiOH, respectively. From the SEM images, it is clear that there is a significant difference in the structure of CaO–0.5LiOH (1 : 0.5 molar ratio) due to the impregnation of lithium ions. The flat surface is possibly due to the impregnation of lithium ions on the surface of CaO (Fig. 3b). Remarkably, the SEM micrographs in Fig. 3 and S1† reveal that the irregular flat surface increases with lithium concentration. This results in the agglomeration of the particles and reduction in the porosity of the catalyst. Fig. 3c illustrates that the regenerated catalyst is in good agreement with lithium-doped CaO before transesterification.

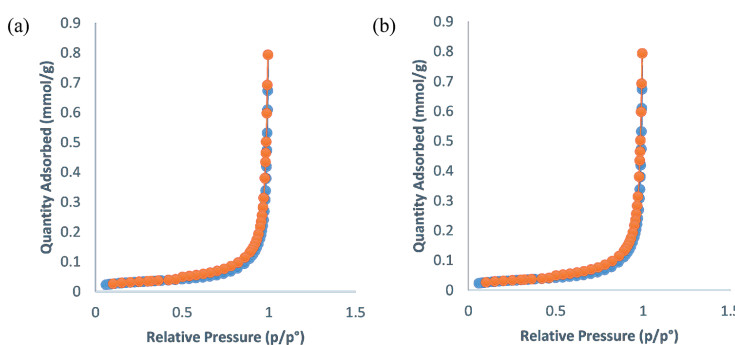
The TEM images of CaO (unmodified), CaO–0.5LiOH, and regenerated CaO–0.5LiOH are depicted in Fig. 4a–c, respectively. The CaO (unmodified), CaO–0.5LiOH, and regenerated CaO–0.5LiOH catalysts have particle sizes in the range of 54.5–127 nm. The TEM results confirmed the size of the particles in the catalysts. Furthermore, after Li-ion impregnation, the agglomeration of particles was also observed (Fig. 4b). Moreover, the agglomeration of irregular shapes with the increase in lithium concentration represents the reduction in catalyst porosity (Fig. 4 and S2†). Fig. 4c indicates that the catalyst after the reaction is also in good agreement with CaO–0.5LiOH. The TEM images are in good agreement with the SEM results.

Nitrogen adsorption/desorption measurements were obtained to determine the surface area, pore volume, and pore size of the catalysts. The surface area analysis of CaO and CaO–

0.5LiOH using BET is shown in Table 2. The decrease in the porosity of CaO–0.5LiOH was probably due to the insertion of lithium ions in the pores. Even though there was decrease in porosity and surface area, we observed increase in the catalytic activity for transesterification, as depicted in Table 1. This may be due to the action of the strength of basic sites in the catalyst, which can enhance the transesterification of lard oil.^{14,15} The addition of alkali metals to the CaO catalyst resulted in the enhancement of catalyst sintering, thus causing decrease in the surface area and increase in the basicity of the catalyst.^{2,31} The BET adsorption–desorption isotherm plots for CaO and CaO–0.5LiOH are given in Fig. 5. The nature of an isotherm specifies the presence of mesoporous materials.

3.3. Characterization of FAME synthesized from lard oil

The representation of the possible mechanism of the transesterification of triglycerides in the presence of the catalyst and FAME obtained after the transesterification of lard oil with CaO–0.5LiOH is shown in Fig. 6a and b, respectively. According to the catalyst characterization analysis, the nature of the synthesized catalyst is basic. During the transesterification reaction, methanol and triglycerides were adsorbed on two nearby sites of the catalyst. Based on previously reported studies, the mechanism of a basic catalyst involves the adsorption of methanol on Brønsted and Lewis base sites of the

**Fig. 5** BET adsorption–desorption isotherm plots of (a) CaO and (b) CaO–0.5LiOH.

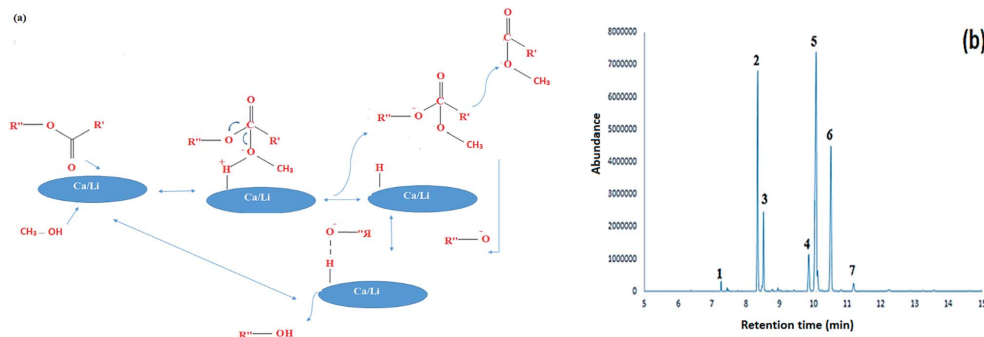


Fig. 6 (a) The possible mechanism of transesterification of triglyceride with methanol in the presence of CaO–0.5LiOH. (b) GC-MS spectrum of FAME obtained after transesterification with CaO–0.5LiOH.

catalyst to form oxygen anions. A tetrahedral intermediate is formed as a result of the nucleophilic attack of the adsorbed alcohol to form esters. Thereafter, two kinds of esters are formed as a result of the cleavage of the hydroxyl (OH) bond. The extension of the process produces di- and mono-glycerides.^{35,36} Each peak corresponding to fatty acid methyl esters present in the sample was recognized with the support of the National Institute of Standards and Technology (NIST) 2014 MS library (Table 3).

FAME characterization and percentage conversion of lard oil to FAME were estimated using ¹³C and ¹H NMR spectroscopic analyses, respectively. The ¹H NMR and ¹³C NMR spectra of the fatty acid methyl ester samples obtained after the transesterification of lard oil using the CaO–0.5LiOH catalyst are depicted in Fig. 7a and b, respectively. They provide sufficient information for FAME characterization and also confirm the presence of fatty acid methyl esters. We calculated 97.33% conversion of lard oil to fatty acid methyl esters with the help of eqn (1) and by using the results from ¹H NMR analysis.

The signals at 3.64 ppm and at 2.27 ppm in the ¹H NMR spectra correspond to the methoxy group (A_{ME}) of FAME and the methylene group (A_{CH_2}). The presence of methyl ester in the

FAME sample obtained *via* transesterification was confirmed by these two peaks. Other comprehensible peaks such as the signals from 0.93 to 0.97 ppm correspond to the latter methyl group. The presence of olefinic groups is confirmed by the signal at 5.3 ppm, whereas the peaks in the range from 1.23 to 2.3 ppm are ascribed to the methylene group.^{3,18} In the ¹³C NMR spectra, the signals at 174 ppm and 51 ppm indicate the existence of ester carbonyl –COO– and C–O groups, respectively. The signals at 132.11 ppm and 126.89 ppm show unsaturation in the synthesized FAME. The signals in the region of 22–34 ppm support the presence of the –CH₂ group. The existence of methyl ester in the FAME sample obtained *via* transesterification was confirmed by the signal at 3.64 ppm and the signal at 2.27 ppm in the ¹H NMR spectrum.^{3,3,18}

3.4. Influence of various parameters on transesterification

The Li–CaO nanocatalyst with 1 : 0.5 molar ratio of CaO : LiOH was found to be the most efficient catalyst for the conversion of lard oil to FAME as a result of the initial screening process. In the present work, optimization was done using the best catalyst CaO–0.5LiOH under different reaction conditions such as varying the oil-to-methanol molar ratio, catalyst amount, reaction time, and reaction temperature.

3.4.1 Influence of the nanocatalyst amount (weight%) on FAME production. The nanocatalyst concentrations from 2 wt% to 8 wt% of oil were used to examine their effect on the FAME production. Fig. 8a shows that the conversion of lard oil to FAME increases with catalyst concentration and the highest conversion (97.33%) is achieved at 4 wt% concentration within 2 h using 1 : 6 oil-to-methanol molar ratio at 65 °C. The rise in the catalyst amount above the optimum concentration (4 wt%) caused reduction in the FAME production due to decrease in the availability of active sites. The extra amount of catalyst leads to the saponification of oils, which finally inhibits the reaction.^{2,3} Based on the comparison with previously reported results, the present catalyst, namely, CaO–0.5LiOH showed better production of FAME.^{15,19,20}

Table 3 The composition of FAME obtained after transesterification with CaO–0.5LiOH

Peak	Retention time (min)	Library match (%)	Compound details
1	7.26	91.7	Tridecanoic acid, 12 methyl-methyl ester
2	8.35	91.5	Hexadecenoic acid, methyl ester
3	8.52	94.35	9-Hexadecenoic acid, methyl ester
4	9.87	93.51	Methyl stearate
5	10.08	96.01	13-Octadecenoic acid, methyl ester
6	10.52	96.53	11,14-Octadecadienoic acid, methyl ester
7	11.21	89.09	9,12,12-Octadecatrienoic acid, methyl ester

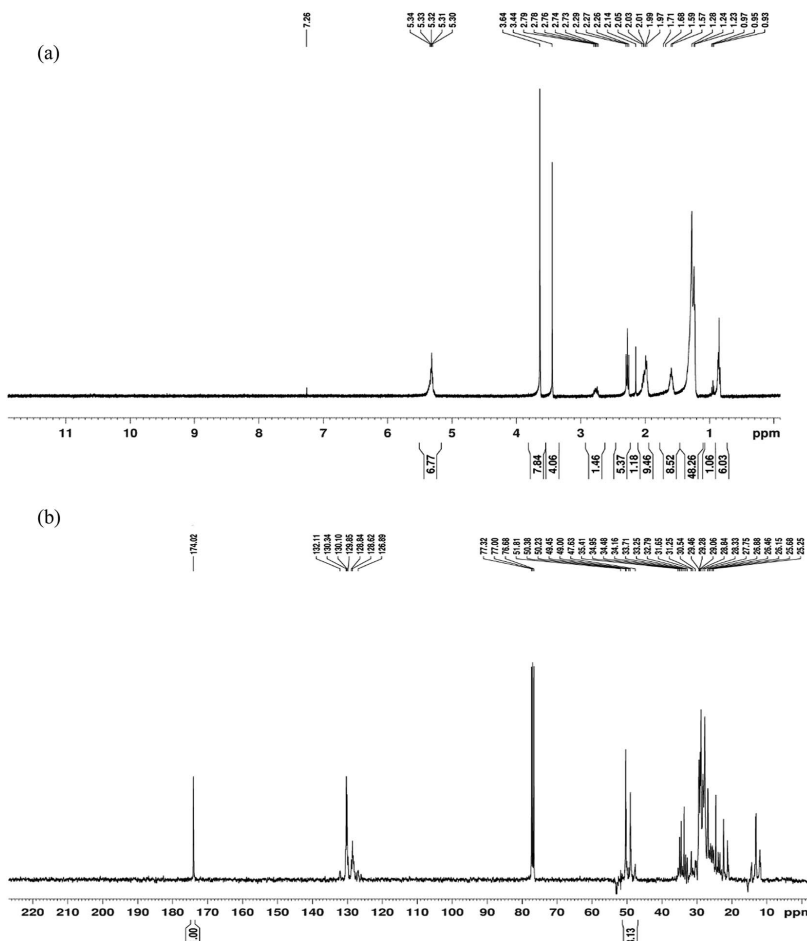


Fig. 7 (a) The ^1H NMR spectrum for the FAME sample obtained with CaO–0.5LiOH. (b) The ^{13}C NMR spectrum for the FAME sample obtained with CaO–0.5LiOH.

3.4.2 Influence of the oil-to-methanol molar ratio on FAME production. The effect of oil-to-methanol molar ratios on the FAME production was investigated by increasing the oil-to-methanol ratio from 1 : 3 to 1 : 12 using 4 wt% catalyst at 65 °C for 2 h reaction time. Fig. 8b shows that the FAME conversion increases with the increase in methanol concentration up to an optimum value (1 : 6) and thereafter, it is adversely affected. The reduction in FAME conversion beyond the optimum value favors the reverse reaction due to increased solubility of glycerol in the FAME phase.^{3,6,21,22} Therefore, 1 : 6 oil-to-methanol ratio was used for rest of the optimization studies.

3.4.3 Influence of reaction temperature on FAME production. A series of transesterification reactions using 4 wt%

catalyst, 1 : 6 oil-to-methanol molar ratio, and 2 h reaction time were performed at various temperatures to determine the effect of temperature on FAME production. The FAME conversion increased progressively up to 65 °C, beyond which the elevated temperature supported the saponification reaction and methanol vaporization. The maximum conversion of lard oil to fatty acid methyl esters observed at 65 °C is shown in Fig. 8c.^{3,23,24}

3.4.4 Influence of reaction time on FAME production. Fig. 8d represents a set of reactions conducted for different time intervals using 4 wt% catalyst and 1 : 6 oil-to-methanol molar ratio at 65 °C. The maximum percentage conversion of FAME was obtained at 120 min and after that, the FAME content remained almost constant.

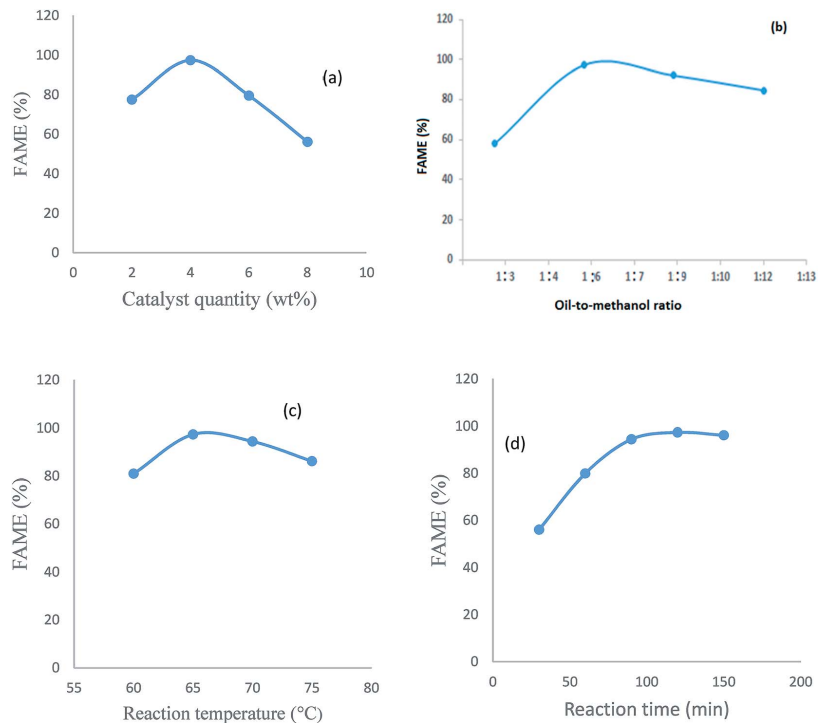


Fig. 8 (a) Influence of catalyst amount (weight%) on the FAME yield. (b) Influence of oil-to-methanol molar ratio on the FAME yield. (c) Influence of reaction temperature on the FAME yield. (d) Influence of reaction time on the FAME yield.

3.5. Properties of the synthesized FAME from lard oil

Table 4 illustrates the properties of lard oil methyl esters obtained using the Li–CaO nanocatalyst with 1 : 0.5 molar ratio of CaO : LiOH. The properties of the synthesized FAME were within the limits of the EN ISO method/ASTM standard methods.^{1,32} The flash point and cetane number of the synthesized FAME were recorded to be 130 °C and 62.6, respectively. The acid value, density, and kinematic viscosity of lard oil methyl esters were found to be 0.282 mg KOH per g, 881.76 kg m⁻³, and 4.08 mm² s⁻¹, respectively. Besides, all other factors of the fuel such as calorific value, cloud point, and pour point were also within the EN ISO/ASTM limits. The higher values for acid value, density, viscosity, cetane number, flash point, and cloud point lead to corrosion, filter clogging, fuel injection problems, fuel quality, and risk in the storage and usage of fuels.^{25–28}

3.6. Regeneration, reusability, and stability of the nanocatalyst

Initially, the regeneration of the catalyst after the transesterification reaction was performed by separating it from the lard oil methyl esters and glycerol by centrifugation. After centrifugation, the obtained catalyst was washed a few times

with heptane to remove the impurities. The washed catalyst was dried at 70 °C and calcined at 400 °C for 4 h to reactivate the catalyst.² Fig. 9a indicates that the catalyst activity decreases

Table 4 Properties of lard oil methyl esters (CaO–0.5LiOH catalyst at concentration of 4 wt%, 1 : 6 oil-to-methanol ratio, reaction temperature 65 °C, reaction time 2 h)

Property	EN 14214 test method	Limits	Methyl ester from lard oil
Acid value (mg KOH per g)	Pr EN14104	0.5 max	0.282
Density at 15 °C (kg m ⁻³)	EN ISO 12185	860–900	881.76
Kinematic viscosity at 40 °C (mm ² s ⁻¹)	EN ISO 3104	3–5	4.08
Flash point (°C)	EN ISO 2719	—	130
Cloud point (°C)	D2500	—	7
Pour point (°C)	ISO 3016	—	5
Cetane point	EN ISO 5165	≥51	62.6
Calorific value (MJ kg ⁻¹)	D6751	—	41.23

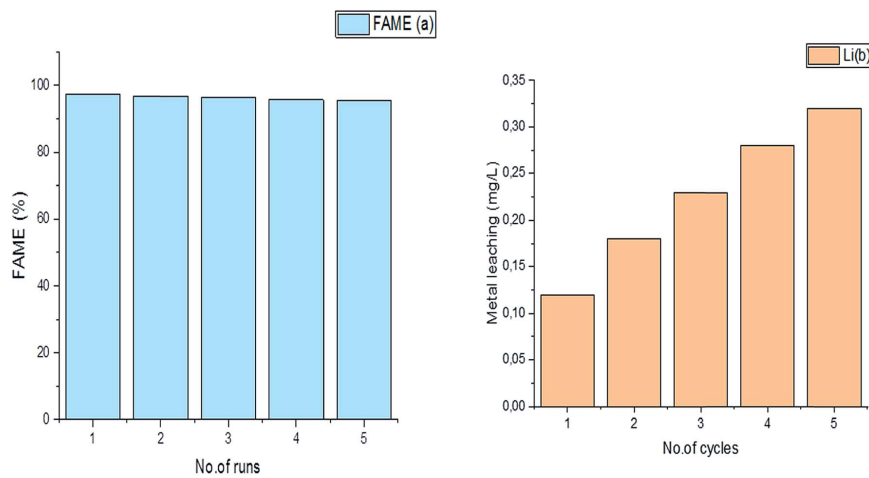


Fig. 9 (a) Reusability analysis of $\text{CaO}-0.5\text{LiOH}$ and (b) stability analysis of $\text{CaO}-0.5\text{LiOH}$.

from 97.33% to 94.4% in five cycles. However, the decrease in the catalytic efficiency might be due to the reduction in the stability of the catalyst. The stability of the catalyst was evaluated by determining the leached metal ion concentration after each run with the help of inductively coupled plasma (ICP, Agilent 5110). Fig. 9b shows that there is no Ca ion leaching up to 5 cycles, whereas the Li concentrations in solutions are less than 0.32 mg L^{-1} .

4. Conclusion

The conversion of lard oil to FAME was successfully conducted with the help of $\text{CaO}-0.5\text{LiOH}$ (1 : 0.5 molar ratio). The improved properties of the nanocatalyst were obtained due to the impregnation of lithium ions into the CaO nanostructure and better conversion in comparison to that for unmodified CaO was obtained. The impregnation of lithium ions into the CaO nanostructure was confirmed by FTIR, XRD, SEM, and TEM. The best activity was attained at the optimum loading of Li ions into CaO in 0.5 : 1 molar ratio. The nanocatalyst showed 97.33% fatty acid methyl ester content using 4 wt% catalyst amount and 1 : 6 oil-to-methanol ratio at 65°C with a reaction time of 120 minutes. The properties of FAME such as acid value, density, kinematic viscosity, and flash point were within the EN 14214 limits. All these results indicate that the lithium ion-impregnated CaO nanocatalyst is an efficient catalyst for the production of superior-quality FAME from lard oil as the feedstock. The reusability of the nanocatalyst exhibits favorable results, which provides an outlook for its expansion and applications.

Conflicts of interest

There are no conflicts to declare.

References

- I. Ambat, V. Srivastava and M. Sillanpää, Recent advancement in biodiesel production methodologies using various feedstock: A review, *Renewable Sustainable Energy Rev.*, 2018, **90**, 356–369.
- I. Ambat, V. Srivastava, E. Haapaniemi, *et al.*, Application of Potassium Ion Impregnated Titanium Dioxide as Nanocatalyst for Transesterification of Linseed Oil, *Energy Fuels*, 2018, **32**, 11645–11655, DOI: 10.1021/acs.energyfuels.8b03310.
- I. Ambat, V. Srivastava, E. Haapaniemi, *et al.*, Nano-magnetic potassium impregnated ceria as catalyst for the biodiesel production, *Renewable Energy*, 2019, **139**, 1428–1436.
- S. H. Teo, A. Islam, F. L. Ng and Y. H. Taufiq-Yap, biodiesel synthesis from photoautotrophic cultivated oleaginous microalgae using a sand dollar catalyst, *RSC Adv.*, 2015, **5**, 47140–47152, DOI: 10.1039/c5ra05801e.
- M. Berrios, M. C. Gutiérrez, M. A. Martín and A. Martín, Application of the factorial design of experiments to biodiesel production from lard, *Fuel Process. Technol.*, 2009, **90**, 1447–1451, DOI: 10.1016/j.fuproc.2009.06.026.
- M. E. Hums, R. A. Cairncross and S. Spatari, Life-Cycle Assessment of biodiesel Produced from Grease Trap Waste, *Environ. Sci. Technol.*, 2016, **50**, 2718–2726, DOI: 10.1021/acs.est.5b02667.
- C. B. Ezekekangha, C. N. Ude and O. D. Onukwuli, Optimization of the methanolysis of lard oil in the production of biodiesel with response surface methodology, *Egypt. J. Pet.*, 2017, **26**, 1001–1011, DOI: 10.1016/j.ejpe.2016.12.004.
- E. F. Aransiola, T. V. Ojumu, O. O. Oyekola, T. F. Madzimbamuto and D. I. O. Ihku-Omoregbe, A review of current technology for biodiesel production: State of the

- art, *Biomass Bioenergy*, 2014, **61**, 276–297, DOI: 10.1016/j.biombioe.2013.11.014.
- 9 J. M. Dias, J. M. Araújo, J. F. Costa, M. C. M. Alvim-Ferraz and M. F. Almeida, Biodiesel production from raw castor oil, *Energy*, 2013, **53**, 58–66, DOI: 10.1016/j.energy.2013.02.018.
- 10 G. Baskar, S. Soumiya and R. Aiswarya, Biodiesel Production from Pongamia oil using Magnetic Composite of Zinc Oxide Nanocatalyst, *International Journal of Modern Science and Technology*, 2016, **1**, 129–137.
- 11 L. Wen, Y. Wang, D. Lu, S. Hu and H. Han, Preparation of KF/CaO nanocatalyst and its application in biodiesel production from Chinese tallow seed oil, *Fuel*, 2010, **89**, 2267–2271, DOI: 10.1016/j.fuel.2010.01.028.
- 12 E. Bet-Moushoul, K. Farhadí, Y. Mansourpanah, A. M. Nikbakht, R. Molaei and M. Forough, Application of CaO-based/Au nanoparticles as heterogeneous nanocatalysts in FAME production, *Fuel*, 2016, **164**, 119–127, DOI: 10.1016/j.fuel.2015.09.067.
- 13 F. Qiu, Y. Li, D. Yang, X. Li and P. Sun, Bioresource Technology Heterogeneous solid base nanocatalyst: Preparation, characterization and application in biodiesel production, 2011, **102**, 4150–4156, DOI: 10.1016/j.biortech.2010.12.071.
- 14 V. Singh, F. Bux and Y. C. Sharma, A low cost one pot synthesis of biodiesel from waste frying oil (WFO) using a novel material, β -potassium dizirconate (β -K₂Zr₂O₅), *Appl. Energy*, 2016, **172**, 23–33, DOI: 10.1016/j.apenergy.2016.02.135.
- 15 J. Boro, L. J. Konwar and D. Deka, Transesterification of non edible feedstock with lithium incorporated egg shell derived CaO for biodiesel production, *Fuel Process. Technol.*, 2014, **122**, 72–78, DOI: 10.1016/j.fuproc.2014.01.022.
- 16 J. F. Puna, J. F. Gomes, J. C. Bordado, M. J. Neiva, A. Paula and S. Dias, Biodiesel production over lithium modified lime catalysts: Activity and deactivation, *Appl. Catal., A*, 2014, **470**, 451–457.
- 17 M. D. Alonso, R. Mariscal, L. M. Granados, et al., Biodiesel preparation using Li/CaO catalysts: Activation process and homogeneous contribution, *Catal. Today*, 2009, **143**, 167–171, DOI: 10.1016/j.cattod.2008.09.021.
- 18 M. Tariq, S. Ali and N. Khalid, Activity of homogeneous and heterogeneous catalysts, spectroscopic and chromatographic characterization of biodiesel: A review, *Renewable Sustainable Energy Rev.*, 2012, **16**, 6303–6316, DOI: 10.1016/j.rser.2012.07.005.
- 19 J. X. Wang, K. T. Chen, S. T. Huang, K. T. Chen and C. C. Chen, biodiesel Production from Soybean Oil Catalyzed by Li₂CO₃, *J. Am. Oil Chem. Soc.*, 2012, 1619–1625, DOI: 10.1007/s11746-012-2074-2.
- 20 D. Kumar and A. Ali, Nanocrystalline Lithium Ion Impregnated Calcium Oxide As Heterogeneous Catalyst for Transesterification of High Moisture Containing Cotton Seed Oil, *Energy Fuels*, 2010, 2091–2097, DOI: 10.1021/ef901318s.
- 21 F. F. Banhani, Transesterification and Production of biodiesel from Waste Cooking Oil: Effect of Operation Variables on Fuel Properties, 2017, **4**, 154–160, DOI: 10.11648/j.ajche.20160406.13.
- 22 G. Kafui, A. Sunnu and J. Parbey, Effect of biodiesel production parameters on viscosity and yield of methyl esters: Jatropha curcas, Elaeis guineensis and Cocos nucifera, *Alexandria Eng. J.*, 2015, **54**, 1285–1290, DOI: 10.1016/j.aej.2015.09.011.
- 23 T. Eevera, K. Rajendran and S. Saradha, Biodiesel production process optimization and characterization to assess the suitability of the product for varied environmental conditions, *Renewable Energy*, 2009, **34**, 762–765, DOI: 10.1016/j.renene.2008.04.006.
- 24 E. C. Abbah, G. I. Nwandikom, C. C. Egwuonwu and N. R. Nwakuba, Effect of Reaction Temperature on the Yield of biodiesel From Neem Seed Oil, *American Journal of Energy Science*, 2016, **3**, 16–20.
- 25 A. B. Chhetri, M. S. Tango, S. M. Budge, K. C. Watts and M. R. Islam, Non-edible plant oils as new sources for biodiesel production, *Int. J. Mol. Sci.*, 2008, **9**, 169–180, DOI: 10.3390/ijms9020169.
- 26 A. Demirbas, *Biodiesel: A realistic fuel alternative for diesel engines. FAME A Realis Fuel Altern Diesel Engines*, 2008, pp. 1–208, DOI: 10.1007/978-1-84628-995-8.
- 27 G. Knothe and K. R. Steidley, Kinematic viscosity of biodiesel fuel components and related compounds. Influence of compound structure and comparison to petrodiesel fuel components, *Fuel*, 2005, **84**, 1059–1065, DOI: 10.1016/j.fuel.2005.01.016.
- 28 H. G. Aleme and P. J. S. Barbeira, Determination of flash point and cetane index in diesel using distillation curves and multivariate calibration, *Fuel*, 2012, **102**, 129–134, DOI: 10.1016/j.fuel.2012.06.015.
- 29 Y. Li, F. Qiu, D. Yang, X. Li and P. Sun, Preparation, characterization and application of heterogeneous solid base catalyst for biodiesel production from soybean oil, *Biomass Bioenergy*, 2011, **35**, 2787–2795, DOI: 10.1016/j.biombioe.2011.03.009.
- 30 R. Luque, R. Luque, L. Herrero-davila, J. M. Campelo, J. H. Clark, J. M. Hidalgo, et al., Biofuels : a technological perspective, *Energy Environ. Sci.*, 2008, **1**, 542–564, DOI: 10.1039/b807094f.
- 31 V. H. Rane and V. R. Choudhary, Influence of alkali metal doping on surface properties and catalytic activity/selectivity of CaO catalysts in oxidative coupling of methane, *J. Nat. Gas Chem.*, 2008, **17**, 313–320, DOI: 10.1016/S1003-9953(09)60001-3.
- 32 A. F. Lee, J. A. Bennett, J. C. Manayil, K. Wilson and A. F. Lee, Heterogeneous catalysis for sustainable biodiesel production via esterification and transesterification, *Chem. Soc. Rev.*, 2014, 437887–437916, DOI: 10.1039/c4cs00189c.
- 33 K. W. Harrison, B. G. Harvey, K. W. Harrison and B. G. Harvey, High cetane renewable diesel fuels prepared from bio-based methyl ketones and diols, *Sustainable Energy Fuels*, 2018, **2**, 367–371, DOI: 10.1039/c7se00415j.
- 34 K. V. Yatish, H. S. Lalithamba, R. Suresh and G. N. Dayananda, Sodium phosphate synthesis through glycerol purifi cation and its utilization for biodiesel production from dairy scum oil to economize production

- cost, *Sustainable Energy Fuels*, 2018, 1299–1304, DOI: 10.1039/c8se00034d.
- 35 S. Yan, M. Kim, S. O. Salley and K. Y. S. Ng, Oil transesterification over calcium oxides modified with lanthanum, *Appl. Catal., A*, 2009, **360**, 163–170, DOI: 10.1016/j.apcata.2009.03.015.
- 36 S. Yan, S. O. Salley and K. Y. S. Ng, Simultaneous transesterification and esterification of unrefined or waste oils over ZnO-La₂O₃ catalysts, *Appl. Catal., A*, 2009, **353**, 203–212, DOI: 10.1016/j.apcata.2008.10.053.
- 37 S. Niju, K. M. M. S. Begum and N. Anantharaman, Continuous flow reactive distillation process for biodiesel production using waste egg shells as heterogeneous catalysts, *RSC Adv.*, 2014, **4**, 54109–54114, DOI: 10.1039/c4ra05848h.
- 38 P. A. Anjana, S. Niju, M. K. M. Sheriffa Begum, *et al.*, Utilization of limestone derived calcium oxide for biodiesel production from non-edible pongamia oil, *Environ. Prog. Sustainable Energy*, 2016, **35**, 1758–1764, DOI: 10.1002/ep.12384.
- 39 G. Knothe, Improving biodiesel fuel properties by modifying fatty ester composition, *Energy Environ. Sci.*, 2009, **2**, 759–766, DOI: 10.1039/b903941d.
- 40 F. Li, J. Jiang, P. Liu, *et al.*, Catalytic cracking of triglycerides with a base catalyst and modification of pyrolytic oils for production of aviation fuels, *Sustainable Energy Fuels*, 2018, **2**, 1206–1215, DOI: 10.1039/c7se00505a.

Publication III

I. Ambat, V. Srivastava, E. Haapaniemi, M. Sillanpää

Nano-magnetic potassium impregnated ceria as catalyst for the biodiesel production

Reprinted with permission from

Renewable Energy

Vol. 139, pp. 1428-1436

© 2019, Elsevier



Nano-magnetic potassium impregnated ceria as catalyst for the biodiesel production



Indu Ambat ^{a,*}, Varsha Srivastava ^a, Esa Haapaniemi ^c, Mika Sillanpää ^{a,b}

^a Department of Green Chemistry, School of Engineering Science, Lappeenranta University of Technology, Sammonkatu 12, FI 50130 Mikkeli, Finland

^b Department of Civil and Environmental Engineering, Florida International University, Miami, FL 33174, USA

^c Department of Organic Chemistry, University of Jyväskylä, Finland

ARTICLE INFO

Article history:

Received 29 May 2018

Received in revised form

5 February 2019

Accepted 9 March 2019

Available online 12 March 2019

Keywords:

Biodiesel

Rapeseed oil

Transesterification

Fe₃O₄-CeO₂ nanocatalyst

ABSTRACT

The main objective of this work comprises the investigation of biodiesel production from rapeseed oil using potassium impregnated Fe₃O₄-CeO₂ nanocatalyst. The various concentration of potassium impregnated Fe₃O₄-CeO₂ was screened for catalytic conversion of rapeseed oil to triglyceride methyl ester. The 25 wt % potassium impregnated Fe₃O₄-CeO₂ nanocatalyst showed best biodiesel production. Nanocatalyst was characterized by FTIR, XRD, SEM, TEM, BET and Hammett indicator for basicity test. The characterization of biodiesel was performed with GC-MS, ¹H and ¹³C NMR. Moreover, the optimum reaction parameters such as catalyst amount (wt %), oil to methanol ratio, reaction time and reaction temperature for transesterification reaction was analyzed and yield was determined by ¹H NMR. The maximum yield of 96.13% was obtained at 4.5 wt % catalyst amount, 1:7 oil to methanol ratio at 65 °C for 120 min. The properties of biodiesel such as acid value and kinematic viscosity were observed as 0.308 mg KOH/g and 4.37 mm²/s respectively. The other fuel parameters such as flash point and density were also determined. The reusability of catalyst was observed and it showed stability up to five cycles without considerable loss of activity. The recovery of excess methanol after transesterification reaction was achieved using distillation process setup.

© 2019 Elsevier Ltd. All rights reserved.

1. Introduction

Now a days, the inadequacy of conventional fuels along with global warming and direct environmental pollution due to massive utilization of fossil fuels leads to the consideration of an alternative fuel for fossil fuels [1,2]. Biodiesel is fatty acid methyl esters obtained after transesterification of oils with methanol [3].

Biodiesel is one of the alternative fuel, which possess all the properties such as renewability, accessibility, sustainable nature, and clean fuel that can meet all the challenges caused by fossil fuels [4,5]. Furthermore, domestically available numerous sources such as vegetable oils, algal oils and animal fat/oils are used as feedstock for the biodiesel production [6]. Various techniques involved in conversion of oils to biodiesel which includes pyrolysis, trans-esterification, supercritical fluid, and dilution [3,7]. Out of these methodologies most commonly and commercially used is transesterification techniques with homogeneous catalyst. Moreover,

there are various catalyst involved in biodiesel production such as homogeneous, heterogeneous and enzyme catalyst [3,7,8]. However, the environmental concern related to usage of homogenous catalyst such as huge amount of chemical waste water, whereas solid heterogeneous and enzyme catalyst have various challenges such as mass transfer resistant, reusability of catalyst [7,9,10].

In recent times nanocatalyst attained special attention in various process such as water treatment, drug delivery, optoelectronics and biodiesel production [4,8,11–13]. Furthermore nanocatalyst plays a major role in biodiesel production due to its various features such as high stability, efficient catalytic activity, easy operational procedure, reusability, and high surface area [8,10,13]. The selection of feedstock for biodiesel production is reliant on the region. For example, in Europe and tropical countries major sources for the production of biodiesel are rapeseed oil and palm oil respectively where as in soybean oil serves as one of the major sources of biodiesel in the United States [3,13].

The focus of this work is to synthesize potassium impregnated nano-magnetic ceria and use this catalyst for the production of biodiesel from rapeseed oil. The magnetic nanoparticles helps in easy separation of catalyst and increases its reusability [14,15].

* Corresponding author.
E-mail address: indu.ambat@lut.fi (I. Ambat).

Nanomagnetic particles has been explored as a catalyst in various fields such as water treatment, bio catalysis, photocatalysis but rarely used in field of biodiesel production [16–19]. Furthermore, as far as our knowledge the transesterification using the potassium impregnated nano-magnetic ceria has not been reported in the literature. The selection of rapeseed oil as a feedstock for biodiesel production is because of its easy availability and comparatively low cost oil in Europe. The CeO₂ magnetic nanoparticles were impregnated with various concentration of potassium ions to determine the doping effect of potassium ions on catalytic activity. The cerium oxide was used in combination with various metal oxides for transesterification reaction [37,38]. Moreover, ceria was used as catalyst for various catalytic reactions [15,39]. The characterization of synthesized nanocatalyst was done using FTIR, XRD, SEM, TEM, BET. Further, the nanocatalyst has been used for transesterification reaction, where the production conditions such as temperature molar ratio of oil and methanol, catalyst amount and time were optimized. The biodiesel was analyzed by GC-MS, ¹H and ¹³C NMR.

2. Materials and methods

2.1. Materials

Rapeseed oil (FFA % = 0.442, average molecular weight = 892.27), Cerium (III) nitrate hexahydrate (Ce (NO₃)₃·6H₂O), Ferrous chloride tetrahydrate (FeCl₂·4H₂O) Ferric chloride hexahydrate (FeCl₃·6H₂O), Ammonia solution, potassium hydroxide (KOH), methanol of analytical grade were purchased from Sigma-aldrich.

2.2. Synthesis and screening of catalyst

The magnetic nanoparticles loaded with 25 wt % of ceria was synthesized by co-precipitation of FeCl₂·4H₂O, FeCl₃·6H₂O, and Ce (NO₃)₃·6H₂O using 25% ammonia solution. The resulted solution was centrifuged and washed several times with water. The obtained precipitate was dried at 60 °C for 24 h and calcinated at 400 °C in muffle furnace (Nabertherm180) for 4 h. The prepared magnetic nanoparticles loaded with 25 wt % ceria was impregnated with different concentration of KOH solution (15, 25, 50 wt %) and stirred continuously for 8 h and later dried at 50 °C for overnight. The dried samples were calcined at 500 °C in muffle furnace for 4 h. A series of potassium impregnated magnetic cerium dioxide nanocatalysts were screened for fatty acid methyl ester (FAME) production from rapeseed oil.

2.3. Characterization of catalyst

FTIR peaks and XRD patterns of synthesized catalyst were examined with Vertex 70 Bruker and PANalytical – Empyrean X-ray diffractometer respectively. SEM images of catalysts were obtained by spreading sample on colloidal graphite with 5 kV accelerating voltage (SEM, Hitachi SU3500). TEM images of the samples were captured using HT7700 (Hitachi). For attaining TEM images the nanocatalyst was dispersed in ethanol and sonicated for 25 min and a drop of suspension was added to carbon coated copper grid. Surface area of synthesized catalysts were determined using BET surface area analyzer (BET, Micromeritics Tristar II plus). Prior to perform BET analysis the catalyst samples were degassed at 35 °C for overnight to remove the moisture from the samples.

The basicity of catalyst was determined with help of Hammett indicator. For basicity test analysis, 350 mg of each catalyst was mixed with 1 mL of Hammett indicators such as bromothymol blue (H_{7.2}), phenolphthalein (H_{9.8}), 2, 4 - dinitroaniline (H₁₅) and 4-nitroaniline were diluted separately in 10 mL of methanol. Later all

the samples were kept for 3 h to settle. The catalyst colour was observed after equilibration time. The catalyst experience colour change indicates that the basicity of catalyst was greater than the weakest indicator whereas no colour change shows that the basic strength of catalyst lower than the strongest indicator [20,21].

2.4. Biodiesel production using potassium impregnated Fe₃O₄-CeO₂

Rapeseed oil was used as feedstock for biodiesel production. The fatty acid methyl ester production from rapeseed oil using different catalyst was done by mixing methanol to oil in 7:1 M ratio and with 3 wt % of each catalyst. The best catalyst for biodiesel production was selected by conducting all the reactions in a 250 mL three neck round bottom flask with mechanical stirrer and reflux condenser at 60 °C for 120 min. The separation of fatty acid methyl ester as well as recovery of excess methanol and catalyst by centrifugation of samples after each reaction. The biodiesel was analyzed by GC-MS (Agilent-GC6890N, MS 5975) with agilent DB-wax FAME analysis GC column dimensions 30 m, 0.25 mm, 0.25 µm. The inlet temperature was 250 °C and oven temperature was programmed at 50 °C for 1 min and it raises at the rate of 25 °C/minute to 200 °C and 3 °C/minute to 230 °C and then it was held for 23 min. Besides, esters of rapeseed oil after transesterification reaction was analyzed by ¹H and ¹³C NMR (Bruker). For NMR analysis, fatty acid methyl esters were analyzed by ¹H NMR and ¹³C NMR at 400 MHz with CDCl₃ as solvent. The percentage of conversion of rapeseed oil to fatty acid methyl esters (C %) and percentage of biodiesel yield are determined by equation (1) and equation (2) respectively [9,13,20,22].

$$C(\%) = \frac{2 \times \text{Intergartion value of protons of methyl ester}}{3 \times \text{Intergartion value of methyl protons}} \times 100 \quad (1)$$

$$\text{Biodiesel yield (\%)} = \frac{\text{mass of biodiesel}}{\text{mass of oil}} \times 100 \quad (2)$$

Moreover, the transesterification reaction was sustained with the best catalyst attained after screening process. However, the biodiesel production was also effected by reaction parameters such as amount of catalyst oil to methanol ratio, temperature and reaction time.

3. Results and discussion

3.1. Screening and selection of nanocatalyst for biodiesel production from rapeseed oil

The catalytic performance of different catalyst such as 15, 25, 50 wt % potassium impregnated Fe₃O₄-CeO₂ were analyzed for the selection of nanocatalyst for the biodiesel production from rapeseed oil at 60 °C by using 3 wt % catalyst and 1:5 oil to methanol molar ratio within 120 min of reaction time. The catalytic activity of each catalyst was indicated in Fig. 1. This is due to the optimum loading of potassium ions to Fe₃O₄-CeO₂, which offers sufficient active sites for the fatty acids to bind with the catalyst as well as the basic nature of the catalyst. Moreover the increased amount of KOH above the optimum value, basicity probably decrease the surface basic sites which led to a fall in the catalytic activity of the catalyst with subsequent reduction in yield [21,23,24]. The 25 wt % potassium impregnated Fe₃O₄-CeO₂ [named as Fe₃O₄-CeO₂-25K] showed best result on preliminary examination on conversion rapeseed oil to biodiesel and hence selected for the optimization studies. Furthermore, reaction parameters for the chosen catalyst was optimized to obtain high yield of fatty acid methyl esters (FAME).

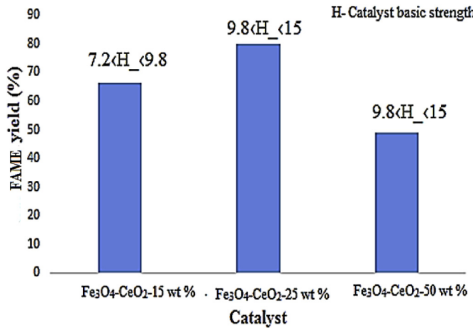


Fig. 1. The efficiency of various catalyst for transesterification of rapeseed oil.

3.2. Characterization of catalyst

The FTIR peaks of Fe₃O₄-CeO₂, Fe₃O₄-CeO₂-25K and regenerated Fe₃O₄-CeO₂-25K were shown in Fig. 2. The FTIR spectrum observed in region of 3286 cm⁻¹ and 1624 cm⁻¹ is due to stretching of the –OH group and bending vibration of water molecule respectively [15]. FTIR bands at around 1370 cm⁻¹ and 1009 cm⁻¹ are due to vibration of CeO₂. The FTIR peaks detected in the range of 500 cm⁻¹ to 700 cm⁻¹ represents Fe–O metal–oxygen bond which indicates the existence of Fe₃O₄ [15]. New peaks at around 833 cm⁻¹ and 1390 cm⁻¹ indicates impregnation of potassium to the catalyst.

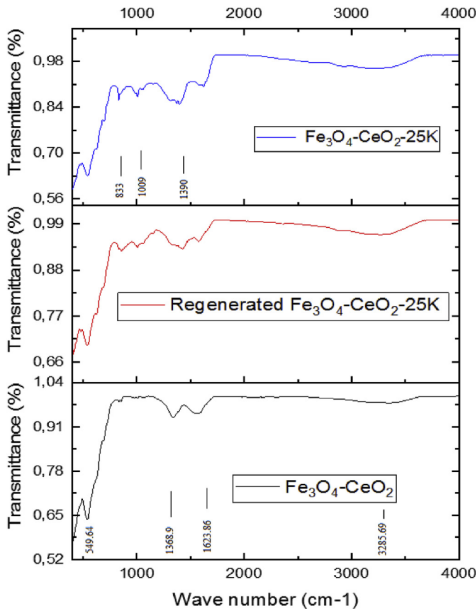


Fig. 2. FTIR spectra of Fe₃O₄-CeO₂, Fe₃O₄-CeO₂-25K and regenerated Fe₃O₄-CeO₂-25K

Fig. 3 shows the XRD pattern of Fe₃O₄-CeO₂, Fe₃O₄-CeO₂-25K and regenerated Fe₃O₄-CeO₂-25. The regenerated catalyst was obtained by separating catalyst after transesterification. The catalyst was with methanol and heptane to remove impurities and dried at 60 °C and calcined at 500 °C for 4 h to reactivate the catalyst. X-ray diffraction patterns of Fe₃O₄-CeO₂ depicts peaks at 35.36°, 41.51°, 50.8°, 63.6°, 67.7°, 74.7°. XRD pattern of Fe₃O₄-CeO₂-25K and regenerated Fe₃O₄-CeO₂-25K showed new peaks at 38.72°, which is due to the impregnation of potassium ions to Fe₃O₄-CeO₂ nanocatalyst [15,25]. Table 1 shows the crystallographic parameters of Fe₃O₄-CeO₂-25K and regenerated Fe₃O₄-CeO₂-25K after five cycles of transesterification.

The TEM image of Fe₃O₄-CeO₂ and Fe₃O₄-CeO₂-25K were depicted in Fig. 4a and b respectively. The Fe₃O₄-CeO₂ and Fe₃O₄-CeO₂-25K catalyst have a particle size of 20–33.9 nm which was confirmed with help of TEM images. Further after impregnation of potassium ions the flat covered surface was observed. The flat covered surface imply to potassium impregnation. The extension of potassium covering depends on the weight percentage of potassium used for impregnation.

The composition and surface structure of nanocatalyst were analyzed by SEM. SEM image and EDS graph of Fe₃O₄-CeO₂ and Fe₃O₄-CeO₂-25K shown in Fig. 5 a and b provides information about its morphology and elemental composition respectively. By comparing two images, it was observed that there was a coating on the catalyst due to doping of potassium. It also confirms the existence of Fe (34.9 wt %), Ce (13.5 wt %), O (28.8 wt %) and K (16.4 wt %) in the nanocatalyst. The elemental distribution in regenerated catalyst obtained after 5 cycles was found to be Fe (33.5 wt %), Ce (12.9 wt %), O (27.7 wt %) and K (15.4 wt %) in the nanocatalyst.

The surface area, pore volume and pore size of Fe₃O₄-CeO₂ and Fe₃O₄-CeO₂-25K were determined by BET analysis. The results of BET analysis of Fe₃O₄-CeO₂ and Fe₃O₄-CeO₂-25K as summarized in Table 2. The BET surface area and pore volume reduced due to loading of potassium and this behavior was quite common with potassium [21,24,26]. The N₂ adsorption-desorption isotherm for Fe₃O₄-CeO₂ and Fe₃O₄-CeO₂-25K from BET analysis were shown in Fig. 6. The hysteretic loop isotherm indicates the presence of mesoporous materials. The pore width and pore volume distribution of Fe₃O₄-CeO₂ and Fe₃O₄-CeO₂-25K depicted in Fig. S1.

The magnetic properties were measured using SQUID magnetometer (Cryogenic S700X-R, UK). The magnetization versus magnetic field dependencies at 300 K was obtained for Fe₃O₄-CeO₂-25K shown in Fig. 7. The remanent magnetization for Fe₃O₄-CeO₂-25K sample is 0.75 emu/g. Fig. 7 also demonstrates the recovery of catalyst from the reaction mixture.

3.3. Characterization of biodiesel

The quality of synthesized biodiesel should satisfy the criteria determined by ASTM/EN 14214 limits. The fatty acid methyl esters made from the rapeseed oil was characterized by GC-MS, ¹H NMR and ¹³C NMR.

The chemical composition of biodiesel was demonstrated with the help of GCMS chromatogram and National Institute of Standards and Technology (NIST) 2014 MS library. The fatty acid methyl esters obtained after transesterification of rapeseed oil with Fe₃O₄-CeO₂-25K illustrated in Fig. S2. Each FAME peak in the sample was identified with the help of library match and represented in Table S1.

3.3.1. ¹H and ¹³C NMR spectroscopy

¹H and ¹³C NMR spectroscopy was used for the analysis of fatty acid methyl esters derived from rapeseed oil. The conversion was calculated using equation (2), which was already mentioned above.

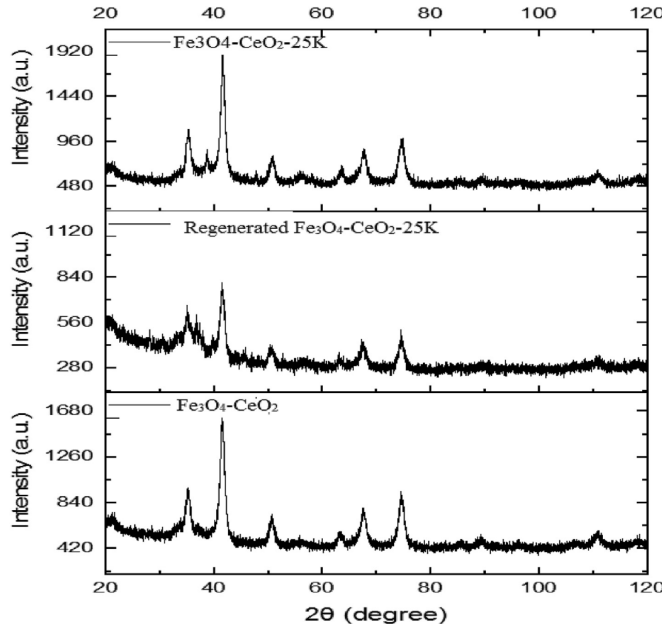


Fig. 3. XRD pattern of Fe₃O₄-CeO₂, Fe₃O₄-CeO₂-25K and regenerated Fe₃O₄-CeO₂-25K

Table 1
The crystallographic parameters of Fe₃O₄-CeO₂-25K and regenerated Fe₃O₄-CeO₂-25K

Catalyst	Crystal structure	a (nm)	b (nm)	c (nm)	α	β	γ
Fe ₃ O ₄ -CeO ₂	Hexagonal	0.48	0.48	0.4	90	90	120
Fe ₃ O ₄ -CeO ₂ -25K	Hexagonal	0.84	0.84	1.2	90	90	120

With the help of ¹H NMR, FAME percentage of sample obtained after transesterification of rapeseed oil with Fe₃O₄-CeO₂-25K was found to be 96.13%. Figs. S3a and S3b demonstrates the ¹H NMR and ¹³C spectrum of fatty acid methyl esters sample obtained with help of Fe₃O₄-CeO₂-25K catalyst respectively. It helps to characterize FAME and can be used to conform the existence of methyl esters in the biodiesel.

In ¹H NMR the signal at 3.64 ppm indicates methoxy group (A_{ME}) of FAME and signal at 2.27 ppm corresponding to methylene group (A_{CH₂}). The presence of these signal in the biodiesel sample verifies the presence of methyl ester. Apart from the signal used for the quantification, there are other identifiable peaks such as signal at 0.87–0.97 ppm for CH₂-CH₃ or for latter methyl group. The peaks in the range of 1.24–2.3 represents CH₂ (methylene group). The signals at 5.3 range indicates presence of CH=CH (double bond) groups or olefinic groups [27]. In ¹³C NMR the signal at the range of 174 ppm and 51 ppm indicates existence of ester carbonyl –COO– and C–O respectively. The unsaturation in biodiesel sample was confirmed with help of signals at 132.11 ppm and 126.89 ppm. The presence of –CH₂ group was showed with help of signals in the region of 21–35 ppm [27].

3.4. Influence of various parameters on biodiesel production

The higher yield of biodiesel was achieved by optimizing the reaction conditions such as oil to methanol ratio, temperature, time, catalyst amount. Based on the preliminary screening of catalysts, the Fe₃O₄-CeO₂-25K catalyst was found to be more capable catalyst for the conversion of rapeseed oil to biodiesel. Series of transesterification reactions were performed using Fe₃O₄-CeO₂-25K in order to achieve the reaction parameters for optimization.

3.4.1. Effect of catalyst amount (weight %) in biodiesel production

The effect of catalyst concentration on biodiesel production was investigated by performing reactions at various catalyst concentration from 1.5 wt % to 6 wt % of oil. The 96.13% of biodiesel yield was obtained within 120 min of reaction time at 65 °C by using 4.5 wt % catalyst and 1:7 oil to methanol molar ratio (Fig. 8a). The conversion of oil to biodiesel raises with increase in amount of catalyst up to 4.5 wt % and extra rise in catalyst concentration beyond the optimum value showed reduction in biodiesel yield due to decrease in the availability of active sites. The additional amount of catalyst aids to saponification of oil which will finally inhibits the reaction [20,21].

3.4.2. Effect of temperature in biodiesel production

The influence of temperature for high yield reaction which was investigated by conducting reaction at various temperatures using 4.5 wt % catalyst, 1:7 oil to methanol molar ratio for 120 min reaction time (Fig. 8b). The yield of biodiesel increased gradually up to 65 °C and resulted in maximum yield of fatty acid methyl esters. After 65 °C biodiesel yield reduced with rise in temperature, which

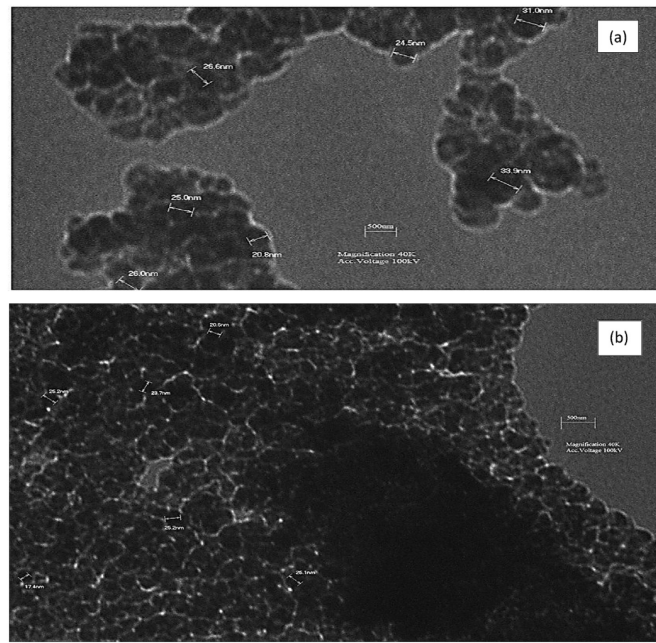


Fig. 4. TEM image of (a) $\text{Fe}_3\text{O}_4\text{-CeO}_2$ and (b) $\text{Fe}_3\text{O}_4\text{-CeO}_2\text{-}25\text{K}$

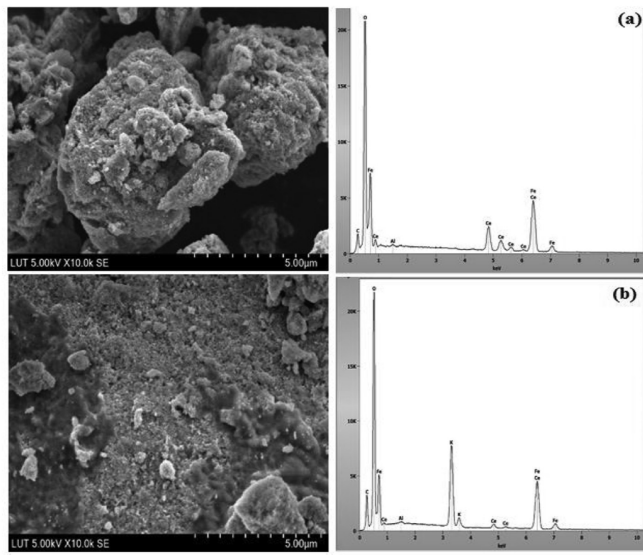
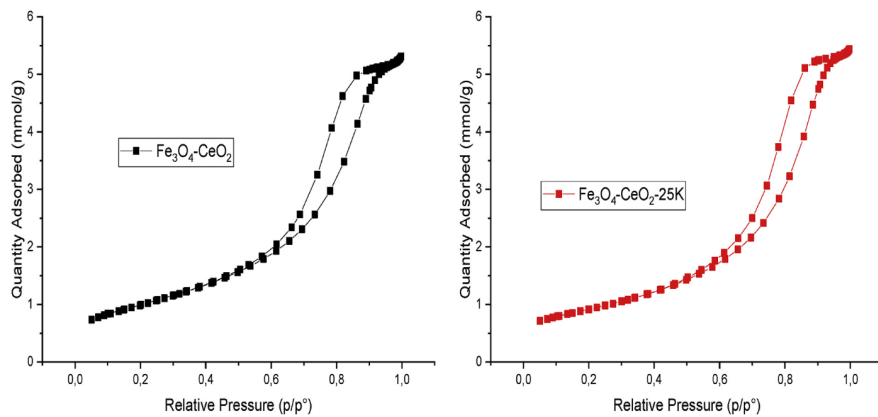
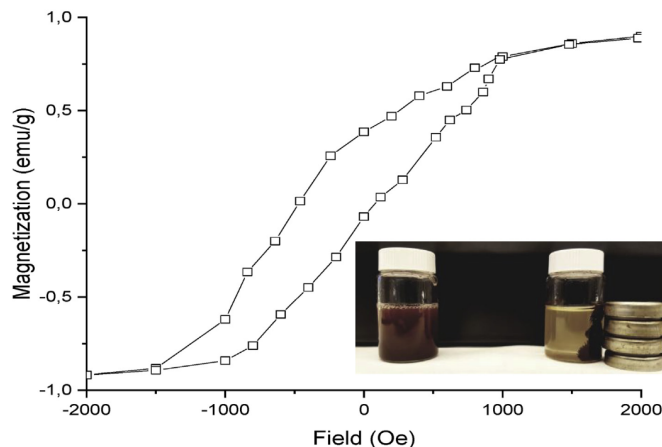


Fig. 5. (a) SEM image and EDS of $\text{Fe}_3\text{O}_4\text{-CeO}_2$ (b) SEM image and EDS of $\text{Fe}_3\text{O}_4\text{-CeO}_2\text{-}25\text{K}$

Table 2

The results of Brunauer-Emmett-Teller surface area analysis.

Parameters	$\text{Fe}_3\text{O}_4\text{-CeO}_2$	$\text{Fe}_3\text{O}_4\text{-CeO}_2\text{-25K}$
Surface area	BET surface area (m^2/g)	80.37
Pore volume	Single point adsorption total pore volume of pores (cm^3/g)	0.177
Pore size	Adsorption average pore width (nm)	8.81
		72.84
		0.18
		9.99

**Fig. 6.** N_2 adsorption-desorption isotherm plot of $\text{Fe}_3\text{O}_4\text{-CeO}_2$ and $\text{Fe}_3\text{O}_4\text{-CeO}_2\text{-25K}$ **Fig. 7.** The magnetization versus magnetic field of $\text{Fe}_3\text{O}_4\text{-CeO}_2\text{-25K}$ at 300 K.

is due to the fact that elevated temperature favors methanol vaporization as well as saponification reaction [20,28,29]. Alkaline catalyst favor the saponification of the triglycerides at elevated prior to the completion of the transesterification process [40,41].

3.4.3. Effect of oil to methanol ratio in biodiesel production

The biodiesel conversion significantly increases as oil to

methanol molar ratios were raised from 1:5 to 1:11 illustrated in Fig. 8c. The reaction was carried out at 4.5 wt % catalyst at 65 °C for 120 min of reaction time. The biodiesel yield was adversely affected on rising methanol concentration above the optimum amount (1:7) which was due to the higher solubility of glycerol to ester phase resulting in difficulty in separation of biodiesel. The excess amount of methanol than optimum limit leads to increasing the solubility of

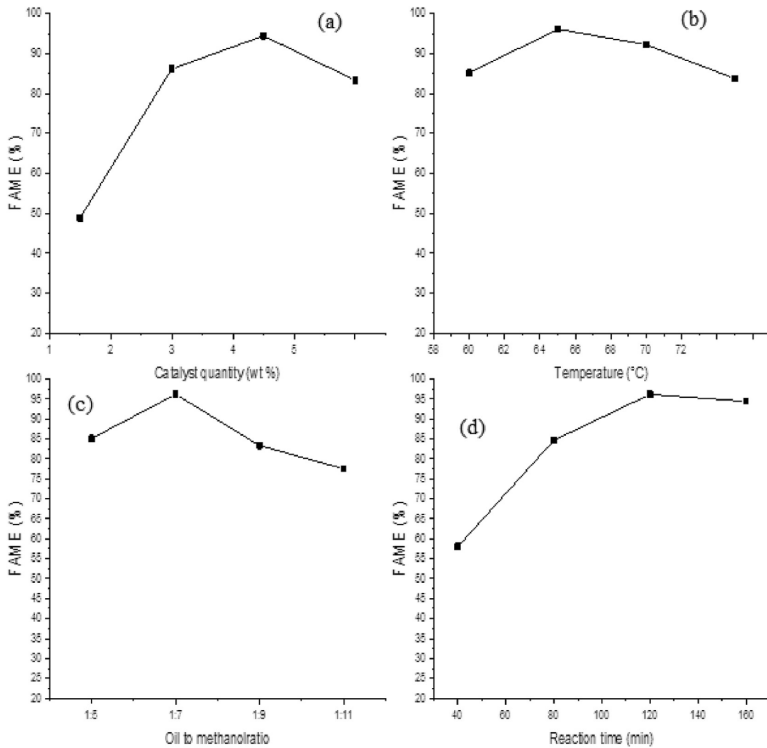


Fig. 8. (a). Effect of catalyst amount (weight %) on FAME yield (b). Effect of reaction temperature on FAME yield (c). Effect of oil to methanol molar ratio on FAME yield (d). Effect of reaction time on FAME yield.

glycerol into the ester phase thereby encouraging the reverse reaction between glycerol and ester which reduces the yield of biodiesel [30,31].

3.4.4. Effect of reaction time in biodiesel production

The effect of reaction time on transesterification reaction was observed by executing reactions for various time intervals using 4.5 wt % catalyst, 1:7 oil to methanol molar ratio at 65 °C depicted in Fig. 8d. The fatty acid methyl ester content rose with increase in reaction time up to 120 min and reached at its maximum. After 120 min FAME percentage remains almost constant, without much reduction in ester content.

3.5. Properties of synthesized biodiesel from rapeseed oil

The properties of rapeseed oil methyl esters were determined using EN 14214 method as presented in Table 3. All these features play a key role in biodiesel quality. The acid value of rapeseed oil methyl ester was found to be 0.32 mg KOH/g and it was within the limits of European International standard organization (EN ISO) method. The increase in acid value can result in difficulties like corrosion of rubber parts of engine and filter clogging [32]. The density and kinematic viscosity are other two main fuel features which influence the fuel injection operation. Higher values of these factors can negatively affect fuel injection process and leads in the formation of engine deposits [33,34]. The density and kinematic viscosity of rapeseed oil methyl esters were 880.30 kg/m³ and

Table 3

Properties of rapeseed oil methyl esters ($\text{Fe}_3\text{O}_4\text{-CeO}_2\text{-25K}$ catalyst at concentration of 4.5 wt %, 1:7 oil to methanol ratio, reaction temperature 65 °C, reaction time 120 min).

Property	EN 14214 test method	Limits	Methyl ester from rapeseed oil
Acid value (mg KOH/g)	Pr EN14104	0.5 max	0.308
Density at 15 °C (kg/m ³)	EN ISO 12185	860–900	880.30
Kinematic viscosity at 40 °C mm ² /s	EN ISO 3104	3–5	4.37
Flash point (°C)	EN ISO 2719	—	171 °C

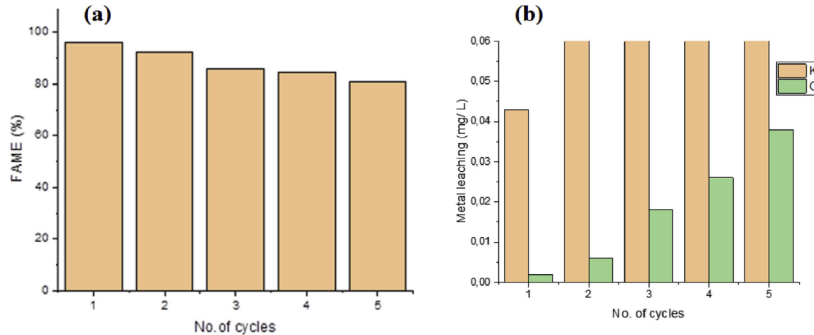


Fig. 9. (a) Reusability analysis and (b) leaching test of $\text{Fe}_3\text{O}_4\text{-CeO}_2\text{-25K}$ catalyst up to five transesterification reactions.

4.37 mm²/s respectively. The other factor is flash point which specifies the minimum temperature at which fuel starts to ignite. It is vital to know flash point value for fuel handling and storage [35].

3.6. Reusability of catalyst

For an environmental friendly biodiesel production process, the concept of reusability of catalyst is a vital element. The deposition of impurities or oil on catalyst surface and thermal deactivation are typical reasons for catalyst deactivation. The cleaning of catalyst with suitable solvent and calcination helps in its regeneration [36]. To analyze the reusability of $\text{Fe}_3\text{O}_4\text{-CeO}_2\text{-25K}$ nanocatalyst, firstly it was separated from rapeseed oil methyl esters and glycerol. After transesterification, the separated catalyst was washed with methanol and heptane to remove impurities. The washed catalyst was dried at 60 °C and calcined at 500 °C for 4 h to reactivate the catalyst. It was detected that activity of catalyst decreased continuously up to the five runs (Fig. 9a). It indicates that catalyst activity decreased from 96.13% to 80.94% in five cycles. In comparison with earlier reported magnetic nanocatalyst, the synthesized catalyst showed greater yield in biodiesel production [16,42].

The leaching test was performed to determine the cause of the decrease in activity of synthesized nanocatalyst and its stability. Fig. 9b represents the concentration of leached metal ion determined using inductively coupled plasma (ICP, Agilent 5110) after different cycles. The concentration of potassium and cerium in the solution after each cycle were less than 0.56 mg/L and 0.038 mg/L respectively.

4. Conclusion

The transesterification of rapeseed oil to biodiesel was successfully done with help of $\text{Fe}_3\text{O}_4\text{-CeO}_2\text{-25K}$. The catalytic activity of different weight percentage of potassium impregnated $\text{Fe}_3\text{O}_4\text{-CeO}_2$ was investigated and best activity was attained at optimum loading of KOH (25 wt %) to $\text{Fe}_3\text{O}_4\text{-CeO}_2$. The characterization of synthesized catalyst and integration of potassium ions to $\text{Fe}_3\text{O}_4\text{-CeO}_2$ nanostructure confirmed by FTIR, XRD, SEM, TEM. The nanocatalyst showed 96.13% fatty acid methyl ester content using 4.5 wt % catalyst amount, 1:7 oil to methanol ratio at 65 °C with in a reaction time of 120 min. The properties of biodiesel such as acid value, density, kinematic viscosity and flash point were within the EN 14214 limits. All these results, indicates $\text{Fe}_3\text{O}_4\text{-CeO}_2\text{-25K}$ is an efficient catalyst for the production of superior quality biodiesel

from rapeseed oil as a feedstock. The reusability of catalyst also exhibited favorable result, which makes it cost effective and more eco-friendly. Moreover, the synthesized catalyst was nontoxic and resulted in higher conversion rate of rapeseed oil to biodiesel compared to other magnetic nanocatalyst.

Appendix A. Supplementary data

Supplementary data to this article can be found online at <https://doi.org/10.1016/j.renene.2019.03.042>.

References

- [1] A. Demirbas, Biodiesel production from vegetable oils by supercritical methanol, *J. Sci. Ind. Res.* 64 (2005) 858–865.
- [2] J.X. Wang, K.T. Chen, S.T. Huang, K.T. Chen, C.C. Chen, Biodiesel Production from Soybean Oil Catalyzed by Li_2CO_3 , 2012, pp. 1619–1625, <https://doi.org/10.1007/s11746-012-2074-2>.
- [3] S.P. Singh, D. Singh, Biodiesel production through the use of different sources and characterization of oils and their esters as the substitute of diesel: a review, *Renew. Sustain. Energy Rev.* 14 (2010) 200–216, <https://doi.org/10.1016/j.rser.2009.07.017>.
- [4] E. Bet-Moushoul, K. Farhadi, Y. Mansourpanah, A.M. Nikbakht, R. Molaei, M. Forough, Application of CaO-based/Al nanoparticles as heterogeneous nanocatalysts in biodiesel production, *Fuel* 164 (2016) 119–127, <https://doi.org/10.1016/j.fuel.2015.09.067>.
- [5] G. Huang, F. Chen, D. Wei, X. Zhang, G. Chen, Biodiesel production by microalgal biotechnology, *Appl. Energy* 87 (2010) 38–46, <https://doi.org/10.1016/j.apenergy.2009.06.016>.
- [6] M.E. Huns, R.A. Cairncross, S. Spatari, Life-cycle assessment of biodiesel produced from grease trap waste, *Environ. Sci. Technol.* 50 (2016) 2718–2726, <https://doi.org/10.1021/es502667>.
- [7] A. Abbaszaadeh, B. Ghobadian, M.R. Omidkhah, G. Najafi, Current biodiesel production technologies: a comparative review, *Energy Convers. Manag.* 63 (2012) 138–148, <https://doi.org/10.1016/j.enconman.2012.02.027>.
- [8] G. Baskar, R. Aliswarya, Trends in catalytic production of biodiesel from various feedstocks, *Renew. Sustain. Energy Rev.* 57 (2016) 496–504, <https://doi.org/10.1016/j.rser.2015.12.101>.
- [9] L. Wen, Y. Wang, D. Lu, S. Hu, H. Han, Preparation of KF/CaO nanocatalyst and its application in biodiesel production from Chinese tallow seed oil, *Fuel* 89 (2010) 2267–2271, <https://doi.org/10.1016/j.fuel.2010.01.028>.
- [10] R. Madhuvilakku, S. Piraman, Biodiesel synthesis by $\text{TiO}_2\text{-ZnO}$ mixed oxide nanocatalyst catalyzed palm oil transesterification process, *Bioresour. Technol.* 150 (2013) 55–59, <https://doi.org/10.1016/j.biortech.2013.09.087>.
- [11] S. Ben, F. Zhao, Z. Safaei, I. Babu, D. Lakshmi, M. Silianpää, Applied Catalysis B: environmental Reactivity of novel Ceria – perovskite composites $\text{CeO}_2\text{-LaMO}_3$ (MCu, Fe) in the catalytic wet peroxidative oxidation of the new emergent pollutant “Bisphenol F”: characterization, kinetic and mechanism studies, *Appl. Catal. B Environ.* 218 (2017) 119–136, <https://doi.org/10.1016/j.apcatb.2017.06.047>.
- [12] B. Gao, Z. Safaei, I. Babu, S. Iftekhar, E. Iakovleva, V. Srivastava, B. Doshi, S. Ben, S. Kallioja, Journal of Photochemistry and Photobiology A: Chemistry Modification of ZnIn_2S_4 by anthraquinone-2-sulfonate doped polypprole as acceptor-donor system for enhanced photocatalytic degradation of

- tetracycline, J. Photochem. Photobiol. A Chem. 348 (2017) 150–160, <https://doi.org/10.1016/j.jphotochem.2017.08.037>.
- [13] I. Ambat, V. Srivastava, M. Sillanpää, Recent advancement in biodiesel production methodologies using various feedstock: A review 90 (2018) 356–369.
- [14] A. Lu, E.L. Salabas, F. Schütt, Magnetic Nanoparticles: Synthesis, Protection, Functionalization, and Application Angewandte, 2007, pp. 1222–1244, <https://doi.org/10.1002/anie.200602866>.
- [15] A. Gogoi, M. Navgire, K. Chandra, P. Gogoi, Fe₃O₄–CeO₂ metal oxide nanocomposite as a Fenton-like heterogeneous catalyst for degradation of catechol, Chem. Eng. J. 311 (2017) 153–162, <https://doi.org/10.1016/j.cej.2016.11.086>.
- [16] S. Hu, Y. Guan, Y. Wang, H. Han, Nano-magnetic catalyst KF/CaO–Fe₃O₄ for biodiesel production, Appl. Energy 88 (2011) 2685–2690, <https://doi.org/10.1016/j.apenergy.2011.02.012>.
- [17] V. Srivastava, T. Kohout, M. Sillanpää, Journal of Environmental Chemical Engineering Potential of cobalt ferrite nanoparticles (CoFe₂O₄) for remediation of hexavalent chromium from synthetic and printing press wastewater, Biochem. Pharmacol. 4 (2016) 2922–2932, <https://doi.org/10.1016/j.jece.2016.06.002>.
- [18] L.H. Andrade, H.E. Toma, M.F.C. Andrade, A.L.A. Parussulo, C.G.C.M. Netto, Lipase immobilized on polydopamine-coated magnetite nanoparticles for biodiesel production from soybean oil, Biofuel Res. J. 10 (2016) 403–409, <https://doi.org/10.18331/BRJ2016.3.2.5>.
- [19] M. Akia, F. Yazdani, E. Motaei, D. Han, H. Arandian, A review on conversion of biomass to biofuel by nanocatalysts, Biofuel Res. J. 1 (2014) 16–25.
- [20] V. Singh, F. Bux, Y.C. Sharma, A low cost one pot synthesis of biodiesel from waste frying oil (WFO) using a novel material, β-potassium diizirconate (β-K₂Zr₂O₅), Appl. Energy (2016), <https://doi.org/10.1016/j.apenergy.2016.02.135>.
- [21] M. Takase, Y. Chen, H. Liu, T. Zhao, L. Yang, X. Wu, Biodiesel production from non-edible Silybum marianum oil using heterogeneous solid base catalyst under ultrasonication, Ultrason. Sonochem. 21 (2014) 1752–1762, <https://doi.org/10.1016/j.ulsonch.2014.04.003>.
- [22] N. Pereira, F. Sávio, G. Pereira, C.C. Galvão, A. Maria, R. Bastos, V. Lins, M. Aparecida, N. Medeiros, D.L. Filho, Biodiesel from residual Oils: less environmental impact with sustainability and simplicity 17 (2016) 1–14, <https://doi.org/10.9734/CSIJ/2016/29455>.
- [23] F. Qiu, Y. Li, D. Yang, X. Li, P. Sun, Heterogeneous solid base nanocatalyst: preparation, characterization and application in biodiesel production, Bioresour. Technol. 102 (2011) 4150–4156, <https://doi.org/10.1016/j.biortech.2010.12.071>.
- [24] Y. Li, F. Qiu, D. Yang, X. Li, P. Sun, Preparation, characterization and application of heterogeneous solid base catalyst for biodiesel production from soybean oil, Biomass Bioenergy 35 (2011) 2787–2795, <https://doi.org/10.1016/j.biomass.2011.03.009>.
- [25] D. Salinas, G. Pecchi, V. Rodríguez, J. Luis, G. Fierro, Effect of Potassium on Sol-Gel Cerium and Lanthanum Oxide Catalysis for Soot Combustion, 2015, pp. 68–77.
- [26] F. Qiu, Y. Li, D. Yang, X. Li, P. Sun, Bioresource Technology Heterogeneous solid base nanocatalyst: Preparation, characterization and application in biodiesel production 102 (2011) 4150–4156, <https://doi.org/10.1016/j.biortech.2010.12.071>.
- [27] M. Tariq, S. Ali, N. Khalid, Activity of homogeneous and heterogeneous catalysts, spectroscopic and chromatographic characterization of biodiesel: a review, Renew. Sustain. Energy Rev. 16 (2012) 6303–6316, <https://doi.org/10.1016/j.rser.2012.07.005>.
- [28] E.C. Abba, G.I. Nwandikom, C.C. Egwuonwu, N.R. Nwakuba, Effect of reaction temperature on the yield of biodiesel from neem seed oil, Am. J. Energy Sci. 3 (2016) 16–20.
- [29] T. Eevera, K. Rajendran, S. Saradha, Biodiesel production process optimization and characterization to assess the suitability of the product for varied environmental conditions, Renew. Energy 34 (2009) 762–765, <https://doi.org/10.1016/j.renene.2008.04.006>.
- [30] G. Kafui, A. Sunnu, J. Parbey, Effect of biodiesel production parameters on viscosity and yield of methyl esters: Jatropha curcas, Elaeis guineensis and Cocos nucifera, Alexandria Eng. J. 54 (2015) 1285–1290, <https://doi.org/10.1016/j.aej.2015.09.011>.
- [31] F.F. Banhani, Transesterification and production of biodiesel from waste cooking oil: effect of operation variables on fuel properties 4 (2017) 154–160, <https://doi.org/10.11648/j.ajche.20160406.13>.
- [32] A.B. Chhetri, M.S. Tango, S.M. Budge, K.C. Watts, M.R. Islam, Non-edible plant oils as new sources for biodiesel production, Int. J. Mol. Sci. 9 (2008) 169–180, <https://doi.org/10.3390/ijms9020169>.
- [33] G. Knothe, K.R. Steidley, Kinematic viscosity of biodiesel fuel components and related compounds: Influence of compound structure and comparison to petrodiesel fuel components, Fuel 84 (2005) 1059–1065, <https://doi.org/10.1016/j.fuel.2005.01.016>.
- [34] A. Demirbas, Biodiesel: A Realistic Fuel Alternative for Diesel Engines, 2008, pp. 1–208, <https://doi.org/10.1007/978-1-84628-995-8>.
- [35] H.G. Aleme, P.J.S. Barbeira, Determination of flash point and cetane index in diesel using distillation curves and multivariate calibration, Fuel 102 (2012) 129–134, <https://doi.org/10.1016/j.fuel.2012.06.015>.
- [36] W.V. Prescott, A.J. Schwartz, Nanorods and Nanomaterials Research Progress, 2008, p. 279, http://books.google.es/books/about/Nanorods_Nanotubes_and_Nanomaterials_Res.html?id=a2Dc3CxrM8w&pgis=1.
- [37] N. Zhang, H. Xue, R. Hu, The activity and stability of CeO₂ @ CaO catalysts for the production of biodiesel, RSC Adv. 8 (2018) 32922–32929, <https://doi.org/10.1039/c8ra06884d>.
- [38] M. Mangkin, D. Berpenyokong, Optimization of process parameters for the production of biodiesel from waste cooking oil in presence of bifunctional γ-Al₂O₃–CeO₂ supported catalysts, Malays. J. Anal. Sci. 19 (2015) 8–19.
- [39] L.M. Orozco, M. Renz, A. Corma, Cerium oxide as a catalyst for the ketonization of aldehydes: mechanistic insights and a convenient way to alkanes without the consumption of external hydrogen 19 (2017) 1555–1569, <https://doi.org/10.1039/c6gc0351f>.
- [40] A.O. Eloka-eboka, O.G. Igbum, F.I. Inambao, Optimization and effects of process variables on the production and properties of methyl ester biodiesel, J. Energy South. Afr. 25 (2014) 39–47.
- [41] R. Saha, V.V. Goud, Ultrasound assisted transesterification of high free fatty acids karanja oil using heterogeneous base catalysts, Biomass Conv. Bioref. 5 (2015) 195–207, <https://doi.org/10.1007/s13399-014-0133-7>.
- [42] M. Feyzi, L. Nourozi, M. Zakarianezhad, Preparation and characterization of magnetic CsH₂PW₁₂O₄₀/Fe–SiO₂ nanocatalysts for biodiesel production, Mater. Res. Bull. 60 (2014) 412–420, <https://doi.org/10.1016/j.materresbull.2014.09.005>.

Publication IV

I. Ambat, V. Srivastava, S. Iftekhar, E. Haapaniemi, M. Sillanpää

**Effect of different co-solvents on biodiesel production from various low-cost feedstocks
using Sr-Al double oxides.**

Reprinted with permission from

Renewable Energy

Vol. 146, pp. 2158–2169

© 2020, Elsevier



Effect of different co-solvents on biodiesel production from various low-cost feedstocks using Sr–Al double oxides



Indu Ambat ^{a,*}, Varsha Srivastava ^a, Sidra Iftekhar ^a, Esa Haapaniemi ^b, Mika Sillanpää ^a

^a Department of Green Chemistry, School of Engineering Science, Lappeenranta University of Technology, Sammonkatu 12, FI-50130, Mikkeli, Finland

^b Department of Organic Chemistry, University of Jyväskylä, Finland

ARTICLE INFO

Article history:

Received 12 September 2018

Received in revised form

12 July 2019

Accepted 10 August 2019

Available online 14 August 2019

Keywords:

Biodiesel

Lard oil

Transesterification

Sr–Al double oxides

Waste cooking oil

ABSTRACT

The main objective of the present paper comprises the investigation of biodiesel production from low-cost feedstock such as lard oil and waste cooking oil (WCO) using Sr–Al double oxides. Nanocatalyst was characterised FTIR, XRD, SEM, TEM, BET and XPS. The Sr:Al with 3:1 M ratio showed the best catalytic activity in the conversion of both oils to fatty acid methyl ester. The effect of acetone and tetrahydrofuran (THF) as a co-solvent for transesterification were compared and the best result was obtained with 5% THF. The mutual effect of the nanocatalyst and co-solvent on biodiesel production was investigated. The characterisation of biodiesel synthesised from lard oil and WCO was performed with GC-MS, ¹H and ¹³C NMR. Moreover, the optimum reaction parameters for transesterification reaction was analysed and the yield was determined by ¹H NMR. The maximum yield of 99.7% and 99.4% of lard oil methyl ester and WCO biodiesel were observed with a 0.9 wt% catalyst amount, 1:5.5 oil to methanol ratio in a reaction time of 45 min at 50 °C and 60 °C, respectively. The properties of biodiesel from lard oil and WCO were determined by the EN 14214 method. The regeneration, characterisation and reusability of regenerated catalyst was observed.

© 2019 Elsevier Ltd. All rights reserved.

1. Introduction

Currently, the perpetual concern is the depletion of conventional fuels due to the massive utilisation of fossil fuels. Moreover, the excessive use of petroleum products leads to global warming and environmental pollution. Due to these issues, there is a need for an alternative fuel [1,2]. Biodiesel is a suitable alternative fuel due to its biodegradability, non-toxicity, renewability, lower emission of sulfur and carbon dioxide and eco-friendly nature [3–5].

Biodiesel comprises fatty acid methyl esters, commonly produced by the transesterification of fats or oils using methanol in the presence of a catalyst [3,6,7]. The bottleneck issues associated with the transesterification process are the selection of suitable feedstock, catalyst and an efficient method for the biodiesel production [2,8–10]. The selection of feedstock for biodiesel production plays an important role in the determination of fuel cost. Hence, keeping this point in mind the raw materials used in the present work includes lard oil and waste cooking oil. Furthermore, the application of nanocatalytic technology for biodiesel production helps to

improve catalytic activity, reusability and stability [2,5,11]. The problems involved in the transesterification reaction such as a lower rate of reaction, poor phase separation and soap formation can be resolved with the help of the co-solvent method [8–10,12].

The present work was targeted to synthesise Sr–Al double oxides with four different molar ratios metal ions. The application of Sr–Al double oxides for biodiesel synthesis is rather scanty and not well explored. Moreover, heterogeneous catalyst offers better stability and reusability with lower cost in comparison with homogeneous or biocatalyst [11]. Later, synthesised Sr–Al double oxides were screened for biodiesel production and the catalyst showed the best catalytic activity when used for the further reaction. Furthermore, as the co-solvent plays an important role in the enhancement of biodiesel yield and, therefore, the role of a different co-solvent with Sr–Al nanocatalyst in biodiesel synthesis was also studied in the present work. The combined effect of the nanocatalyst and co-solvent in biodiesel production from different feedstock was investigated. Furthermore, to the best of our knowledge, the transesterification of lard oil and waste cooking oil (WCO) using Sr–Al nanocatalysts and co-solvent have not been investigated. The selection of oil was due to its low cost and availability.

The characterisation of synthesised nanocatalyst was done

* Corresponding author.
E-mail address: indu.ambat@lut.fi (I. Ambat).

using Fourier transform infrared spectroscopy (FTIR), Scanning electron microscopy (SEM), X-ray diffraction (XRD), Transmission electron microscopy (TEM) and Brunauer–Emmett–Teller (BET) and X-ray photoelectron spectroscopy (XPS). The biodiesel obtained after a transesterification reaction was analysed by gas chromatography with mass spectrometry (GC-MS), ^1H and ^{13}C nuclear magnetic resonance (NMR). The reaction parameters such as co-solvent percentage, reaction temperature, molar ratio of oil and methanol, catalyst amount and reaction time were analysed. The physic-chemical properties of obtained biodiesel was determined using EN 14214 method.

2. Experimental

2.1. Chemicals

Lard oil (FFA% = 0.423) and waste cooking oil (FFA% = 0.634) were obtained from Sigma-Aldrich and household oil waste, respectively. The aluminium nitrate nonahydrate, citric acid monohydrate ACS reagent, methanol, acetone, tetrahydrofuran (THF) anhydrous and heptane were purchased from Sigma-Aldrich. The strontium nitrate was obtained from VWR International. All the chemicals were of analytical grade.

2.2. Synthesis and screening of the catalyst

Four different samples of Sr-Al mixed oxides were synthesised using the sol-gel citrate method. The samples were prepared by mixing metal nitrate of Sr/Al in different molar ratios of 1:1, 1:0.51, 1:0.33, and 1:0.25 respectively and stirred for 1 h. Thereafter, stoichiometric amount of citric acid was added to metal nitrate solution followed by additional stirring for 1 h [45]. The molar ratios of citric acid to total metal cations concentration were kept 2 [46]. The mixture was then heated over 100 °C until a clear transparent gel was obtained. The resultant gel was dried at 110 °C overnight and then dried gel was grounded to get fine powder which was further calcined at 700 °C for 5 h. The catalysts were screened for fatty acid methyl ester (FAME) production from lard oil and WCO.

2.3. Characterisation of catalyst

XRD patterns of synthesised catalyst were captured with PANalytical – Empyrean X-ray diffractometer over a 2 θ range of 10–120° with an X-ray source Co-K α of 0.178 nm at 40 mA and 40 kV. FTIR (Vertex 70 model by Bruker) used to analyse functional groups of synthesised catalyst by capturing IR spectra from 400 to 4000 cm $^{-1}$. SEM images of nanocatalysts were obtained by spreading the sample on colloidal graphite with 5 kV accelerating voltage (SEM, Hitachi SU3500). TEM images of the samples were captured using HT7700 (Hitachi). For attaining TEM images, the nanocatalyst was dispersed in ethanol and sonicated for 25 min and a drop of suspension was added to the carbon coated copper grid. Surface area, pore diameter and pore volume of synthesised catalysts were determined using BET surface area analyser (BET, Micromeritics Tristar II plus). Prior to performing BET analysis, the catalyst samples were degassed at 35 °C overnight to remove the moisture from the samples. The surface composition and the binding energies of elements in nanocatalysts were examined by ESCALAB 250 model XPS with an Al-K X-ray source of 1486.6 eV.

2.4. Reaction procedure

Lard and waste cooking oil were used as feedstock for biodiesel production. The fatty acid methyl ester production from each oil

using different ratios of Sr-Al double oxides was done in a 250 ml three neck round bottom flask with mechanical stirrer and reflux condenser at 60 °C by mixing methanol to oil in a 5:1 M ratio and with 2.5 wt% of each catalyst for 120 min. The various methanol to oil ratios were reported for transesterification studies and theoretically 3: 1 M ratio is enough for transesterification reaction [11,35–37]. All the reactions were conducted in triplicates. The phase separation of fatty acid methyl ester, glycerol and catalyst were achieved by the centrifugation of the samples after each reaction. The selection of the best catalyst for further studies was completed by analysing the obtained FAME concentration. In addition, excess methanol in ester phase and catalyst after the reaction were recovered after the transesterification reaction. The separated catalyst was washed with methanol and heptane to remove impurities. After washing, the catalyst reactivation was achieved by drying the recovered catalyst at 60 °C followed by calcination at 700 °C for 5 h.

As an extension of this work, the influence of a different co-solvent like acetone and THF on biodiesel production was investigated. The transesterification reactions were conducted for the comparison of co-solvents by varying its amount from 5 to 20 wt % in each reaction with the best catalyst obtained after the screening procedure. The resulting optimised amount of the best co-solvent with the greatest performing nanocatalyst was used for further biodiesel production studies.

2.5. Analytical methods

The biodiesel attained after the transesterification reaction of lard and WCO was analysed by GC-MS (Agilent-GC6890N, MS 5975) with Agilent DB-wax FAME analysis GC column dimensions 30 m, 0.25 mm, 0.25 μm . The inlet temperature was 250 °C and the oven temperature was programmed at 50 °C for 1 min and it raises at the rate of 25 °C/min to 200 °C and 3 °C/min to 230 °C and then it was held for 23 min. Moreover, ^1H and ^{13}C NMR (Bruker) were used for the estimation of fatty acid esters content and conformation of esters in each sample, respectively. For NMR analysis, fatty acid methyl esters were examined by ^1H NMR and ^{13}C NMR at 400 MHz with CDCl $_3$ as a solvent. The percentage conversion of oil to fatty acid methyl esters (C%) and biodiesel yield are determined by equations (1) and (2), given below [11,37].

$$C(\%) = \frac{2 \times \text{Integration value of protons of methyl ester}}{3 \times \text{Integration value of methyl protons}} \times 100 \quad (1)$$

$$\text{Biodiesel yield (\%)} = \frac{\text{mass of biodiesel}}{\text{mass of oil}} \times 100 \quad (2)$$

However, the biodiesel production was also affected by the reaction parameters such as the amount of catalyst, oil to methanol ratio, reaction temperature and reaction time.

3. Result and discussion

3.1. Screening and selection of nanocatalyst for biodiesel production

The catalytic performance of different molar ratio of Sr:Al catalyst was analysed for the biodiesel production from waste cooking oil and lard oil. The catalytic activity of each catalyst and the viscosity of different FAME samples was indicated in Table 1. The high catalytic activity of Sr:Al with 1.033 M ratio is due to the optimum loading of aluminium ions and strontium ions to nanocatalyst, which offers a proper interaction between the components of the catalyst. Hence, the appropriate structure of the catalyst

Table 1

The efficiency of various catalyst for transesterification.

No.	Catalyst	Molar ratio	Biodiesel yield	Viscosity at 40 °C mm ² /s	
			%	Lard oil WCO	Lard oil (FAME)
1	Sr:Al	1:1	71.25	66.98	5.02
2	Sr:Al	1:0.51	80.93	79.89	4.82
3	Sr:Al	1:0.33	85.09	83.41	4.37
4	Sr:Al	1:0.25	69.42	62.23	5.96
					6.23

provides sufficient active sites for the fatty acids to bind with the nanocatalysts. Moreover, only the biodiesel obtained using Sr:Al with molar ratio 1:0.51 and 1:0.33 were within the EN ISO 3104 limits. Considering the following results, Sr:Al with molar ratio 1:0.33 catalyst was chosen for further optimisation studies. Thereafter, Sr:Al with molar ratio 1:0.33 denoted as Sr: 0.33Al.

3.2. Characterisation of catalyst

The IR bands of Sr: 0.33Al and regenerated Sr: 0.33Al were shown in Fig. 1. The spectra clearly demonstrate the intensity of the IR band and were lower in regenerated Sr: 0.33Al compared to Sr: 0.33Al. The FTIR peaks in the region of 445 cm⁻¹ to 602 cm⁻¹ of the spectrum indicates the frequency vibrations of AlO₆ groups. Moreover, the peaks observed around 723 cm⁻¹ to 872 cm⁻¹ corresponding to the stretching and vibration of AlO₄ [13,14]. The band at 1440.64 cm⁻¹ indicates the presence of Sr–O vibrations. The bending vibrations of OH groups and water molecule crystallisation correspond to the IR spectra of about 3400 cm⁻¹, 3600 cm⁻¹ and 1640 cm⁻¹, respectively [13,15].

Fig. 2 shows the strong and fine XRD pattern of Sr:Al double oxides and regenerated Sr:0.33Al over the 10–120° attribute to the crystalline nature of the synthesised nanocatalyst. The X-ray diffraction patterns at 37.1°, 45.8°, 56°, 57.1°, 58.6°, 67.1° were consigned to the typical peaks of Sr₂Al₂O₆ and show as a match to the earlier report in JCPDS file No. 24–1187. The Sr₂Al₂O₆ termed as a superstructure of the nanocatalysts, Al₂O₃ [41]. The less intense diffraction patterns around 18°, 24.3°, 29.9°, 34.9°, 40.5°, 49.9°, 53.6°, 60.5°, 70.24° indicate the slight existence of SrCO₃ [13,16].

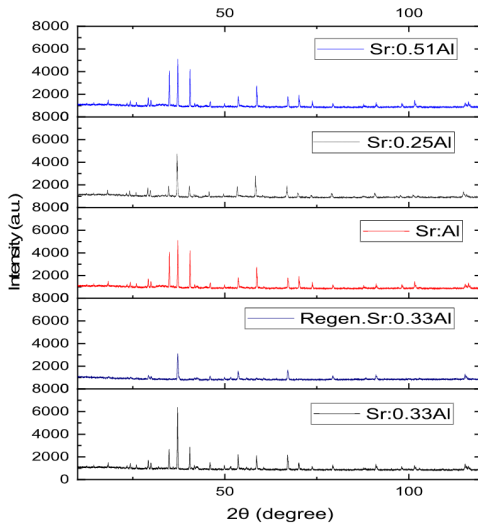


Fig. 2. XRD pattern of Sr: Al double oxides and regenerated Sr: 0.33Al

Concisely, the diffractogram shows that a clear difference happened to Sr: 0.33Al after transesterification. In comparison with Sr: 0.33Al, XRD patterns at 18°, 24°, 40.5°, 58.6° and 70.2° disappeared in the regenerated Sr: 0.33Al and the intensity of rest of the peaks was reduced. This might be due to slight leaching of Sr and Al ions after reuse of the catalyst.

The SEM images of Sr: 0.33Al and regenerated Sr: 0.33Al are shown in Fig. 3, which provide information about the surface structure of the nanocatalyst and the morphological alterations which occurred to the catalyst after biodiesel production. The SEM image of Sr: 0.33Al shows more similar morphology of particles

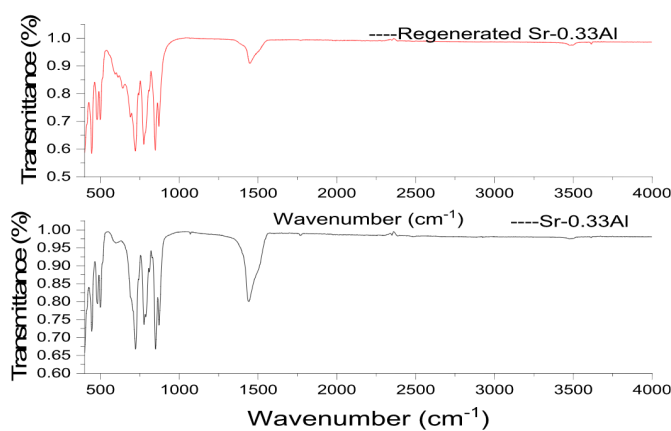


Fig. 1. FTIR spectra of Sr: 0.33Al and regenerated Sr: 0.33Al

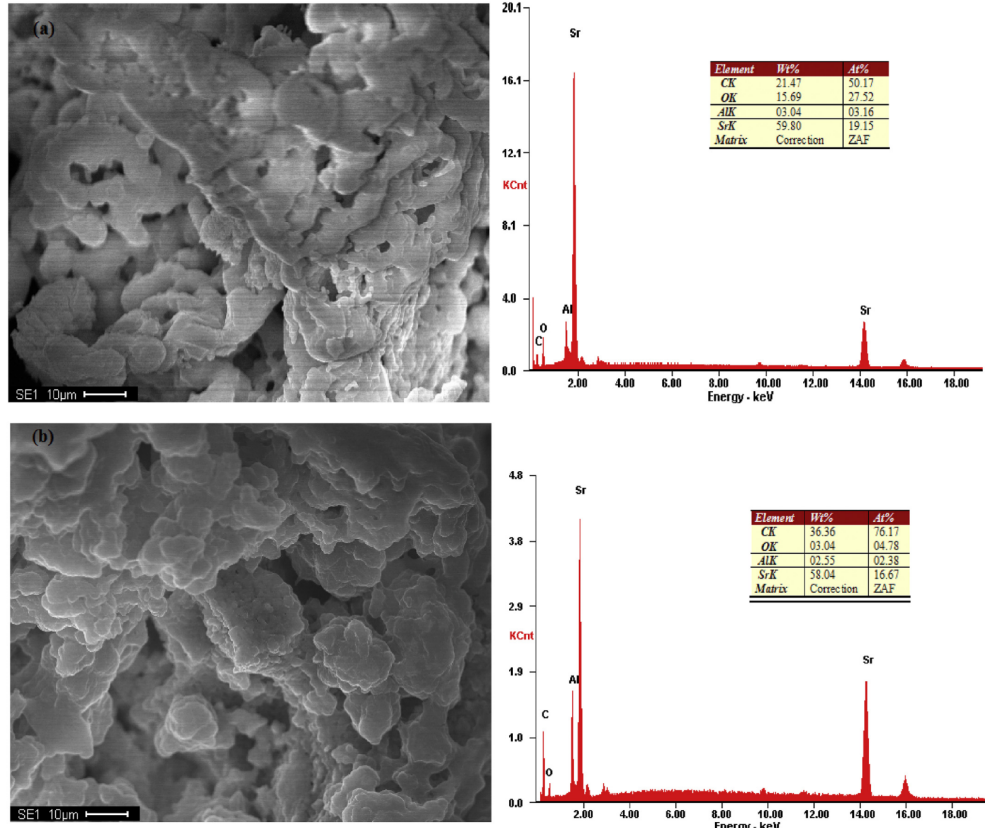


Fig. 3. (a) SEM image and EDS of Sr: 0.33Al (b) SEM image and EDS of regenerated Sr: 0.33Al

throughout the image with slight agglomeration. The minor distortion in the Sr: 0.33Al morphology of the catalyst is directly visible from the SEM images. The EDS graph of Sr: 0.33Al and regenerated Sr: 0.33Al shows the elemental composition of the catalyst before and after the reaction, respectively. The minor variation in the composition of catalyst possibly due to slight leaching of Sr and Al ions after regeneration and reuse of catalyst.

The TEM image of Sr: 0.33Al and regenerated Sr: 0.33Al were depicted in Fig. 4a and b, respectively. The TEM images are strong agreement with the SEM results. The Sr: 0.33Al and regenerated Sr: 0.33Al catalyst have a particle size of 57–100 nm, which was confirmed with help of TEM images. The slight variation in particle form of Sr: 0.33Al and regenerated Sr: 0.33Al were also visible in TEM images.

The specific surface area, pore volume and pore size of Sr: 0.33Al and regenerated Sr: 0.33Al were summarised in Table 2. The BET surface area and average adsorption pore width and pore volume were reduced after the reaction procedure. This result explains one of the reasons for the slight reduction in catalytic activity of the regenerated Sr: 0.33Al. The N₂ adsorption-desorption isotherm for

Sr: 0.33Al and regenerated Sr: 0.33Al from BET analysis is shown in Fig. 5. The hysteresis loop of isotherm indicates the presence of mesoporous materials.

XPS was applied to examine the surface properties and binding energies (BE) of elements in Sr-Al double oxides. The chemical environment of Sr, Al, O, C were simulated by Gaussian curve-fitting of the Sr 3d, Al 2p, O 1s and C 1s spectra. Fig. 6 (a) and (b) depicts XPS fitted spectra of Sr: 0.33Al and the regenerated Sr: 0.33Al nanocatalyst. The Sr-Al double oxides depicts Sr3d signals with two peaks at binding energies of 133.1 and 134.9 eV assigned to Sr 3d_{5/2} and 3d_{3/2}, respectively [17]. The Al 2p spectra of Sr: 0.33Al and regenerated Sr: 0.33Al show binding energy at 73 eV, which corresponds to pure Al. The pure Al helps in the formation of defective oxides that helps in trapping charges [18]. The presence of weakly adsorbed oxygen, stronger binding with adsorbed oxygen and aluminium atoms was described by a signal at 531 eV represented in O 1s spectra of Sr: 0.33Al and regenerated Sr: 0.33Al correspondingly [19]. The binding energies at 284.6 eV and 289 eV in C 1s core level spectrum of Sr: 0.33Al consigned to C–C, C=O respectively. Furthermore, the C 1s spectra of regenerated Sr: 0.33Al

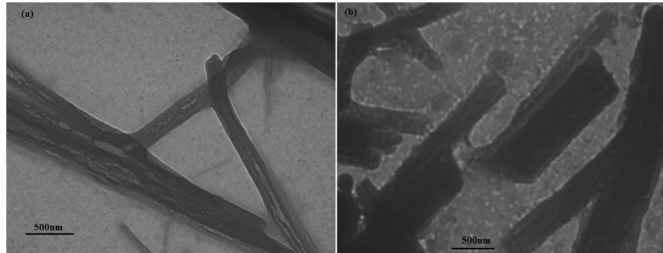


Fig. 4. TEM image of (a) Sr: 0.33Al and (b) Regenerated Sr: 0.33Al

Table 2
The results of Brunauer-Emmett-Teller surface area analysis.

	Parameters	Sr: 0.33Al	Regenerated Sr: 0.33Al
Surface area	BET surface area (m^2/g)	0.95	0.50
	BJH adsorption cumulative surface area of pores (m^2/g)	0.49	0.20
	BJH desorption cumulative surface area of pores (m^2/g)	0.60	0.26
	Single point adsorption total pore volume of pores (cm^3/g)	0.002	0.0009
	BJH adsorption cumulative volume of pores (cm^3/g)	0.0052	0.0027
	BJH desorption cumulative volume of pores (cm^3/g)	0.0056	0.0030
Pore size	Adsorption average pore width (nm)	8.5	6.2
	BJH adsorption average pore diameter (nm)	43.1	53.2
	BJH desorption average pore diameter (nm)	37.1	44.8

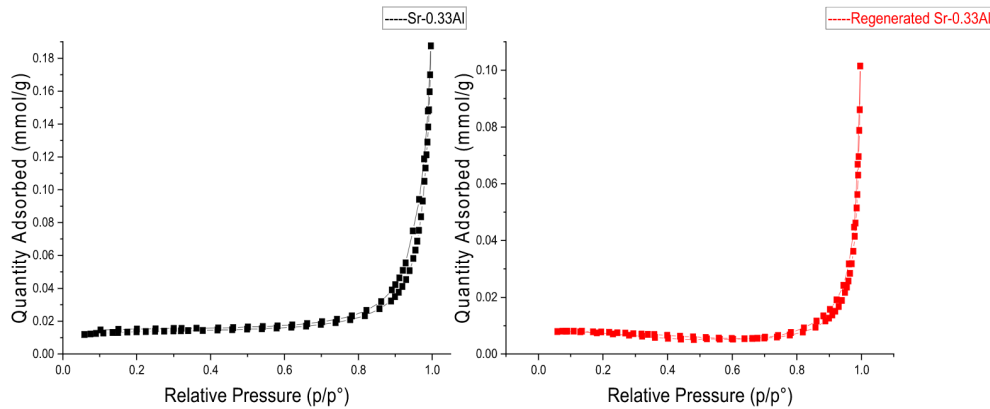


Fig. 5. N_2 adsorption-desorption isotherm plot of Sr: 0.33Al and regenerated Sr: 0.33Al

indicates only the presence of C–C binding energies [20,21].

3.3. Characterisation of biodiesel

The fatty acid methyl esters made from the lard oil and WCO were characterised by GC-MS, ^1H NMR and ^{13}C NMR. The quality of the produced biodiesel should satisfy the criteria determined by ASTM/EN 14214 limits.

The chemical composition of biodiesel was demonstrated with the help of GC-MS chromatogram and National Institute of Standards and Technology (NIST) 2014 MS library. The fatty acid methyl

esters obtained after the transesterification of lard oil and waste cooking oil with Sr: 0.33Al illustrated in Fig. 7. Each FAME peak in the sample was recognised with the help of a library match and the obtained outcomes were represented in Table 3.

The yield of fatty acid methyl esters derived from lard and waste cooking oil was estimated using ^1H and ^{13}C NMR spectroscopy. The conversion was calculated using equation (2), which was already mentioned hereinabove. With the help of ^1H NMR, FAME percentage of sample obtained after transesterification of lard oil and waste cooking oil with Sr: 0.33Al was found to be 99.7% and 99.4% correspondingly. Fig. 8a and b demonstrates the ^1H NMR spectrum

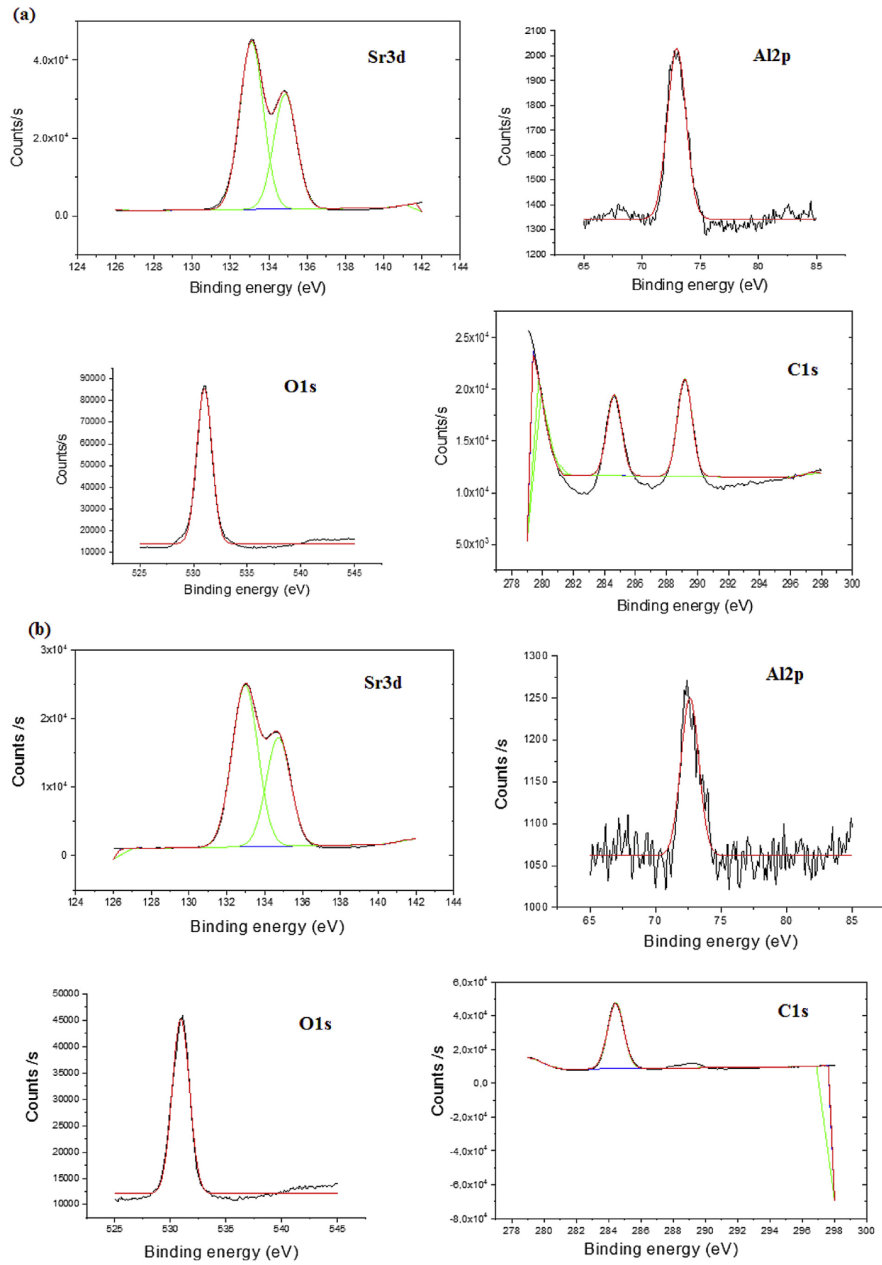


Fig. 6. XPS spectra of (a) bare Sr: 0.33Al and (b) regenerated Sr: 0.33Al nanocatalyst.

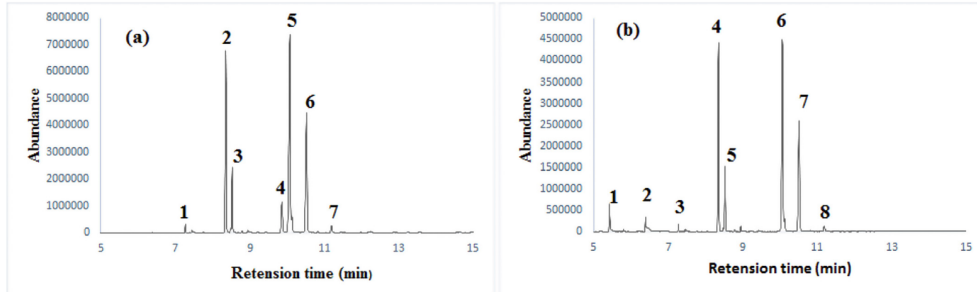


Fig. 7. Illustrates the GC-MS spectrum of biodiesel obtained from (a) lard oil and (b) waste cooking oil, after transesterification with 0.6 wt Sr: 0.33Al, 1:4.5 oil to the methanol molar ratio at 40 °C for 30 min.

Table 3
The composition of biodiesel obtained after transesterification with Sr: 0.33Al.

Peak	Lard oil FAME		Compound name
	Retention time (min)	Library match (%)	
1	7.3	92.6	methyl 12-methyltridecanoate
2	8.4	91.5	methyl hexadecanoate
3	8.5	94.4	methyl (Z)-hexadec-9-enolate
4	9.9	93.5	methyl octadecanoate
5	10.1	96	methyl (E)-octadec-13-enolate
6	10.5	96.5	methyl (11E,14E)-octadeca-11,14-dienoate
7	11.2	89	methyl (9Z,12Z,15Z)-octadeca-9,12,15-trienoate

Peak	Waste cooking oil FAME		Compound name
	Retention time (min)	Library match (%)	
1	5.4	89.9	methyl decanoate
2	6.4	84.6	methyl dodecanoate
3	7.3	92.9	methyl 12-methyltridecanoate
4	8.4	90.3	methyl hexadecanoate
5	8.8	85	methyl 14-methylpentadecanoate
6	10.1	96.8	methyl (E)-octadec-13-enolate
7	10.5	96.4	methyl (11E,14E)-octadeca-11,14-dienoate
8	11.2	93.2	methyl (9Z,12Z,15Z)-octadeca-9,12,15-trienoate

of fatty acid methyl esters sample obtained from lard and waste cooking oil with help of Sr: 0.33Al as catalyst, respectively. It helps to characterise FAME and can be used to conform the existence of methyl esters in the biodiesels.

In ^1H NMR, the signal at 3.63 ppm indicates methoxy group (A_{ME}) of FAME and signal at 2.27 ppm corresponding to the methylene group (A_{CH_2}). The presence of these signal in the biodiesel sample verifies the presence of methyl ester. Apart from the signal used for the quantification, there are other identifiable peaks such as the signal at 0.83–0.86 ppm for CH_2-CH_3 or for latter methyl group. The peaks in the range of 1.22–2.3 represents CH_2 (methylene group). The signals at 5.3 range indicates the presence of $\text{CH}=\text{CH}$ (double bond) groups or olefinic groups [22,23]. The 3.45 ppm corresponds to solvent residual signal [42]. Fig. S1 (a) and S1 (b) represents ^{13}C NMR spectra of biodiesel obtained after transesterification of lard and waste oil with Sr: 0.33Al as nanocatalyst. In ^{13}C NMR, the signal in the range of 174 ppm and 51 ppm indicates the existence of ester carbonyl $-\text{COO}-$ and $\text{C}-\text{O}$, respectively. The unsaturation in biodiesel sample was confirmed with help of signals over the ppm range 126–132 ppm. The presence of the $-\text{CH}_2$ group was shown with the help of the signals in the region of 21–35 ppm [23]. The peaks 0–55 ppm corresponds to aliphatic carbon in fatty acid esters [43,44].

3.4. Influence of various parameters on biodiesel production

The higher yield of biodiesel was achieved by optimising the reaction conditions such as the amount of co-solvent, oil to methanol ratio, reaction temperature, reaction time and catalyst amount. Based on the preliminary screening of catalysts, the Sr: 0.33Al catalyst was found to be a more capable catalyst for the conversion of lard and waste cooking oil to biodiesel. A series of transesterification reactions were performed using Sr: 0.33Al and optimised in order to achieve the reaction parameters for optimisation.

3.4.1. Effect of various co-solvents on biodiesel production

Fig. 9. (a) Shows the influence of various co-solvent on biodiesel production from different oils. The quantity of co-solvent varied over the range of 5–20 wt% based on the weight of oil used for the transesterification reaction. Based on reported studies co-solvent enhance interaction between reactants in presence of minimum amount of catalyst and oil to methanol ratio [8–10]. Therefore slightly higher theoretical minimum of oil to methanol ratio is used to determine effect of co-solvent on transesterification reaction. The evaluation of the effect of the co-solvent on the biodiesel production procedure was attained by performing the transesterification of each oil at 40 °C by using 0.6 wt% catalyst and 1:3.5

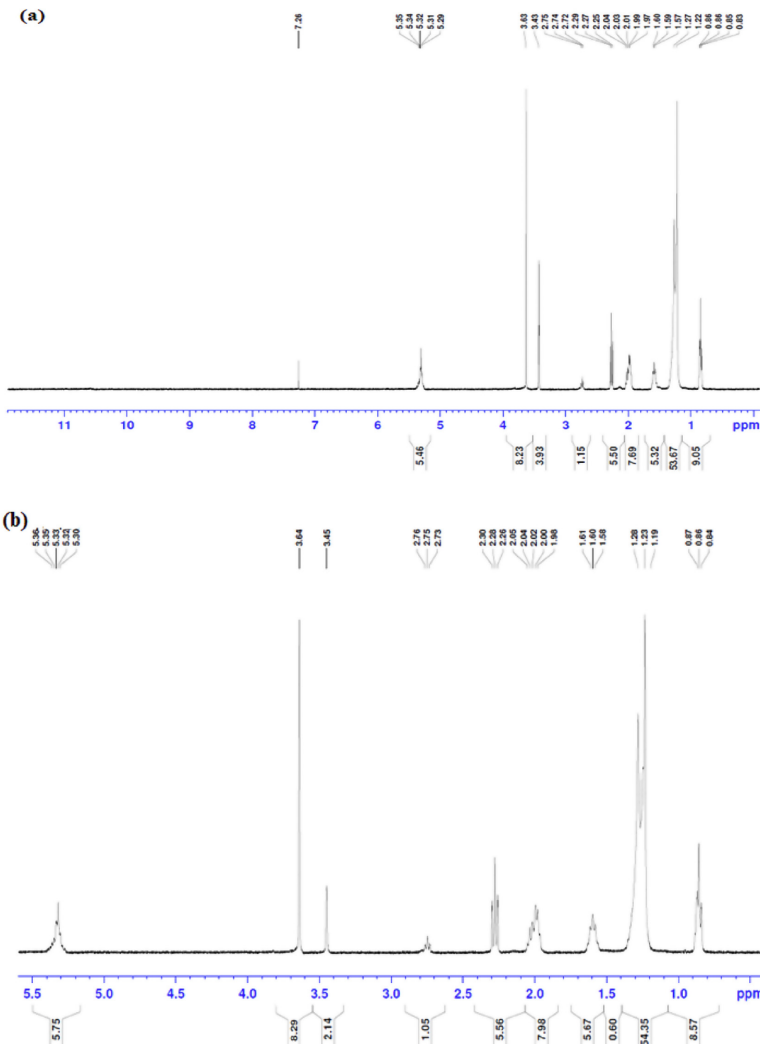


Fig. 8. **a.** The ^1H NMR for the biodiesel sample obtained from lard oil with Sr: 0.33Al
b. The ^1H NMR for the biodiesel sample obtained from waste cooking oil with Sr: 0.33Al.

oil to the methanol molar ratio for 40 min in the presence of various weight percentage of acetone and THF, respectively. Generally, the co-solvent helps to increase the miscibility of reactants in a transesterification reaction and thereby results in a higher yield of fatty acid methyl esters. On the contrary, a larger amount of co-solvent above the optimum value hinders the phase separation of biodiesel and glycerol [8–10]. In the present study, it was observed that the samples with 5 wt% of THF resulted in the maximum yield of FAME from both lard and waste cooking oil. This can be

interpreted to means 5 wt% of THF is enough and efficient to enhance the following factors such as the solubility of methanol and oil, phase separation of FAME and glycerol and for separation of glycerol from reaction mixture.

3.4.2. Effect of temperature on biodiesel production

The influence of temperature on transesterification reaction was investigated by conducting a reaction at various temperatures using 0.9 wt% catalyst, 5 wt% THF, 1:5.5 oil to methanol molar ratio for

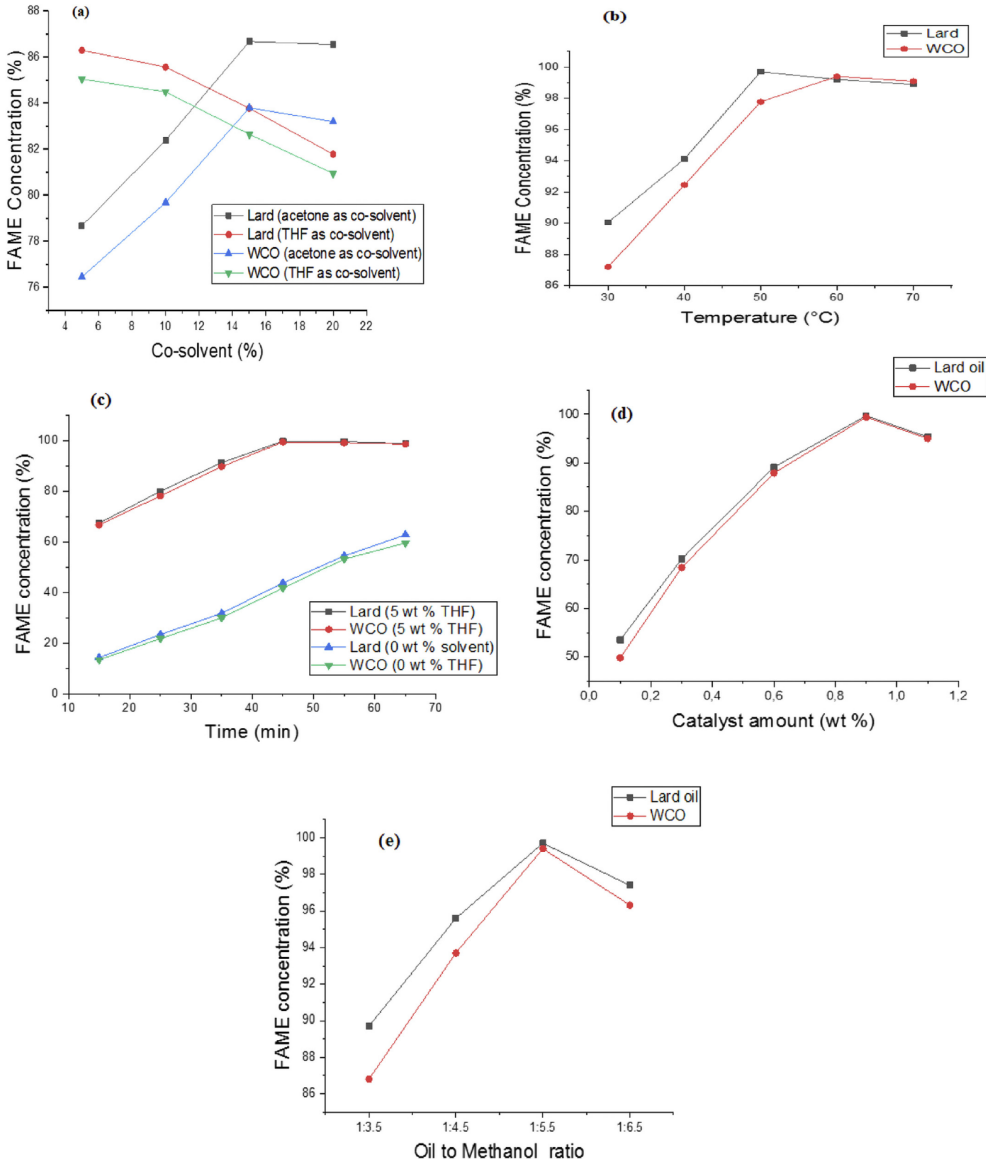


Fig. 9. (a). Effect of various co-solvents on the biodiesel yield (b). Effect of the reaction temperature on the biodiesel yield (c). Effect of the reaction time on the biodiesel yield (d). Effect of the catalyst amount (weight %) on the biodiesel yield (e) Effect of the oil to methanol molar ratio on the biodiesel yield.

45 min reaction time (Fig. 9b). The temperature range chosen for the reaction was lower than the boiling point of THF. The yield of biodiesel from lard oil and WCO increased gradually up to 99.7% and 99.4% at 50 °C and 60 °C, respectively, and resulted in the maximum yield of fatty acid methyl esters. Moreover, the temperature has a direct effect on the rate of the reaction but elevation in temperature after the optimum value decreases the yield of biodiesel which is due to the fact that an elevated temperature favours methanol or co-solvent vaporisation [10,24,25]. Further experiments were conducted at 50 °C and 60 °C for lard and WCO, respectively.

3.4.3. Effect of the reaction time on biodiesel production

The effect of the reaction time on the transesterification reaction of lard oil and WCO was observed by executing reactions for various time intervals using 0.9 wt% catalyst, 1:5.5 oil to methanol molar ratio at 50 °C and 60 °C correspondingly were depicted in Fig. 9c. The present investigation was employed to represent the effect of THF on the rate of the transesterification reaction. The fatty acid methyl ester content rose with the increase in reaction time and reached its maximum with a shorter interval of time in the reaction mixtures with the co-solvent. This is due to the reduction of the phase boundary in reactants and a faster separation of biodiesel and glycerol.

3.4.4. Effect of the catalyst amount (weight%) in biodiesel production

Fig. 9d was applied to determine the effect of the catalyst concentration on biodiesel production by performing reactions at various catalyst concentration from 0.2% to 1.2 wt% of oil. The 99.7% and 99.4% of biodiesel yield was obtained from lard oil and waste cooking oil using 0.9 wt% catalyst, 5 wt% THF as the co-solvent and 1:5.5 oil to methanol molar ratio within 45 min of the reaction time at 50 °C and 60 °C correspondingly. The conversion of oil to biodiesel raises with an increase in the amount of catalyst up to 0.9 wt % and extra rise in the catalyst concentration beyond the optimum value showed reduction in biodiesel yield due to a decrease in the availability of active sites and hindrance to phase separation [9,26,27].

3.4.5. Effect of oil to methanol ratio in biodiesel production

The biodiesel conversion significantly increases as oil to methanol molar ratios were raised from 1:3.5 to 1:6.5 as illustrated in Fig. 9e. The lard oil and waste cooking oil transesterification process was carried out with 0.9 wt% catalyst for 45 min of reaction time at 50 °C and 60 °C, respectively. The biodiesel yield was negatively affected by a rising methanol concentration above the optimum amount (1:5.5) which was due to the higher solubility of glycerol to ester phase resulting in difficulty for the separation of biodiesel. It may also support a reverse reaction than the production of biodiesel [28,29].

3.5. Properties of synthesised biodiesel

The properties of fatty acid methyl esters were determined using the EN 14214/ASTM D6751 method as shown in Table 4. All of these features play a key role in the biodiesel quality. The acid value of lard oil methyl ester and WCO methyl ester were found to be 0.29 mg KOH/g and 0.31 mg KOH/g, respectively. The resulted acid values were within the limits of the European International standard organisation (EN ISO) method. The increase in acid value can result in difficulties like corrosion of rubber parts of engine and filter clogging [30]. The density and kinematic viscosity are other two main fuel features that influence the fuel injection operation. Higher values of these factors can negatively affect the fuel injection process and leads in the formation of engine deposits [31,32]. The density and kinematic viscosity of both methyl esters were within EN ISO 12185 and EN ISO 3104 limits correspondingly. The other factor is flash point, which specifies the minimum temperature at which fuel starts to ignite. It is vital to know the flash point value for fuel handling and storage [33]. Cloud point is important when fuel is exposed to lower temperature where as cetane number directly connects to quality of fuel. The rest of the preferred features such as calorific value, cloud point, cetane number, and pour point are also within EN ISO/ASTM limits.

3.6. Reusability of catalyst

The concept of catalyst reusability plays a vital role in an environmentally friendly biodiesel production process. Therefore, the catalyst recovered after the transesterification reaction was subjected to a cleaning process to remove the deposited oil, products or glycerol. The cleaning of the catalyst with a suitable solvent and calcination helps in its regeneration [11,34]. The catalytic reusability of the Sr:0.25Al nanocatalyst was analysed by the separation of the catalyst from fatty acid methyl esters and glycerol. The catalytic reusability Sr: 0.33Al over lard oil and waste cooking oil using 0.9 wt% catalyst, 5 wt% THF as co-solvent and 1:5.5 oil to methanol molar ratio within 45 min of reaction time at 50 °C and 60 °C correspondingly depicted in Fig. 10. Lard oil and WCO biodiesel yields were decreased from 99.7% to 95.1% and 99.4%–93.7%, respectively, in four cycles. Compared to other reported studies the current catalyst showed higher stability and better biodiesel yield even after five cycles of reaction [11,26,38–40]. The minor changes in the catalyst structure and composition, reduction in BET surface area illustrated in catalyst characterisation findings agrees with the drop in catalytic activity. The reusability test showed that the regenerated catalyst was quite efficient even after four cycles with the significant conversion of oil into biodiesel. The nanocatalyst stability after various cycles were evaluated based on the leached metal ion concentration. The Agilent 5110 Inductively coupled plasma (ICP) was used to measure metal concentration. It was detected that from cycle 1 to cycle 5, the Al and Sr concentrations in solution were less than 0.0072 and 0.024 mg/L.

Table 4
Properties of fatty acid methyl esters from different feedstocks.

Property	EN 14214/ASTM D6751 test method	Limits	Methyl ester from Lard oil	Methyl ester from WCO
Acid value (mg KOH/g)	Pr EN14104	0.5 max	0.29	0.31
Density at 15 °C (kg/m ³)	EN ISO 12185	860–900	882.1	885.6
Kinematic viscosity at 40 °C mm ² /s	EN ISO 3104	3–5	3.98	4.01
Calorific value (MJ/kg)	D6751		39.92	40.45
Flash point (°C)	EN ISO 2719	—	131 °C	138 °C
Cetane number	EN ISO 5165	≥51	63	67
Cloud point (°C)	D2500		8	9
Pour point (°C)	ISO 3016		5	7

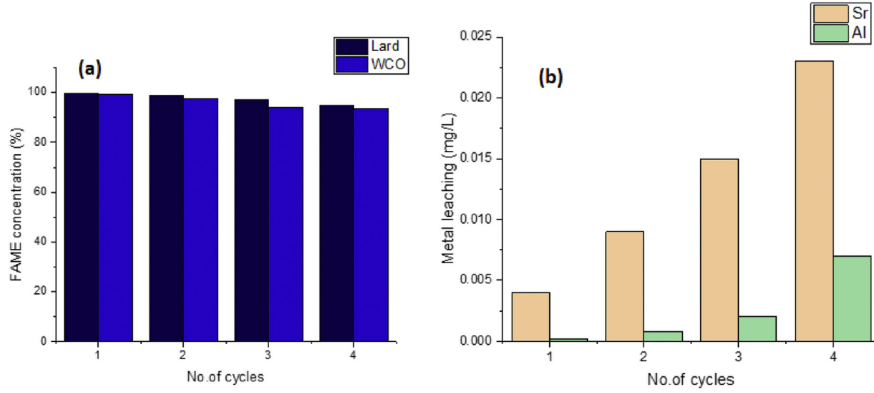


Fig. 10. (a) Reusability analysis of Sr: 0.33Al catalyst and (b) Stability of Sr: 0.33Al catalyst up to four transesterification reactions.

4. Conclusion

The Sr-Al doubleoxides were synthesised and employed for the transesterification reaction of lard and waste cooking oil to biodiesel. The influence of acetone and THF as a co-solvent on biodiesel production were investigated. The combined effect of a co-solvent and nanocatalyst on lard and waste cooking oil were examined. The best catalytic activity was attained with Sr: 0.33Al as a nanocatalyst and THF as a co-solvent. The characterisation of synthesised catalyst and regenerated catalyst were performed by FTIR, XRD, SEM, TEM, XPS and BET. It helps to determine the morphology, composition and stability of the catalyst before and after the transesterification reaction. The factors affecting biodiesel production were optimised. The maximum yield of 99.7% and 99.4% of lard oil methyl ester and WCO biodiesel was observed with 5 wt% THF, 0.9 wt% catalyst amount, 1:5.5 oil to methanol ratio with in a reaction time of 45 min at 50 °C and 60 °C, respectively. The presence of the co-solvent increases the reaction rate and reduction in methanol consumption compared to the usual transesterification reaction. The reusability of the catalyst also exhibited a favourable result, which makes it cost effective and eco-friendlier. The properties of biodiesel such as acid value, density, kinematic viscosity and flash point were within the EN 14214 limits. All these results summarise the efficiency of Sr-Al nanocatalysts as a potential catalyst and THF as a better co-solvent for the production of superior quality biodiesel from different feedstock.

Appendix A. Supplementary data

Supplementary data to this article can be found online at <https://doi.org/10.1016/j.renene.2019.08.061>.

References

- [1] J. Hossain, Bio-Diesel from mustard oil: a renewable alternative fuel for small diesel engines, *Mod. Mech. Eng.* 1 (2011) 77–83, <https://doi.org/10.4236/mme.2011.12010>.
- [2] L. Wen, Y. Wang, D. Lu, S. Hu, H. Han, Preparation of KF/CaO nanocatalyst and its application in biodiesel production from Chinese tallow seed oil, *Fuel* 89 (2010) 2267–2271, <https://doi.org/10.1016/j.fuel.2010.01.028>.
- [3] W. Roschat, T. Sirisanon, T. Kaewpuang, B. Yoosuk, Economical and green biodiesel production process using river snail shells-derived heterogeneous catalyst and co-solvent method, *Bioresour. Technol.* 209 (2016) 343–350, <https://doi.org/10.1016/j.biortech.2016.03.038>.
- [4] I. Thushari, S. Babel, Bioresource Technology Sustainable utilization of waste palm oil and sulfonated carbon catalyst derived from coconut meal residue for biodiesel production, *Bioresour. Technol.* 248 (2018) 199–203, <https://doi.org/10.1016/j.biortech.2017.06.106>.
- [5] G. Baskar, I.A.E. Selvakumari, R. Aiswarya, Biodiesel production from castor oil using heterogeneous Ni-doped ZnO nanocatalyst, *Bioresour. Technol.* 250 (2018) 793–798, <https://doi.org/10.1016/j.biortech.2017.12.010>.
- [6] L.T. Thanh, K. Okitsu, L. Van Boi, Y. Maeda, Catalytic technologies for biodiesel fuel production and utilization of glycerol: a review, *Catalysts* 2 (2012) 191–222, <https://doi.org/10.3390/catal2010191>.
- [7] S.P. Singh, D. Singh, Biodiesel production through the use of different sources and characterization of oils and their esters as the substitute of diesel: a review, *Renew. Sustain. Energy Rev.* 14 (2010) 200–216, <https://doi.org/10.1016/j.rser.2009.07.017>.
- [8] L. Tu, K. Okitsu, Y. Sadanaga, N. Takenaka, Y. Maeda, A new co-solvent method for the green production of biodiesel fuel – optimization and practical application, *Fuel* 103 (2013) 742–748, <https://doi.org/10.1016/j.fuel.2012.09.029>.
- [9] J.M. Encinar, A. Pardal, N. Sánchez, An improvement to the transesterification process by the use of co-solvents to produce biodiesel, *Fuel* 166 (2016) 51–58.
- [10] V. Singh, M. Yadav, Y.C. Sharma, Effect of co-solvent on biodiesel production using calcium aluminium oxide as a reusable catalyst and waste vegetable oil, *Fuel* 203 (2017) 360–369, <https://doi.org/10.1016/j.fuel.2017.04.111>.
- [11] I. Ambat, V. Srivastava, M. Sillanpää, Recent advancement in biodiesel production methodologies using various feedstock: a review, *Renew. Sustain. Energy Rev.* 90 (2018) 356–369.
- [12] S. Sakhivel, S. Halder, P.D. Gupta, Influence of Co-solvent on the production of biodiesel in batch and continuous process, *Int. J. Green Energy* 10 (2013) 876–884, <https://doi.org/10.1080/15435075.2012.727365>.
- [13] M. Feyzi, N. Hosseini, N. Yaghobi, R. Ezzati, Preparation, characterization, kinetic and thermodynamic studies of MgO-La₂O₃ nanocatalysts for biodiesel production from sunflower oil, *Chem. Phys. Lett.* 677 (2017) 19–29, <https://doi.org/10.1016/j.cplett.2017.03.014>.
- [14] M. Sangher, Al-0 infrared vibrational frequencies of y-alumina, *Mater. Lett.* 22 (1995) 109–113.
- [15] L. Song, Y. Li, P. He, S. Zhang, X. Wu, S. Fang, J. Shan, D. Sun, Ultrasonics Sonochemistry Synthesis and sonocatalytic property of rod-shape Sr(OH)₂·8H₂O, *Ultrason. Sonochem.* 21 (2014) 1318–1324.
- [16] E. Rashtizadeh, F. Farzaneh, Z. Talebpour, Synthesis and characterization of SrAl₂O₅ nanocomposite as catalyst for biodiesel production, *Bioresour. Technol.* 154 (2014) 32–37, <https://doi.org/10.1016/j.biortech.2013.12.014>.
- [17] W. Chen, Q. Liu, One-step in situ synthesis of strontium ferrites and strontium ferrites/graphene composites as microwave absorbing materials, *RSC Adv.* (2017) 40650–40657, <https://doi.org/10.1039/C7RA05700H>.
- [18] H. Kang, M.S.P. Reddy, D. Kim, Effect of oxygen species on the positive flat-band voltage shift in Al₂O₃/GaN metal – insulator – semiconductor capacitors with post-deposition annealing, *J. Phys. D Appl. Phys.* 46 (2013), <https://doi.org/10.1088/0022-3727/46/15/155101>.
- [19] C.J. Maldonado, C.J. Lucio-Ortiz, Low Concentration Fe-Doped Alumina Catalysts Using Sol-Gel and Impregnation Methods: The Synthesis, Characterization and Catalytic Performance during the Combustion of Trichloroethylene, *Materials*, 2014, pp. 2062–2086, <https://doi.org/10.3390/ma7032062>.
- [20] M. Wang, J. Han, Y. Hu, R. Guo, C. Mesoporous, N-codoped TiO₂ hybrid shells with enhanced visible light photocatalytic performance, *RSC Adv.* 7 (2017) 15513–15520, <https://doi.org/10.1039/C7RA00985B>.

- [21] S.S. Pitale, I.M. Nagpure, V. Kumar, O.M. Ntwaeborwa, J.J. Terblans, H.C. Swart, Investigations on the low voltage cathodoluminescence stability and surface chemical behaviour using Auger and X-ray photoelectron spectroscopy on, Mater. Res. Bull. 46 (2011) 987–994, <https://doi.org/10.1016/j.materresbull.2011.03.022>.
- [22] M. Tariq, S. Ali, F. Ahmad, M. Ahmad, M. Zafar, N. Khalid, M.A. Khan, Identification, FT-IR, NMR (^1H and ^{13}C) and GC/MS studies of fatty acid methyl esters in biodiesel from rocket seed oil, Fuel Process. Technol. 92 (2011) 336–341, <https://doi.org/10.1016/j.fuproc.2010.09.025>.
- [23] M. Tariq, S. Ali, N. Khalid, Activity of homogeneous and heterogeneous catalysts, spectroscopic and chromatographic characterization of biodiesel: a review, Renew. Sustain. Energy Rev. 16 (2012) 6303–6316, <https://doi.org/10.1016/j.rser.2012.07.005>.
- [24] E.C. Abba, G.I. Nwandikom, C.C. Egwuonwu, N.R. Nwakuba, Effect of reaction temperature on the yield of biodiesel from neem seed oil, Am. J. Energy Sci. 3 (2016) 16–20.
- [25] T. Evera, K. Rajendran, S. Saradha, Biodiesel production process optimization and characterization to assess the suitability of the product for varied environmental conditions, Renew. Energy 34 (2009) 762–765, <https://doi.org/10.1016/j.renene.2008.04.006>.
- [26] V. Singh, F. Bux, Y.C. Sharma, A low cost one pot synthesis of biodiesel from waste frying oil (WFO) using a novel material, β -potassium dizirconate (β - $\text{K}_2\text{Zr}_2\text{O}_5$), Appl. Energy (2016), <https://doi.org/10.1016/j.apenergy.2016.02.135>.
- [27] M. Takase, Y. Chen, H. Liu, T. Zhao, L. Yang, X. Wu, Biodiesel production from non-edible Silybum marianum oil using heterogeneous solid base catalyst under ultrasonication, Ultrason. Sonochem. 21 (2014) 1752–1762, <https://doi.org/10.1016/j.ulsonch.2014.04.003>.
- [28] G. Kafui, A. Sunnu, J. Parbey, Effect of biodiesel production parameters on viscosity and yield of methyl esters: jatropha curcas, Elaeis guineensis and Cocos nucifera, Alexandria Eng. J. 54 (2015) 1285–1290, <https://doi.org/10.1016/j.aej.2015.09.011>.
- [29] F.F. Banhani, Transesterification and production of biodiesel from waste cooking Oil : effect of operation variables on fuel properties, Am. J. Chem. Eng. 4 (2017) 154–160, <https://doi.org/10.11648/j.jache.20160406.13>.
- [30] A.B. Chhetri, K.C. Watts, M.R. Islam, Waste cooking oil as an alternate feedstock for biodiesel production, Energies 1 (2008) 3–18, <https://doi.org/10.3390/en1010003>.
- [31] G. Knithe, K.R. Steidley, Kinematic viscosity of biodiesel fuel components and related compounds, Influence of compound structure and comparison to petrodiesel fuel components, Fuel 84 (2005) 1059–1065, <https://doi.org/10.1016/j.fuel.2005.01.016>.
- [32] A. Demirbas, Biodiesel: a realistic fuel alternative for diesel engines, Biodiesel A Realis, Fuel Altern. Diesel Engines (2008) 1–208, <https://doi.org/10.1007/978-1-84628-995-8>.
- [33] H.G. Aleme, P.J.S. Barbeira, Determination of flash point and cetane index in diesel using distillation curves and multivariate calibration, Fuel 102 (2012) 129–134, <https://doi.org/10.1016/j.fuel.2012.06.015>.
- [34] W.V. Prescott, A.I. Schwartz, Nanorods and Nanomaterials Research Progress, 2008, p. 279, http://books.google.es/books/about/Nanorods_Nanotubes_and_Nanomaterials.Res.html?id=a2De3CxRm8wC&pgis=1.
- [35] N. Kaur, A. Ali, Lithium ions-supported magnesium oxide as nano-sized solid catalyst for biodiesel preparation from mutton fat, Energy Sources, Part A Recover Util Environ Eff 35 (2013) 184–192.
- [36] K. Tahvildari, Y.N. Anaraki, R. Fazaeli, S. Mirpanji, E. Delrish, The study of CaO and MgO heterogeneous nano-catalyst coupling on transesterification reaction efficacy in the production of biodiesel from recycled cooking oil, Iran, J Environ Heal Sci Eng 13 (2015) 1–9, <https://doi.org/10.1186/s40201-015-0226-7>.
- [37] I. Ambat, V. Srivastava, E. Haapaniemi, et al., Nano-magnetic potassium impregnated ceria as catalyst for the biodiesel production, Renew. Energy 139 (2019) 1428–1436.
- [38] G. Galván, R. Romero, A. Ramírez, S. Luz, R. Baeza-jiménez, R. Natividad, Biodiesel production from used cooking oil and sea sand as heterogeneous catalyst, Fuel 138 (2014) 143–148, <https://doi.org/10.1016/j.fuel.2014.07.053>.
- [39] M. Berrios, M.C. Gutiérrez, M.A. Martín, A. Martín, Application of the factorial design of experiments to biodiesel production from lard, Fuel Process. Technol. 90 (2009) 1447–1451, <https://doi.org/10.1016/j.fuproc.2009.06.026>.
- [40] C.B. Ezekamnagh, C.N. Ude, O.D. Onukwuli, Optimization of the methanolysis of lard oil in the production of biodiesel with response surface methodology, Egypt J Pet 26 (2017) 1001–1011, <https://doi.org/10.1016/j.ejpe.2016.12.004>.
- [41] J.A. Alonso, I. Rasines, J.L. Souleyroux, Tristrontium dialuminum hexaoxide: an intricate superstructure of nanocatalyst, Chemlnform 29 (1990) 4768–4771, <https://doi.org/10.021/ci0348a035>.
- [42] G.R. Fulmer, A.J.M. Miller, N.H. Sherdan, H.E. Gottlieb, A. Nudelman, B.M. Stoltz, et al., NMR chemical shifts of trace Impurities : common laboratory solvents , organics , and gases in deuterated solvents relevant to the organometallic chemist, Organometallics 29 (2010) 2176–2179, <https://doi.org/10.1021/oj00106e>.
- [43] E. Alexandri, R. Ahmed, H. Siddiqui, M.J. Choudhary, C.G. Tsiafoulis, I.P. Gerothanassis, High resolution NMR spectroscopy as a structural and analytical tool for unsaturated lipids in solution, Molecules 22 (2017) 1–71, <https://doi.org/10.3390/molecules22101663>.
- [44] A.V. Piterina, J. Barlett, J.T. Pembroke, C-NMR assessment of the pattern of organic matter transformation during domestic wastewater treatment by autothermal aerobic digestion (ATAD), Int. J. Environ. Res. Public Health (2009) 2288–2306, <https://doi.org/10.3390/ijerph6082288>.
- [45] U. Megha, K. Shijina, G. Varghese, Nanosized $\text{LaCo}_{0.5}\text{Fe}_{0.4}\text{O}_3$ perovskites synthesized by citrate sol gel auto combustion method, Processing and Application of Ceramics 8 (2014) 87–92, <https://doi.org/10.2298/PAC1402087M>.
- [46] Y. Xu, Y. He, X. Yuan, Preparation of Nanocrystalline $\text{Sr}_3\text{Al}_2\text{O}_6$ Powders via Citric Acid Precursor, vol. 172, 2007, pp. 99–102, <https://doi.org/10.1016/j.powtec.2006.10.045>.

Publication V

I. Ambat, S. Bec, E. Peltomaa, A. Ojala, V. Srivastava, M. Sillanpää

Phototropic technology for aquaculture wastewater treatment coupled with biodiesel production using the co-solvent method of lipid extraction

Submitted

Phototropic technology for aquaculture wastewater treatment coupled with biodiesel production using the co-solvent method of lipid extraction

Indu Ambat^{a*}, Sabina Bec^a, Elina Peltomaa^{b,c,d}, Anne Ojala^{b,c,d} Varsha Srivastava^a, Mika Sillanpää^a

^a Department of Green Chemistry, LUT University, Sammonkatu 12, FI-50130 Mikkeli, Finland.

^b Faculty of Biological and Environmental Sciences, Ecosystems and Environment Research Programme, University of Helsinki, Niemenkatu 73, FI -15140 Lahti, Finland.

^c Institute of Atmospheric and Earth System Research (INAR)/Forest Sciences, University of Helsinki, P.O. Box 27, FI-00014 Helsinki, Finland.

^d Helsinki Institute of Sustainability Science (HELSUS), Yliopistonkatu 3, 00014 Helsingin yliopisto, Finland.

*Corresponding Author (E-mail: indu.ambat@lut.fi)

Abstract

The current work focused on nutrient removal from aquaculture wastewater integrated with biodiesel production. During this process, freshwater microalgae such as *Chlamydomonas* sp., *Scenedesmus ecornis*, and *Scenedesmus communis* were used for the treatment of two sets of wastewater (AqWW1 and AqWW2) collected from recirculating aquaculture system (RAS). The growth pattern of different algal species in AqWW1 and AqWW2 was examined. The optimization of physical parameters such as temperature, light intensity, and carbon dioxide amount for all the algal species was studied in two sets of wastewater samples. The biomass productivity, lipid content, lipid productivity, nutrient removal of all three algal species in AqWW1 and AqWW2 were monitored. The *Chlamydomonas* sp. showed higher percentage removal of chemical oxygen demand (COD), total nitrogen (TN), and total phosphorus (TP) in AqWW1 but for *S. communis*, and *S. ecornis* in AqWW2. The extraction of lipids from different algal species using 1-ethyl-3-methyl imidazolium diethyl phosphate, [Emim] DEP, and methanol were performed. The *Chlamydomonas* sp. showed the highest biomass productivity in AqWW1 while *S. ecornis* and *S. communis* showed maximum biomass productivity in AqWW2. The lipid content of all algal species was maximum in AqWW1. The co-solvent extraction method of lipids resulted in higher total fatty acid methyl ester, FAME (%DW). The properties of obtained algal biodiesel are within limits of the EN14214 method.

Keywords: Aquaculture wastewater, biodiesel production, co-solvent extraction, microalgae, nutrient removal

1. Introduction

The drastic increase in population results in an enormous consumption of fossil fuels and water resources which leads to scarcity of water and fuels [1, 2]. Besides, the overutilization of conventional fuels results in pollution of the environment and global warming^{3,4}. Hence, there is a need for sustainable alternative fuels and the management of water resources using wastewater treatment technologies [2, 5]. Biodiesel is one of the sustainable alternative fuels composed of fatty acid methyl esters (FAME). FAME can act as an alternative fuel source due to its renewability, biodegradability, eco-friendly nature and non-toxicity [6-8].

The intensive aquaculture is also developed to support the escalating demand for aquatic food sources for the growing population. Furthermore, the fast-growing aquaculture industry produces a large amount of wastewater discharge rich in nitrogen, phosphorus, and organic matter. To avoid eutrophication, the aquaculture wastewater discharge needs to be treated before disposing to the environment or before reuse [2, 9-11].

Currently, there are different ongoing techniques used for the removal of nutrients from wastewater, such as biological nitrification/denitrification and chemical precipitation. All these methods are energy demanding and also result in by-products that are not environmentally friendly [2, 9, 11]. Microalgae serves as a sustainable source for biodiesel production due to its low cost, availability, high oil content, high growth rate, and the capability to reduce greenhouse gases (GHGs) in the atmosphere and it does not compete with vegetable oils^{5,12-14}. Recently, there were reported studies involving the cultivation of algal species on wastewater for nutrient removal coupled with sustainable biodiesel production [2, 9-11, 15-19]. Algae offer efficient nutrient removal process by the utilization of nutrients in wastewater for its growth and production of biomass for biodiesel production [19, 20]. The aquaculture wastewater treatment using bioremediation techniques with algal species is a developing technology, in which the wastewater serves as a feasible medium for algal growth. The combination of wastewater treatment using algal species and biomass production is also one of the eco-friendly and economical ways of biodiesel production [2, 10,11,14,18, 21, 22].

Algal cultivation, cell harvesting, lipid extraction, and transesterification of lipids are the steps involved in the conversion of algae to biodiesel production. Algal lipid extraction can be carried

out using different methods such as solvent extraction methods, osmotic shock method, enzyme extraction method, bead beating, microwave-assisted extraction method, sonication method and ionic liquid extraction method [2, 14, 22, 23]. Ionic liquids (ILs) are salts that remain liquid at moderate to room temperature (0-140 °C). Primarily, ILs can act as an attractive alternative for volatile organic solvents due to their non-volatile nature and thermal stability. Usually, cation of ILs comprises of a nitrogen-containing ring structure (e.g.: pyridine or imidazolium) to which a wide range of functional side groups can be attached. Besides, the low vapor pressure, shorter reaction time, specific stability, polarity, and high-performance yield, make ILs as an attractive substitute for volatile solvents [22, 24-26]. Earlier research work indicates that 1-ethyl-3-methyl imidazolium diethyl phosphate, [Emim] DEP showed as best ionic liquid²². Polar covalent molecules (PCM), are solvents that possess a polar functional group covalently bonded hydrocarbon chain. The solvents with strong polarity can enhance the extraction of oils and fats. The previous reported studies shows methanol as good choice as co-solvent for lipid extraction [27].

The present work was targeted to an integrated approach of cultivation of *Chlamydomonas* sp., *Scenedesmus ecornis*, and *Scenedesmus communis* in aquaculture wastewater collected from a recirculating aquaculture system for nutrient removal and biodiesel production. Furthermore, to the best of our knowledge, the cultivation of these algal species on wastewater for biodiesel production has not been reported. The growth pattern of different algal species in aquaculture wastewater samples was observed, and physical conditions such as temperature, light intensity, and carbon dioxide amount for maximum biomass productivity were investigated. The nutrient removal efficiency and lipid productivity of different algal species were studied. The extraction of lipids using greener solvent such as 1-ethyl-3-methyl imidazolium diethylphosphate, [Emim] DEP ionic liquid coupled with PCM as methanol to enhance the lipid yield was also investigated. Moreover, the extraction of lipids using this co-solvent system has not been explored before.

2. Materials and methods

2.1 Microalgae species and pre- cultivation

The *Chlamydomonas* sp., *Scenedesmus ecornis*, and *Scenedesmus communis* were provided by one of the authors (E. Peltomaa, University of Helsinki, Finland). All the cultures were maintained in Modified WC Medium (MWC). MWC contains the following ingredients: (1) chemicals CaCl₂.2H₂O (36.80 g L⁻¹), MgSO₄.7H₂O (37.00 g L⁻¹), NaHCO₃ (12.60 g L⁻¹), K₂HPO₄.3H₂O (11.40 g L⁻¹), NaNO₃ (85.00 g L⁻¹), Na₂O₃Si.5H₂O (21.20 g L⁻¹); (2) trace elements EDTANa₂ (4.36 g L⁻¹), FeCl₃.6H₂O (3.15 g L⁻¹), CuSO₄.5H₂O (0.01 g L⁻¹), ZnSO₄.7H₂O (0.022 g L⁻¹), CoCl₂.6H₂O (0.01 g L⁻¹), MnCl₂.4H₂O (0.18 g L⁻¹), Na₂MoO₄.2H₂O(0.006 g L⁻¹), H₃BO₃ (1 g L⁻¹); (3) vitamin mix thiamine HCL (0.1 g L⁻¹), biotin (0.0005 g L⁻¹), cyanocobalamin (0.0005 g L⁻¹); (4) TES buffer (0.115 g L⁻¹)[28]. All the pre-cultures were grown in a growth cabinet (SANYO MLR-350 H; 294 L) at 20 °C, in tissue culture flasks containing 250 mL of MWC medium with a continuous light intensity of 150 μmol m⁻² s⁻¹.

2.2 Wastewater collection and characterization

Aquaculture wastewater (AqWW) was collected from a recirculating aquaculture system (RAS) operated at the Laukaa fish farm of the Natural Resources Institute Finland. The two sets of wastewater were collected from the RAS platform; (a) bottom-drained rearing tank (AqWW1) and (b) concentrated stream from drum filters (AqWW2)[29]. Initially, the pre-treatment of wastewater samples were carried out by filtration and centrifugation. The substrate obtained after the pre-treatment process was sterilized using autoclaving [15, 17]. The physicochemical parameters of the collected wastewater sample before and after pre-treatment and sterilization process were examined. The initial inoculum concentration for *Chlamydomonas* sp., *S. ecornis*, and *S. communis* were 0.25 gL⁻¹, 0.24gL⁻¹, and 0.25gL⁻¹, respectively. The algal culture was introduced into each 800 ml of batch culture flask with a working volume of 500 ml of the respective wastewater samples. All the three microalgae species were cultivated as triplicates separately in batch culture flasks for 10 days at 20 °C with a continuous light intensity of 150 μmol m⁻² s⁻¹. Microalgae were also grown in MWC medium under the same condition for comparative analysis. COD, total nitrogen (TN) and total phosphorus (TP) of aquaculture wastewater were analysed according to standard methods (APHA, 2012) and measured with a spectrophotometer DR3900 (Hatch, Germany) [30].

2.3 Analytical procedures

2.3.1 Sampling, microalgae growth rate, and biomass analysis

The growth of each algal species was examined on alternative days by measuring optical density (OD) at 680 nm using spectrophotometric method and was confirmed by dry weight measurements[10, 15-17]. The algal biomass of each algal species was determined gravimetrically at the initial phase, log phase, and late log phase. The effect of physical parameters such as temperature, light intensity, and CO₂ on biomass productivity was studied. The Equation1 represents the gravimetric method used for the calculation of biomass productivity at late lag phase [10,11]. The biomass of each algal species was collected separately using centrifugation and then freeze-dried (Christ Alpha 2-4 LD plus).

$$\text{Biomass productivity } (\text{mgL}^{-1}\text{d}^{-1}) = \frac{\text{Biomass yield } (\text{mgL}^{-1})}{\text{No. of days}} \quad (\text{Eq. 1})$$

2.3.2 Determination of nutrient removal efficiency

The nutrient removal efficiency of each algae species was determined by collecting 20 ml of samples on alternative days from different cultures separately. The samples were then centrifuged and filtered using 0.45 µm syringe filters from VWR. The filtered samples were analysed for COD, total nitrogen (TN) and total phosphorus (TP) according to standard methods [30] and measured with a spectrophotometer DR3900 (Hatch, Germany). The nutrient removal efficiency of each algal species was determined according to the Equation 2.

$$\text{Removal percentage } (\%) = \frac{\text{Initial concentration} - \text{Final concentration}}{\text{Initial concentration}} \times 100 \quad (\text{Eq. 2})$$

2.3.3 Extraction of lipids and determination of lipid productivity

The lipid extraction was carried out by suspending 500 mg of dried algal biomass in a co-solvent prepared by mixing 1-ethyl-3-methyl imidazolium diethylphosphate, [Emim] DEP and methanol as PCM in 1.2:1 (v/v) ratio. The biomass –co-solvent system was mixed continuously for 18h at 65 °C and later, it was then cooled at room temperature. Hexane was added to the mixture to

dissolve the extracted lipids. The separation of ionic liquid- methanol phase, and lipid containing hexane phase was obtained by centrifugation. The hexane was removed by rotary evaporator for lipid recovery [22, 26, 27]. The total content of lipid in each algal species was determined gravimetrically and lipid content of each algae was expressed as a percentage of dry weight. The lipid productivity of each algal species was calculated using Equation 3[10, 17, 26].

$$\text{Lipid productivity } (\text{mg L}^{-1} \text{d}^{-1}) = \text{Biomass productivity} \times \frac{\text{Lipid content}}{100} \quad (\text{Eq. 3})$$

2.4.3 FAME characterization

All algal lipids cannot be converted to fatty acid methyl esters (FAME). Therefore it is crucial to analyze the FAME composition of selected algal species after growing in aquaculture wastewater. The preparation was carried out using transesterification of lipids which was performed using 2M potassium hydroxide in analytical grade methanol. The supernatant was collected for gas chromatography with mass spectrometry (GC-MS) after phase separation of the samples. During the analysis of ester, FAME mix C₄-C₂₄ and pentadecanoic acid methyl ester (Sigma-Aldrich) were used as a quantitative standard and as an internal standard, respectively[31-34]. The obtained FAME was analyzed by GC-MS (Agilent-GC6890N, MS 5975) with Agilent DB-wax FAME analysis, and GC column dimensions 30 m, 0.25 mm, 0.25 μm. The inlet temperature was 250 °C and oven temperature was programmed at 50 °C for 1 min and it raised at the rate of 25 °C/min to 200 °C and 3 °C/min to 230 °C where it was held for 23 min. The FAME composition was identified and quantified with the help of GCMS chromatogram and National Institute of Standards and Technology (NIST) 2014 MS library [7, 35]. The algal FAME properties such as cetane number (CN), saponification value (SV), and iodine value (IV) were determined using empirical formula given below [36-39].

$$\text{Cetane number } (\text{CN}) = 46.3 + \frac{5458}{\text{SV}} - 0.225 \times \text{IV} \quad (\text{Eq 4})$$

Where SV is saponification value (mg KOH g⁻¹) and IV is iodine value ((g I 100g⁻¹)

The iodine value and saponification value of algal FAME can be calculated using empirical formula given below [37-39].

$$IV = \sum \frac{254 \times F \times D}{MW} \quad (Eq\ 5)$$

$$SV = \sum \frac{560 \times F \times D}{MW} \quad (Eq\ 6)$$

Where, F is the percentage weight of each fatty acid, D is the number of double bonds and MW is the molecular weight of the respective fatty acid.

All the experiments were performed in triplicates and average values were reported.

3. Results and discussion

3.1 Wastewater characterization

The characteristic features of AqWW collected from the RAS for algal cultivation are presented in Table 1. The chemical oxygen demand (COD), total nitrogen (TN), total phosphorus (TP), and salinity of aquaculture wastewater from bottom-drained rearing tank (AqWW1) after pre-treatment process and sterilization were lower than concentrated stream from drum filters (AqWW2). The pH of both wastewater samples was similar before algal cultivation.

Table 1. The characterization of aquaculture wastewater before and after pre-treatment and sterilization					
Parameters	Units	Prior to pre-treatment and sterilization AqWW1	After pre-treatment and sterilization AqWW1	Prior to pre-treatment and sterilization AqWW2	After pre-treatment and sterilization AqWW2
pH	-	7.09	7.00	7.58	7.32
COD	mgL ⁻¹	180	172	593	583
TN	mgL ⁻¹	28	23	47	41
TP	mgL ⁻¹	4.08	3.7	8.4	7.5
Salinity	mgL ⁻¹	0.21	0.2	0.30	0.28

3.2 Algal growth and biomass production

The growth pattern of *Chlamydomonas* sp., *S. ecornis*, and *S. communis* in MWC medium, AqWW1, and AqWW2 are summarized in (Fig. 1). The algal species showed a lag phase of two days in aquaculture wastewater compared to MWC medium. The fast growth in MWC medium was due to the high amount of nutrients compared to aquaculture wastewater [10, 40]. Later, the algal growth moved to an exponential phase where, *Chlamydomonas* sp., *S. ecornis*, and *S. communis* showed a significant rise in biomass production on day eight. The *Chlamydomonas* sp. showed maximum biomass yield of $2.48 \pm 0.01 \text{ gL}^{-1}$ in AqWW1 compared to AqWW2. For *S. ecornis* and *S. communis* highest biomass yield was 1.43 ± 0.02 and 1.61 ± 0.04 respectively in AqWW2 than AqWW1. The obtained results might be due to the effect of COD, nitrogen and phosphorus concentration on each algal species [10, 19, 40, 41].

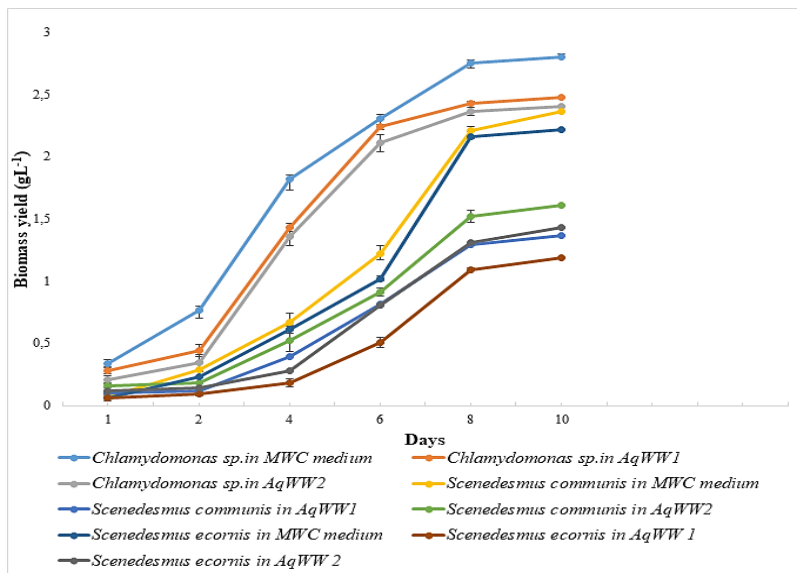


Fig .1 Growth curves of *Chlamydomonas* sp., *S. ecornis*, and *S. communis* in MWC medium, AqWW1, and AqWW2 for 10 days (mean \pm SD).

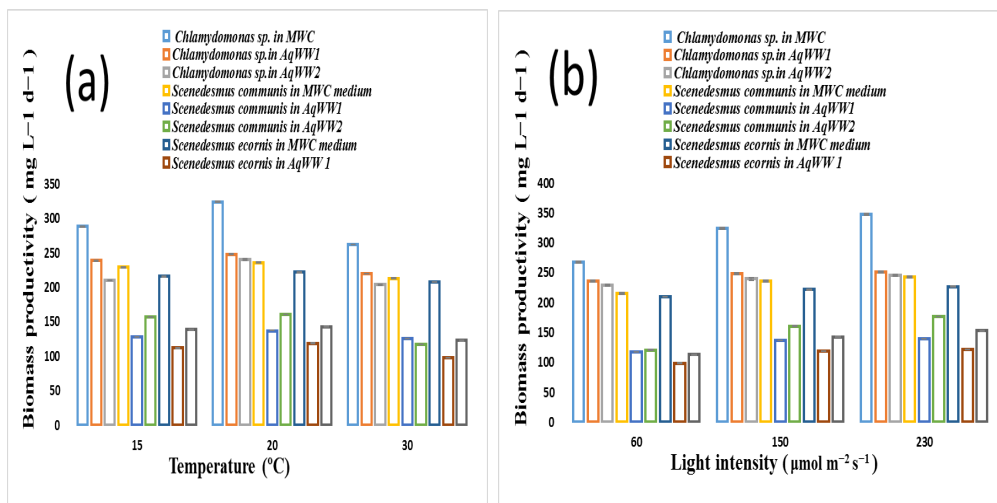
3.2 Effect of physical factors on biomass productivity

The algal growth can be enhanced or inhibited by varying the physical parameters used for cultivation of algae. Therefore the effect of different algal species under different physical conditions was studied to select the best parameters suitable for algal cultivation [19, 42, 44]. The influence of temperature on biomass productivity of *Chlamydomonas* sp., *S. ecornis*, and *S. communis* were studied by cultivating each algal species in batch cultures with a continuous light intensity of $150 \mu\text{mol m}^{-2} \text{s}^{-1}$ and at different temperatures such as 15°C , 20°C , and 30°C respectively represented in (Fig. 2a). The maximum yield of biomass productivity was obtained at 20°C for all species in this study which matches with the findings reported by Abbas et al., 2013 [43]. The temperature lower or higher than optimum value can inhibit the cellular metabolism and growth of algal species [41, 42]. The highest biomass productivity was obtained with *Chlamydomonas* sp. followed by *S. communis* and then *S. ecornis* in MWC. The biomass productivity of *Chlamydomonas* sp. was higher in AqWW1 whereas for *S. ecornis* and *S. communis* in AqWW2. The values of biomass productivity were $324 \pm 3.6 \text{ mg L}^{-1} \text{ d}^{-1}$, $248 \pm 1.2 \text{ mg L}^{-1} \text{ d}^{-1}$, and $240 \pm 2.5 \text{ mg L}^{-1} \text{ d}^{-1}$ in *Chlamydomonas* sp. in MWC medium, AqWW1, and AqWW2, respectively. The biomass productivity of *S. ecornis* and *S. communis* in AqWW1 was $119 \pm 2.1 \text{ mg L}^{-1} \text{ d}^{-1}$, and $137 \pm 1.8 \text{ mg L}^{-1} \text{ d}^{-1}$ respectively whereas in AqWW2 it was $143 \pm 2.4 \text{ mg L}^{-1} \text{ d}^{-1}$, and $161 \pm 3.6 \text{ mg L}^{-1} \text{ d}^{-1}$.

The optimum light intensity for *Chlamydomonas* sp., *S. ecornis*, and *S. communis* were examined by cultivating each algal species as batch cultures at 20°C under various light intensities such as $60 \mu\text{mol m}^{-2} \text{s}^{-1}$, $150 \mu\text{mol m}^{-2} \text{s}^{-1}$, and $230 \mu\text{mol m}^{-2} \text{s}^{-1}$ correspondingly depicted in the (Fig 2b). The maximum biomass productivity for *Chlamydomonas* sp., *S. ecornis*, and *S. communis* were obtained at $230 \mu\text{mol m}^{-2} \text{s}^{-1}$. At this intensity the biomass productivities of $246 \pm 1.78 \text{ mg L}^{-1} \text{ d}^{-1}$, $153 \pm 1.4 \text{ mg L}^{-1} \text{ d}^{-1}$ and $177 \pm 1.2 \text{ mg L}^{-1} \text{ d}^{-1}$ were obtained by *Chlamydomonas* sp., *S. ecornis*, and *S. communis* in AqWW2, respectively, whereas productivities of $251 \pm 1.9 \text{ mg L}^{-1} \text{ d}^{-1}$, $122 \pm 1.2 \text{ mg L}^{-1} \text{ d}^{-1}$ and $139 \pm 1.6 \text{ mg L}^{-1} \text{ d}^{-1}$ were recorded in AqWW1, respectively.

The optimum carbon dioxide (CO_2) amount for *Chlamydomonas* sp., *S. ecornis*, and *S. communis* were examined by cultivating each algal species as batch cultures by changing the amount of CO_2 from 0 (%v/v) to 50 (%v/v) at 20°C with a continuous light intensity of $230 \mu\text{mol}$

$\text{m}^{-2} \text{s}^{-1}$ shown in (Fig. 2c). The different volumes of 99.8 % pure CO₂ were introduced to the algal cultivation using venting filters (Acro® 37, VWR). The biomass productivity of algal species can increase or decrease depending on the CO₂ tolerance of each algal species. The biomass productivity of *Chlamydomonas* sp. decreased with increase in CO₂ amount, but *S. ecornis* and *S. communis* showed an increase in biomass productivity until 20% (v/v) amount of CO₂ [19, 34,45]. The maximum biomass productivity of $181 \pm 1.5 \text{ mg L}^{-1} \text{ d}^{-1}$, and $159 \pm 1.3 \text{ mg L}^{-1} \text{ d}^{-1}$ were shown by *Scenedesmus communis* and *Scenedesmus ecornis*, respectively, in AqWW2, whereas productivity was $143 \pm 1.0 \text{ mg L}^{-1} \text{ d}^{-1}$, and $129 \pm 0.9 \text{ mg L}^{-1} \text{ d}^{-1}$ in AqWW1 at 20 °C with a continuous light intensity of 230 $\mu\text{mol m}^{-2} \text{ s}^{-1}$ and 20 % (v/v) amount of CO₂.



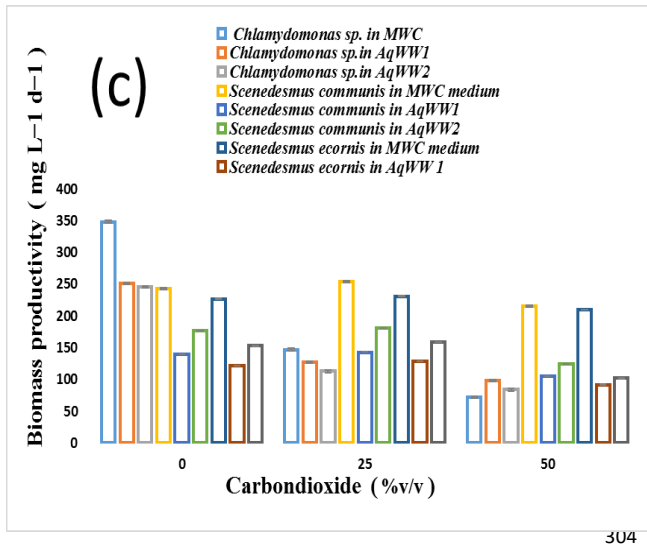


Fig .2 Biomass productivity of *Chlamydomonas* sp., *S. ecornis*, and *S. communis* at (a) different temperature (b) different light intensity (c) CO₂ (%v/v)

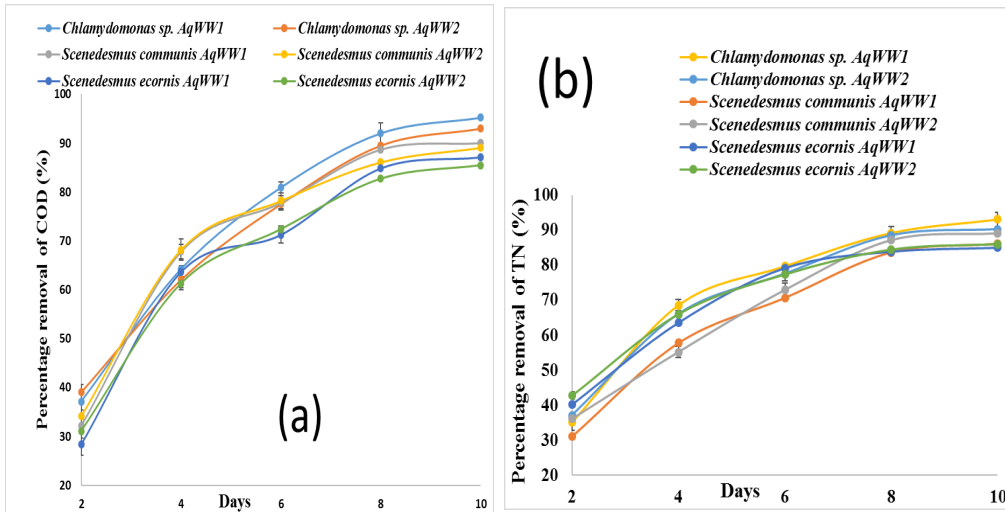
3.3 Nutrient removal

The percentage removal of COD by *Chlamydomonas* sp., *S. ecornis*, and *S. communis* in the aquaculture wastewater samples (AqWW1 and AqWW2) are summarized in Fig. 3a. In earlier studies algal species were used for the treatment of different types of wastewater [19, 42, 46]. The present work shows that there is a drastic decrease in COD level in all experiments. The *Chlamydomonas* sp. showed higher removal of COD in AqWW1 but *S. communis*, and *S. ecornis* in AqWW2. This finding is in good agreement with the research outcome of Kamyab et al., (2015) and Ma et al., (2017) in palm oil effluent and molasses wastewater treatment [41, 47]. The *Chlamydomonas* sp., *S. communis*, and *S. ecornis* exhibited 95.5 %, 89.1 %, and 85.4 % of COD removal in AqWW1 respectively whereas 92.9 %, 91.9 %, and 87 % in AqWW2 correspondingly within ten days.

The maximum percentage removal of TN in AqWW1 by *Chlamydomonas* sp., *S. communis*, and *S. ecornis* was 93.8 %, 86.1 %, and 85 % correspondingly (Fig. 3b). The *Chlamydomonas* sp.,

S. communis, and *S. ecornis* showed 90.2 %, 89.1 %, and 86 % removal of TN in AqWW2, respectively within ten days. The current work indicates that *Chlamydomonas* sp. showed higher removal of TN when the initial concentration of nitrogen was lower in the wastewater samples and this result matches with the reported study by Tao et al., (2016) and Kamyab et al., (2015)[47, 48]. The *Scenedesmus* sp. showed a rise in TN removal with an increase in COD level until certain limit (Ma et al., 2017)[41]. Moreover, in this current study *S. communis*, and *S. ecornis* showed maximum removal of TN in wastewater samples with a higher level of nitrogen.

Within ten days of cultivation *Chlamydomonas* sp., *S. communis*, and *S. ecornis* in AqWW1 showed 94 %, 87.1 %, and 85.9 % removal of TP respectively (Fig. 3c). The TP removal was 91.2%, 91.1%, 90% by *Chlamydomonas* sp., *S. communis*, and *S. ecornis* in AqWW2 correspondingly. The TP removal by *Chlamydomonas* sp. was higher in wastewater samples with a low concentration of phosphorus which is in good agreement with the findings reported by Tao et al., (2016)[48]. Ma et al. (2017) stated that *Scenedesmus* sp. showed an increase in TP removal with an increase in COD content until a specific limit which matches with the current findings. *S. communis*, and *S. ecornis* showed a rise in TP removal compared to other reported studies [41]. The rise in TP removal is due to the accumulation of precipitated phosphorus in the algal cell as a result of a rise in the pH of culture from 7 to 9 [49].



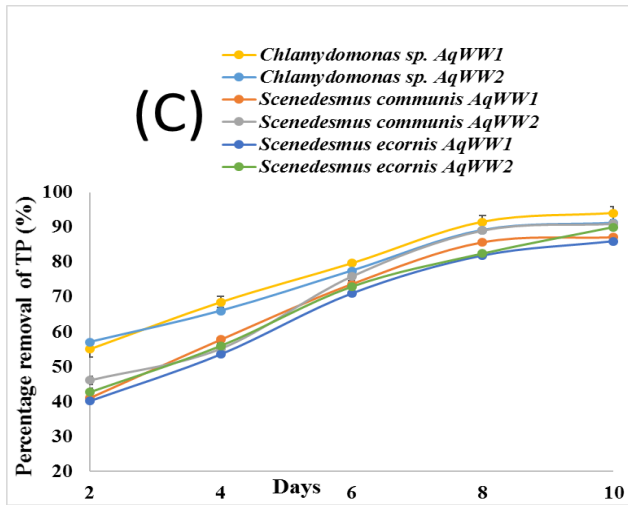


Fig.3 The aquaculture wastewater treatment performance by *Chlamydomonas* sp., *S. ecornis*, and *S. communis* at their optimum condition as percentage removal of (a) COD (b) TN and (c) TP

3.4 Lipid content and productivity

The maximum lipid content was observed in *Chlamydomonas* sp. (38.5%) followed by *S. communis* (31.1 %) and *S. ecornis* (29 %) in AqWW1 while 19.9%, 22.9% and 24.7% of lipid content was detected in *Chlamydomonas* sp., *S. ecornis* and *S. communis* in MWC medium (Fig. 4). The biomass productivity of *Chlamydomonas* sp. was $348 \text{ mg L}^{-1}\text{d}^{-1}$, and $251 \text{ mg L}^{-1}\text{d}^{-1}$ in MWC medium and AqWW1 respectively. The reduction in biomass productivity from MWC medium to AqWW1 by *S. communis* and *S. ecornis* were $243 \text{ mg L}^{-1}\text{d}^{-1}$ to $142.9 \text{ mg L}^{-1}\text{d}^{-1}$ and $231 \text{ mg L}^{-1}\text{d}^{-1}$ to $139 \text{ mg L}^{-1}\text{d}^{-1}$ correspondingly. The biomass productivity of *Chlamydomonas* sp. was higher in AqWW1 and in *S. ecornis*, and *S. communis* in AqWW2. All the algae species in this study shows higher lipid content in the following order AqWW1 >AqWW2>MWC, of the medium used for the cultivation. The resulted algal performance is possible due to the limited amount of nutrients [19, 42, 50]. The lower level of COD helps algal cells to activate lipid production and storage. Moreover, the lower amount of nitrogen and phosphorus enhanced the lipid content [10, 17, 40, 50, 51]. The present study showed higher lipid content for *Chlamydomonas* sp. and

Scenedesmus sp. relative to results by Kong et al., 2010 and Ansari et al., (2017), respectively [11,52]. The obtained result is maybe due to the low concentration of nitrogen and phosphorus in AqWW1 compared to the previously reported studies [50].

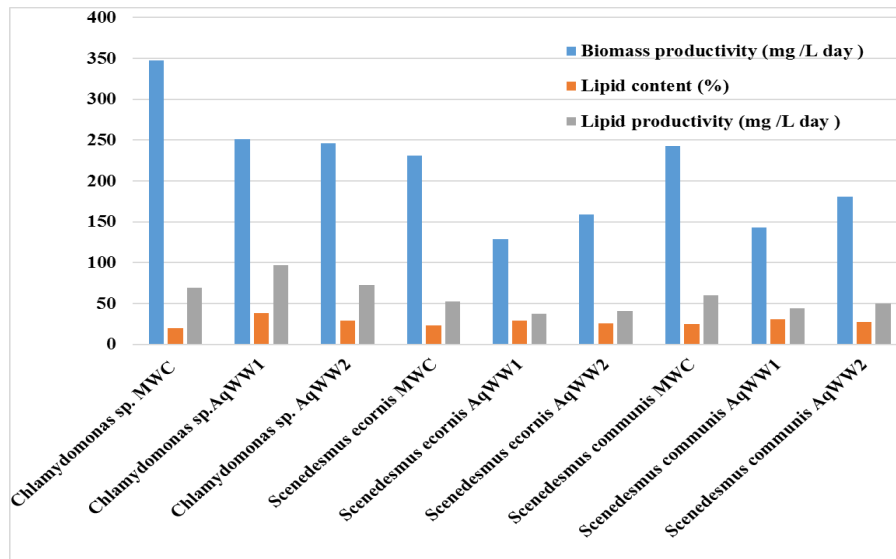


Fig. 4. The lipid content and productivity of *Chlamydomonas* sp., *S. ecornis*, and *S. communis* in MWC medium and aquaculture wastewater samples (AqWW1 and AqWW2) after co-solvent extraction.

3.5 FAME profile and properties

The current work shows that the FAME of *Chlamydomonas* sp., *S. ecornis*, and *S. communis* mainly consisted of palmitic acid methyl ester (C16:0), palmitoleic acid methyl ester (C16:1), stearic acid methyl ester (C18:0), oleic acid methyl ester (C18:1n9c), linoleic acid methyl ester (C18:2n6c), and α -linolenic acid methyl ester (C18:3n3) (Table 2). The FAME yields of 23.1%, 11.0%, and 10.5% of DW were correspondingly attained by *Chlamydomonas* sp, *S. communis*, and *S. ecornis* in AqWW1. The present work represents higher FAME (% DW) for *Scenedesmus* sp. than in Duong et al. (2015) and Tossavainen et al. (2018)[53, 54]. The increased content of FAME

is possibly due to the extraction of lipid using the co-solvent method. The previous work by Choi et al. (2014) observed higher fatty acid content with ionic liquid extraction compared to organic solvent extraction²², which supports the present findings.

The properties of algal biodiesel such as cetane number, saponification value, and iodine value were estimated with help of empirical formula, and fatty acid methyl ester profiles were also summarized in Table 2. The fatty acid composition of algal species depends on the environmental conditions such as nutrient concentration, salinity, temperature, and light intensity [34,40,41,51,53]. The lower concentration of nitrogen and phosphorus in the medium increases the content of triglycerides (TGA) and also enhance the concentration of oleic fatty acid and reduces the linolenic fatty acid amount [34, 50]. The drop in linolenic fatty acid or a lower amount of unsaturated fatty acid increases oxidation stability [5, 50, 55]. The lower amount of long-chain fatty acid reduces filter clogging at a lower temperature [5, 56]. The pour point of fuel decreases with an increase in unsaturated fatty acid content [17]. The calculated cetane number and iodine value of all algal FAME were within EN 14214 limits [5, 38].

Table 2. Summary of FAME composition and properties of different algal species in MWC and aquaculture wastewater with in ten days

FAME Composition	<i>Chlamydomonas</i> sp			<i>S. communis</i>			<i>S. ecornis</i>		
	MWC	AqWW1	AqWW2	MWC	AqWW1	AqWW2	MWC	AqWW1	AqWW2
Saturated fatty acids (% of total FAME)									
C16:0	24.6	28.24	26.12	33.05	37.45	35.56	20.35	23.12	21.51
C18:0	5.21	2.80	3.1	4.1	2.1	2.9	3.31	1.50	2.42
Unsaturated fatty acids (% of total FAME)									
C 16:1	1.40	2.79	2.18	1.13	2.55	1.89	1.32	3.4	2.64
C18:1n9c	8.8	27.20	23.42	35.02	44.5	40.03	21.14	32.18	25.72
C18:2n6c	20.9	26.4	22.10	2.4	3.6	2.84	6.60	9.16	6.57
C18:3n3	16.2	5.0	6.94	14.6	10.4	12.67	15.8	12.3	14.10
Total FAME (%DW)	8.92	23.12	14.65	8.78	11.04	9.38	6.58	10.45	7.92
Iodine value (g I 100g ⁻¹)	91.49	88.74	82.25	76.19	77.54	77.69	75.51	82.57	76.24

4. Conclusions

The findings of the current work clearly illustrate that the removal of nutrients from aquaculture wastewater (AqWW1 and AqWW2) was efficiently achieved by *Chlamydomonas* sp., *S. erconis*, and *S. communis* within ten days. The biomass productivity, lipid content, and optimum growth conditions differ among the chosen algal species. In contrast to *Chlamydomonas* sp., the *Scenedesmus* sp. showed improved biomass productivity with an increased amount of CO₂ up to 20% (v/v). It is important to note the *Chlamydomonas* sp. maximum biomass productivity (251 ±1.9 mg L⁻¹ d⁻¹) and lipid content (38.5%) in AqWW1. The wastewater treatment efficiency and total FAME (% DW) was highest in the following order (a) *Chlamydomonas* sp., (b) *S. communis*, and (c) *S. erconis*. The estimated fuel properties of obtained algal FAME are suitable for proper fuel. The present study revealed that a synergetic approach of growing microalgae in aquaculture wastewater and utilizing microalgae lipid for the low-cost biodiesel can be a sustainable solution of nutrient recovery, wastewater treatment, and production of fuel.

Acknowledgement

We would like to gratefully acknowledge Dr. Jouni Vielma, Principal Research Scientist in Natural Resources Institute Finland (Luke) for providing guidance with recirculation aquaculture systems (RAS). We also like to express our gratitude to Jani Pulkkinen for helping with aquaculture wastewater sample collection from Laukaa fish farm of the Natural Resources Institute Finland.

References

- [1] Ambat I, Srivastava V, Haapaniemi E et al. Application of Potassium Ion Impregnated Titanium Dioxide as Nanocatalyst for Transesterification of Linseed Oil. *Energy & Fuels* **2018**, 32, 11645–11655. doi:10.1021/acs.energyfuels.8b03310.
- [2] Gouveia L, Graça S, Sousa C, Ambrosano L, Ribeiro B, Botrel EP, et al. Microalgae biomass production using wastewater: Treatment and costs. Scale-up considerations. *Algal Res* **2016**, 16,167–176. doi:10.1016/j.algal.2016.03.010.
- [3] Ambat I, Srivastava V, Haapaniemi E et al. Nano-magnetic potassium impregnated ceria as catalyst for the biodiesel production . *Renew Energy* **2019**, 139,1428–1436.
- [4] Demirbas A. Biodiesel production from vegetable oils by supercritical methanol. *J Sci Ind Res* **2005**,64,858–865.
- [5] Ambat I, Srivastava V, Sillanpää M. Recent advancement in biodiesel production methodologies using various feedstock : A review. *Renew Sustain Energy Rev* **2018**, 90, 356–369.
- [6] Ambat I, Srivastava V, Iftekhar S, Haapaniemi E et al. Dual application of divalent ion anchored catalyst: biodiesel synthesis and photocatalytic degradation of carbamazepine. *Catal Green Chem Eng* **2019**, 2, 25–42.
doi:<http://dx.doi.org/10.1615/CatalGreenChemEng.2019030878>.
- [7] Ambat I, Srivastava V, Haapaniemi E et al. Effect of lithium ions on the catalytic efficiency of calcium oxide as a nanocatalyst for the transesterification of lard oil. *Sustain Energy Fuels* **2019**, 3, 2464–2474. doi:10.1039/C9SE00210C.
- [8] Renato J, Lima DO, Abdul Y, Rondenelly B, Marcos F, Batista C, et al. Strontium zirconate heterogeneous catalyst for biodiesel production : Synthesis , characterization and catalytic activity evaluation. *Applied Catal A, Gen* **2012**, 445–446, 76–82.
doi:10.1016/j.apcata.2012.08.005.
- [9] Gao F, Li C, Yang Z, Zeng G, Feng L, Liu J, et al. Continuous microalgae cultivation in aquaculture wastewater by a membrane photobioreactor for biomass production and nutrients removal. *Ecol Eng* **2016**, 92, 55–61. doi:10.1016/j.ecoleng.2016.03.046.
- [10] Guldhe A, Ansari FA, Singh P et al. Heterotrophic cultivation of microalgae using aquaculture wastewater_ A biorefinery concept for biomass production and nutrient remediation *Ecol Eng* **2017**, 99, 47–53. doi:<https://doi.org/10.1016/j.ecoleng.2016.11.013>.

- [11] Ansari FA, Singh P, Guldhe A et al. Microalgal cultivation using aquaculture wastewater_ Integrated biomass generation and nutrient remediation. *Algal Res* **2017**, 21, 169–77. doi:<https://doi.org/10.1016/j.algal.2016.11.015>.
- [12] Ravindran B, Kurade M, Kabra AN et al. Algal Biofuels. In: Gupta SK, Malik A, Bux F, editors. *Algal biofuels*, Springer International Publishing; **2017**, p. 1–38.
- [13] Galadima A, Muraza O. Biodiesel production from algae by using heterogeneous catalysts : A critical review. *Energy* **2014**, 78, 72–83. doi:[10.1016/j.energy.2014.06.018](https://doi.org/10.1016/j.energy.2014.06.018).
- [14] Patil PD, Reddy H, Muppaneni T, Mannarswamy A, Schuab T. Power dissipation in microwave-enhanced in situ transesterification of algal biomass to biodiesel. *Green Chem* **2012**, 14, 809–18. doi:[10.1039/c2gc16195h](https://doi.org/10.1039/c2gc16195h).
- [15] López CVG, García CC, Sevilla FJM et al. Medium recycling for Nannochloropsis gaditana cultures for aquaculture. *Bioresour Technol* **2013**, 129, 430–438.
- [16] Michels MHA, Vaskoska M, Al VMH et. Growth of *Tetraselmis suecica* in a tubular photobioreactor on wastewater from a fish farm. *Water Res* **2014**, 65, 290–296.
- [17] Zhu L, Wang Z, Shu Q, Takala J, Hiltunen E, Feng P, et al. Nutrient removal and biodiesel production by integration of freshwater algae cultivation with piggery wastewater treatment. *Water Res* **2013**, 47, 4294–302. doi:[10.1016/j.watres.2013.05.004](https://doi.org/10.1016/j.watres.2013.05.004).
- [18] Guo Z, Liu Y, Guo H et al. Microalgae cultivation using an aquaculture wastewater as growth medium for biomass and biofuel production. *J Environ Sci* **2013**, 25, 85–8.
- [19] Ambat I, Tang W, Sillanpää M. Statistical analysis of sustainable production of algal biomass from wastewater treatment process. *Biomass and Bioenergy* **2019**, 120, 471–478. doi:<http://dx.doi.org/10.1016/j.biombioe.2018.10.016>.
- [20] Zhou W, Li Y, Min M, Hu B, Chen P, Ruan R. Local bioprospecting for high-lipid producing microalgal strains to be grown on concentrated municipal wastewater for biofuel production. *Bioresour Technol* **2011**, 102, 6909–6919. doi:[10.1016/j.biortech.2011.04.038](https://doi.org/10.1016/j.biortech.2011.04.038).
- [21] Kothari R, Pathak V V., Kumar V, Singh DP. Experimental study for growth potential of unicellular alga *Chlorella pyrenoidosa* on dairy waste water: An integrated approach for treatment and biofuel production. *Bioresour Technol* **2012**, 116, 466–470. doi:[10.1016/j.biortech.2012.03.121](https://doi.org/10.1016/j.biortech.2012.03.121).
- [22] Choi SA, Oh YK, Jeong M-J et al. Effects of ionic liquid mixtures on lipid extraction from *Chlorella vulgaris*. *Renew Energy* **2014**, 65, 169–174.

- [23] Kumar RR, Rao PH, Arumugam M. Lipid extraction methods from microalgae : a comprehensive review. *Front Energy Res* **2015**, 2, 1–9. doi:10.3389/fenrg.2014.00061.
- [24] Fulmer GR, Miller AJM, Sherden NH, Gottlieb HE, Nudelman A, Stoltz BM, et al. NMR Chemical Shifts of Trace Impurities : Common Laboratory Solvents , Organics , and Gases in Deuterated Solvents Relevant to the Organometallic Chemist. *Organometallics* **2010**, 2176–2179. doi:10.1021/om100106e.
- [25] Shim YY, Gui B, Arnison PG, Wang Y, Reaney MJT. Flaxseed (*Linum usitatissimum L.*) bioactive compounds and peptide nomenclature: Areview. *Trends Food Sci Technol* **2014**, 38, 5–20. doi:10.1016/j.tifs.2014.03.011.
- [26] Kim Y-H, Choi Y-K, Park J et al. Ionic liquid-mediated extraction of lipids from algal biomass . *Bioresour Technol* **2012**, 109, 312–315.
- [27] Young G, Nippgen F, Titterbrandt S et al. Lipid extraction from biomass using co-solvent mixtures of ionic liquids and polar covalent molecules _ Elsevier Enhanced Reader.pdf. Sep Purif **2010**, 72, 118–121.
- [28] Guillard RRL, Lorenzen CJ. Yellowgreen Algae with Chlorophyllide C. *JPhycol* **1972**, 8, 10–4.
- [29] Pulkkinen JT, Kiuru T, Aalto SL et al. Startup and effects of relative water renewal rate on water quality and growth of rainbow trout (*oncorhynchus mykiss*) in a unique RAS research platform. *Aquac Eng* **2018**, 82, 38–45.
- [30] Rice EW, Baird RB, Eaton AD et al, editors. Standard methods for the examination of water and wastewater. 22nd editi. American Public Health Association (APHA), American Water Works Association (AWWA) and Water Environment Federation (WEF), Washington, D.C., USA.; **2012**.
- [31] Christie WW. Advances in lipid methodology. The Oily Press; **1993**.
- [32] Júnior OOS, Montanher PF, Bonafé EG. Efficiencies of Acid and Base-Catalyzed Methylation of Vegetable Oils by Ambient Mass Spectrometry. *J Braz Chem Soc* **2013**, 24, 1764–1771. doi:<http://dx.doi.org/10.5935/0103-5053.20130221> J.
- [33] Thoai DN, Photaworn S, Kumar A, Prasertsit K, Tongurai C. A novel chemical Method for Determining Ester Content in Biodiesel. *Energy Procedia* **2017**, 138, 536–543.
- [34] Ho S, Nakanishi A, Ye X, Chang J, Hara K, Hasunuma T. Optimizing biodiesel production in marine Chlamydomonas sp . JSC4 through metabolic profiling and an innovative salinity-

gradient strategy. *Biotechnol Biofuels* **2014**, *7*, 1–16.

- [35] Ambat I, Srivastava V, Iftekhar S, Haapaniemi E et al. Effect of different co-solvents on biodiesel production from various low-cost feedstocks using Sr-Al double oxides. *Renew Energy* **2020**, *146*, 2158–69. doi:<https://doi.org/10.1016/j.renene.2019.08.061>.
- [36] Krisnangkura K. A simple method for estimation of cetane index of vegetable oil methyl esters. *J Am Oil Chem Soc* **1986**, *63*, 552–3.
- [37] Kalayasiri P, Jeyashoke N, Krisnangkura K. Survey of seed oils for use as diesel fuels. *J Am Oil ChemSoc* **1996**, *73*, 471–4.
- [38] Islam MA, Magnusson M, Brown RJ et al. Microalgal Species Selection for Biodiesel Production Based on Fuel Properties Derived from Fatty Acid Profiles. *Energies* **2013**, *6*, 5676–702. doi:10.3390/en6115676.
- [39] Karpagam R, Preeti R, Ashokkumar B et al. Enhancement of lipid production and fatty acid profiling in *Chlamydomonas reinhardtii*, CC1010 for biodiesel production. *Ecotoxicol Environ Saf* **2015**, *121*, 253–7.
- [40] Yang L, Chen J, Qin S, Zeng M, Jiang Y, Hu L, et al. Growth and lipid accumulation by different nutrients in the microalga *Chlamydomonas reinhardtii*. *Biotechnol Biofuels* **2018**, *11*, 1–12.
- [41] Ma C, Wen H, Xing D, Pei X, Zhu J, Ren N, et al. Molasses wastewater treatment and lipid production at low temperature conditions by a microalgal mutant *Scenedesmus* sp. Z-4. *Biotechnol Biofuels* **2017**, *10*, 111. doi:10.1186/s13068-017-0797-x.
- [42] Singh SP, Singh P. Effect of temperature and light on the growth of algae species—A review. *Renew Sustain Energy Rev* **2015**, *50*, 431–44.
- [43] Abbas S, Saeed S, Ammar M, Aman S, Shakeel SN. Effect of High Temperature on Activities and Lipid Production in Mutants of *Chlamydomonas reinhardtii*. *Int J Agric Biol* **2013**, *20*, 1331–8. doi:10.17957/IJAB/15.0634.
- [44] Bonente G, Pippa S, Castellano S, Bassi R, Ballottari M. Acclimation of *Chlamydomonas reinhardtii* to Different Growth Irradiances. *J Biol Chem* **2012**, *287*, 5833–47. doi:10.1074/jbc.M111.304279.
- [45] Yadav G, Sen R. Microalgal green refinery concept for biosequestration of carbon-dioxide vis-à-vis wastewater remediation and bioenergy production: Recent technological advances in climate research. *J CO₂ Util* **2017**, *17*, 188–206. doi:10.1016/j.jcou.2016.12.006.

- [46] Bhatt NC, Panwar A, Bisht TS, Tamta S. Coupling of algal biofuel production with wastewater. *Sci World J* ;**2014**. doi:10.1155/2014/210504.
- [47] Kamyab H, Din MFM, Keyvanfar A et al. Efficiency of Microalgae Chlamydomonas on the Removal of Pollutants from Palm Oil Mill Effluent (POME). *Energy Procedia* **2015**,75, 2400–8.
- [48] Tao G, Yaakob Z, Sobri M. Biomass production and nutrients removal by a newly-isolated microalgal strain Chlamydomonas sp in palm oil mill effluent (POME) *Int J Hydrogen Energy* **2016**,4888–95. doi:10.1016/j.ijhydene.2015.12.010.
- [49] Ruiz-Martin A, Mendoza-Espinosa LG, Stephenson T. Growth and nutrient removal in free and immobilized green algae in batch and semi-continuous cultures treating real wastewater. *Bioresour Technol* **2010**,101,58–64.
- [50] Sharma KK, Schuhmann H, Schenk PM. High Lipid Induction in Microalgae for Biodiesel Production. *Energies* **2012**, 5, 1532–53. doi:10.3390/en5051532.
- [51] Shin SE, Koh HG, Kang NK, Suh WI, Jeong B, Lee B. Isolation , phenotypic characterization and genome wide analysis of a Chlamydomonas reinhardtii strain naturally modified under laboratory conditions : towards enhanced microalgal biomass and lipid production for biofuels. *Biotechnol Biofuels* **2017**,1–15. doi:<https://doi.org/10.1186/s13068-017-1000-0>.
- [52] Kong Q, Li L, Martinez Bl et al. Culture of Microalgae Chlamydomonas reinhardtii in Wastewater for Biomass Feedstock Production. *Appl Biochem Biotechnol* **2010**,160. doi:<https://doi.org/10.1007/s12010-009-8670-4>.
- [53] Duong VT, Ahmed F, Thomas-hall SR, Quigley S. High protein- and high lipid-producing microalgae from northern Australia as potential feedstock for animal feed and biodiesel. *Front Bioeng Biotechnol* **2015**,3,1–7. doi:10.3389/fbioe.2015.00053.
- [54] Tossavainen M. , Chopra K, Silja K, Kalle V, K SA, Suvigya S, et al. Conversion of biowaste leachate to valuable biomass and lipids in mixed cultures of Euglena gracilis and chlorophytes. *Algal Res* **2018**,35,76–84.
- [55] Huo S, Wang Z, Zhu S et al. Cultivation of Chlorella zofingiensis in bench-scale outdoor ponds by regulation of pH using dairy wastewater in winter, South China. *Bioresour Technol* **2012**,121, 76–82.
- [56] P'erez A, Casas A, Fernández CM et al. Winterization of peanut biodiesel to improve the

cold flow properties. *Bioresour Technol* **2010**,*101*,7375–81.

ACTA UNIVERSITATIS LAPPEENRANTAENSIS

- 862.** KHADIJEH, NEKOUEIAN. Modification of carbon-based electrodes using metal nanostructures: Application to voltammetric determination of some pharmaceutical and biological compounds. 2019. Diss.
- 863.** HANSKI, JYRI. Supporting strategic asset management in complex and uncertain decision contexts. 2019. Diss.
- 864.** OTRA-AHO, VILLE. A project management office as a project organization's strategizing tool. 2019. Diss.
- 865.** HILTUNEN, SALLA. Hydrothermal stability of microfibrillated cellulose. 2019. Diss.
- 866.** GURUNG, KHUM. Membrane bioreactor for the removal of emerging contaminants from municipal wastewater and its viability of integrating advanced oxidation processes. 2019. Diss.
- 867.** AWAN, USAMA. Inter-firm relationship leading towards social sustainability in export manufacturing firms. 2019. Diss.
- 868.** SAVCHENKO, DMITRII. Testing microservice applications. 2019. Diss.
- 869.** KARHU, MIIKKA. On weldability of thick section austenitic stainless steel using laser processes. 2019. Diss.
- 870.** KUPARINEN, KATJA. Transforming the chemical pulp industry – From an emitter to a source of negative CO₂ emissions. 2019. Diss.
- 871.** HUJALA, ELINA. Quantification of large steam bubble oscillations and chugging using image analysis. 2019. Diss.
- 872.** ZHIDCHENKO, VICTOR. Methods for lifecycle support of hydraulically actuated mobile working machines using IoT and digital twin concepts. 2019. Diss.
- 873.** EGOROV, DMITRY. Ferrite permanent magnet hysteresis loss in rotating electrical machinery. 2019. Diss.
- 874.** PALMER, CAROLIN. Psychological aspects of entrepreneurship – How personality and cognitive abilities influence leadership. 2019. Diss.
- 875.** TALÁSEK, TOMÁS. The linguistic approximation of fuzzy models outputs. 2019. Diss.
- 876.** LAHDENPERÄ, ESKO. Mass transfer modeling in slow-release dissolution and in reactive extraction using experimental verification. 2019. Diss.
- 877.** GRÜNENWALD, STEFAN. High power fiber laser welding of thick section materials - Process performance and weld properties. 2019. Diss.
- 878.** NARAYANAN, ARUN. Renewable-energy-based single and community microgrids integrated with electricity markets. 2019. Diss.
- 879.** JAATINEN, PEKKO. Design and control of a permanent magnet bearingless machine. 2019. Diss.
- 880.** HILTUNEN, JANI. Improving the DC-DC power conversion efficiency in a solid oxide fuel cell system. 2019. Diss.

881. RAHIKAINEN, JARKKO. On the dynamic simulation of coupled multibody and hydraulic systems for real-time applications. 2019. Diss.
882. ALAPERÄ, ILARI. Grid support by battery energy storage system secondary applications. 2019. Diss.
883. TYKKYLÄINEN, SAILA. Growth for the common good? Social enterprises' growth process. 2019. Diss.
884. TUOMISALO, TEEMU. Learning and entrepreneurial opportunity development within a Finnish telecommunication International Venture. 2019. Diss.
885. OYEDEJI, SHOLA. Software sustainability by design. 2019. Diss.
886. HUTTUNEN, MANU. Optimizing the specific energy consumption of vacuum filtration. 2019. Diss.
887. LIIKANEN, MIIA. Identifying the influence of an operational environment on environmental impacts of waste management. 2019. Diss.
888. RANTALA, TERO. Operational level performance measurement in university-industry collaboration. 2019. Diss.
889. LAUKKANEN, MINTTU. Sustainable business models for advancing system-level sustainability. 2019. Diss.
890. LOHRMANN, CHRISTOPH. Heuristic similarity- and distance-based supervised feature selection methods. 2019. Diss.
891. ABDULLAH, UMMI. Novel methods for assessing and improving usability of a remote-operated off-road vehicle interface. 2019. Diss.
892. PÖLLÄNEN, ILKKA. The efficiency and damage control of a recovery boiler. 2019. Diss.
893. HEKMATMANESH, AMIN. Investigation of EEG signal processing for rehabilitation robot control. 2019. Diss.
894. HARMOKIVI-SALORANTA, PAULA. Käyttäjät liikuntapalvelujen kehittäjinä - Käyttäjälähtöisessä palveluinnovaatioprosessissa käyttäjien tuottama tieto tutkimuksen kohteena. 2020. Diss.
895. BERGMAN, JUKKA-PEKKA. Managerial cognitive structures, strategy frames, collective strategy frame and their implications for the firms. 2020. Diss.
896. POLUEKTOV, ANTON. Application of software-defined radio for power-line-communication-based monitoring. 2020. Diss.
897. JÄRVISALO, HEIKKI. Applicability of GaN high electron mobility transistors in a high-speed drive system. 2020. Diss.
898. KOPONEN, JOONAS. Energy efficient hydrogen production by water electrolysis. 2020. Diss.
899. MAMELKINA, MARIA. Treatment of mining waters by electrocoagulation. 2020. Diss.



ISBN 978-952-335-494-4

ISBN 978-952-335-495-1 (PDF)

ISSN-L 1456-4491

ISSN 1456-4491

Lappeenranta 2020